

# ORIGIN OF ATMOSPHERIC AEROSOLS TRANSPORTED ACROSS THE NORTH ATLANTIC FREE TROPOSPHERE

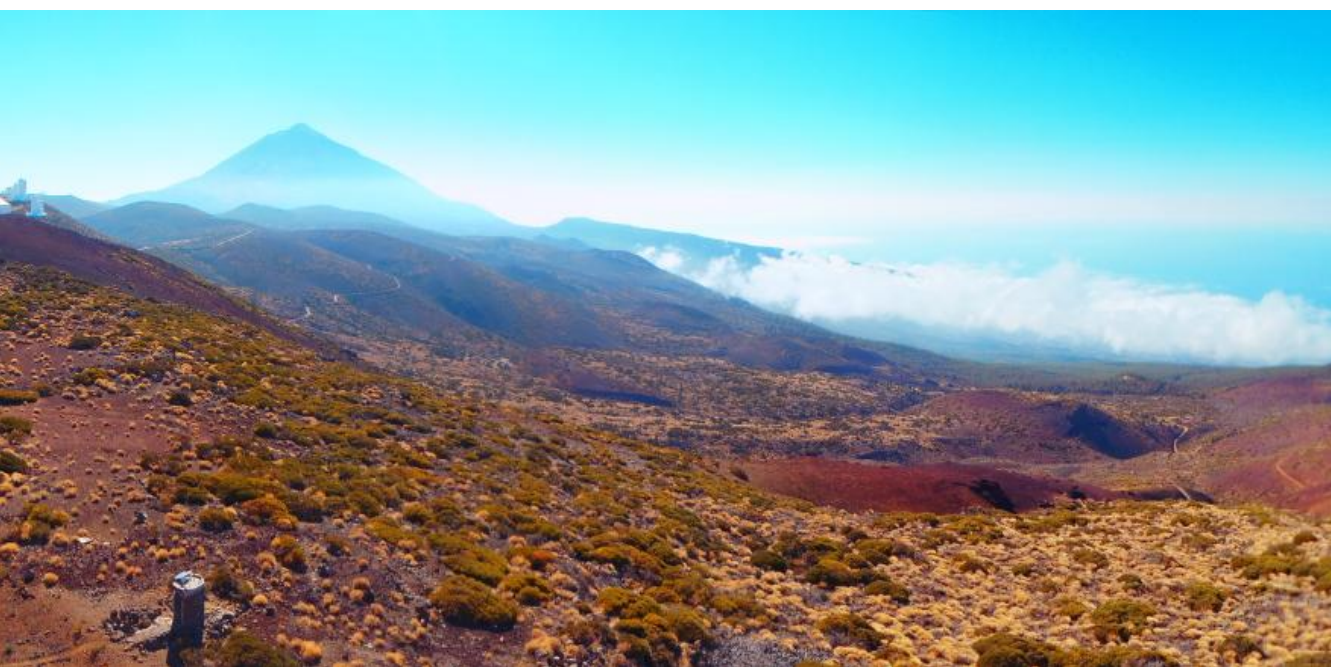
María Isabel García Álvarez

Supervisor:  
Dr. Sergio Rodríguez González.

Co-supervisors:  
Dr. Andrés Alastuey Urós.  
Dr. Barend L. Van Drooge.

Tutor:  
Dr. Luis R. Galindo Martín.

University of La Laguna  
PhD thesis, 2017





# ORIGIN OF ATMOSPHERIC AEROSOLS TRANSPORTED ACROSS THE NORTH ATLANTIC FREE TROPOSPHERE

ORIGEN DE LOS AEROSOLES ATMOSFÉRICOS  
TRANSPORTADOS A TRAVÉS DE LA TROPOSFERA  
LIBRE DEL ATLÁNTICO NORTE

María Isabel García Álvarez

Department of Chemistry (T.U. Analytical Chemistry) – Faculty of Science  
University of La Laguna  
Santa Cruz de Tenerife  
July 2017



Academic thesis submitted to obtain the Degree of Doctor from the University of La Laguna in the doctoral programme of Chemistry and Chemical Engineering.

María Isabel García Álvarez: **Origin of atmospheric aerosols transported across the North Atlantic free troposphere.**

Supervisor:

Dr. Sergio Rodríguez González.

Co-supervisors:

Dr. Andrés Alastuey Urós.

Dr. Barend L. Van Drooge.

Tutor:

Dr. Luis R. Galindo Martín.

Faculty of Science.

Department of Chemistry (T.U. Analytical Chemistry).

Santa Cruz de Tenerife.

July 2017.

# Declaration

Dr. Sergio Rodríguez González (Doctor of the Polytechnic University of Catalonia), Dr. Andrés Alastuey Urós (Doctor of the University of Barcelona), Dr. Barend L. Van Drooge (Doctor of the Autonomous University of Barcelona) and Dr. Luis R. Galindo Martín (Doctor of the University of La Laguna)

declare,

that María Isabel García Álvarez – with the Degree of Chemistry from the University of La Laguna – has performed the doctoral thesis ‘Origin of atmospheric aerosols transported across the North Atlantic free troposphere’, submitted to obtain the degree of Doctor by the University of La Laguna in the doctoral programme of Chemistry and Chemical Engineering, under our supervision.

In witness thereof, we authorize the submission of the here presented thesis and sign it,

Santa Cruz de Tenerife, July 2017

Supervisor:  
Dr. Sergio Rodríguez González

Co-Supervisor:  
Dr. Andrés Alastuey Urós

Tutor:  
Dr. Luis R. Galindo Martín

Co-Supervisor:  
Dr. Barend L. Van Drooge



*A mi familia,  
en especial a mi abuelo Juan*



# Acknowledgements

I would like to express my sincere thanks to Sergio for being the first to have confidence in me, for having dedicated his time, and for his great patience. He has not only focused on his work of supervising, but also guiding, forming and fostering curiosity and fascination for science. I have no words to thank you for your support and dedication; always in a good mood and with enthusiasm. To Barend and Andres for having welcomed me so warmly in Barcelona, for having gave me all the possible facilities and for having guided and helped me at all times. I am very grateful that this experience has been of the hand of these three people, of great value as researchers and more so as persons.

To Luis Galindo and Miguel Angel (University of La Laguna), because they were the ones who showed me the existence of Izaña and opened the possibility of a collaboration with them.

I also want to express my gratitude to Joseph M. Prospero (University of Miami) for having gave me the great opportunity to work with him, and to Paquita Zuidema (University of Miami) for having welcomed me to the lab.

A mis padres, Isabel y Juan, agradecer es decir poco. Si soy quien soy, y he llegado hasta aquí, es por ellos. Por haberme formado como persona, por su apoyo incondicional, por haberme dado todas las oportunidades y más, por ser ejemplo a seguir. A mi madre, por tirar de mí en el día a día y empujarme hasta aquí. A mi padre, por motivar mi interés por la ciencia y enseñarme que hay que entender el ‘por qué’ de lo que ocurre. A mi hermano Daniel, no sé qué haría sin ti, para lo bueno y para lo malo. A mis abuelos, que aunque ya no están, forman parte de la persona que soy y las decisiones que he tomado. A mis tíos y mis primos; no se puede tener una familia mejor y tan unida. Especialmente to Bea, who along with Jordi and Aldo, welcomed me in Barcelona several times; thank you for the good memories.

To my friends, because they are the family that is chosen. Thank you for your moral support, concern and interest in what I do.

I am grateful to my co-workers (IARC), those who still are in the centre and those who are no longer here, because they have been part of this experience. Especially to Elisa, for her support and willingness to help me at all times; and Javi, for his advice and quick resolution of problems. At the same time, I want to thank to Ramón, the meteorological watchers, the computer technicians and SIELTEC Canarias their great help with the maintenance of the instruments and the technical work.

Of course, also my sincere thanks to the people with whom I was lucky to share part of this

experience at the Institute of Environmental Assessment and Water Research in Barcelona, and the Rosenstiel School of Marine and Atmospheric Science in Miami. To Guillermo, Bibi, MariCruz, Noemi, Ana, Lillian, Ingrid, Sam and Claudia, thank you very much for your warm welcome and for using part of your time to teach me and help me during my stay.

Also, I am very grateful to all the people with whom I have shared part of my training in campaigns (REDMAAS in Huelva, CALIMA at Izaña), courses (Hyytiälä summer school, GAWTECH and PMF) and short-term stays (IDAEA and RSMAS); very grateful to have met them all and to have made friends along the way.

And to all those people who have passed through my life and who, in one way or another, have influenced the person I am, and the decisions I have made in my life.

To all of you, thank you.

# Contents

	<b>Page</b>
<b>Abstract</b>	<b>3</b>
<b>Resumen</b>	<b>5</b>
<b>1 Introduction to aerosols</b>	<b>9</b>
1.1 Properties, impacts and sources . . . . .	9
1.2 The North Atlantic Ocean . . . . .	15
<b>2 Objectives</b>	<b>23</b>
<b>3 Methodology</b>	<b>25</b>
3.1 Sampling and measurement site . . . . .	26
3.2 Data Set . . . . .	27
3.2.1 Size distribution . . . . .	28
3.2.2 Particulate Matter . . . . .	29
3.2.3 Chemical composition . . . . .	31
3.2.3.1 Inorganic and carbonaceous species . . . . .	31
3.2.3.2 Organic species . . . . .	33
3.2.4 Meteorological products . . . . .	34
3.2.4.1 In-situ meteorology at Izaña . . . . .	34
3.2.4.2 Back-trajectories . . . . .	35
3.2.4.3 NCAR/NCEP re-Analysis data . . . . .	35
3.2.5 Additional parameters . . . . .	36
3.2.5.1 Radiation . . . . .	36
3.2.5.2 Reactive gases . . . . .	36
3.2.5.3 Global fires . . . . .	36
3.2.5.4 Aerosol Index . . . . .	37
3.2.5.5 Tornado climatology . . . . .	37
3.3 Data Analysis . . . . .	37
3.3.1 Size distribution . . . . .	37
3.3.1.1 Classification of events . . . . .	37
3.3.1.2 Size distribution–dependent particle loss parameters . . . . .	37
3.3.1.3 Determination of Formation and Growth Rates . . . . .	38
3.3.1.4 Determination of sulfuric acid contribution . . . . .	41
3.3.2 Median Concentration At Receptor Plots . . . . .	41

---

3.3.3	Multivariate Curve Resolution Alternating Least Squares / Multilinear Regression Analysis . . . . .	42
<b>4</b>	<b>Results</b>	<b>43</b>
4.1	Article 1 . . . . .	45
4.2	Article 2 . . . . .	65
4.3	Article 3 . . . . .	105
<b>5</b>	<b>Discussion</b>	<b>145</b>
<b>6</b>	<b>Conclusions</b>	<b>153</b>
<b>7</b>	<b>Future Prospects</b>	<b>157</b>
<b>A</b>	<b>Annex I</b>	<b>159</b>
	<b>References</b>	<b>165</b>
	<b>List of figures</b>	<b>I</b>
	<b>List of tables</b>	<b>III</b>
	<b>Acronyms</b>	<b>V</b>
	<b>Scientific Contribution</b>	<b>IX</b>

# Abstract

This study deals on the origin of atmospheric aerosols transported across the North Atlantic, paying special attention on identifying the impact of human activities. It is based on records of aerosol and other atmospheric components collected at Izaña Global Atmospheric Watch Observatory in Tenerife Island (2367 m a.s.l.).

The aerosol composition has been studied in the two main airflows of the North Atlantic free troposphere: the westerlies – prevailing airstreams that flows from North America eastward across the North Atlantic at subtropical and mid-latitudes – and the Saharan Air Layer – the warm, dry and dusty airstream that expands from North Africa to the Americas at tropical and subtropical latitudes – . The results of this study provide new insights on the processes that contribute to the variability of the aerosols composition in the North Atlantic free troposphere.

The seasonal evolution observed in the composition of the aerosols carried by the westerlies is influenced by (i) the spatial distribution of their sources in North America, and (ii) the seasonal shift of the westerly jet and the associated eastward moving cyclones. The westerlies carry maximum loads of (i) mineral dust from February to May, associated with the occurrence of the westerly jet at rather low latitudes ( $35^{\circ}$ – $40^{\circ}$ N), dust emissions in a region that extends from Southwest Texas to the High Plains, and subsequent dust export to the Atlantic, (ii) none-sea-salt-sulphate and ammonium from March to May, linked to the presence of the westerly jet and to the export of polluted air from Northeastern United States, where the highest  $\text{SO}_2$  emissions in North America occur, (iii) organic matter from February to May, associated with the westerly jet and export from regions of Eastern United States rich in organic aerosols, (iv) elemental carbon in August and September, associated with the occurrence of the westerly jet at rather high latitudes ( $50^{\circ}$ – $55^{\circ}$ N) and the consequent export from the regions (Chicago to New York) where the highest concentrations of elemental carbon occur in North America.

Results evidence how dust is a major component of the aerosols transported from North America across the North Atlantic by the westerly winds. The concentrations of sub- $10\ \mu\text{m}$  aerosols that reach the Izaña Observatory, after transatlantic transport from North America, typically ranges between  $1.2$  and  $4.2\ \mu\text{g}\cdot\text{m}^{-3}$  ( $20^{\text{th}}$  and  $80^{\text{th}}$  percentiles). The main contributors to background levels ( $1^{\text{st}}$ – $50^{\text{th}}$  percentiles =  $0.15$ – $2.54\ \mu\text{g}\cdot\text{m}^{-3}$ ) are North American dust (53 %), non-sea-salt- $\text{SO}_4^-$  (14 %) and organic matter (18 %), whereas aerosol composition during high  $\text{PM}_{10}$  events ( $75^{\text{th}}$ – $95^{\text{th}}$  percentiles =  $3.9$ – $8.9\ \mu\text{g}\cdot\text{m}^{-3}$ ) is dominated by North American dust (56 %), organic matter (24 %) and nss- $\text{SO}_4^-$  (9 %).

About the 64 % of the organic aerosol transported in the summer westerlies has been chemically identified. The most abundant organic compounds are (i) secondary organic aerosols from isoprene oxidation and (ii) dicarboxylic acids (mainly succinic and phthalic, indicating aged aerosols after the long-range atmospheric transport). Compounds linked to soil emissions (i.e. saccharides) are found but in minor amounts. High concentrations of organic matter and of some organic species (e.g. levoglucosan, succinic and malic acids) are linked to North American fires; air mass impacted by fires has the highest contribution of aged organic aerosols (di-acids formed during the long-range atmospheric transport) and the lowest contributions of secondary organic aerosols from oxidation of isoprene and  $\alpha$ -pinene (further oxidized under the biomass burning air). This long-range atmospheric transport of biomass burning plumes from North America supports the idea that, under certain conditions, levoglucosan is stable in the atmosphere to experience long range transport. In the westerlies, the organic matter sources are associated with soils, biomass burning and combustion.

This research also provides novel results on the composition and sources of organic aerosols exported over the Atlantic Ocean in the summer Saharan Air Layer. The speciation of the organic matter shows how most of this aerosol has a natural origin. Organic species are associated with (i) primary compounds of surface soils (i.e. saccharides) and terrestrial higher plants (i.e. nC27, nC29 and nC31 n-alkanes), (ii) secondary organic aerosols linked to the oxidation of biogenic isoprene and  $\alpha$ -pinene, (iii) primary vehicles emissions (i.e. hopanes), and (iv) bio-accumulative and toxic organic compounds (i.e. polycyclic aromatic hydrocarbons). Saccharides from soils and secondary organic compounds derived from the oxidation of isoprene and  $\alpha$ -pinene accounts for more than a 70 % of the organic matter. In the Saharan Air Layer, the sources of organic aerosols have been associated mostly with soils and combustion. Of special relevance is the enhancement in the formation of biogenic secondary organic aerosols due to interaction with anthropogenic NO<sub>x</sub> emissions – as suggested by the correlation between nitrate and secondary organic aerosols from isoprene oxidation –, which may exert a large-scale impact as a result of the synoptic scale of the Saharan Air Layer.

This study also includes a research on new particle formation, which has been found to be a frequent source of aerosols above Tenerife. The climatology of the new particle formation events at Izaña shows that these episodes occur a 30 % of the days, with a clearly marked new particle formation season (May–August). Monthly mean values of the formation and growth rates in this season exhibited values within the ranges of 0.49–0.92 cm<sup>3</sup>·s<sup>-1</sup> and 0.48–0.58 nm·h<sup>-1</sup>, respectively. New particle formation is observed during periods of upslope winds that bring gaseous precursors from the boundary layer to the interface with the low free troposphere. Sulphuric acid played a key role as gas precursor, contributing with a ~70 % to the observed growth rate. Organic species, such as oxidation products of biogenic volatile organic compounds, probably also contribute. It was found that year-to-year variability of the frequency of new particle formation events is correlated with mean sulphur dioxide concentrations. This study also has found an interaction between dust and the freshly formed new particles in the Saharan Air Layer; dust may play a significant role acting as coagulation sink of freshly formed nucleation particles.

The results of this study provide a comprehensive view of the sources and atmospheric processes that influence on the composition of the aerosol transported across the North Atlantic free troposphere. The conceptual models presented will be useful in further studies on transboundary air pollution, long-term evolution of aerosols, their effects physical properties and their influence on processes related to climate.

# Resumen

Este estudio se centra en la investigación del origen de los aerosoles atmosféricos transportados a través del Atlántico Norte, haciendo especial énfasis en la identificación del impacto de las actividades humanas. El trabajo se basa en observaciones de la composición química y las propiedades físicas de los aerosoles, y de otros componentes atmosféricos realizadas en el Observatorio de Izaña en la isla de Tenerife (2367 m a.s.l.).

Se ha estudiado la composición y el origen de los aerosoles transportados en las dos corrientes de aire asociadas a la circulación general de la atmósfera en la troposfera libre del Atlántico Norte: (i) la circulación del oeste – que fluye desde Norteamérica a través del Atlántico a latitudes medias y subtropicales – y (ii) la capa de aire sahariano – que fluye desde el Norte de África hacia las Américas a latitudes tropicales y subtropicales –. Este estudio proporciona nuevos resultados sobre los procesos que contribuyen a la variabilidad de la composición de los aerosoles en la troposfera libre del Atlántico Norte.

La evolución estacional observada en la composición de los aerosoles, transportados por la circulación del oeste, está influenciada por (i) la distribución espacial de las fuentes de los aerosoles y de sus precursores en Norteamérica y, (ii) el desplazamiento latitudinal y estacional de la circulación del oeste, cuya corriente principal se ubica a latitudes bajas en invierno ( $35^{\circ}$ – $40^{\circ}$ N) y altas en verano ( $50^{\circ}$ – $55^{\circ}$ N). Estos vientos del oeste transportan altas concentraciones de (i) polvo del suelo entre febrero y mayo, época en la que los vientos del oeste ocurren a latitudes relativamente bajas ( $35^{\circ}$ – $40^{\circ}$ N), favoreciendo las emisiones de polvo en una región que se extiende desde el suroeste de Texas hasta la Gran Llanura Central Norteamericana, y la posterior exportación al Atlántico, (ii) sulfato no marino y amonio entre marzo y mayo, cuando la circulación del oeste favorece la exportación de aire contaminado desde el noreste de los Estados Unidos, donde tienen lugar altas emisiones de  $\text{SO}_2$  debido a la combustión del carbón, (iii) materia orgánica entre febrero y mayo, asociado a procesos de exportación desde el este de Estados Unidos, (iv) carbono elemental en agosto y septiembre, cuando la circulación del oeste tiene lugar a latitudes altas y favorece la exportación de aire contaminado desde el extremo noreste de Estados Unidos (Chicago a Nueva York), región donde tienen lugar emisiones importantes de este contaminante.

Los resultados muestran que el polvo es un componente importante de los aerosoles transportados desde Norteamérica a través del Atlántico Norte. La concentración de los aerosoles (de diámetros aerodinámicos inferiores a  $10\ \mu\text{m}$ ) que llegan al Observatorio de Izaña, tras el transporte transatlántico desde Norteamérica, oscilan entre  $1.2$  and  $4.2\ \mu\text{g}\cdot\text{m}^{-3}$  (percentiles 20 y 80). Los principales componentes que contribuyen a los niveles de fondo (percentiles 1–50 =  $0.15$ – $2.54\ \mu\text{g}\cdot\text{m}^{-3}$ ) son el polvo (53 %), el sulfato no marino (14 %) y la materia orgánica

(18 %) de Norteamérica, mientras que la composición de estos aerosoles durante los eventos de altas concentraciones (percentiles 75–95 =  $3.9\text{--}8.9\ \mu\text{g}\cdot\text{m}^{-3}$ ) está dominada por el polvo (56 %), la materia orgánica (24 %) y el sulfato no marino (9 %) de Norteamérica.

Aproximadamente el 64 % de la materia orgánica transportada en los vientos del oeste en verano ha sido identificada químicamente; los compuestos más abundantes son (i) aerosoles orgánicos secundarios formados a partir de la oxidación del isopreno y (ii) ácidos dicarboxílicos (principalmente succínico y ftálico, indicando que se trata de un aerosol envejecido tras sufrir transporte atmosférico de largo alcance). Los compuestos ligados a las emisiones del suelo (sacáridos) están presentes en menores cantidades. Altas concentraciones de materia orgánica y de algunas especies orgánicas (como el levoglucosano, ácidos succínico y málico) están relacionadas con la quema de biomasa en Norteamérica; estas masas de aire influenciadas por incendios tienen las mayores contribuciones de aerosoles orgánicos envejecidos (diácidos formados durante el transporte atmosférico de larga distancia) y las menores contribuciones de aerosoles orgánicos secundarios formados por la oxidación del isopreno y del  $\alpha$ -pineno (oxidados en mayor proporción en el aire afectado por la quema de biomasa). Este transporte atmosférico de largo recorrido asociado a las emisiones de quema de biomasa procedente de Norteamérica apoya la idea de que, bajo ciertas condiciones, el levoglucosano es estable en la atmósfera y experimenta transporte de largo alcance. Las fuentes de los aerosoles orgánicos transportados por la corriente del oeste están asociadas a emisiones del suelo, quema de biomasa y la quema de combustibles fósiles.

Esta investigación también proporciona nuevos resultados sobre la composición y las fuentes de los aerosoles orgánicos exportados hacia el Atlántico Norte en la capa de aire sahariano durante el verano, época en la que las emisiones de polvo tienen lugar principalmente en la región central del desierto del Sáhara. La especiación de la materia orgánica muestra cómo la mayor parte de este aerosol tiene un origen natural. Las especies orgánicas están asociadas con (i) compuestos primarios de suelos (como los sacáridos) y plantas superiores terrestres (es decir nC27, nC29 y nC31 n-alcenos), (ii) aerosoles orgánicos secundarios ligados a la oxidación del isopreno y del  $\alpha$ -pineno, (iii) emisiones primarias de vehículos (hopanos), y (iv) compuestos orgánicos bioacumulativos y tóxicos (como los hidrocarburos aromáticos policíclicos). Los sacáridos del suelos y los compuestos orgánicos secundarios derivados de la oxidación del isopreno y del  $\alpha$ -pineno representan más del 70 % de la materia orgánica. En la capa de aire sahariano, las fuentes de aerosoles orgánicos se han asociado principalmente a los suelos y la quema de combustibles fósiles. De especial relevancia es la formación de aerosoles orgánicos secundarios debido a la interacción entre los óxidos de nitrógeno (principalmente ligado a emisiones antropogénicas) y compuestos derivados de la oxidación del isopreno (ligado a emisiones biogénicas). La correlación observada entre el nitrato y los compuestos oxidados del isopreno, presentes en la capa de aire sahariano, indica que esta interacción tiene un impacto a gran escala, ligado al alcance sinóptico de esta corriente de aire.

Este estudio incluye una investigación sobre la formación de nuevas partículas. La climatología de los eventos de formación de nuevas partículas en Izaña muestra que estos episodios se producen un 30 % de los días del periodo estudiado ( $\sim 5$  años). Estos episodios son más frecuentes entre mayo y agosto (50–60 % de los días), época en que las tasas de formación y crecimiento tienen valores medios entre  $0.49\text{--}0.92\ \text{cm}^3\cdot\text{s}^{-1}$  y  $0.48\text{--}0.58\ \text{nm}\cdot\text{h}^{-1}$ , respectivamente. La formación de nuevas partículas se observa durante el día, periodo en el que se desarrollan vientos ascendentes que transportan precursores gaseosos desde la capa límite

a la interfase con la baja troposfera libre. Los resultados muestran que el ácido sulfúrico desempeña un papel clave como gas precursor, contribuyendo con un  $\sim 70\%$  a la tasa de crecimiento observada; es probable que también contribuyan especies orgánicas, como los productos de la oxidación de compuestos orgánicos volátiles biogénicos. Los datos tomados dentro de la capa de aire sahariano aportan información sobre la interacción entre el polvo y las partículas de nucleación recién formadas; el polvo puede desempeñar un papel importante actuando como sumidero de coagulación de partículas de nucleación recién formadas. También se hizo un estudio de variabilidad inter-anual, en el que se encontró que la frecuencia de formación de nuevas partículas correlaciona con las concentraciones medias de dióxido de azufre, lo cual indica que la regulación en las emisiones de este contaminante tiene implicaciones en el número de partículas.

Los resultados de este estudio proporcionan una visión multidisciplinaria de las fuentes y los procesos atmosféricos que influyen en la composición de los aerosoles transportados a través de la troposfera libre del Atlántico Norte. Los modelos conceptuales presentados serán útiles en futuros estudios sobre la contaminación atmosférica transfronteriza, la evolución a largo plazo de los aerosoles, sus propiedades físicas y su influencia en los procesos relacionados con el clima.



## CHAPTER

# 1

# Introduction to aerosols

## 1.1 Properties, impacts and sources

Atmospheric aerosols, or particulate matter, are a complex mix of liquid and solid particles blowing in the air from natural and anthropogenic sources (Seinfeld and Pandis, 2006). Emissions from natural sources (i.e. oceans, deserts, volcanoes, vegetation and wild-fires) dominate on a global scale over those derived from human activities (e.g. industry, traffic, waste and biomass burning, and agriculture), with annual emission estimated to be about  $20 \cdot 10^2$ – $90 \cdot 10^2$  and  $1.5 \cdot 10^2$ – $4.8 \cdot 10^2$  Tg $\cdot$ y $^{-1}$ , respectively (IPCC, 2013 and references therein). Particles can be emitted directly into the atmosphere or be formed by the oxidation of precursor gases (e.g. sulphur dioxide, nitrogen oxides and volatile organic compounds) by gas-particle conversion such as nucleation, condensation, heterogeneous and multiphase chemical reaction (Hallquist et al., 2009); particulate matter formed through these two routes are referred to as primary and secondary particles, respectively. Atmospheric lifetimes of aerosols range from a few hours to several weeks (Kristiansen et al., 2016) and this depends heavily on removing mechanisms, such as dry (strongly size dependent) and wet (i.e. incorporation into cloud droplets during the formation or precipitation) deposition.

The chemical composition and size distribution influence on aerosol impacts. The chemical composition includes sea salt, mineral dust, organic matter (thousands of organic species), black carbon, secondary inorganic species (sulphate, nitrate and ammonium) and trace elements (IPCC, 2013). The particle diameters ( $d_p$ ) comprise sizes from a few nanometres to tens of micrometers (Fig. 1) and can be classified into fine ( $d_p < 1 \mu\text{m}$ ) and coarse ( $d_p > 1 \mu\text{m}$ ) particles. Particles of these two size ranges have different formation mechanisms and physicochemical properties that influence the atmospheric lifetime (Seinfeld and Pandis 2006). At the same time, the fine fraction can be further sub-divided in nucleation ( $d_p < 0.01 \mu\text{m}$ ), aitken ( $d_p \approx 0.01$ – $0.1 \mu\text{m}$ ) and accumulation ( $d_p \approx 0.1$ – $1.0 \mu\text{m}$ ) modes (Fig. 1). Nucleation particles (lifetime  $\sim$  hours) form through nucleation of atmospheric gases and growth by condensation of low-volatility vapour species, thus it is mainly constituted of secondary species

(mainly sulphate, ammonia and organic compounds), whereas the aitenken particles (lifetime  $\sim$  days) form mostly through coagulation of the nucleation mode or condensation on them and of some fresh primary emissions, specially soot vehicle exhaust emissions after fuel combustion (Fig. 1). In spite of the fact that these two classes (i.e. nucleation and aitenken) are the most abundant in particle number, they only account for a small fraction of the total mass (Fig. 1). The third size fraction, the accumulation mode (lifetime  $\sim$  few weeks), is generated by coagulation of particles belonging to the smaller modes and condensation of low-volatility vapours on pre-existing particles; it includes secondary inorganics (e.g. sulphate, nitrate and ammonium) and carbonaceous aerosols (Fig. 1). Largest particles (e.g. mineral dust and sea salt), belonging to the coarse fraction (lifetime  $\sim$  hours), are generated through mechanical processes (e.g. abrasion and fragmentation) and chemical reaction of gases with marine or crustal particles (e.g. sodium-nitrate, sodium-sulphate); the coarse mode account for the highest fraction of the total aerosol mass (Fig. 1).

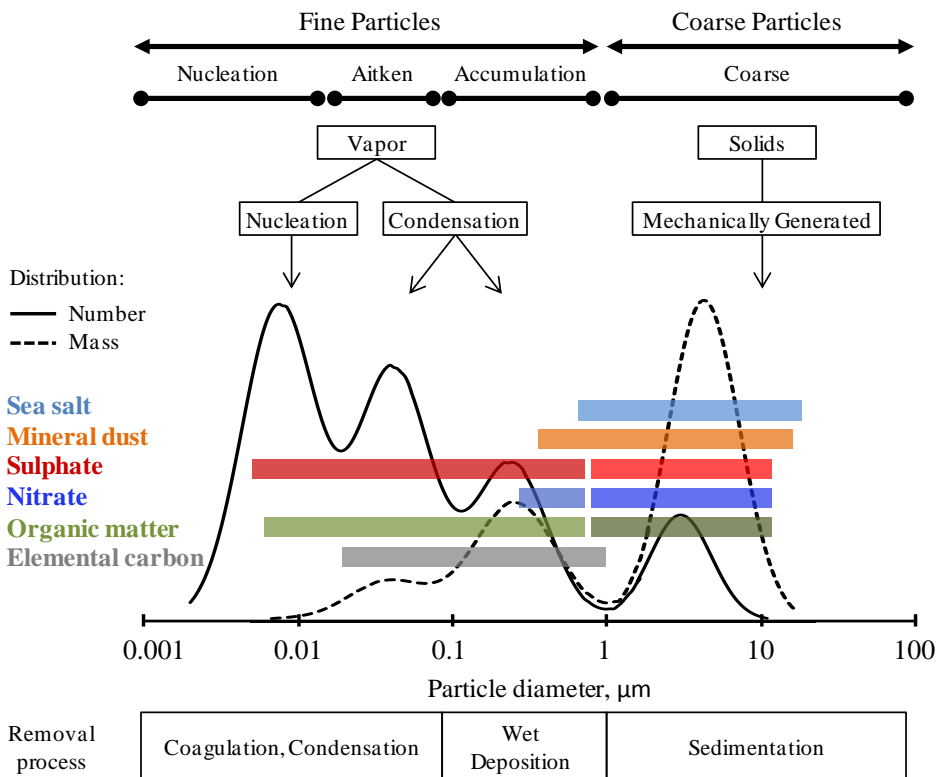


**Figure 1:** Aerosol size distribution in number (continuous line) and mass (dotted line). Major chemical species distribution, formation and removal processes are shown. Figure adapted from Seinfeld and Pandis (2006) and Gieré et al. (2010).

## 1.1. PROPERTIES, IMPACTS AND SOURCES

---

Aerosols exert a great concern globally, mainly because of their influence on:

- (i) Continental and marine ecosystems, providing fundamental nutrients as iron and phosphorous (e.g. to the Amazon rainforest fertilizing plants; Koren et al., 2006; Ben-Ami et al., 2010; Abouchami et al., 2013; and to the remote ocean influencing the phytoplankton growth; De Baar et al., 2005; Ravelo et al., 2016).
- (ii) Heterogeneous chemistry in the troposphere and stratosphere (Ravishankara, 1997; Finlayson-Pitts and Pitts, 2000), by providing a medium for chemical reactions (e.g. destruction of stratospheric ozone).
- (iii) Degradation of visibility, as a consequence of light extinction (Xiao et al., 2014).
- (iv) Human health, promoting ischaemic heart disease, stroke, chronic obstructive pulmonary disease, lung cancer and acute lower respiratory infections in children (Davidson et al., 2007; Dominguez-Rodríguez et al., 2016). According to the World Health Organization (WHO, 2014), exposure to aerosols and reactive gases in ambient air pollution is associated with  $\sim 3.7$  million deaths $\cdot y^{-1}$ .
- (v) Climate change, forcing the Earth's radiative equilibrium directly by scattering and absorbing solar and infrared radiation (i.e. aerosol-radiation interaction), and indirectly by serving as cloud condensation nuclei (CCN) or ice nucleating particles (INPs) (i.e. aerosol-cloud interaction, which affects precipitation and rain patterns) (IPCC, 2013; Myhre et al., 2013).

The most important aerosol properties influencing the radiative forcing are the particle size distribution and chemical composition (Penner et al., 2001). The particle size distribution is critical as sub-micron aerosols ( $d_p < 1\mu\text{m}$ ) scatter more light per unit mass and have longer atmospheric lifetimes. The chemical composition and relative contribution of different species are also significant because are linked to the absorbing or scattering properties; a completely scattering aerosol (e.g. sulphate) will has a cooling effect, whereas an absorbing aerosol (e.g. black carbon) will has a warming effect. The IPCC (2013) considers the 'best estimates' of globally average radiative forcing due to aerosol-radiation and aerosol-clouds interactions of about  $-0.9 \text{ W}\cdot\text{m}^{-2}$ , being the aerosol-radiation contribution of  $-0.35 \text{ W}\cdot\text{m}^{-2}$  as a result of the net contributions of dust (-0.1), organics (-0.12), black carbon (+0.4), sulphate (-0.4) and nitrate (-0.11) (Myhre et al., 2013). This estimation of forcing is subject to uncertainties due to the spacio-temporal variability of aerosols (linked to their variety of sources and short lifetime) and uncertainties on the changes in aerosol properties during aging processes. Aerosols contribute with the largest uncertainty to estimates and interpretations of the radiative forcing of the Earth's atmosphere, according to the IPCC (2013).

Satellite observations and three-dimensional models are frequently used to study aerosol from a global point of view. Figure 2 shows the global distribution of major aerosol components provided by the Coupled Model Intercomparison Project Phase 5 (CMIP5), experiment coordinated by the World Climate Research Programme's (WCRP) Working Group on Coupled Modelling (WGCM) (<http://cmip-pcmdi.llnl.gov/cmip5/index.html?submenuheader=0>) (Taylor et al., 2012).

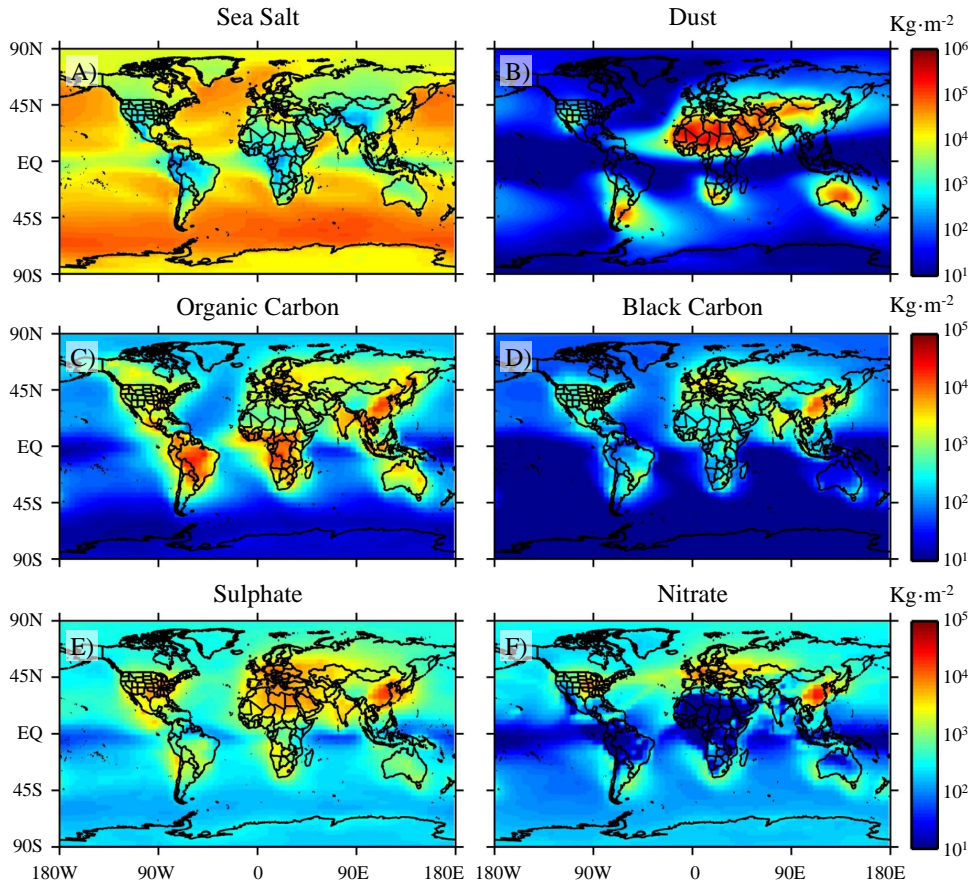


**Figure 2:** Annual mean aerosol loads of (A) sea salt, (B) mineral dust, (C) organic carbon, (D) black carbon, (E) sulphate and (F) nitrate. Simulations from Phase 5 of the Coupled Model Intercomparison Project (CMIP5) for 2000; source data: <https://data.giss.nasa.gov/modelforce/trop.aer/>.

- a) The highest sea salt loads occur at mid-latitudes, being specially high in the Southern Hemisphere due to the highest wind speed; it is also high in the subtropics linked to the trade winds (Fig. 2A). This is the consequence of sea-spray formation increasing with wind speed (Fairall et al., 1983) as sea salt is produced when wind and waves force air bubbles to burst at the sea surface during the whitecap formation (Blanchard, 1983; Monahan et al., 1986). Sea salt is the major contributor to the global aerosol budget, with an estimated annual emission of  $30\cdot 10^{22}$ – $80\cdot 10^{22}$   $\text{Tg}\cdot\text{y}^{-1}$  (Jaenicke, 2005; Tsigaridis et al., 2006).
- b) Dust also contributes significantly to the total aerosol budget, with global emissions estimated to be about  $8\cdot 10^{22}$ – $30\cdot 10^{22}$   $\text{Tg}\cdot\text{y}^{-1}$  (Choobari et al., 2014). The largest and most active dust sources are located in the Northern Hemisphere in a broad region so-called ‘dust belt’ (Prospero et al., 2002) that extends from the west coast of North Africa (e.g. Sahara desert), over the Middle East (e.g. Arabian desert, Syrian Desert), Central and

## 1.1. PROPERTIES, IMPACTS AND SOURCES

---

South Asia (e.g. Thar desert), to China (e.g. Gobi and Taklamakan) (Fig. 2B). This dust belt is mostly located along the subtropical anticyclonic regions, consequence of the descending dry air of the downward branch of the Hadley cell circulation after having lost most of its water vapour in the upward branch over the Intertropical Convergence Zone (ITCZ). In a global scale, dust mobilization is dominated by natural sources, although anthropogenic dust related to cropland, pastureland, and urbanized regions also contributes to the total dust load (Huang et al., 2015).

- c) The highest loads of organic matter are located in the tropical forests of South America, South Africa and Southeast Asian (Fig. 2C), where biogenic emissions and biomass burning are frequent. Figure 2C also shows high loads of organic aerosols over highly industrialized regions such as Europe and Eastern Asia – among others – where fossil fuel combustion is important (Chung et al., 2002). The contribution of primary and secondary organic aerosol (POA and SOA respectively) to the total organic matter is highly variable (Kanakidou et al., 2005). Globally, major POA emissions ( $34\text{--}144\text{ Tg}\cdot\text{y}^{-1}$ ; Tsigaridis et al., 2014) are associated with vegetation fires (Bond et al., 2004; Kanakidou et al., 2005), whereas about 90 % of SOA ( $13\text{--}121\text{ Tg}\cdot\text{y}^{-1}$ ; Tsigaridis et al., 2014) are linked to biogenic volatile organic carbon (BVOC) emissions and subsequent (homogeneous or heterogeneous) nucleation. SOA is formed from the oxidation of VOCs emissions, whose major component is isoprene ( $\sim 50\%$ ; Guenther et al., 2012). Although most sources of VOCs are mainly derived from terrestrial ecosystems, human activities (e.g. fossil fuel combustion and biomass burning) also contribute; the amount of SOA linked to anthropogenic activities is considered low, estimated within the range  $2\text{--}12\text{ Tg}\cdot\text{y}^{-1}$  (Henze et al., 2008). Other important sources of POA are fossil fuel combustion, biogenic aerosols (e.g. viruses, bacteria, fungal spores and plant debris), phytoplankton blooms and soils.
- d) High loads of black carbon (BC) occur over regions affected by urban and industrial fossil fuel combustion and biomass burning such as Europe, Eastern Asia and other populated areas of America and Africa (Fig. 2D). BC results from the incomplete combustion of biomass and fossil fuels; it is a metric for quantifying the black (light absorbing) soot particles. Studies performed at different European background sites (Zanatta et al., 2016) have found that BC light absorption is enhanced (through the so-called ‘lensing effect’) as a consequence of its internal mixing with other components. Global emissions are estimated to be in the range  $5.6\text{--}14.4\text{ Tg}\cdot\text{y}^{-1}$  (Wang et al., 2014), with main fluxes linked to (i) fossil ( $\sim 3\text{ Tg}\cdot\text{y}^{-1}$ ; Bond et al. 2004) and bio ( $\sim 1.6\text{ Tg}\cdot\text{y}^{-1}$ ; Bond et al. 2004) fuels combustion, with maximums in highly populated areas of Europe, North America, Asia, Southern Africa and South America, and (ii) vegetation fires ( $\sim 3.3\text{ Tg}\cdot\text{y}^{-1}$ ; Bond et al. 2004) with maximum in the tropical forest (Fig. 2D).
- e) Sulphate ( $\text{SO}_4^-$ ) is present in high loads in regions of North America, Europe and Eastern Asia where fossil fuel combustion is important (Fig. 2E). Most of sulphate in the atmosphere is formed by the oxidation of its gaseous precursor sulphur dioxide ( $\text{SO}_2$ ) – both human-generated and naturally-occurring – followed by new particle formation.  $\text{SO}_2$  has dramatically increased from  $10\text{ Tg}\cdot\text{y}^{-1}$  in pre-industrial times (1880) to  $70\text{--}75\text{ Tg}\cdot\text{y}^{-1}$  in 2000 (Dentener et al., 2006; Ganzeveld et al., 2006) due to anthropogenic activity (Smith et al., 2011), although in the last decades there has been a clear decreasing trend in North America and Europe, with an increasing role of Asia (Klimont et al., 2013; Maas et al., 2016). Natural sources also contribute to the sulphur atmospheric budget, mainly due

to volcanic emissions (which accounts  $\sim 30\%$  of total  $\text{SO}_2$ ; Fioletov et al., 2016) and to oxidation of oceanic dimethyl-sulphide – formed by marine biota – (which release  $\sim 23.4 \text{ TgS}\cdot\text{y}^{-1}$ ; Mahajan et al., 2015).

- f) Ammonium-nitrate ( $\text{NH}_4\text{NO}_3$ ) exhibits high loads in Eastern North America, Europe and Eastern Asia (Fig. 2F), associated with emissions of their precursors: nitrogen oxides ( $\text{NO}_x$ , generated mostly in urban and industrial areas) and ammonia ( $\text{NH}_3$ , from several sources including agriculture and decomposition of organic wastes). Global  $\text{NO}_x$  emissions are estimated in  $10\text{--}20 \text{ Tg}\cdot\text{y}^{-1}$  (Bauer et al., 2007), mostly of an anthropogenic origin (IPCC, 2013). Nitrate ( $\text{NO}_3^-$ ) can be present not only as (i) ammonium-nitrate, usually at temperatures lower than  $15^\circ\text{C}$  and relative humidity conditions below the deliquescence point (Stelson and Seinfeld, 1982; Seinfeld and Pandis, 2006), but also as (ii) calcium-nitrate ( $\text{Ca}(\text{NO}_3)_2$ ) and magnesium-nitrate ( $\text{Mg}(\text{NO}_3)_2$ ), due to reaction of nitric acid ( $\text{HNO}_3$ ) with dust minerals (Laskin et al., 2005; Gibson et al., 2006), and (iii) sodium nitrate ( $\text{NaNO}_3$ ), due to reaction of nitric acid with sea salt (ten Brink, 1998; Liu et al., 2007). The formation of these species will depend on temperature, humidity and the availability of dust, sea salt, ammonia and sulphate. If there is an excess of ammonium, the existing sulphate is totally neutralized resulting in ammonium-sulphate ( $(\text{NH}_4)_2\text{SO}_4$ ) and ammonium-bisulphate ( $\text{NH}_4\text{HSO}_4$ ); the remaining ammonium is available to react with nitric acid to form submicron ( $< 1\mu\text{m}$ ) ammonium-nitrate. If there is a lack of ammonium, the existing sulphate cannot be totally neutralized and the aerosol phase will be acidic. Under this acidic conditions, mineral dust and sea salt particles also play a key role in nitrate formation, serving as reactive surfaces for heterogeneous reactions of the gaseous species (i.e. nitric acid) (Dentener et al., 1996; Zhuang et al., 1999); compounds such as calcium-nitrate and magnesium-nitrate can be formed, shifting nitrate from the fine to the coarse mode. It is estimated that more than a  $40\%$  of the global total nitrate concentration is associated with mineral dust (Usher et al., 2003). Therefore, the highest fine aerosol nitrate concentration corresponds to urban and industrialized areas and the coarse aerosol nitrate is highest close to deserts (Karydis et al., 2016).

A better understanding on the spatial and temporal distribution of the aerosol components and on aerosol properties is needed to reduce the uncertainties on the relationship of aerosols and climate variability processes, such as the radiative forcing highlighted by the IPCC (2013) and cited above. The important technological development experienced by satellite remote sensing and modelling during the last two decades have improved our understanding on global distribution of aerosols; however, there are still important limitations that need to be complemented with aerosol observations based on in-situ techniques.

Satellite remote sensing has gradually been developed to monitor atmospheric aerosols, providing routine measurements on a global scale (Lee et al., 2009). These sensors (e.g. CALIOP, MODIS, AVHRR or TOMS/OMI) are able to detect aerosols present in high amounts (e.g. dust or smokes linked to biomass burning, Chin et al., 2002; Jeong and Li, 2005), but have difficulties to provide other aerosol species present in lower concentrations (e.g. nitrate or sulphate; Kaufman et al., 2005; Clarisse et al., 2013). Most of the sensors provide vertically integrated aerosol measurements (e.g. Aerosol Optical Depth by MODIS) and only some of them can perform vertically resolved measurements (e.g. CALIOP). Moreover, remote sensing is not still able to quantify the amount of each aerosol specie (e.g. sulphate, dust, organic matter, etc.) to provide a mass closure (Clarisse et al., 2013).

Global models (e.g. GEOS-Chem, Megan, GOCART) simulate spatial and temporal distribution of aerosols and some aerosol properties on a global scale, including their effects on clouds, atmospheric chemistry, radiation, and other climate related processes. Models need to be validated with measurements (e.g. Textor et al., 2006; Jaeglé et al., 2011; Huneus et al., 2011), whose availability is very heterogeneous, being more abundant on continental regions of Europe and North America than on oceanic regions (e.g. Lee et al., 2009; Huneus et al., 2011).

Ground-based in-situ techniques have some limitations for providing information on spatial variability on aerosols; in contrast, they allow performing rather high precision measurements of chemical composition, size distribution and other aerosol properties for complementing the satellite remote sensing observations. These in-situ aerosol measurements are especially relevant in remote oceanic regions, where they are rather scarce, where the prevailing low aerosol loads do not always allow using satellite observations and where these measurements allow model and satellite validation.

Of high importance is the case of the oceanic stations providing observations in the free troposphere. Once particles are lifted and transported to this layer, their atmospheric lifetime increases considerably as there are fewer removal processes and the wind speed is higher than in the planetary boundary layer (Freney et al., 2016). The higher lifetime results in aerosol aging, i.e. change in the composition, size, and mixing state through condensation, cloud processing or coagulation. At the same time, the higher wind speed provides aerosols with the ability to be transported over long distances by prevailing winds. This aged and processed long-range transported aerosol is spatially representative of the remote background and exerts higher influences on climate (Winker et al., 2013) from regional to global scales. Aerosol characterization in remote-free troposphere stations is of vital importance to understand the background aerosol features (i.e. physicochemical properties and transport mechanisms) that are driving and influencing the particle concentration in regional and global scales. Remote observatories reaching the free troposphere are considered as ‘supersites’ for atmospheric aerosol research and are limited as they cannot be influenced by local pollution.

## 1.2 The North Atlantic Ocean

Aerosols over the North Atlantic have received attention since long time ago. Within the first aerosol studies in this region, we find those made by C. Darwin in the mid-1840s, who studied dust deposits on board vessels (Darwin, 1846). More detailed analysis was performed by Christian E. Junge, who studied aerosols at Miami in the mid-1950s (Junge, 1956) and at Izaña Observatory in Tenerife (off the North African coast) in the mid-1960s (Abel et al., 1969). These observations suggested that North African dust could experience transatlantic transport to the Caribbean, which was subsequently confirmed by A. C. Delany in the mid-1960s with observations performed at Barbados Island in the Caribbean (Delany et al., 1967). This scenario led to a scientific research program on aerosols, mainly focused on understudying the transatlantic transport of North African dust, its connection to climate variability and its impacts. Pioneering long-term research programs were led by J. M. Prospero, who started aerosol records in several sites of the North Atlantic, including Barbados (since 1965 to present, Prospero and Mayol-Bracero, 2013), Miami (since 1974 to present, Prospero and Mayol-Bracero, 2013) and Izaña (1970s, 1987-1999, and subsequently reactivated in 2002 by the Meteorological State Agency and the Scientific Research Council of

Spain, Rodríguez et al., 2012). In the mid-1980s the Atmosphere-Ocean Chemistry Experiment (AEROCE, 1987–1991) focused on studying the export of sulphuric and nitrogen aerosols from North America, North African dust and ozone background, by measurements at Barbados, Bermuda, Mace Head and Izaña-Tenerife (Levy, 1988). In the mid-1990s, the Aerosol Characterization Experiment (ACE-2, 1996–1998; Raes et al., 2000) studied the radiative effects and controlling processes of anthropogenic aerosols from Europe and desert dust from Africa, as they were transported over the North Atlantic Ocean. Subsequently, a number of scientific projects and programs on the North Atlantic aerosols have developed at Izaña-Tenerife (e.g. IZA2, 2001–2003, Alastuey et al., 2005; POLLINDUST, 2012–2014, Rodríguez et al., 2011; AEROATLAN, 2016–2018), Cape Verde (e.g. CV-Dust, 2010–2013, Almeida-Silva et al., 2013), Pico Nare-Azores (e.g. AGS-1110059, 2011–2016, Dzepina et al., 2015), Barbados (e.g. AGS-0962256, 2010–2015, Prospero et al., 2014), Miami (e.g. OCE-0623189, 2007–2010, Prospero et al., 2010) and Puerto Rico (e.g. PRIDE, 2000, Reid et al., 2003). These studies have evidenced that the North Atlantic receives a diversity of aerosols by several routes from America, Africa and Europe.

In this study, aerosol records at the Izaña supersite Observatory (2367 m a.s.l.), in Tenerife Island, have been used to address a set of specific topics on the aerosols in the North Atlantic free troposphere.

### **Organic aerosols in the Saharan Air Layer**

Desert dust from North Africa is the most studied aerosol type over the North Atlantic. Dust particles are transported in the so-called Saharan Air Layer (SAL), the warm, dry and dusty airstream that expands from North Africa to the Americas at tropical and subtropical latitudes (Fig. 3) (Prospero and Carlson, 1972). The Sahara-Sahel region is the largest and most active dust source in the world (800–3000 Tg·y<sup>-1</sup>; Ginoux et al., 2004, 2012; Huneus et al., 2011), accounting for 60–70 % of the global desert dust emissions; reason which has motivated a number of studies on the meteorology and aerosol composition, linked to the SAL, connected to dust impacts.

Dust export experiences a marked seasonality (Fig. 3) linked to the shift of trade winds and the ITCZ (Engelstaedter and Washington, 2007). In winter, dust is exported westward at low tropical latitudes (<15°N, 0–3 km a.s.l.), whereas in summer, dust exportation takes place at higher subtropical latitudes (15–30°N, 1–5 km a.s.l.) (Tsamalis et al., 2013). The ITCZ acts as an efficient aerosol removal mechanism (Andronache et al., 2002; Prospero et al., 2014), controlling the southerly edge of the SAL and not allowing dust transport to the Southern Atlantic (Huang et al., 2009, 2010; Adams et al., 2012). Dust export also experiences an important year-to-year variability. In winter, most of dust mobilization occurs in Southern Sahara and in the Sahel, being the interannual variability influenced by the North Atlantic Oscillation (NAO, Chiapello et al., 2005). There have been many uncertainties about the processes affecting summer-to-summer variability in dust export; a recent study based on 28-years dust records at Izaña (in which the PhD candidate has participated) has shown that summer-to-summer variability in dust export is modulated by the North African Dipole Intensity (NAFDI), i.e. the intensity of the subtropical Saharan high to the tropical monsoon low, measured as the difference of the 850 hPa geopotential heights anomaly between the subtropics (30–32°N) and the tropics (10–13°N) (Rodríguez et al., 2015). Summer-to-summer variability in NAFDI is associated with north-south shifts in the SAL and in the tropical rain

## 1.2. THE NORTH ATLANTIC OCEAN

bands and is correlated with the intensity of Harmattan winds in inner Sahara, where most of dust emissions occurs.

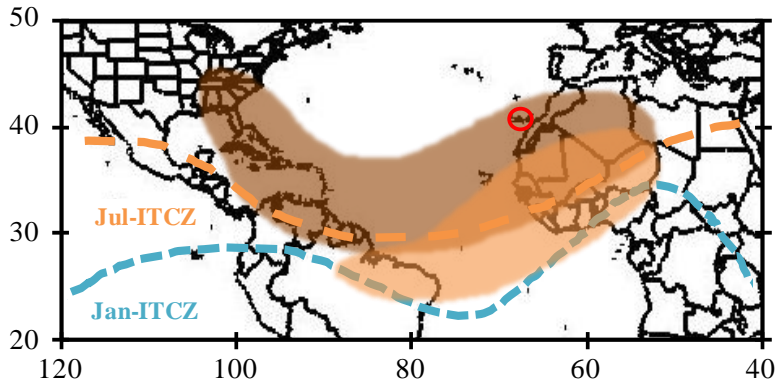


**Figure 3:** Expanse of the Saharan Air Layer (SAL) in winter (orange shade) and in summer (brown shade). Discontinuous lines mark the Intertropical Convergence Zone (ITCZ) band in January (Jan) and July (Jul). The location of Izaña-Tenerife is highlighted (red circle). Figure adapted from Garrison et al., 2014 and Rodríguez et al 2015.

Composition of the SAL has also been widely studied. In this layer, the aerosol population is by far dominated by dust, which is mixed with some amounts of particulate pollutants (Putaud et al., 2000; Savoie et al., 2002; Formenti et al., 2003; Rodríguez et al., 2011; Fomba et al., 2014; Salvador et al., 2016), trace metals (Arimoto et al., 1995; Alastuey et al., 2005), organic aerosols (Capes et al., 2008; Fomba et al., 2014; Garrison et al., 2014; Gonçalves et al., 2014) and bioaerosols (e.g. pollens, virus, bacteria and fungi) (Griffin et al., 2003; Izquierdo et al., 2011).

The presence of particulate pollutants mixed with dust was described by Prospero et al. (1995), who in the mid-1990s pointed that these pollutants could be original from Europe. More recently, the Izaña in-situ aerosols group found that the amount of sulphate, ammonium and nitrate mixed with dust in the SAL was high when air masses had previously flown over industrialized regions of Morocco, Algeria and Tunisia, where oil refineries, fertilizer industries and power plants are placed (Rodríguez et al., 2011). The mixing of acids with dust may change its original physicochemical properties, having implications on how dust minerals influence on climate-related processes. For instance, the particle size can be altered due to changes in the hygroscopicity of the dust particles as a consequence of the condensation of inorganic acids; the reaction dust–nitric acid results in the neutralization product calcium-nitrate, which takes up ambient water vapour changing the dust particle radius (Laskin et al., 2005; Gibson et al., 2006; Karydis et al., 2016). This alteration of particle size affects the light scattering efficiency, the cloud condensation nuclei activation (Li and Shao, 2009; Lance et al., 2013; Abdelkader et al., 2017) and increase the wet and dry removal of the dust particles (Abdelkader et al., 2017). Similarly, two studies based on data collected at Izaña Observatory (in which this PhD candidate has participated during the development of this thesis) found that the fractional iron solubility (% of soluble iron) and the number of ice nuclei (at  $-40^{\circ}\text{C}$ ) to dust ratio were correlated with the ammonium-sulphate to dust ratio (Ravelo et al. 2016; Boose et al. 2016). These findings suggest that the mixing of ammonium-sulphate with dust

influences on the solubility of some minerals, with implications on the amount of soluble iron released on the ocean (Ravelo et al., 2016) and on the ability of some minerals to act as ice nuclei (Boose et al., 2016).

The existence of carbonaceous aerosols has also implications. In a recent study, Grigas et al. (2017) has evidenced the important contribution of anthropogenic organics to particulate matter (PM) in the North-eastern Atlantic (Mace Head Station, Ireland); under polluted conditions, organic matter contribute  $\sim 50\%$  to the PM mass of the fine particles ( $dp < 1\ \mu\text{m}$ ), reaching up to  $90\%$  in extremely polluted conditions. There are also evidences of the transport of anthropogenic bio-accumulative and toxic organic compounds (i.e. organochlorine and organophosphate pesticides, polycyclic aromatic hydrocarbons and polychlorinated biphenyl) from Western Sahara to the Caribbean (Risebrough et al., 1968; Prospero and Seba, 1972; Garrison et al., 2014); their connection with human-related activities (e.g. to control agriculture pests and disease vectors) has been suggested (Garrison et al., 2014). In winter, dust particles exported in the SAL are frequently mixed with organic and black carbon linked to biomass burning in the Sahel during the dry season (Formenti et al., 2003; Hand et al., 2010; Kandler et al., 2011; Salvador et al., 2016), having implication on the SAL radiative properties (Hand et al., 2010; Heinold et al., 2011). In summer, organic aerosols have also been observed mixed with dust in the subtropical SAL (Van Drooge et al., 2001, 2010; Alastuey et al., 2005). In this season, dust emissions occur in inner subtropical Sahara, where the human-derived activities (i.e. industry, biomass burning, etc.) are extremely low. It is believed that organic aerosols play a role as ice nuclei at warm temperatures ( $-8^\circ\text{C}$ ), as pointed a recent study in the SAL at Izaña Observatory among other sites (Conen et al., 2015). Organic aerosols in the SAL may also affect dust optical properties and health effects as a result of the adsorption of aromatic and nitrated polycyclic aromatic hydrocarbons (Jacobson, 1999; Garrido et al., 2014). This aerosol type is constituted by tens of thousands organic species (Goldstein and Galbally, 2007) and there are large gaps in the knowledge of the composition and potential sources of the organic aerosol within the SAL. The summer SAL has a large-scale impact on the North Atlantic, so some key questions arise:

- *Which is the composition of the organic aerosols?*
- *What are the sources of the organic aerosols?*
- *Are the organic aerosols only linked to primary emissions?*
- *Are there contributions to the organic aerosols in linked to long-range transport?*

### **Aerosols in the westerlies**

The westerlies (WES) are the prevailing airstreams that flows from North America eastward across the North Atlantic at subtropical and mid-latitudes ( $30^\circ\text{N}$ – $60^\circ\text{N}$ ). Studies about the impact of North America emissions on other regions have mostly focused on relatively long lifetime (LT) reactive gases such as CO (LT $\sim 60$  days) and O<sub>3</sub> (LT $\sim 25$  days), which are exported to the North Atlantic free troposphere, enhanced by the mid-latitude cyclones (Fig. 4A–B) (Dickerson et al., 1995; Merrill and Moody, 1996; Moody et al., 1996) and convective processes (Fig. 4C) (Dickerson et al., 1987; Talbot et al., 1998).

Mid-latitude cyclones (i) frequently form at lee side of the Rocky Mountains and propagate eastward, with associated cold fronts southeastward across the eastern United States (U.S.;

Zishka and Smith, 1980; Whittaker and Horn, 1984); (ii) occur every 5 days – as average – in summer (Li et al., 2005), although in spring the frequency may even be higher, and (iii) have four airstreams associated (Fig. 4A–B): the warm conveyor belt ahead of the cold front, the cold conveyor belt, the dry airstream subsiding behind the cold front, and the post cold front boundary layer airstream (Cooper et al., 2002 a, b). The northeastward ascending airstream, represented by the warm conveyor belt, prompts the upward transport of pollutants from North America to the free troposphere over the North Atlantic (Eckhardt et al., 2004).

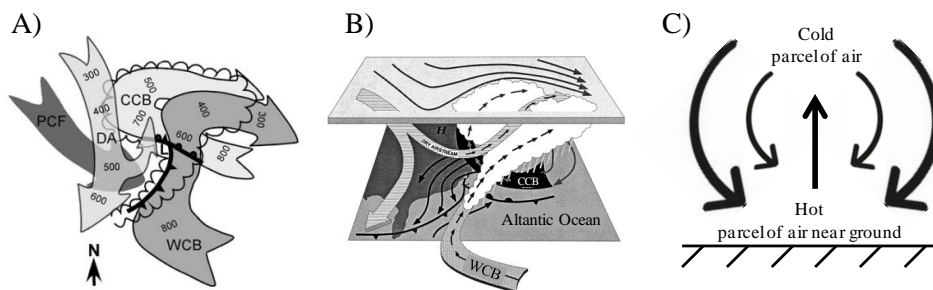


**Figure 4:** Airstreams associated with the mid-latitude cyclones: (A) top view and (B) three-dimensional scheme. Figure adapted from Cooper et al., 2002 a. **WCB:** warm conveyor belt. **CCB:** cold conveyor belt. **DA:** dry airstream. **PCF:** post cold front. (C) Convection mechanism.

Convection (Fig. 4C) is also an important mechanism for ventilating the boundary layer; the convective outflow prompts the upward transport of pollutants (Dickerson et al., 1987; Talbot et al., 1998), which may remain for several days over the North America prompting ozone production and its subsequent export to the North Atlantic (Li et al., 2005). This mechanism is important in Southeastern U.S. in summer, as the warm conveyor belt of the mid-latitude cyclones is shifted northward (Li et al., 2005).

Once in the free troposphere, CO and O<sub>3</sub> enter in the westerly circulation at the north of the Azores high (Li et al., 2005), with the subsequent transatlantic transport. There are a number of observation-based evidences on the large-scale impact of the CO and O<sub>3</sub> pollution events in the North Atlantic linked to North American fires and pollution export (Moody et al., 1996; Parrish et al., 1998; Honrath et al., 2004; Owen et al., 2006).

Although aerosols have been less studied, some researches have found evidences of their export to the Atlantic in the cyclones modulated North American outflow (Li et al., 2005), even if they have a relatively short lifetime (LT~ 15 days). By ground-based and airborne Laser Imaging Detection and Ranging (LIDAR) measurements, Ancellet et al. (2016) detected the transatlantic transport of North American biomass burning aerosols and dust to the Mediterranean. At Pico Observatory (Azores Islands) free troposphere transport of North American BC aerosols linked to boreal fires (Val Martin et al., 2006) and sulphate, nitrate, elemental carbon and organic aerosols has been detected (Dzepina et al., 2015). The impact of biomass aerosols has been documented: these particles effectively scatter and absorb solar radiation and are good cloud condensation nuclei (Reid et al., 2005 and references therein). The few available studies on the export of aerosols from North American have been based on rather short-term measurement campaigns (weeks to a few months). There is a clear need to get a comprehensive view on the North American aerosols over the North Atlantic, which

requires long term measurements to answer some key questions:

- *What is the composition of the aerosol population?*
- *What are the sources of the aerosol population?*
- *Is there any seasonal evolution of the composition of the aerosol population?*
- *Does the aerosol population experience transatlantic transport?*

## **New particle formation**

New Particle Formation (NPF) is a two-step process, not fully understood, that comprises: nucleation and growth up to stable sizes (Fig. 5A). Several theories have been proposed to explain the Nucleation step: (i) binary (water–sulphuric acid) nucleation (Nilsson and Kulmala, 1998; Vehkamäki et al., 2002), (ii) ternary (water–sulphuric acid–ammonia) nucleation (Coffman and Hegg, 1995; Korhonen et al., 1999; Kulmala et al., 2002; Napari et al., 2002), (iii) ion-induced nucleation (Laakso et al., 2002), (iv) low-pressure organic vapours nucleation (Marti et al., 1997; Zhang et al., 2004), and (v) halogen oxide nucleation (Hoffmann et al., 2001); but still fail to explain some of the field observations. Semi-empirical new mechanisms such as cluster activation and kinetic nucleation have been developed to explain the observed measurements (Laakso et al., 2004; Kulmala et al., 2006; Metzger et al., 2010). The growth step occurs under certain scenarios, when clusters are activated to result in stable aerosols with a size  $\geq 50$  nm (i.e. during the so-called ‘banana-type’ events; Fig. 5B). Proposed mechanisms for growth include: (i) condensation of sulphuric acid–sulphate and low-volatility organic vapours, including biogenic volatile compounds such as isoprene and monoterpenes (Laaksonen et al., 2008; Kulmala et al., 2013; Patoulias et al., 2015) and (ii) acid–organics heterogeneous reactions (Zhang and Wexler, 2002). Understanding how nucleated clusters grow is important to study the influence of aerosols on climate, as it depends on particle size. Particles able to grow beyond 50 nm may act as Cloud Condensation Nuclei (CCN), and may consequently increase the indirect aerosol-cloud interaction (McMurry et al., 2011). In fact, NPF is the source of over half of the atmosphere’s CCN (Merikanto et al., 2009).

NPF has been studied in different locations: from polluted urban areas (e.g. Dunn et al., 2004), rural environments (e.g. Rodríguez et al., 2005; Hamed et al., 2007), coastal areas (e.g. Lee et al., 2008), forests (e.g. Dal Maso et al., 2005), to remote high-mountains (e.g. Venzac et al., 2008) and recently, even in the free troposphere (e.g. Rose et al., 2015; Bianchi et al., 2016). Typical values for formation and growth rates of new particles are within the range  $\sim 0.01\text{--}3\text{ cm}^{-3}\cdot\text{s}^{-1}$  and  $\sim 0.4\text{--}10\text{ nm}\cdot\text{h}^{-1}$  in remote and  $\sim 1\text{--}70\text{ cm}^{-3}\cdot\text{s}^{-1}$  and  $\sim 2\text{--}40\text{ nm}\cdot\text{h}^{-1}$  in polluted environments, respectively (Kulmala et al., 2004 and references there in; Yli-Juuti et al., 2011 and references there in; Järvinen et al., 2013).

In the continental boundary layer at mid-latitudes, NPF is frequently observed under the clean air conditions that occur after cold front passages and/or rainfalls, normally associated with low relative humidity and high solar radiation (Rodríguez et al., 2005; Wu et al., 2007). However, in high-mountains reaching the free troposphere, NPF has been observed in different contexts. For instance, Weber et al. (1995, 1999) found that NPF in the remote Pacific Ocean (Mauna Loa, 3400 m a.s.l.), was led by sulphuric acid, whereas Boulon et al. (2011) did not find any correlation between sulphuric acid and NPF events in continental Europe (Puy de Dome, 1465 m a.s.l.). Although it is accepted that pre-existing particles behave as

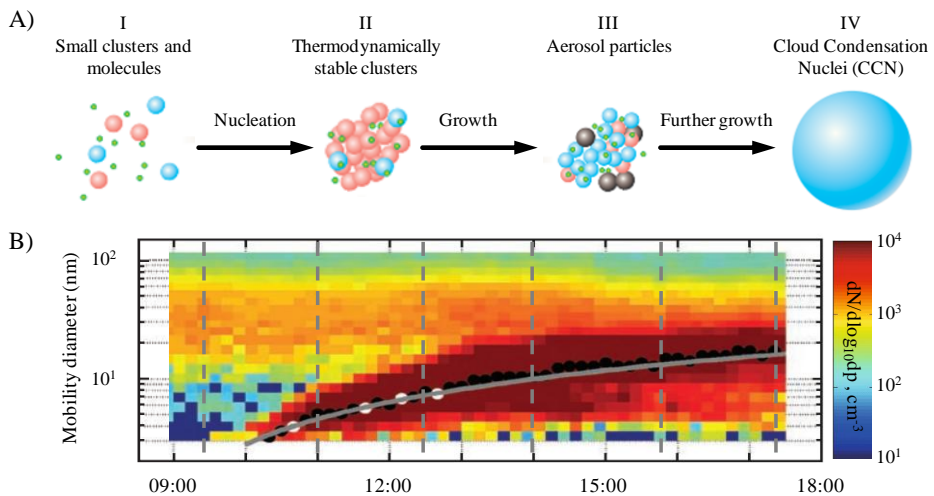


**Figure 5:** (A) New particle formation steps. Figure adapted from Kulmala et al. (2003). (B) New Particle Formation or ‘banana type’ event where the above named steps are pointed. Black dots indicate the growth of the particle geometric mean diameter. The gray line is the linear least-squares fit to these points. Figure adapted from Kulmala et al. (2012).

a condensation sink for the vapour phase and, consequently, for freshly new particles – as observed in Norikura mount in Asia, 2770 m a.s.l. (Nishita et al., 2008) –, NPF has been observed under high concentrations of pre-existing particles in Europe (Jungfraujoch, 3580 m a.s.l, Boulon et al., 2010) and Antarctica (Dome C, 3200 m a.s.l., Järvinen et al., 2013); measurements performed by Nie et al. (2014) in South China (Mount Heng, 1290 m a.s.l.), even evidenced how NPF and growth were enhanced by heavy dust plumes mixed with anthropogenic pollution as a result of dust-induced heterogeneous photochemical processes. UV radiation also plays a key role for oxidizing  $\text{SO}_2$  to form sulphuric acid and prompt NPF (e.g. Boulon et al., 2010; Hallar et al., 2011). Bianchi et al. (2016) found that – in addition to sulphuric acid-ammonia nucleation – NPF in the free troposphere mainly occurs by condensation of highly oxygenated organic molecules; they observed that neutral nucleation is more than 10 times faster than ion-induced nucleation and that NPF occurs from 1 to 2 days after contact of the air masses with the planetary boundary layer, the time needed for oxidation of organic compounds. Long-term records ( $\geq 1$  y) of aerosol size distribution and of other parameters involved in NPF (e.g. sulphur dioxide and UV radiation) at high-mountain sites that reach the free troposphere are scarce, and are needed to understand the context in which NPF take place. According to the long term record at Izaña Observatory:

- *In what context does new particle formation occur?*
- *Is there an interannual variability in NPF?*
- *Is NPF influenced by the Saharan Air Layer?*



## CHAPTER

# 2

## Objectives

Taking into consideration the previous studies performed in the North Atlantic Ocean and in view of the current shortcomings in the knowledge of (i) the sources of the organic aerosols, (ii) the origin of the aerosols in the westerlies and (iii) the new particle formation at Izaña, the present study aims to fill these research gaps related to the origin of the atmospheric aerosol in the North Atlantic free troposphere. The specific objectives are:

1. To assess the relevance of new particle formation processes.  
More specifically:
  - (a) Identifying the context in which NPF occurs.
  - (b) Identifying factors affecting interannual variability.
2. To study the origin of the aerosols in the North Atlantic free troposphere westerlies.  
More specifically:
  - (a) Identifying the source regions of each aerosol component.
  - (b) Identifying the meteorological processes that modulate the aerosols transatlantic transport
3. To study the origin of organic aerosols in the Saharan Air Layer.

Obtained results will allow (i) progressing in the knowledge of the chemical characteristics of background aerosol and of the context involved in the formation of new particles, which will help in a better estimation of aerosols effects on climate, (ii) identifying potential source regions of background atmospheric particles, which will help in further development of climate change policies, and (iii) understanding how large-scale meteorological processes influence long-range transport from regional to global scales, which will improve our understanding of trans-boundary pollution transport processes.

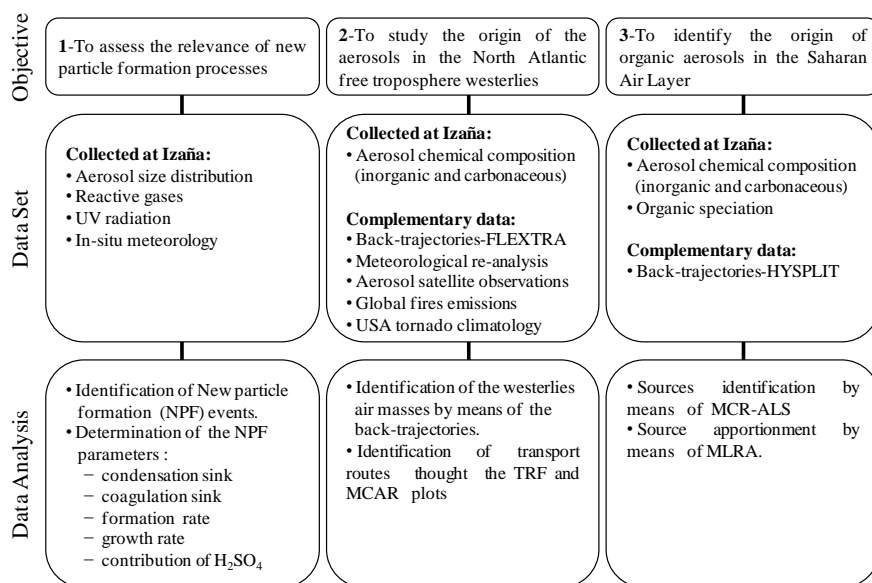
This thesis presents a high multidisciplinary involving a combination of atmospheric chemistry, meteorology and computational methods. The research topic is highly important within the context of aerosols-climate interactions and trans-boundary pollution and it is motivated by the potential impact of atmospheric aerosols on climate.

CHAPTER

# 3

## Methodology

The present thesis is mostly based on aerosol data collected at the Izaña Observatory. This data set was complemented with other atmospheric measurements at Izaña, meteorological products and additional observations. A brief description of the methodology used for each objective is shown:



The methods used to measure the chemical and physical properties of the aerosols are the recommended and reference methods of the Global Atmospheric Watch program, which ensure traceability and comparability of measurements. A detailed description of the measurement site, data set and analysis is given in the following sections.

### 3.1 Sampling and measurement site

Sample collection was performed at the Izaña Global Atmospheric Watch (GAW) Observatory ( $16^{\circ} 29'N$   $58^{\circ}W$ ,  $28^{\circ} 18'N$   $32^{\circ}N$ ; Tenerife, Canary Islands, Spain; Fig. 6A) at 2367 m a. s.l. The Izaña Observatory is located in the subtropical North Atlantic Ocean, above an almost permanent temperature inversion layer (TIL) which separates two well differentiated air masses (Fig. 6B): the moist and cool marine boundary layer (MBL) and the dry free troposphere (FT); these two airflows are differentiated fundamentally by their relative humidity (MBL  $\gg$  FT; Rodríguez et al., 2009). The MBL top (frequently located just below the TIL) is characterized by the formation of a stratocumulus layer as a result of the condensation of water vapour onto the available pre-existing particles.

The wind regime in the FT is dominated by NW dry subsiding airflows (connected to the westerlies circulation) throughout the year except in summer, when they are frequently alternated with SE airflows from North Africa (associated with the Saharan Air Layer). In the moist and cool MBL, the NNE trade winds prevail.

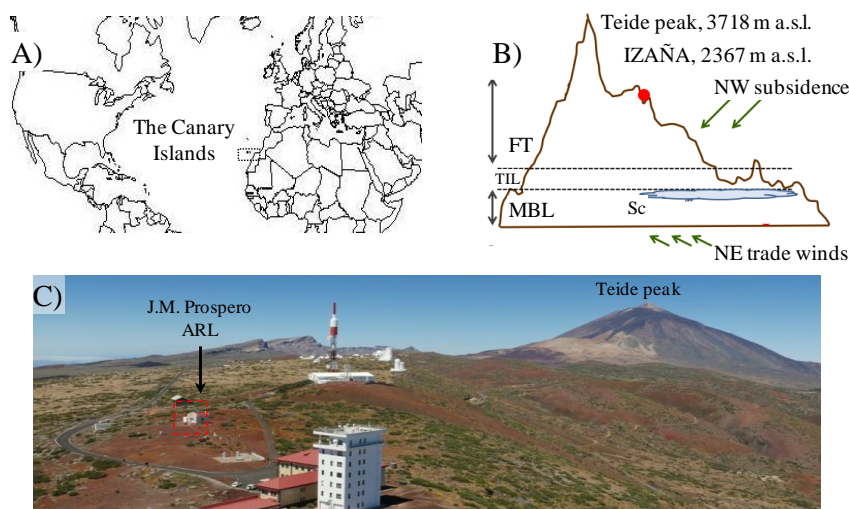


**Figure 6:** (A) Location of the Canary Islands. (B) Vertical cross-section of Tenerife, where the altitude of the Izaña Observatory and the Teide peak are indicated; the stratification of the troposphere at the Island and the wind regimen are also represented. Figure adapted from Rodríguez et al., 2009. (C) View of Izaña GAW Observatory; the main building of the aerosol program (J.M. Prospero Aerosol Research Laboratory) is highlighted.

Izaña is within the pre-national park (Teide National Park) close to the Mount Teide – the highest peak of the Island – (Fig. 6B–6C). The area is environmentally protected by the ‘Sky Law’ and was declared a UNESCO World Heritage Site in 2007. The Observatory is surrounded by a forest of an endemic specie of pine (*Pinus canariensis* Chr, *Sm.ex DC*) limited between  $\sim 500$ – $2300$  m a.s.l.

During daytime, heating of terrain prompts upslope winds that may transport trace amounts of chemical compounds that are emitted by biogenic and anthropogenic sources in the MBL. Although the impact is minimum for the aerosol mass concentration (Rodríguez et al., 2009),

### 3.2. DATA SET

---

it is substantial for the number of ultrafine particles, reactive gases and water vapour concentrations (Rodríguez et al., 2009).

Administratively, the Izaña Atmospheric Research Centre belongs to the State Meteorological Agency of Spain (AEMET) and is a joint research unit of the National Research Council of Spain (CSIC), through the Institute of Environmental Assessment and Water Research (IDAEA). Since 1989, the Izaña Observatory is one of the 31 super-site stations (Fig. 7) which form part of the Global Atmosphere Watch (GAW) programme coordinated by the World Meteorological Organization. The main objective of the GAW aerosol program is ‘to determine the spatio-temporal distribution of aerosol properties related to climate forcing and air quality up to multi-decadal time scales’ (<http://www.wmo.int/pages/prog/arep/gaw/aerosol.html>). The data collected at the GAW monitoring stations are particularly essential to further understanding of the relationship between changing atmospheric composition and changes of global and regional climate.



**Figure 7:** Global Atmospheric Watch (GAW) stations (<http://www.wmo.int/pages/prog/arep/gaw/measurements.html>); Izaña GAW Station is highlighted in red.

## 3.2 Data Set

The aerosol instrumentation is located in a 6 m-high building (Fig. 6C), where the indoor temperature is set to 20°C. Temperature, relative humidity (RH) and pressure are monitored in the aerosol flow (stretch of sampling pipe into the building, just before the aerosol monitors) and in the outdoor ambient air. Outdoor ambient RH is usually low (70<sup>th</sup> percentile is ~ 40 % for hourly annual data). Because of the higher indoor temperature, the RH in the sample is usually much lower, within the range 10–25 % (25<sup>th</sup>–75<sup>th</sup> percentiles for annual hourly data). Thus, dry aerosol measurements are performed without using any system for reducing RH (membrane/nafion driers, or dilutors). The filter treatment is performed at the weighing room, where the indoor temperature is set to 20°C and the relative humidity between 30 and 35 %.

### 3.2.1 Size distribution

Particle size distribution within the range 10–600 nm was measured with a Scanning Mobility Particle Sizer (SMPS, model 3996, TSI). The SMPS spectrometer (Fig. 8A) is formed by an Electrostatic Classifier (EC; Fig. 8B) and a Condensation Particle Counter (CPC). The EC uses a bipolar charger to ionize the particles to a known charge distribution for which the equilibrium is reached (Fuchs, 1963; Wiedensohler, 1988; Reischl et al., 1996). The sample (charged and neutral particles) is then conducted to a Differential Mobility Analyzer (DMA), where particles are classified according to their electrical mobility, which is proportional to the particle diameter. The complete particle size distribution is obtained by applying a ramp of voltages. Particles in the size-classified monodisperse aerosol, coming out the DMA, are counted by a Condensation Particle Counter (CPC). Two different CPCs were used as detectors: a CPC-3025A (diameter cut-off: 3 nm) from June 2008 to March 2009 and a CPC-3010 (diameter cut-off: 10 nm) from March 2009 on. The Aerosol Instrument Manager® Software for SMPS spectrometer collects and stores sample data. Correction for diffusion losses in the sampling pipe and inside the SMPS was applied (Hinds, 1999).

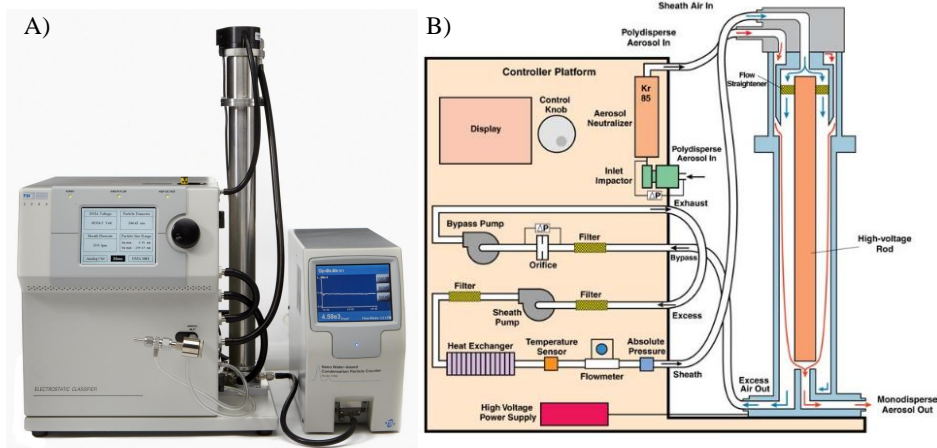


**Figure 8:** (A) Scanning Mobility Particle Sizer (SMPS, model 3996, TSI™). (B) Schematic diagram of the electrostatic classifier (TSI, 2009).

The SMPS has been subjected to several quality assurance and quality control activities:

- (i) The 50 % efficiency diameters ( $D_{p50}$ ) were determined in the World Calibration Centre for Aerosol Physics (WCCAP, Institute for Tropospheric Research, Leipzig, Germany).  $D_{p50} = 2.4$  nm for the CPC-3025A unit (SN: 1160; September 2002) and  $D_{p50} = 9.6$  nm for the CPC-3010 unit (SN: 70431239; September 2011).
- (ii) The SMPS was intercompared, measuring ambient air aerosol, with similar TSI SMPS instruments in April 2010 and November 2012 within the REDMAAS network ([www.redmaas.com](http://www.redmaas.com); Gómez-Moreno et al., 2013). In these exercises the sizing accuracy was also assessed with monodisperse polystyrene latex spheres of 80 and 190 nm; a discrepancy of -1 and -1.2 % was found, respectively.

### 3.2. DATA SET

- (iii) During the regular operations at Izaña, the SMPS is subject to weekly checks of aerosol and sheath airflows, zeroes and leak tests using absolute filters.

Particle size distribution within the range 0.7–20  $\mu\text{m}$  aerodynamic diameter was measured with an Aerodynamic Particle Sizer (APS, model 3321, TSI). The APS (Fig. 9A) classifies the particles according to their time-of-flight (Fig. 9B). An inner nozzle focuses the aerosol flow, which is surrounded by the sheath air flow, to be accelerated through the outer nozzle. Particle with different aerodynamic diameters have different acceleration rates directly behind the nozzle, with larger particles accelerating more slowly due to increased inertia. Two laser beams are positioned directly behind the outer nozzle and the time-of-flight – time difference between the two pulse maxima – is recorded and converted to aerodynamic diameter using a calibration curve.

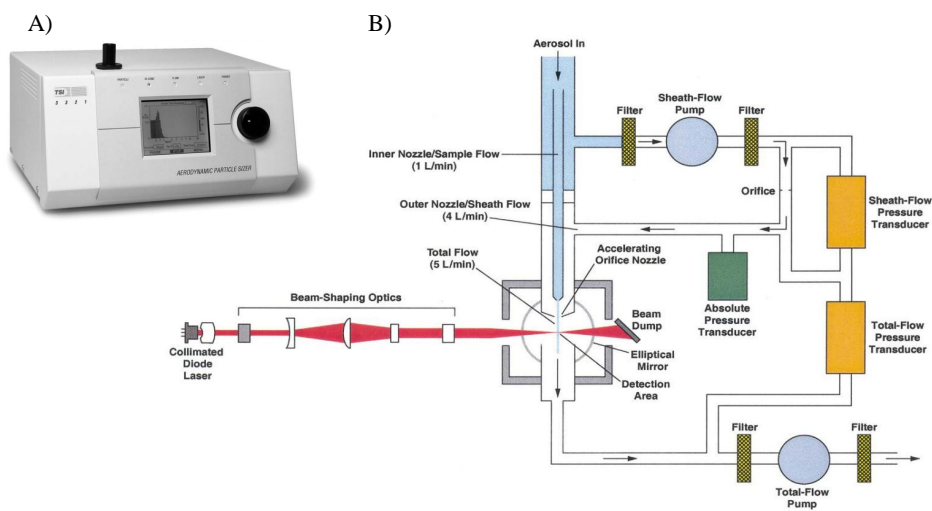


**Figure 9:** (A) Aerodynamic Particle Sizer (APS, model 3321, TSI<sup>TM</sup>). (B) Schematic diagram of the APS (TSI, 2005).

The APS has been subjected to several quality assurance and quality control activities:

- (i) During the regular operations at Izaña, the APS is subject to weekly checks of aerosol and sheath airflows, zeroes and leak tests using absolute filters.
- (ii) The APS was intercompared, measuring ambient air aerosol, with the gravimetry of the samples collected in quartz micro fiber filters ( $R^2$ :  $\sim 0.9$ ) during the study period.

#### 3.2.2 Particulate Matter

Particulate matter (PM) was gathered in several size fractions. Total Particulate Matter ( $\text{PM}_T$ ), and PM smaller than 10  $\mu\text{m}$  ( $\text{PM}_{10}$ ) and 2.5  $\mu\text{m}$  ( $\text{PM}_{2.5}$ ) aerodynamic diameters were collected on pre-heated (205°C during 5 h to remove potentially adsorbed volatile carbon)

quartz micro fiber filters (Pall Science, 150 mm diameter) with high volume air samplers (Fig. 10A; Hi-Vol, MCZ;  $30 \text{ m}^3 \cdot \text{h}^{-1}$  of flow rate). Concentrations of  $\text{PM}_x$  were gravimetrically determined in the weighing room (Fig. 10B) following the EN-14907 procedure (except that filter conditioning was performed at 30–35 % relative humidity instead of 50 %). The manual gravimetric method is considered optimal for PM concentrations  $> 10 \mu\text{g} \cdot \text{m}^{-3}$  (EN-14907), so uncertainties are significant below this threshold value.

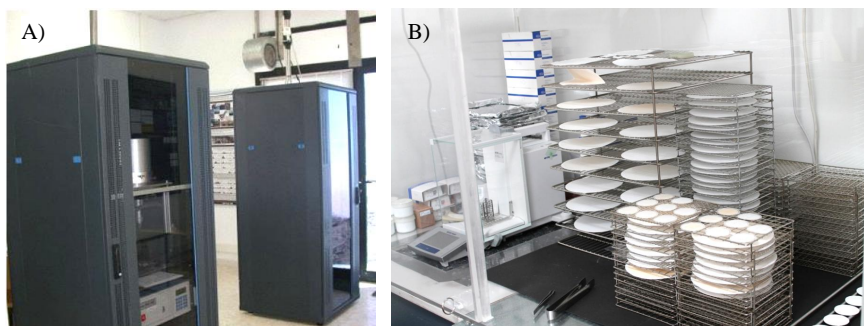


**Figure 10:** (A) High volume air samplers (HVS; MCZ) and (B) the weighing room.

The combined standard uncertainty ( $u_c$ ), associated with a specific  $\text{PM}_x$  concentration, is expressed as the combination of the individual sources of uncertainty identified in EN-14907; by multiplying  $u_c$  by the coverage factor  $k=2$ , the expanded uncertainty ( $U$ ) is obtained.  $U$  implies that there is a 95 % probability that the true value lies within  $\pm U$  of the measured value and it was calculated for individual samples, with the Izaña sampling conditions (sampling time: 8h; sampler flow:  $30 \text{ m}^3 \cdot \text{h}^{-1}$ ), as represented in Fig. 11. The expanded uncertainty associated for  $\text{PM}_x < 10 \mu\text{g} \cdot \text{m}^{-3}$  is  $\pm 5 \mu\text{g} \cdot \text{m}^{-3}$ .  $U$  (%) will depend on the sample mass, with  $U > 50 \%$  for  $\text{PM}_x < 10 \mu\text{g} \cdot \text{m}^{-3}$ .

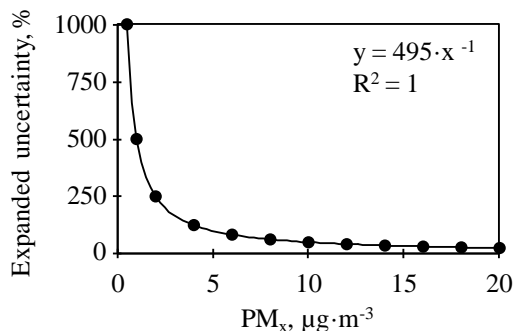


**Figure 11:** Expanded uncertainty ( $U$ ) of the gravimetric method for individual  $\text{PM}_x$  samples as described in EN-14907.

Blank weighing room and blank field filters (treated like the samples regarding preparation, transport and storage) were collected and weighed as part of the quality assurance / quality control (QA/QC) protocol.

## 3.2. DATA SET

From September to July,  $PM_{10}$  and  $PM_{2.5}$  samples were collected every 3 days at night (22–6 GMT; FT conditions), whereas in August,  $PM_x$  were gathered daily as part of the annual aerosol summer campaign. During the 2013 campaign, a set of  $PM_{2.5}$  samples were collected during the day (10–16 GMT; FT potentially mixed with MBL) at non-consecutive days. In August, additional  $PM_x$  samples were collected with Low Volume Samplers (LVS) to assess the accuracy of the High Volume Samplers (HVS) measurements.

### 3.2.3 Chemical composition

#### 3.2.3.1 Inorganic and carbonaceous species

Filter samples gathered during the study period (2008–2013) were stored and sent periodically to the Institute of Environmental Assessment and Water Research (IDAEA-CSIC) in Barcelona for the inorganic and carbonaceous chemical analysis (Fig. 12). The methods used for the chemical analysis are described in detail in previous articles (Querol et al., 2001; Rodríguez et al., 2015).

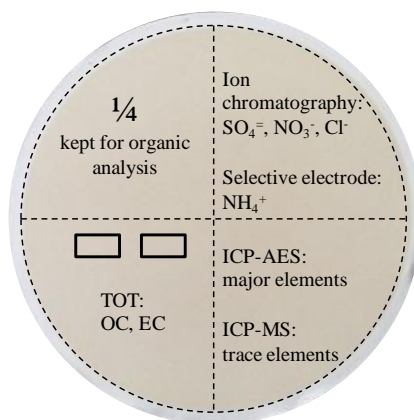


**Figure 12:** Scheme of the inorganic and carbonaceous species analyzed and the amount of filter used. **TOT:** thermal-optical transmittance; **ICP-AES:** Inductively Coupled Plasma Atomic Emission Spectrometry; **ICP-MS:** Inductively Coupled Plasma Mass Spectrometry.

One quarter of the filter was leached with de-ionized water to extract soluble species. The solution was subsequent heated at 60°C for 6 h and filtered for the analysis of  $SO_4^{2-}$ ,  $NO_3^-$ ,  $Cl^-$  by high-performance liquid chromatography (HPLC, ICpak™ anion column and 432 conductivity detector, WATERS; detection limits 0.113, 0.113 and 0.505  $\mu\text{g}\cdot\text{m}^{-3}$ , respectively) and  $NH_4^+$  by selective electrode (SE, 710 A+, THERMO Orion; detection limit 0.056  $\mu\text{g}\cdot\text{m}^{-3}$ ) (Fig. 12).

Other quarter of the filter was acid digested (HF and  $HNO_3$ ) at 90°C for 8 h to dissolve elemental and trace elements. Once the solution was cooled,  $HClO_4$  was added to dissolve the organic matter resistant to  $HNO_3$ . The acids were evaporated on a heating plate at 230°C and the remaining dry residue dissolved with  $HNO_3$  and de-ionized water. The resulting solution was analysed to determine elemental composition by Inductively Coupled Plasma

Atomic Emission Spectrometry (ICP-AES, IRIS Advantage TJA Solutions, THERMO; detection limit  $0.4 \text{ ng}\cdot\text{m}^{-3}$ ) and trace elements by Inductively Coupled Plasma Mass Spectrometry (ICP-MS, X Series II, THERMO; detection limit  $0.02 \text{ ng}\cdot\text{m}^{-3}$ ) respectively (Fig. 12).

Two punches (1 cm x 1.5 cm) of the filter were used to determine organic and elemental carbon by thermal-optical transmittance (TOT, Sunset Laboratory Inc.; detection limits 0.8 and  $0.032 \mu\text{g}\cdot\text{m}^{-3}$  respectively) (Fig. 12) following the EUSAAR2 protocol (Cavalli et al., 2010). The thermal-optical method analyse the carbonaceous material according to a pre-arranged temperature protocol, first in an inert atmosphere (He), where the organic carbon (OC) is desorbed in 4-steps (OC1, OC2, OC3 and OC4) and then in an oxidizing atmosphere (He/O<sub>2</sub>), where the elemental carbon (EC) combust in 4-steps (EC1, EC2, EC3 and EC4). Under the inert He atmosphere the temperature set points and residence times are the followings: (i) 200°C for 120 s, (ii) 300°C for 150 s, (iii) 450°C for 180 s and (iv) 650°C for 180 s, whereas under the oxidizing atmosphere He/O<sub>2</sub> the temperature set points and residence times are: (i) 500°C for 120 s, (ii) 550°C for 20 s, (iii) 700°C for 70 s and (iv) 850°C for 80 s. During the analysis in the inert atmosphere, some thermally unstable organic compounds pyrolyse and form pyrolytic carbon (Py), which is desorbed off the filter in the oxidizing atmosphere; to correct for pyrolysis, a laser beam monitors the optical properties of the sample before and during the analysis. The carbonaceous species desorbed from the filter are converted to CO<sub>2</sub>, which is reduced to CH<sub>4</sub> and subsequent quantified into a flame ionization detector (FID). At Izaña, OC and EC concentration are relatively low and artefacts are important. To identify possible artefacts – related to filter treatment, sampling, transport and storage – a short-campaign was performed in 2013. Results indicated that quartz microfiber filters may adsorb volatile carbon very easily due to the high active surface – as previously indicated by Chai et al. (2012) – and the more unstable part of the organic carbon (OC1 and OC2) was decided to be discarded to calculate OC.

The following empirically determinations were done:

- Organic matter (OM) was determined by using the ratio  $\text{OM}/\text{OC} = 1.8$  observed in the North American aerosol collected at Pico Observatory in the Azores (Dzepina et al., 2015).
- Sulphate was split into sea salt sulphate ( $\text{ss}\text{-SO}_4^-$ ) and non-sea salt sulphate ( $\text{nss}\text{-SO}_4^-$ ) using the empirical ratio of marine Na and sulphate ( $\text{SO}_4^-/\text{Na}^+ = 0.25$ ) in seawater (Gravenhorst, 1978).
- Sea salt was calculated as  $\text{ss}\text{-Cl} + 1.47\cdot\text{ss}\text{-Na}$  (Holland, 1978).
- $\text{CO}_2^{3-}$  was calculated from the amount of Ca not present as Ca-sulphate and Ca-nitrate, and then assuming this fraction of Ca is present as calcite ( $\text{CaCO}_3$ ;  $\text{CO}_3^- = 1.5\cdot\text{Ca}$ ; Rodríguez et al., 2011).
- SiO<sub>2</sub> was determined from the Al content on the basis of prior experimental equations ( $\text{SiO}_2 = 3\cdot\text{Al}_2\text{O}_3$ , see Querol et al., 2001).
- Mineral dust was calculated as the sum of  $\text{Al}_2\text{O}_3 + \text{SiO}_2 + \text{Fe} + \text{CaCO}_3 + \text{K} + \text{nss}\text{-Na} + \text{P} + \text{Ti} + \text{Sr}$  (see details in Rodríguez et al., 2011, 2015) and normalized so Al accounts for 8 % of the dust mass (see discussion in Pérez et al., 2016).

### 3.2.3.2 Organic species

The speciation of the organic matter was performed for a set of PM<sub>10</sub> and PM<sub>2.5</sub> samples collected during August 2013. The analytical procedure was carried at the Institute of Environmental Assessment and Water Research (IDAEA) during a short-term research stay in the course of this thesis. A detailed description of the analytical method is given elsewhere (Fontal et al. 2015, Van Drooge and Grimalt 2015). One quarter of the filter sample was used for the organic compounds speciation by gas-chromatography coupled to mass-spectrometry (GC-MS) (Fig. 13).

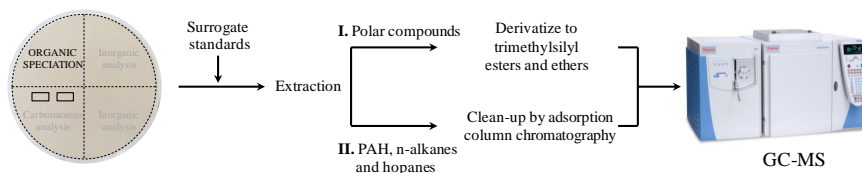


**Figure 13:** Scheme of the organic speciation analysis.

Briefly, before extraction, surrogate standards levoglucosan-D7, n-C24-D50 (Cambridge Isotopic Laboratories, UK), succinic acid-D4 (Sigma Aldrich, Steinheim, U.S.A.), anthracene-D10, benz[a]anthracene-D12, benzo[b]fluoranthene-D12, benzo[a]pyrene-D12 and benzo[ghi]perylene-D12 (Dr. Ehrenstorfer, Ausburg, Germany) were added on the filters. Filter samples were ultrasonically extracted three times in 15 ml of a solvent mixture of dichloromethane and methanol (2:1 (v/v); Merck, Germany) for 15 min and filtered over 0.45  $\mu\text{m}$  glass-fiber filter (Whatman, U.S.A.) to remove insoluble particles. Extracts were then concentrated to 1 ml by rotovap and to 0.5 ml using a gentle nitrogen stream.

For the analysis of polar compounds, i.e. acids and saccharides, a 25  $\mu\text{l}$  aliquot of the extract was evaporated until dryness, and 25  $\mu\text{l}$  of bis-(trimethylsilyl)-trifluoroacetamide (BSFTA) + trimethylchlorosilane (99:1) (Supelco, Bellefonte, PA, U.S.A.) and 10  $\mu\text{l}$  of pyridine (Merck, Darmstadt, Germany) were added and left overnight to derivatize the polar compounds to their trimethylsilyl esters and ethers in order to analyse them by GC-MS. The remaining extract was used for the analysis of polycyclic aromatic hydrocarbons (PAH), n-alkanes and hopanes, and was clean-up by adsorption column chromatography, packed with 1 g of aluminium oxide (Merck, Germany). The analytes were eluted with 10 ml of hexane: dichloromethane (1:2 (v/v), Merck, Germany) solvent, which was collected and concentrated to 1 ml by rotovap and to 25  $\mu\text{l}$  under a gentle nitrogen stream for quantification by GC-MS.

All prepared extracts were injected into a Thermo GC-MS (Thermo Trace GC Ultra-DSQ II). For derivatized polar compounds, the GC-MS was equipped with a 60 m fused capillary column; while non-polar compounds were analysed using a 30 m column (HP-5MS, 0.25 mm x 25  $\mu\text{m}$  film thickness). The oven temperature program started at 60°C for the polar compounds and 90°C for the non-polar compounds (holding time 1 min) and then heated to 120°C at 12°C·min<sup>-1</sup> and to 310°C at 4°C·min<sup>-1</sup>, at which point it was held for 10 min. The injector, ion source, quadrupole and transfer line temperatures were 280, 200, 150 and 280°C, respectively. Helium was used as a carrier gas at 0.9 ml·min<sup>-1</sup>. The MS detector was operated in full scan ( $m/z$  from 50 to 650) and electron impact (70 eV) ionization mode for the polar compounds. The sample extracts for the analysis of non-polar compounds was performed in selected ion monitoring mode for the corresponding ions.

Organic species were identified by their GC retention time and characteristic ions in the MS. Retention time was compared to those of the standards or with literature and the National Institute of Standards and Technology (NIST) library data (Claeys et al., 2007; Kourtchev et al., 2005; Clements and Seinfeld, 2007; Medeiros and Simoneit 2007; Fontal et al., 2015). The organic species analyzed and their characteristic ions are:

- (i) Dicarboxylic acids  
succinic acid ( $m/z$  247), glutaric acid ( $m/z$  261), adipic acid ( $m/z$  275), pimelic acid ( $m/z$  289), suberic acid ( $m/z$  303), azelaic acid ( $m/z$  317), malic acid ( $m/z$  233), phthalic acid ( $m/z$  295).
- (ii) Saccharides  
 $\alpha$ - and  $\beta$ -glucose ( $m/z$  204), mannitol ( $m/z$  319), sucrose and fructose ( $m/z$  361).
- (ii) Levoglucosan ( $m/z$  204)
- (iii) Secondary aerosols from isoprene oxidation (SOA ISO)  
2-methylglyceric acid (2-MGA;  $m/z$  219), 2-methylthreitol (2-MT1) and 2-methylerythritol (2-MT2;  $m/z$  219).
- (iv) Secondary aerosols from  $\alpha$ -pinene oxidation (SOA PIN)  
cis-pinonic acid ( $m/z$  171), 3-hydroxyglutaric acid (3-HGA;  $m/z$  349), 3- methyl-1,2,3-butanetricarboxylic acid (MBTCA;  $m/z$  405).
- (v) n-alkanes ( $m/z$  71).
- (vi) Hopanes  
17(H) $\alpha$ ,21(H) $\beta$ -29-Norhopane, 17(H) $\alpha$ ,21(H) $\beta$ -hopane ( $m/z$  191).
- (vii) Polycyclic aromatic hydrocarbon (PAH)  
benzo[a]anthracene ( $m/z$  228), chrysene ( $m/z$  228), benzo[b+k]fluoranthene ( $m/z$  252), benzo[e]pyrene ( $m/z$  252), benzo[a]pyrene ( $m/z$  252), indeno[1,2,3-cd] pyrene ( $m/z$  276), benzo[ghi]perylene ( $m/z$  276).

The limits of quantification in the applied methodologies were  $0.02 \text{ ng}\cdot\text{m}^{-3}$  for the saccharides,  $0.01 \text{ ng}\cdot\text{m}^{-3}$  for the acids and  $0.002 \text{ ng}\cdot\text{m}^{-3}$  for PAHs, hopanes and n-alkanes. The concentrations were corrected by the recoveries of the above mentioned surrogates. The recoveries of the surrogate standards were higher than 60 %. The field blanks concentrations of the reported compounds were between 1 and 30 % of the sample concentration. Organic compounds, such as carboxylic acids are not reported due to higher blank concentrations. No corrections for the blank concentrations were applied on the sample concentrations.

## 3.2.4 Meteorological products

### 3.2.4.1 In-situ meteorology at Izaña

Meteorological parameters were provided by the Izaña Observatory. Pressure was measured with a Setra 470, temperature and relative humidity with a Rotronic, and wind with a Thies sonic anemometer. Vertical wind was only recorded from June 2011 to October 2011. Concentrations of water vapour were calculated from the improved Magnus equation (Goff and Gratch, 1946).

## 3.2. DATA SET

---

### 3.2.4.2 Back-trajectories

The air mass origin and transport was tracked by means of backward trajectory analysis. Three-dimensional ten-days back-trajectories arriving at 2400 m.a.s.l were computed at 00 GMT for Izaña with:

- (i) The FLEXible TRAjectories model (FLEXTRA; <https://folk.nilu.no/~andreas/flextra/flextra3.html>; Stohl et al., 1995; Stohl and Seibert., 1998), developed at the Institute of Meteorology and Geophysics in Vienna. FLEXTRA was run with the European Centre for Medium-Range Weather Forecasts (ECMWF) data set and back-trajectories were used as input in a self-developed Matlab script (The Mathworks, Natick, U.S.A.) which segregates air masses coming from North America and the North Atlantic, from those of Africa, attending to its latitude and longitude values along the transport path towards Izaña.
- (ii) The HYbrid Single-Particle Lagrangian Integrated Trajectory model (HYSPLIT, <http://ready.arl.noaa.gov/HYSPLIT.php>; Draxler and Hess, 1998; Draxler and Rolph, 2003; Stein et al., 2015), developed by the National Oceanic and Atmospheric Administration (NOAA). HYSPLIT was run with the National Centre for Environmental Prediction's (NCEP) Global Data Assimilation System (GDAS, 1 degree) data set.

The use of FLEXTRA or HYSPLIT back-trajectories was subject to their availability during the course of the thesis. Both lagrangian models show a good agreement when their trajectories are compared (e.g. Klein et al., 2011; Madonna et al., 2013), but they were applied separately and not mixed: FLEXTRA back-trajectories were used to reach objective-2 and HYSPLIT back-trajectories were used to reach objective-3.

### 3.2.4.3 NCAR/NCEP re-Analysis data

Meteorological re-analysis data for the period 2008–2013 was downloaded from the National Centre for Environmental Prediction and the National Centre for Atmospheric Research (NCEP/NCAR; <https://www.esrl.noaa.gov>; Kalnay et al., 1996); both divisions are part of the National Oceanic and Atmospheric Administration (NOAA). The NCEP/NCAR Re-analysis Project produces a retroactive – 1948 on – record of global analyses of atmospheric fields. To achieve this goal the recovery of land surface, ship, rawinsonde, pibal, aircraft, satellite and other data is needed (Kistler et al., 2001). These data are quality controlled and assimilated with a data assimilation system (DAS) which is kept unchanged over the re-analysis period. This avoids the problem of inhomogeneous meteorological analyses, which had to support real-time weather forecasting, due to the changes in the DAS. The output consists of a globally gridded data set of the chosen variables (e.g. precipitation, vector winds, etc.). The analysis in the present thesis includes geopotential heights, winds and omega (vertical wind) at several standard levels (925, 850 and 700 hPa) as well as precipitations rates. Data was used to study the processes involved in the export and transatlantic transport of aerosols from North America.

### 3.2.5 Additional parameters

#### 3.2.5.1 Radiation

Radiation data was provided by the Baseline Surface Radiation Network (BSRN). The Izaña observatory has been part of the BSRN since 2009 (García, 2011). We used short-wave downward radiation (SDR) irradiance (global, direct and diffuse), and UV-A and UV-B measurements. The global and diffuse SDRs were measured with unshaded and shaded Kipp Zonen CM-21 pyranometers, respectively. The spectral range covers 335–2200 nm (95 % points), and the expected uncertainty is  $\pm 2\%$  for hourly totals. The direct SDR is measured with a Kipp Zonen CH1 pyrhelimeter, with a field of view limited to  $5^\circ \pm 0.2^\circ$ , placed on a sun tracker with a tracking accuracy of  $0.1^\circ$ . The spectral range goes from 200 to 4000 nm (50 % points), and the uncertainty of this measurement is  $\pm 2\%$  for hourly totals. The UV-A is measured with Kipp Zonen UVS-A-T radiometer. The spectral range covers 315–400 nm with daily uncertainty lower than 5 %. The UV-B is measured with Yankee Environmental System (YES) UV-B-1 pyranometer. The spectral range goes from 280 to 320 nm. All radiation parameters are measured with 1 min resolution. Radiation was used to study the context in which NPF takes place.

#### 3.2.5.2 Reactive gases

Reactive gases (RG) were provided by the Izaña Reactive gases GAW program. RG measured using different principle of measurements: UV fluorescence analyser for  $\text{SO}_2$  (Thermo™, model 43C-TL), UV absorption for  $\text{O}_3$  (Thermo™, model 49C) and chemiluminescence for NO,  $\text{NO}_2$  and  $\text{NO}_x$  (Thermo™, model 42C-TL). In order to avoid the  $\text{NO}_2$  overestimation linked to the use of molybdenum converters, a photolytic  $\text{NO}_2$  to NO converter was used (Parrish and Fehsenfeld, 2000; Steinbacher et al., 2007). Quality assurance and quality control activities included (i) 15 min zero measurements, performed every 24 h in the  $\text{SO}_2$  and  $\text{O}_3$  and every 6 h in the  $\text{NO}_x$  analysers; (ii) the use of linear fittings between consecutive zeros for applying zero correction to data; (iii) five-point span calibrations every 3 months with certified  $\text{SO}_2$  and  $\text{NO}_x$  concentrations; and (iv) calibration of the  $\text{O}_3$  analyser versus an  $\text{O}_3$  primary standard (49C PS). A high linearity was commonly observed in these calibrations ( $R^2 \sim 0.999$ ). Detection limit is 60 ppt for  $\text{SO}_2$ , 50 ppt for NO and  $\text{NO}_x$  (5 min average) and 1 ppb for  $\text{O}_3$  (1 min average). Reactive gases were used to study the context in which NPF takes place.

#### 3.2.5.3 Global fires

The Global Fire Emissions Database Version 4 including small fires data (GFEDv4.1s; Randerson et al., 2015; <http://www.globalfiredata.org/index.html>) was downloaded from the Oak Ridge National Laboratory Distributed Active Archive Centre for biogeochemical dynamics ([https://daac.ornl.gov/cgi-bin/dsviewer.pl?ds\\_id=1293](https://daac.ornl.gov/cgi-bin/dsviewer.pl?ds_id=1293)), which is one of the NASA Earth Observing System Data and Information System data centres. The data set has  $0.25^\circ$  latitude by  $0.25^\circ$  longitude spatial resolution and provides global estimates of monthly burned area (i.e. the fraction of each grid cell that burned in that month) derived from the 500-m direct broadcast burned area product (MCD64A1) combined with 1-km thermal anomalies (active fires) of the Moderate Resolution Imaging Spectroradiometer (MODIS). GFEDv4.1s

### 3.3. DATA ANALYSIS

---

was used to estimate the monthly average burned fraction – of each  $0.25^\circ \times 0.25^\circ$  grid cell – in North America from 2008 to 2013.

#### 3.2.5.4 Aerosol Index

Level 3 UV Aerosol Index (AI) data, from the Ozone Monitor Instrument spectrometer onboard satellite Aura, was downloaded from the Giovanni online data system of the NASA Goddard Earth Sciences Data and Information Services Centre (<http://disc.sci.gsfc.nasa.gov/>). AI was used to study the spatial and temporal variability of dust in North America from 2008 to 2013. Graphs were provided by the Izaña aerosol group.

#### 3.2.5.5 Tornado climatology

The Severe Weather Database Files (1950–2015) for U.S. tornadoes were downloaded from the Storm Prediction Centre (<http://www.spc.noaa.gov/>) as part of the NOAA National Weather service. The data set contains several fields such as date of occurrence and starting latitude and longitude. The tornado climatology was used to study convective processes in Central and Northeastern United States.

## 3.3 Data Analysis

### 3.3.1 Size distribution

#### 3.3.1.1 Classification of events

The SMPS aerosol number size distribution (10–600 nm) was plotted for each day of the period 2008–2012, visually analysed and classified to distinguish NPF – or ‘banana-type’ events – following the criteria of Dal Maso et al., (2005). Seven types of events were considered (Table 1 and Fig. 14). In class I and II events a clear particle formation and growth was observed for at least 4 and 2 h, respectively. In class III events no particle growth was observed after the particle burst (apple-type events; Yli-Juuti et al., 2009). The remaining data were sorted as follows: non-event (no increase in the concentration of particles  $<25$  nm was observed), undefined (event was not clearly observed) or bad data (invalid or missing data). We attempted to determine the Formation Rate (FR) and Growth Rate (GR) for all class I events. However, this was not possible for a set of episodes in which a noisy signal was observed, mostly induced by a significant variability in the horizontal and/or vertical components of wind. Thus, events in which the FR and GR could be determined were sub-classified as class Ia; the remaining events were labelled as class Ib (Table 1).

#### 3.3.1.2 Size distribution–dependent particle loss parameters

When analyzing NPF events, losses of new particles during the formation and growth steps have to be taken into account. Condensation Sink (CS) describes how fast condensable vapour is removed by collisions with the pre-existing aerosol particles, which is the main sink for the smallest particles, and Coagulation Sink (CoagS) represents the self-coagulation

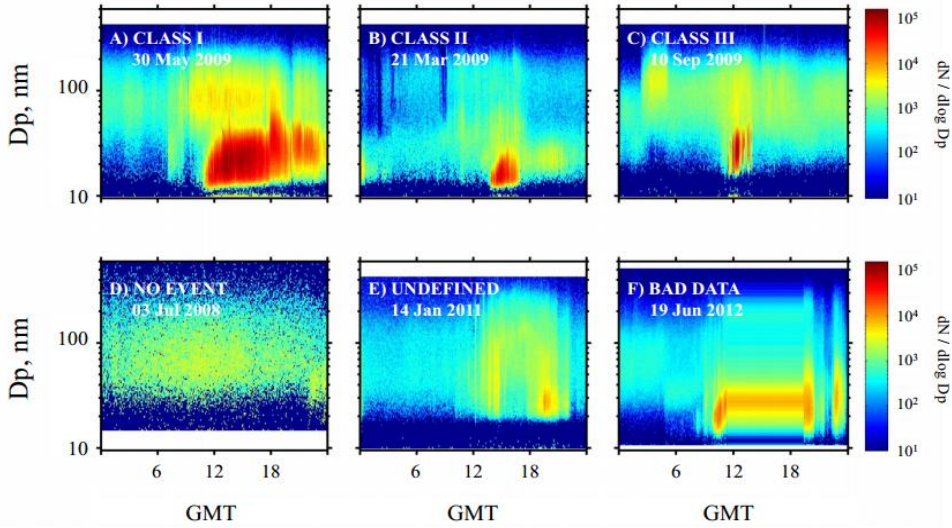


**Figure 14:** Examples of type of events and cases identified in the data analysis.

of the growing particle population. CS and CoagS were calculated for each size distribution following the equations described by Kulmala et al., (2012).

$$\begin{aligned} CS &= 2\pi D \cdot \int_0^\infty Dp \cdot \beta_m(Dp) \cdot n(Dp) \cdot dDp \\ &= 2\pi D \cdot \sum_i Dp_i \cdot \beta_{m,Dp,i} \cdot N_{Dp,i}, \end{aligned} \quad (3.1)$$

where  $D$  is the condensable vapour (assumed to be sulfuric acid) diffusion coefficient,  $Dp_i$  and  $N_{Dp,i}$  the particle diameter and concentration in the size section  $i$ , and  $\beta_{m,Dp,i}$  the size dependent transitional correction factor in the size section  $i$  calculated as (Fuchs and Sutugin, 1971):

$$\beta_m = \frac{1 + Kn}{1 + 1.677Kn + 1.333Kn^2}, \quad (3.2)$$

where  $Kn$  is the Knudsen number  $= 2\lambda/dp$ . Particles between 10 nm and 20  $\mu\text{m}$  were used to calculate the CS. CoagS is linked to CS by the simplified relation (Lehtinen et al., 2007):

$$CoagS_{nuc} = \left(\frac{Dp}{0.71}\right)^m \cdot CS, \quad (3.3)$$

where  $Dp$  is the geometric mean diameter of the nucleation mode and  $m$  is an empirical factor that generally can be assumed to be constant ( $m \approx -1.7$ ; Dal Maso et al., 2008).

### 3.3.1.3 Determination of Formation and Growth Rates

The FR and GR were calculated for the nucleation mode particles ( $Dp < 25$  nm) using equations described by Kulmala et al. (2012):

### 3.3. DATA ANALYSIS

**Table 1:** Type of events considered in this study. **FR:** formation rate. **GR:** growth rate.

Type	Criteria
Class Ia (banana type)	A new mode with growing mean diameter under 25 nm is observed. The growth is observed during at least 4 h. FR and GR can be calculated.
Class Ib (banana type)	A new mode with growing mean diameter under 25 nm is observed. The growth is observed during at least 4 h, but FR and GR could not be calculated.
Class II (short banana type)	A new mode with growing mean diameter under 25 nm is observed. The growth period lasts from 2 to 4 h.
Class III (apple/burst)	A new mode with growing mean diameter under 25 nm is observed. The growth period is lower than 2 h.
Non-event	No new particle mode with mean diameter under 25 nm is observed.
Undefined	Event is not clearly observed.
Bad data	Missing or invalid data.

$$FR = \frac{\Delta N_{nuc}}{\Delta t} + CoagS_{nuc} \cdot N_{nuc} + \frac{GR}{\Delta Dp} \cdot N_{nuc} + S_{losses}, \quad (3.4)$$

where the first term is the temporal variation of nucleation mode particles number concentration; it is the slope obtained from the first-order polynomial fitting during the episode when representing the nucleation mode particle concentration as a function of time (Fig. 15). The second term is the self-coagulation loss, i.e. the mean coagulation sink of nucleation mode particles. The third term is the flux of particles growing out of the nucleation mode size range, with GR being the growth rate and  $\Delta Dp$  the particle diameter increase during the growth. Slosses takes into account additional losses, but neglected in this study. Similarly,

$$GR = \frac{dDp}{dt} = \frac{\Delta Dp}{\Delta t} = \frac{Dp_2 - Dp_1}{t_2 - t_1}, \quad (3.5)$$

where  $dp_1$  and  $dp_2$  are the representative particle diameters at times  $t_1$  and  $t_2$ . GR is the slope obtained from the first-order polynomial fitting during the episode when representing the nucleation mode geometric mean diameter as a function of time (Fig. 15). The FR and GR were determined using Eqs. (1) and (2) in two different approaches.

#### Method 1: SMPS data

The FR and GR were determined for the nucleation mode particles ( $Dp < 25$  nm) using the number concentration ( $N_{nuc}$ ; Dal Maso et al., 2005) and the geometric mean diameter (GMD,  $Dp_{nuc}$ ; Järvinen et al., 2013) of the 5 min resolution SMPS data. We used the GMD to avoid the human bias associated with other methods such as visual determination of the mode size change. Figure 15 shows an illustration of the linear fittings used for determining the slopes FR (Eq. 1) and GR (Eq. 2).

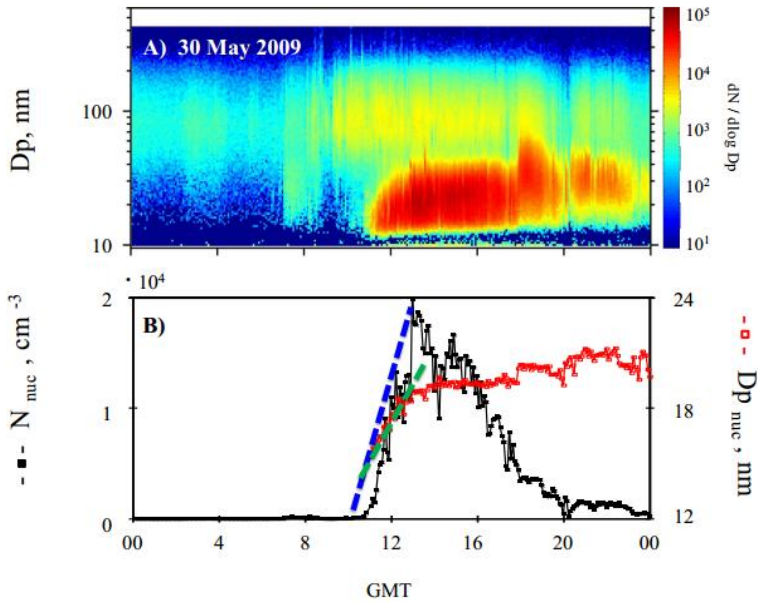


**Figure 15:** (A) Example of type Ia event. (B) Time evolution of the number of particles and of the geometric mean diameter (GMD) for the nucleation mode. Lines illustrate the fitting that are performed for determining the formation (blue) and growth (green) rates.

## Method 2: lognormal size distribution

This method was implemented in two steps. First, each 5 min average size distribution was fitted to a linear combination of lognormal distributions:

$$\frac{dN}{d\ln D_p} = \sum_{(i=1)}^n \frac{N_i}{\sqrt{2\pi \ln \sigma_{(g,i)}}} \exp\left(-\frac{(\ln D_p - \ln D_{p(g,i)})^2}{2 \ln^2 \sigma_{(g,i)}}\right),$$

Each lognormal distribution is characterized by three parameters: (i) mean number concentration  $N_i$ , (ii) geometric variance  $\sigma_{(g,i)}^2$  and (iii) the geometric mean diameter  $D_{p(g,i)}$ . The fitting procedure was performed using a self-developed software in MATLAB 7.4 (The Mathworks, Natick, U.S.A.) within the frame of this thesis. The fitting accuracy was assessed by the least squares quadratic (LSQ) value between the measured particle number size distribution and its fitting. This method is usually applied considering a single nucleation mode ( $< 25$  nm) (e.g. Dal Maso et al., 2005; Boy et al., 2008; Yli-Juuti et al., 2009; Salma et al., 2011). However, we observed that, in many cases, the LSQ value was significantly reduced if the nucleation mode was fitted with 2 lognormal fittings instead of 1. In many cases a simple visual analysis of the 5 min size distributions evidenced that the nucleation mode growth was prompted by one of these lognormal distribution. In a second step, GR was determined using Eq. (2).

#### 3.3.1.4 Determination of sulfuric acid contribution

In order to quantify the contribution of H<sub>2</sub>SO<sub>4</sub> to particle growth, we determined the experimental Concentration of Condensable Vapour (C<sub>v</sub>) and its Source Rate (Q) (Dal Maso et al., 2005) as well as the theoretical H<sub>2</sub>SO<sub>4</sub> proxy.

$$C_v = A \cdot \frac{dDp}{dt}, \quad (3.6)$$

where A is a constant for a vapour with molecular properties of sulfuric acid ( $A = 1.37 \cdot 10^{-7} \text{ h} \cdot \text{cm}^{-3} \cdot \text{nm}^{-1}$ ; Dal Maso et al., 2005). If changes in the source rate are slow compared to the characteristic lifetime of the vapour, we can assume a steady-state situation, resulting in the following equation for Q:

$$Q = CS \cdot C_v = CS \cdot A \cdot \frac{dDp}{dt}, \quad (3.7)$$

For estimating the theoretical concentrations of H<sub>2</sub>SO<sub>4</sub> by the proxy of Petäjä et al. (2009), we used experimental data of SO<sub>2</sub> and UV-B radiation at Izaña with Hyytiälä's parameters ( $k = 9.9 \times 10^{-7} \text{ m}^2 \text{ W}^{-1} \text{ s}^{-1}$ ); the use of this value for k instead of the actual (unknown) value at Izaña could have an influence on the absolute value of the H<sub>2</sub>SO<sub>4</sub> concentration, but not on the correlations.

$$\text{Proxy}[\text{H}_2\text{SO}_4] = k \cdot \frac{\text{SO}_2 \cdot \text{UVB}}{CS}, \quad (3.8)$$

This proxy and the C<sub>v</sub> equation were used to calculate the theoretical growth rate due to sulfuric acid (GRSA) (Nieminen et al., 2010).

### 3.3.2 Median Concentration At Receptor Plots

The possible source regions of the main PM<sub>10</sub> chemical components (i.e. nss-SO<sub>4</sub><sup>2-</sup>, NO<sub>3</sub><sup>-</sup>, NH<sub>4</sub><sup>+</sup>, OM, EC, Ca, Al, dust and sea salt) arriving in Izaña in the period 2008–2013, were identified by means of the Median Concentrations At Receptor (MCAR) plots.

MCAR plots were built with a software using the method described by Rodríguez et al. (2011). These plots have 1° latitude by 1° longitude spatial resolution and show the typical (median) concentration of each aerosol component recorded at Izaña when the air mass has passed by each grid cell. Briefly, the software (i) build a 3D matrix where X, Y and Z dimensions correspond to longitude, latitude and the number of samples respectively, (ii) intersects the latitude-longitude cell grids (i.e. X–Y) with the FLEXTRA 10-days back-trajectory, for each Z value (i.e. back-trajectory of a specific sample), assigning to these X–Y cells the value corresponding to the aerosol concentration of the plotted specie, (iii) calculates the median concentration of each Z vector (i.e. concentration for a latitude-longitude cell grid), and (iiiv) plots the resulting matrix of median concentrations with a smoothly coloured outputs.

The MCAR plots were fed with FLEXTRA back-trajectories representative of transatlantic transport from North America (westerlies air masses) for the sampled days. Westerlies (WES) and Saharan Air Layer (SAL) air masses were separated with a software which

scanned the latitude and longitude points for each day classifying samples, as WES or SAL, depending on if the air masses passed over Africa or came from North America and the Atlantic Ocean. Events linked to (i) back-trajectories from North Africa or (ii) associated with Saharan dust re-circulated over the North Atlantic (exported from North Africa westward and then re-circulated eastward, e.g. as described by Ancellet et al., 2016) were removed; for visually identifying these latter type of events we used the forecast of the BSC-DREAM8b model (Pérez et al., 2006; Basart et al., 2012) storages in the Barcelona Supercomputing Centre web site (<http://www.bsc.es/earth-sciences/mineral-dust-forecast-system/bsc-dream8b-forecast/north-africa-europe-and-middle-ea-1>).

Similar plots were used to analyse the seasonality of the westerlies frequency arriving in Izaña, which is linked to the export North American pollutants. The monthly Transport Route Frequency (TRF) plots of the period 2008–2013 were calculated in a similar way to the MCAR plots, but instead of the median concentration, the total number of back-trajectories passing for each  $1^\circ \times 1^\circ$  cell grid (i.e. the sum in each Z vector instead of the median) is represented. TRF plots were fed with FLEXTRA back-trajectories representative of transatlantic transport from North America for all days from 2008 to 2013.

The software packages used to build the MCAR and TRF plots, as well as to sort the Westerlies and Saharan Air Layer air masses, were self-developed in MATLAB 7.4 (The Mathworks, Natick, U.S.A.) within the scope of this thesis.

### 3.3.3 Multivariate Curve Resolution Alternating Least Squares / Multilinear Regression Analysis

Potential OA sources and processes were identified by merging organic compounds concentrations for evaluation with Multivariate Curve Resolution Alternating Least Squares (MCR-ALS) and the OM was apportioned between the OA sources using receptor modelling. This technique was applied to the  $PM_T$  (22–6 GMT) and  $PM_{2.5}$  (10–16 GMT) samples collected in August 2013.

The joint dataset was imported into MATLAB 7.4 (The Mathworks, Natick, U.S.A.) for subsequent calculations using MATLAB PLS 5.8 Toolbox (Eigenvector Research Inc, Masson WA, U.S.A.) (Jaumot et al. 2005). The MCR-ALS method decomposes the data matrix using an Alternating Least Squares algorithm under a set of constraints such as non-negativity, unimodality, closure, trilinearity or selectivity (Tauler et al., 1995 a, b). The MCR-ALS method has been applied successfully in previous studies on organic aerosol in urban and rural areas (Alier et al. 2013; Van Drooge and Grimalt 2015). The explained variance by the different components is similar to a Principal Components Analysis (PCA), but not orthogonal. Since natural sources in the environment are rarely orthogonal, the MCR-ALS method provides more realistic descriptions of the components than the orthogonal database decomposition methods.

The data matrix was decomposed in two factors: loadings (i.e. the relative amount of the chemical compounds in the source) and scores (i.e. the relative contribution of the potential sources to the organic aerosol) (Tauler et al., 2009). The loading factors obtained in the MCR-ALS were used to identify OA sources, whereas the score factors were used as independent variables in the Multilinear Regression Analysis (MLRA) to apportion the determined fraction of OM between the identified sources.

CHAPTER

# 4

## Results

The present thesis is the result of the compilation of three peer-reviewed articles published in atmospheric science journals. The articles and their corresponding authors are the followings:

### Article 1

**Title:** Climatology of new particle formation at Izaña mountain GAW observatory in the subtropical North Atlantic.

**Authors:** M. I. García, S. Rodríguez, Y. González, R. D. García.

**Reference:** García, M. I., Rodríguez, S., González, Y., and García, R. D.: Climatology of new particle formation at Izaña mountain GAW observatory in the subtropical North Atlantic, *Atmos. Chem. Phys.*, 14, 3865-3881, doi:10.5194/acp-14-3865-2014, 2014.

In this article, a climatology of new particle formation at Izaña is presented. The events of new particle formation are identified and described, along with the context in which take place and the factors affecting the interannual variability. This article covers the objective 1.

## Article 2

- Title:** Impact of North America on the aerosol composition in the North Atlantic free troposphere.
- Authors:** M. I. García, S. Rodríguez, A. Alastuey.
- Reference:** García, M. I., Rodríguez, S., and Alastuey, A.: Impact of North America on the aerosol composition in the North Atlantic free troposphere, *Atmos. Chem. Phys. Discuss.*, doi:10.5194/acp-2017-60, in review, 2017.

In this article, the composition of the aerosols transported in the westerlies and its seasonal variability is presented. The potential aerosol source regions in North America are identified along with the meteorological processes that modulate the aerosols transatlantic transport. This article covers the objective 2.

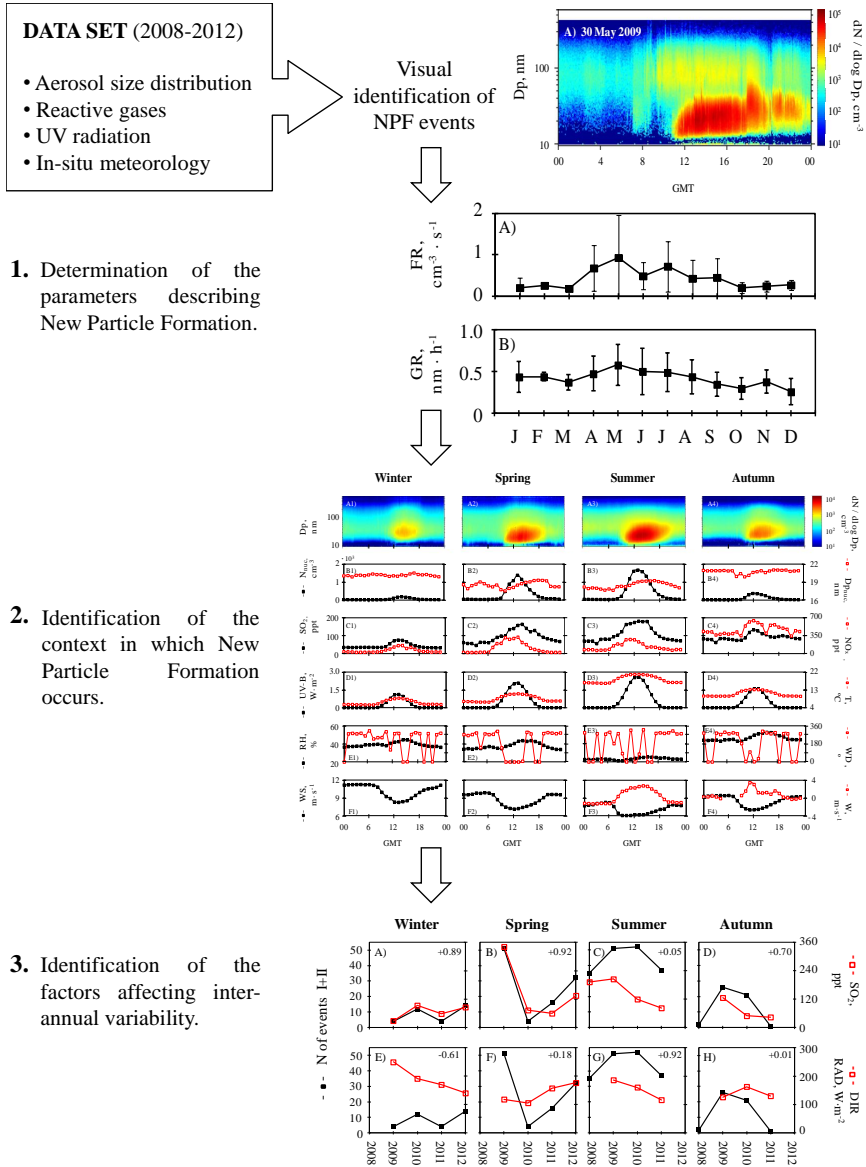
## Article 3

- Title:** Speciation of organic aerosols in the Saharan Air Layer and in the free troposphere westerlies.
- Authors:** M. I. García, B. L. Van Drooge, S. Rodríguez and A. Alastuey.
- Reference:** García, M. I., Van Drooge, B. L., Rodríguez, S., and Alastuey, A.: Speciation of organic aerosols in the Saharan Air Layer and in the free troposphere westerlies, *Atmos. Chem. Phys. Discuss.*, doi:10.5194/acp-2017-108, in review, 2017.

In this article, the speciation of the organic aerosols in the Saharan Air Layer and in the westerlies is presented. The contribution of the analyzed organic groups to the Izaña organic matter is analyzed, along with the identification of potential sources and the source apportionment to the Izaña organic matter. This article covers the objectives 2 and 3.

# 4.1 Article 1

Graphical abstract:





Atmos. Chem. Phys., 14, 3865–3881, 2014  
www.atmos-chem-phys.net/14/3865/2014/  
doi:10.5194/acp-14-3865-2014  
© Author(s) 2014. CC Attribution 3.0 License.



Atmospheric  
Chemistry  
and Physics  
Open Access

## Climatology of new particle formation at Izaña mountain GAW observatory in the subtropical North Atlantic

M. I. García<sup>1,2</sup>, S. Rodríguez<sup>1</sup>, Y. González<sup>1</sup>, and R. D. García<sup>1,3</sup>

<sup>1</sup>Izaña Atmospheric Research Centre, AEMET Joint Research Unit of CSIC “Studies on Atmospheric Pollution”, La Marina 20, Planta 6, E38071, Santa Cruz de Tenerife, Canary Islands, Spain

<sup>2</sup>Department of Analytical Chemistry, Nutrition and Food Science, University of La Laguna, Avda. Astrofísico Fco. Sánchez s/n, 38200, La Laguna, Tenerife, Canary Islands, Spain

<sup>3</sup>Atmospheric Optic Group, University of Valladolid (GOA, UVA), Paseo de Belén 7, 47011, Valladolid, Spain

Correspondence to: M. I. García (isabel\_garciaalvarez@hotmail.es)

Received: 20 August 2013 – Published in Atmos. Chem. Phys. Discuss.: 13 September 2013

Revised: 25 February 2014 – Accepted: 27 February 2014 – Published: 17 April 2014

**Abstract.** A climatology of new particle formation (NPF) events at high altitude in the subtropical North Atlantic is presented. A 4-year data set (June 2008–June 2012), which includes number size distributions (10–600 nm), reactive gases (SO<sub>2</sub>, NO<sub>x</sub>, and O<sub>3</sub>), several components of solar radiation and meteorological parameters, measured at Izaña Global Atmosphere Watch (GAW) observatory (2373 m above sea level; Tenerife, Canary Islands) was analysed. NPF is associated with the transport of gaseous precursors from the boundary layer by orographic buoyant upward flows that perturb the low free troposphere during daytime. On average, 30 % of the days contained an NPF event. Mean values of the formation and growth rates during the study period were 0.46 cm<sup>-3</sup> s<sup>-1</sup> and 0.42 nm h<sup>-1</sup>, correspondingly. There is a clearly marked NPF season (May–August), when these events account for 50–60 % of the days per month. Monthly mean values of the formation and growth rates exhibit higher values in this season, 0.49–0.92 cm<sup>-3</sup> s<sup>-1</sup> and 0.48–0.58 nm h<sup>-1</sup>, respectively. During NPF events, SO<sub>2</sub>, UV radiation and upslope winds showed higher values than during non-events. The overall data set indicates that SO<sub>2</sub> plays a key role as precursor, although other species seem to contribute during some periods. Condensation of sulfuric acid vapour accounts for most of the measured particle growth during most of the year (~70 %), except for some periods. In May, the highest mean growth rates (~0.6 nm h<sup>-1</sup>) and the lowest contribution of sulfuric acid (~13 %) were measured, suggesting a significant involvement of other condensing vapours. The SO<sub>2</sub> availability seems also to be the

most influencing parameter in the year-to-year variability in the frequency of NPF events. The condensation sink showed similar features to other mountain sites, showing high values during NPF events. Summertime observations, when Izaña is within the Saharan Air Layer, suggest that dust particles may play a significant role acting as coagulation sink of freshly formed nucleation particles. The contribution of dust particles to the condensation sink of sulfuric acid vapours seems to be modest (~8 % as average). Finally, we identified a set of NPF events in which two nucleation modes, which may evolve at different rates, occur simultaneously and for which further investigations are necessary.

### 1 Introduction

The growth of nucleated clusters is an important source of atmospheric aerosols (Kulmala, 2003). It is considered that the so-called new particle formation (NPF) is a two-step (decoupled) process: nucleation and growth. It has been proposed that the nucleation of sulfuric acid gas molecules results in the formation of clusters (< 2 nm size; Kulmala et al., 2006; Kulmala and Kerminen, 2008) that are simultaneously being stabilized by amines, ammonia, or organic vapours (Kulmala et al., 2013). Under certain scenarios these clusters are activated in such a way that they grow up to result in stable aerosols with a size ≥ 50 nm (e.g. during the so-called “banana-type” growth events). Processes involved in the NPF (nucleation and growth up to stable sizes) are not

fully understood. For the first phase, or nucleation, the most studied mechanisms are binary (water–sulfuric acid), ternary (water–sulfuric acid–ammonia) and ion-induced nucleation (see the Kulmala, 2003, discussion), but fail to explain field observations. Semi-empirical new mechanisms such as cluster activation and kinetic nucleation have been developed to explain the observed measurements (Kulmala et al., 2006; Laakso et al., 2004; Metzger et al., 2010). For the second phase, or growth, the proposed mechanisms include condensation of sulfuric acid – sulfate and organic vapours (Laaksonen et al., 2008; Kulmala et al., 2013).

Understanding how nucleated clusters and particles grow is important for studying the influence of aerosols on climate, including feedbacks (IPCC, 2007). This influence depends on particle size. Nucleation not followed by growth processes (e.g. bursts, also so-called “apple”-type events) typically results in high concentrations of particles < 20 nm size. These particles have a short lifetime (~hours), have a low ability to act as cloud condensation nuclei (McFiggans et al., 2006) and exhibit Rayleigh scattering features (as gases). In contrast, accumulation mode particles (100–1000 nm) are long-lived (~few weeks), are good condensation nuclei and scatter light more efficiently. Because of the influence of thermodynamic variables (e.g.  $T$  and RH), UV radiation and meteorology on the NPF processes, climate may also affect NPF. Emission rates of gaseous precursors also play a key role. The decadal decrease (2001–2010) in the total particle number concentration (a metric dominated by particles < 20 nm) observed at background and remote sites in Europe, North America and the Pacific has been attributed to a decrease of anthropogenic emissions of gaseous precursors (Asmi et al., 2012). In contrast, Dal Maso et al. (2005) observed how the frequency of NPF events increased from 1998 to 2003 in the Finnish boreal forest.

Long-term studies ( $\geq 1$  yr) on NPF, which include the determination of the new particle formation rate (FR) and growth rate (GR), at mountain sites that reach the free troposphere are scarce (Fig. 1; see also Kulmala et al., 2004). These long-term studies have mostly been performed in the continental boundary layer (e.g. Birmili and Wiedensohler, 2000; Dal Maso et al., 2005; Hamed et al., 2007). Studies of NPF at mountain sites are of interest for several reasons. Because mountain upslope winds are frequently linked to high ultrafine particle concentrations (Weber et al., 1995; Venzac et al., 2008), elevated mounts may act as source regions for new particles in the free troposphere (FT), where these grown particles may experience long-range transport due to the much higher wind speeds and the longer lifetime of particles than in the boundary layer.

The objective of this work is to study the origin and processes that influence the NPF at high altitude in the subtropical North Atlantic. We analysed and interpreted the variability in the NPF frequency, growth rates and formation rates, and estimated the contribution of sulfuric acid to particle growth. As the study region is within the Saharan Air Layer

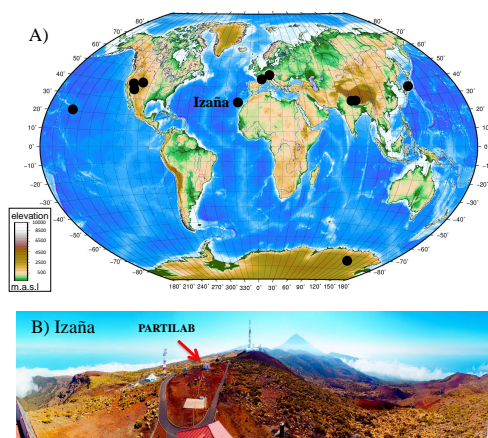


**Fig. 1.** (A) Global map highlighting the location of Izaña and of other high-altitude observatories where studies on NPF have been performed. From west to east: Mauna Loa, Hawaii (3400 m.a.s.l.; Weber et al., 1995, 1999); Storm Peak Laboratory, Colorado (3210 m.a.s.l.; Hallar et al., 2011); Mount Lemmon, Arizona (2700 m.a.s.l.; Shaw et al., 2007); Rocky Mountains, Colorado (2900 m.a.s.l.; Boy et al., 2008); Izaña, Tenerife (2373 m.a.s.l.; this study); Puy de Dôme, France (1465 m.a.s.l.; Venzac et al., 2007; Boulon et al., 2011); Jungfrauoch, Swiss Alps (3580 m.a.s.l.; Boulon et al., 2010); Mukteshwar, Indian Himalayas (2180 m.a.s.l.; Neitola et al., 2011); Pyramid, Nepal (5079 m.a.s.l.; Venzac et al., 2008); Norikura, Japan (2770 m.a.s.l.; Nishita et al., 2008); and Dome C, Antarctica (3200 m.a.s.l.; Järvinen et al., 2013). (B) View of the PARTILAB (particles laboratory) from the Izaña observatory main building.

in summer, we also investigated how dust particles may influence NPF.

## 2 Methodology

### 2.1 Study area

Izaña Global Atmosphere Watch (GAW) observatory ( $16^{\circ}29'58''$  W,  $28^{\circ}18'32''$  N) is located in Tenerife island, at 2373 m a.s.l (Fig. 1a). The observatory (Fig. 1b) remains almost permanently above the marine stratocumulus layer typical of the subtropical oceans. NW dry subsiding airflows dominate throughout the year except in summer, when they are frequently alternated with SE airflows from North Africa. Below the stratocumulus layer, the humid and cool NNE trade winds dominate. The development of orographic thermal-buoyant upward flows during daytime results in the upward transport of water vapour and trace gases emitted at low altitudes by biogenic and anthropogenic sources (see details in Rodríguez et al., 2009).

## 2.2 Measurements

This study is based on a 4 yr data set (June 2008–June 2012) of particle size distributions (10–600 nm), reactive gases ( $\text{SO}_2$ ,  $\text{NO}_x$ ,  $\text{O}_3$ ), meteorological parameters (temperature, humidity, water vapour, wind speed, wind direction) and radiation (global, direct, diffuse, UV-B, UV-A).

### 2.2.1 Particle size distribution

Particle size distribution within the range 10–600 nm was measured with a TSI<sup>TM</sup> Scanning Mobility Particle Sizer (SMPS, model 3996). Two different condensation particle counters (CPCs) were used as detectors: a CPC-3025A from June 2008 to March 2009 and a CPC-3010 from March 2009 on. These instruments have been subjected to several quality assurance and quality control activities. The 50 % efficiency diameters ( $\text{Dp}_{50}$ ) were determined in the World Calibration Centre for Aerosol Physics (WCCAP, Institute for Tropospheric Research, Leipzig, Germany): 2.4 nm for the CPC-3025A unit (SN: 1160; September 2002) and 9.6 nm for the CPC-3010 unit (SN: 70431239; September 2011). The SMPS was intercompared, measuring ambient air aerosol, with similar TSI<sup>TM</sup> SMPS instruments in April 2010 and November 2012 within the REDMAAS network ([www.redmaas.com](http://www.redmaas.com); Gómez-Moreno et al., 2013). In these exercises the sizing accuracy was also assessed with monodisperse polystyrene latex spheres of 80 and 190 nm; a discrepancy of  $-1$  and  $-1.2$  % was found, respectively. During the regular operations at Izaña, the SMPS is subject to weekly checks of aerosol and sheath airflows, zeroes and leak tests using absolute filters.

At Izaña, the aerosol instrumentation (SMPS and other devices) is located in a 6 m-high building called PARTILAB (particles laboratory; Fig. 1b), where the indoor temperature is set to 20 °C. Temperature, relative humidity (RH) and pressure are monitored in the aerosol flow (stretch of sampling pipe into the building, just before the aerosol monitors) and in the outdoor ambient air. Temperature and RH in the aerosol flow and in the outdoor ambient air are shown in Fig. 2. Outdoor ambient RH is usually low (70th percentile is  $\sim 40$  % for hourly annual data). Because of the higher indoor temperature, the RH in the sample is usually much lower, within the range 10–25 % (25th–75th percentiles for annual hourly data). Thus, dry aerosol measurements are performed without using any system for reducing RH (membrane/nafiion driers, or dilutors).

The SMPS data availability is 74 % for the study period (June 2008–June 2012). Non-valid data were flagged and not analysed. Correction for diffusion losses in the sampling pipe and inside the SMPS was applied (Hinds, 1999).

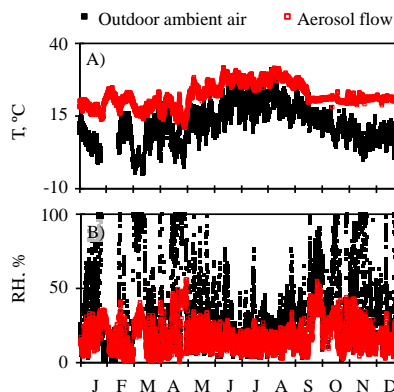


**Fig. 2.** Hourly mean values of temperature and relative humidity in the outdoor ambient air and in the aerosol flow of the SMPS during 2011.

### 2.2.2 Reactive gases and dust

Reactive gases were measured using different principle of measurements: UV fluorescence analyser for  $\text{SO}_2$  (Thermo<sup>TM</sup>, model 43C-TL), UV absorption for  $\text{O}_3$  (Thermo<sup>TM</sup>, model 49C) and chemiluminescence for  $\text{NO}$ ,  $\text{NO}_2$  and  $\text{NO}_x$  (Thermo<sup>TM</sup>, model 42C-TL). In order to avoid the  $\text{NO}_2$  overestimation linked to the use of molybdenum converters, a photolytic  $\text{NO}_2$  to  $\text{NO}$  converter was used (Parish and Fehsenfeld, 2000; Steinbacher et al., 2007). Quality assurance and quality control activities included (i) 15 min zero measurements, performed every 24 h in the  $\text{SO}_2$  and  $\text{O}_3$  and every 6 h in the  $\text{NO}_x$  analysers; (ii) the use of linear fittings between consecutive zeros for applying zero correction to data; (iii) five-point span calibrations every 3 months with certified  $\text{SO}_2$  and  $\text{NO}_x$  concentrations; and (iv) calibration of the  $\text{O}_3$  analyser versus an  $\text{O}_3$  primary standard (49C PS). A high linearity was commonly observed in these calibrations ( $r^2 \sim 0.999$ ). Detection limit is 60 ppt for  $\text{SO}_2$ , 50 ppt for  $\text{NO}$  and  $\text{NO}_x$  (5 min average) and 1 ppb for  $\text{O}_3$  (1 min average).

As Izaña is within the Saharan Air Layer in summer, the measurement programme includes (1) size distributions with the Aerodynamic Particle Sizer (APS, TSI<sup>TM</sup>) for the range 0.7–20  $\mu\text{m}$  aerodynamic diameter ( $\sim 0.7$ –12  $\mu\text{m}$  geometric diameter for dust) and (2) dust concentrations with the methods described by Rodríguez et al. (2011).

### 2.2.3 Radiation

The Izaña observatory has been part of the Baseline Surface Radiation Network (BSRN) since 2009 (García, 2011). We used short-wave downward radiation (SDR) irradiance (global, direct and diffuse), and UV-A and UV-B measurements. The global and diffuse SDRs were measured with

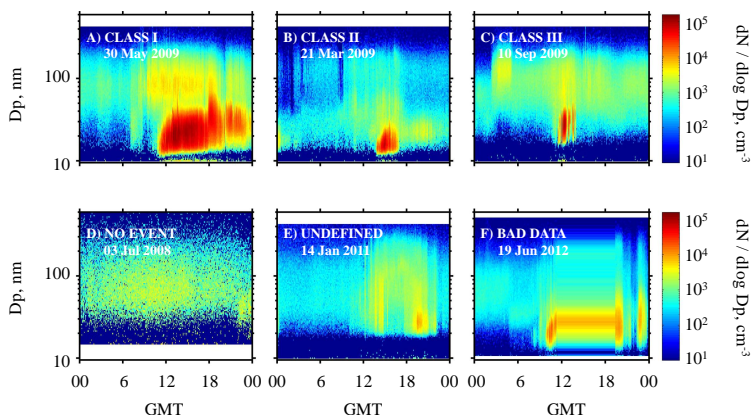


Fig. 3. Examples of type of events and cases identified in the data analysis.

unshaded and shaded Kipp & Zonen CM-21 pyranometers, respectively. The spectral range covers 335–2200 nm (95 % points), and the expected uncertainty is  $\pm 2\%$  for hourly totals. The direct SDR is measured with a Kipp & Zonen CH1 pyrheliometer, with a field of view limited to  $5^\circ \pm 0.2^\circ$ , placed on a sun tracker with a tracking accuracy of  $0.1^\circ$ . The spectral range goes from 200 to 4000 nm (50 % points), and the uncertainty of this measurement is  $\pm 2\%$  for hourly totals. The UV-A is measured with Kipp & Zonen UVS-A-T radiometer. The spectral range covers 315–400 nm with daily uncertainty lower than 5 %. The UV-B is measured with Yankee Environmental System (YES) UV-B-1 pyranometer. The spectral range goes from 280 to 320 nm. All radiation parameters are measured with 1 min resolution.

## 2.2.4 Meteorology

Meteorological parameters were measured using a Setra 470 instrument for pressure, a Rotronic for temperature and relative humidity, and a Thies sonic anemometer for wind. Concentrations of water vapour were calculated with the Magnus equation. Vertical wind was only recorded from June 2011 to October 2011.

## 2.3 Characterization of NPF events

### 2.3.1 Classification of events

Daily aerosol number size distribution plots were visually analysed for identifying the “banana-type” NPF events (Dal Maso et al., 2005). Seven types of events were considered (Table 1 and Fig. 3). In events class I and II a clear particle formation and growth was observed for at least 4 and 2 h, respectively. In class III events no particle growth was observed after the particle burst (apple-type events; Yli-Juuti et

al., 2009). The remaining data were sorted as follows: non-event (no increase in the concentration of particles < 25 nm was observed), undefined (event was not clearly observed) or bad data (invalid or missing data).

### 2.3.2 Determination of formation (FR) and growth rate (GR)

We attempted to determine the FR and GR for all class I events. However, this was not possible for a set of episodes in which a noisy signal was observed, mostly induced by a significant variability in the horizontal and/or vertical components of wind. Thus, events in which the FR and GR could be determined were sub-classified as class Ia; the remaining events were labelled as class Ib (Table 1).

The FR ( $J_D$ ) and GR were calculated for the nucleation mode particles ( $D_p < 25$  nm) using equations described by Kulmala et al. (2012):

$$J_D = \frac{\Delta N_{D_p, D_{p_{\max}}}}{\Delta t} + \text{CoagS}_{D_p} \cdot N_{D_p} + \frac{\text{GR}}{\Delta D_p} \cdot N_{D_p} + S_{\text{losses}}, \quad (1)$$

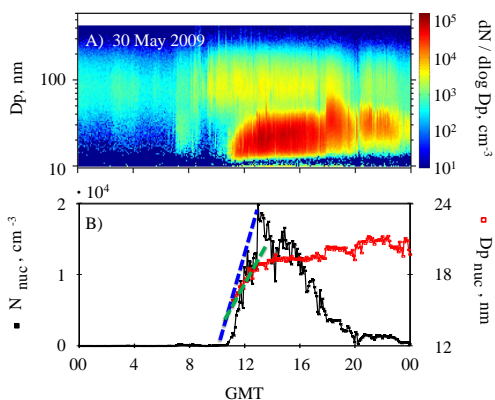
where the first term is the slope obtained from the first-order polynomial fitting during the episode when representing the nucleation mode particle concentration as a function of time (Fig. 4).  $\text{CoagS}$  is the coagulation of particles in the size range  $[D_p, D_{p_{\max}}]$ .  $D_{p_{\max}}$  is the maximum size that the critical clusters may reach because of their growth during  $\Delta t$  (GR).  $S_{\text{losses}}$  takes into account additional losses, neglected in this study. Similarly,

$$\text{GR} = \frac{dD_{p_m}}{dt} = \frac{\Delta D_{p_m}}{\Delta t}, \quad (2)$$

where  $D_{p_m}$  belongs to the size range  $[D_p, D_{p_{\max}}]$ . GR is the slope obtained from the first-order polynomial fitting during

**Table 1.** Type of events considered in this study. FR: formation rate. GR: growth rate.

Type	Criteria
Class Ia (banana type)	A new mode with growing mean diameter under 25 nm is observed. The growth is observed during at least 4 h. FR and GR can be calculated.
Class Ib (banana type)	A new mode with growing mean diameter under 25 nm is observed. The growth is observed during at least 4 h, but FR and GR could not be calculated.
Class II (short banana type)	A new mode with growing mean diameter under 25 nm is observed. The growth period lasts from 2 to 4 h.
Class III (apple/burst)	A new mode with growing mean diameter under 25 nm is observed. The growth period is lower than 2 h.
Non-event	No new particle mode with mean diameter under 25 nm is observed.
Undefined	Event is not clearly observed.
Bad data	Missing or invalid data.

**Fig. 4.** Example of type Ia event. (A) Time evolution of the particle size distribution of the number of nucleation particles and (B) of the geometric mean diameter for the nucleation mode. Lines illustrate the fitting that are performed for determining the formation and growth rates.

the episode when representing the nucleation mode geometric mean diameter as a function of time (Fig. 4). The FR and GR were determined using Eqs. (1) and (2) in two different approaches.

#### Method 1: SMPS data

The FR and GR were determined for the nucleation mode particles ( $D_p < 25$  nm) using the number concentration ( $N_{\text{nuc}}$ ; Dal Maso et al., 2005) and the geometric mean diameter (GMD,  $D_{p,\text{nuc}}$ ; Järvinen et al., 2013) of the 5 min resolution SMPS data. We used the GMD to avoid the human bias associated with other methods such as visual determination

of the mode size change. Figure 4b shows an illustration of the linear fittings used for determining the slopes FR (Eq. 1) and GR (Eq. 2).

#### Method 2: lognormal size distribution

This method was implemented in two steps. First, each 5 min average size distribution was fitted to a linear combination of lognormal distributions:

$$\frac{dN}{d \ln Dp} = \sum_{(i=1)}^n \frac{N_i}{\sqrt{2\pi \ln \sigma_{(g,i)}}} \exp\left(-\frac{(\ln Dp - \ln D_{p(g,i)})^2}{2 \ln^2 \sigma_{(g,i)}}\right). \quad (3)$$

Each lognormal distribution is characterized by three parameters: mean number concentration  $N_i$ , geometric variance  $\sigma_{(g,i)}^2$  and the geometric mean diameter  $D_{p(g,i)}$ . The fitting procedure was performed in a script programmed in Matlab™. The fitting accuracy was assessed by the least squares quadratic (LSQ) value between the measured particle number size distribution and its fitting. This method is usually applied considering a single nucleation mode ( $< 25$  nm), e.g. by Boy et al. (2008); Dal Maso et al. (2005); Salma et al. (2011); Yli-Juuti et al. (2009). However, we observed that, in many cases, the LSQ value was significantly reduced if the nucleation mode was fitted with 2 lognormal fittings instead of 1. In many cases a simple visual analysis of the 5 min size distributions evidenced that the nucleation mode growth was prompted by one of these lognormal distribution. In the second step, GR was determined using Eq. (2).

#### 2.3.3 Determination of event parameters

In order to quantify the contribution of  $\text{H}_2\text{SO}_4$  to particle growth, we determined the following parameters: condensation sink (CS) and coagulation sink (CoagS) for each size

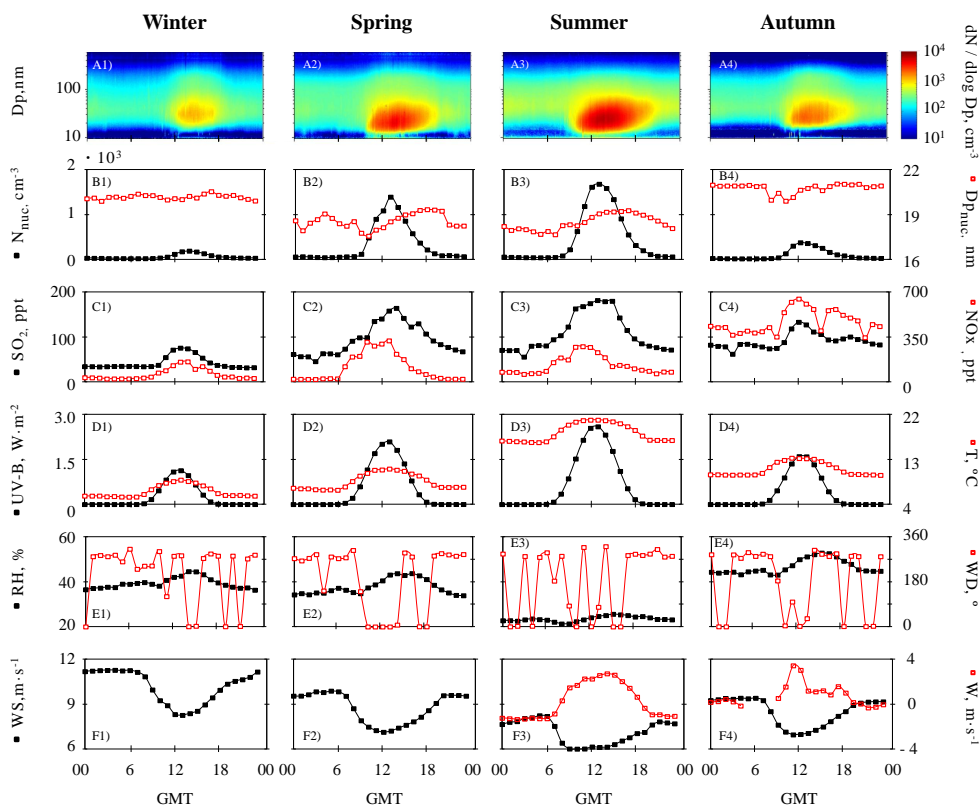


**Fig. 5.** Daily evolution (hourly mean values) per season of (A) aerosol particle number size distribution, (B) nucleation mode particle concentrations ( $N_{\text{nuc}}$ ) and the geometric mean diameter ( $D_{\text{p,nuc}}$ ), (C)  $\text{SO}_2$  and  $\text{NO}_x$ , (D) UV-B and temperature ( $T$ ), (E) relative humidity (RH) and wind direction (WD), and (F) horizontal wind (WS) and vertical (W) wind.

distribution (Kulmala et al., 2012); and concentration of condensable vapour ( $C_v$ ) and its source rate ( $Q$ ) (Dal Maso et al., 2005). For estimating concentrations of  $\text{H}_2\text{SO}_4$  by the proxy of Petäjä et al. (2009), we used experimental data of  $\text{SO}_2$  and UV-B radiation at Izaña with Hyytiälä's parameters ( $k = 9.9 \times 10^{-7} \text{ m}^2 \text{ W}^{-1} \text{ s}^{-1}$ ); the use of this value for  $k$  instead of the actual (unknown) value at Izaña could have an influence on the absolute value of the  $\text{H}_2\text{SO}_4$  concentration, but not the correlations. This proxy and the  $C_v$  equation were used to calculate the theoretical growth rate due to sulfuric acid ( $\text{GR}_{\text{SA}}$ ) (Nieminen et al., 2010).

### 3 Results and discussion

#### 3.1 Upward transport of particle precursors

The daily evolution (hourly mean values throughout the day) of the particle size distribution, particle concentration and geometric mean diameter of the nucleation mode,  $\text{SO}_2$ ,  $\text{NO}_x$ , UV-B radiation and some meteorological parameters, averaged for each season is shown in Fig. 5. At Izaña, the number of particles exhibits strongly marked daily cycles, with much higher values during daytime than at night (Fig. 5b). This daytime increase is associated with a parallel increment in the RH and in the concentrations of  $\text{SO}_2$ ,  $\text{NO}_x$  and RH, which is prompted by the arrival of air from lower altitudes due to the development of orographic buoyant upward flows. The influence of these upward airflows on the concentrations

**Table 2.** Total number and percentage of events observed from June 2008 to June 2012.

Event type	Number of events	%
Class Ia	109	9.3
Class Ib	26	2.2
Class II	227	19.3
Class III	101	8.6
Non-event	514	43.6
Undefined	50	4.2
Bad data	151	12.8
Total days	1178	100.0

of precursors and nanoparticles ( $< 10$  nm) at Izaña was previously described in detail by Rodríguez et al. (2009). These upward airflows were also observed in other mountain observatories located on islands, such as Pico in Azores (Kleissl et al., 2007) and Mauna Loa in Hawaii (Weber et al., 1995, 1999). This ascent of air masses tends to occur during daytime linked to the heating of the terrain (Fig. 5F3 and F4). Previous studies at Mauna Loa and Izaña concluded that NPF is favoured in the boundary layer to the free troposphere transition region due to the low surface area of pre-existing particles (prompted by in-cloud particle scavenging), the high solar radiation conditions above the marine cloud layer and the gaseous precursor supply by the upward flows.

The high frequency of NPF events at Izaña results in a strongly marked daily cycle in the mean particle size distributions (Fig. 5a and b); after the increase in the number of particles  $< 25$  nm (hereinafter so-called nucleation particles,  $N_{\text{nuc}}$ ) typically observed between 10:30 and 13:30 GMT (depending on the season), a progressive increase in the geometric mean diameter is observed, in some cases even until the evening. These observations indicate that formation and growth of new particles  $> 10$  nm tend to occur during the daytime upward flow period. This evidences that the nanoparticles ( $< 10$  nm) observed by Rodríguez et al. (2009) at Izaña frequently grow up to reach higher and stable diameters.

### 3.2 Classification of episodes

A total of 1178 days were classified in the study period (June 2008 to June 2012). The distribution of these events among the seven considered categories is shown in Table 2. Figure 6 shows the monthly distribution of episodes. Events in which a burst of nucleation particles ( $< 25$  nm) followed by particle growth (banana events) was observed during at least 2 h (type Ia + Ib + II; examples in Fig. 3) accounted for  $\sim 30\%$  of the 4 yr observations. Events with a duration longer than 4 h ( $I = \text{Ia} + \text{Ib}$ ) accounted for  $\sim 11\%$  of the days. These banana events ( $I + \text{II}$ ) mostly occurred from May to October, when they accounted for more than 30% of the days of each month (Fig. 6a). The frequency of these

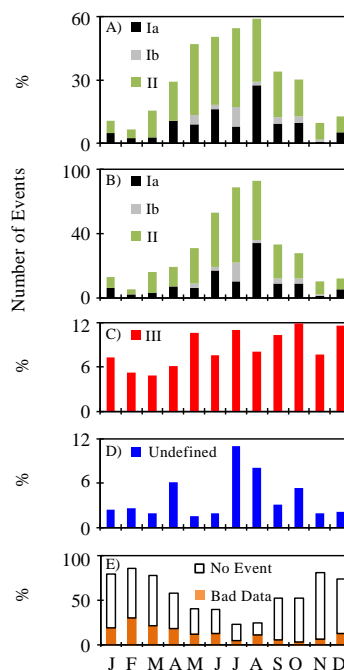


**Fig. 6.** (A, and C–E) Number of days per month (%) in which each event (Ia, Ib, II, III, undefined, non-event and bad data) was observed. (B) Accumulated number of days (for the period 2008–2012) in which an event (Ia, Ib and II) was observed in each month.

events was at a maximum from June to August, when they accounted for 50–60% of the days per month (Fig. 6a). In each of these months, the accumulated number of events observed during the 4 study years was 50–75 (Fig. 6b). Events type III (burst of nucleation particles not followed by particle growth, also so-called apple-type events) occurred throughout the year, with a frequency within the range 5–12%, without any significant seasonal behaviour (Fig. 6c). This indicates that although the formation of nucleation particles occurs throughout the different seasons (Fig. 6c), conditions for the particle growth mostly occur from May to October (Fig. 6a and b). Undefined events showed a higher frequency in July–August (Fig. 6d), whereas non-events mostly occurred from November to March (Fig. 6d).

The percentage of event days ( $I + \text{II}$ ) we observed ( $\sim 30\%$ ; Table 2) is somewhat lower than that observed at 3210 m a.s.l. on the summit of Mount Werner in North America ( $\sim 50\%$ ; Hallar et al., 2011), at 5079 m a.s.l. in the Nepal Himalayas ( $\sim 43\%$ ; Venzac et al., 2008) and in Puy de Dôme ( $\sim 38\%$ ; Manninen et al., 2010), but higher than those observed at 2180 m a.s.l. in the Indian Himalayas ( $\sim 11\%$ ;

Neitola et al., 2011) and at 3580 m a.s.l. in the Swiss Alps ( $\sim 20\%$ ; Jungfraujoch; Boulon et al., 2010; Manninen et al., 2010).

At Izaña site, the NPF season occurs from May to August, when events (I+II) present a frequency of  $\sim 50\%$  (Fig. 6a). At Jungfraujoch these events occur from the end of spring to early autumn ( $\sim 25\%$  frequency during the season) as well, linked to the transport of precursors from the boundary layer (Boulon et al., 2010; Manninen et al., 2010). In the European continental boundary layer, these events are mostly observed in spring (Dal Maso et al., 2005; Hamed et al., 2007; Manninen et al., 2010), although in NW Italy they were mostly observed in autumn linked to specific north foehn meteorological conditions (Rodríguez et al., 2005). In Puy de Dôme mount the maximum frequency of events was found during early spring and early autumn (Boulon et al., 2011). In the Nepal Himalayas these events were observed in the monsoon (July–September) and post-monsoon (October–December) seasons ( $\sim 50\%$ ), whereas in the Indian Himalayas they occur in spring ( $\sim 80\%$  from March to June; Neitola et al., 2011). In the upper plateau of East Antarctica, Järvinen et al. (2013) reported that these events take place more often during summer.

### 3.3 Formation and growth rates of new particles

Figure 7 shows the monthly averages of the formation rates (FRs), growth rates (GRs) and other parameters during NPF events at Izaña from June 2008 to June 2012. As already described above, the FRs and GRs of the nucleation particles ( $< 25$  nm) could only be calculated for a set of events class I, which were labelled as class Ia. These determinations were performed for a total of 109 Ia events using the method 1 described in Sect. 2.3.2. At Izaña, NPF class Ia events (a) exhibit higher monthly averaged FR from April to September ( $0.43\text{--}0.92\text{ cm}^{-3}\text{ s}^{-1}$ ) than from October to March ( $0.19\text{--}0.27\text{ cm}^{-3}\text{ s}^{-1}$ ; Fig. 7a), (b) show slightly higher GR from April to July ( $0.48\text{--}0.58\text{ nm h}^{-1}$ ) than from August to March ( $0.26\text{--}0.44\text{ nm h}^{-1}$ ; Fig. 7b), and (c) are longer from April to October (6–7 h) than from November to March (5–6 h; Fig. 7c). This shift in the duration is also associated with a shift in the starting and ending time of the events, clearly linked with the seasonal shift in the daytime length (Fig. 7d).

Mean values of FR and GR at Izaña were compared with those observed at other mountain sites (Table 3). Unfortunately, because of the lack of long-term studies, just mean values (and not seasonal behaviour) could be compared in most of the cases. GRs at Izaña and Mauna Loa are quite similar ( $\sim 0.4\text{ nm h}^{-1}$ ). These are significantly lower than those observed in mountains located in continental areas ( $2\text{--}12\text{ nm h}^{-1}$ ), where the higher regional emission of gaseous precursors and the enhanced vertical transport over the continental platform may account for the significantly higher GRs. FRs at Izaña and Mauna Loa are also similar; however, the low number of reported observations at mountain sites does

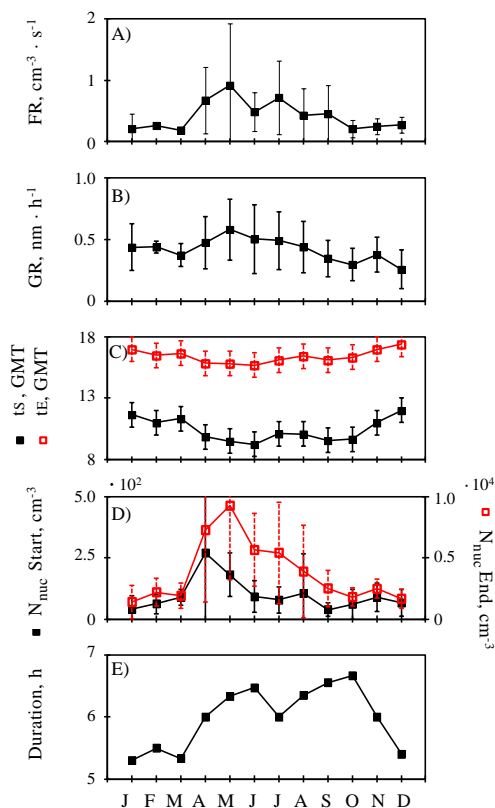


**Fig. 7.** Monthly mean  $\pm$  standard deviation values, during Ia episodes, of (A) formation rates (FRs), (B) growth rates (GRs), (C) start ( $t_s$ ) and end ( $t_e$ ) time of the events, (D) nucleation particle concentration at the start ( $N_{\text{nuc start}}$ ) and burst peak of the event ( $N_{\text{nuc end}}$ ), and (E) duration of events.

not allow reaching any conclusion about differences between remote islands and continental areas. The amplitude of the seasonal variation of the FR at Izaña (min:  $0.19\text{ cm}^{-3}\text{ s}^{-1}$ ; max:  $0.92\text{ cm}^{-3}\text{ s}^{-1}$ ) is higher than that observed at Pyramid, Himalayas (min:  $0.14\text{ cm}^{-3}\text{ s}^{-1}$ ; max:  $0.20\text{ cm}^{-3}\text{ s}^{-1}$ ; Venzac et al., 2008), with max-FR to min-FR ratios equal to 4.7 at Izaña and 1.4 at Pyramid, Himalayas.

### 3.4 Context during NPF events

#### 3.4.1 Type Ia events

In order to identify the parameters that influence, the NPF a set of analyses were performed. Mean values of the reactive

**Table 3.** Values of formation rates and growth rates observed in this and in other studies at mountain sites. Footnotes indicate the references.

Mount/ observatory	FR, $\text{cm}^{-3} \text{s}^{-1}$	Size range	GR, $\text{nm h}^{-1}$	Size range	$\text{CS} \times 10^{-3}$ , $\text{s}^{-1}$	$\text{Cv} \times 10^7$ , $\text{molecules cm}^{-3}$	$Q \times 10^5$ , $\text{molecules cm}^{-3} \text{s}^{-1}$	Region	Altitude, m a.s.l.
Izaña	$0.46 \pm 0.57^1$	10–25 nm	$0.43 \pm 0.21^1$	10–25 nm	$1.55^1$	$0.6^1$	$0.095^1$	Atlantic Ocean	2400
Mauna Loa	$0.50 \pm \text{N/A}^{2a}$	3–10 nm	$0.40 \pm \text{N/A}^{2b}$	3–10 nm				Pacific Ocean	3400
Jungfraujoch	$0.90 \pm \text{N/A}^{3a}$	2–3 nm	$6.00 \pm \text{N/A}^{3a,3b}$	7–20 nm	$0.29^{3b}$		$0.051^{3b}$	Europe	3580
Puy de Dôme	$1.38 \pm 0.20^{4a}$	2–3 nm	$6.20 \pm 0.12^{4a}$	1.3–20 nm	$5.80^{4b}$			Europe	1465
Pyramid	$0.18 \pm \text{N/A}^5$	10–20 nm						Asia, Everest	5079
Mukteshwar	$0.40 \pm \text{N/A}^6$	15–20 nm	$2.43 \pm \text{N/A}^6$	15–20 nm	$7.30^6$			Asia, Himalaya	2180
Norikura			$2.85 \pm \text{N/A}^7$	10–20 nm	$2.00^7$	$2-3^7$	$0.1-1^7$	Asia, Japan	2770
Mount Lemmon			$12.00 \pm \text{N/A}^8$	> 16 nm		$1-10^8$	$1-10^8$	North America	2790
Rocky Mountains Storm Peak Laboratory	$7.47 \pm 5.1^{10}$	6–10 nm	$0.65 \pm 0.14^{10}$	> 8 nm	$1.20^{10}$			North America	2900
Dome C	$0.023 \pm \text{N/A}^{11}$	10–25 nm	$2.50 \pm \text{N/A}^{11}$	10–25 nm	$0.18^{11}$	$5.7^{11}$		Antarctica	3200

<sup>1</sup> this study; <sup>2a</sup> Weber et al. (1999); <sup>2b</sup> Weber et al. (1995); <sup>3a</sup> Manninen et al. (2010); <sup>3b</sup> Boulon et al. (2010); <sup>4a</sup> Boulon et al. (2011); <sup>4b</sup> Venzac et al. (2007); <sup>5</sup> Venzac et al. (2008); <sup>6</sup> Neitola et al. (2011); <sup>7</sup> Nishita et al. (2008); <sup>8</sup> Shaw (2007); <sup>9</sup> Boy et al. (2008); <sup>10</sup> Hallar et al. (2011); <sup>11</sup> Järvinen et al. (2013).

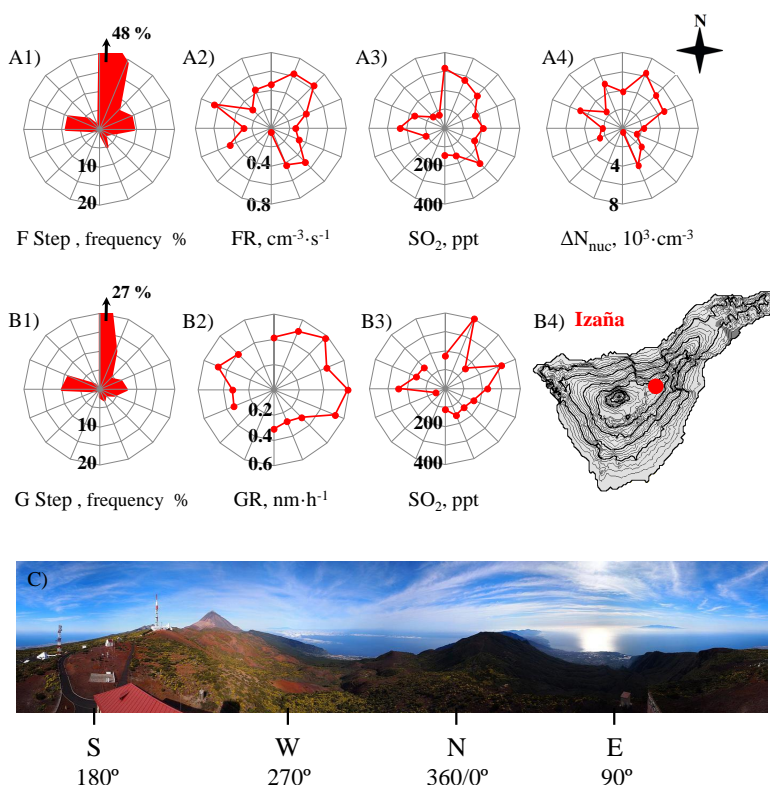


**Fig. 8.** Wind rose for formation step parameters ((A) frequency, formation rates,  $\text{SO}_2$  and nucleation particles concentration) and for growth step parameters ((B) frequency, growth rates and  $\text{SO}_2$  concentration). (B4) Topographic map of Tenerife. (C) 360° view from Izaña observatory.

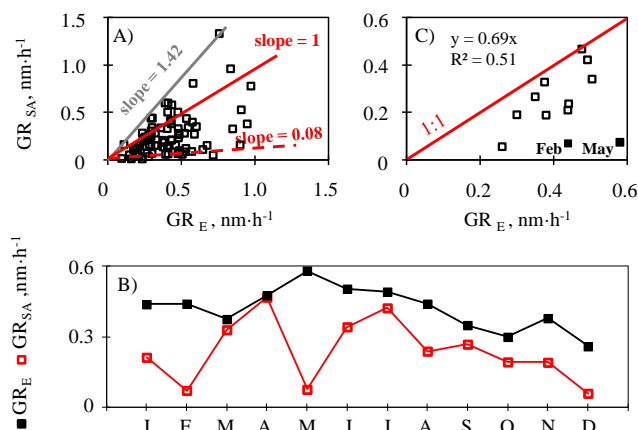


**Fig. 9.** (A) Growth rates of sulfuric acid ( $GR_{SA}$ ) versus experimental growth rates ( $GR_E$ ) in type Ia events. (B) Time series of monthly mean values of  $GR_{SA}$  and  $GR_E$ . (C) Monthly mean values of  $GR_{SA}$  versus  $GR_E$  in type Ia events; fitting was performed excluding February and May.

**Table 4.** Mean values of a set of parameters in three different periods: (a) from 11:00–16:00 GMT for days with no particle formation (non-events), (b) during the formation (*F*) of the nucleation mode particles step in the NPF episodes, (c) during the particle growth (*G*) step in the NPF episodes. Ratios of the mean “*F* step to non-events” data, and of “*G* step to non-events”. Ratios > 1.2 are highlighted in italic.

Parameter	(a) Non-events, mean	(b) <i>F</i> step, mean	(c) <i>G</i> step, mean	<i>F</i> step, ratio	<i>G</i> step, ratio
Ozone (ppb)	43.3	42.3	42.9	1.0	1.0
SO <sub>2</sub> (ppt)	83.2	238.3	233.7	2.9	2.8
NO <sub>x</sub> (ppt)	317.9	204.0	196.7	0.6	0.6
Global (W m <sup>-2</sup> )	719.2	881.5	833.1	1.2	1.2
Diffuse (W m <sup>-2</sup> )	796.1	940.4	884.0	1.2	1.1
Direct (W m <sup>-2</sup> )	160.2	128.4	129.5	0.8	0.8
UV-B (W m <sup>-2</sup> )	1.2	1.7	1.6	1.4	1.3
UV-A (W m <sup>-2</sup> )	46.2	56.3	53.4	1.2	1.2
<i>T</i> (°C)	10.9	18.4	18.1	1.7	1.7
Relative humidity (%)	44.8	29.2	32.0	0.7	0.7
Water vapour (g cm <sup>-3</sup> )	3.2	2.8	3.1	0.9	1.0
Wind speed (m s <sup>-1</sup> )	8.9	4.6	4.7	0.5	0.5
Wind <i>X</i> component (m s <sup>-1</sup> )	2.6	0.8	1.1	0.3	0.4
Wind <i>Y</i> component (m s <sup>-1</sup> )	-4.2	0.0	-0.4	0.0	0.1
Vertical wind (m s <sup>-1</sup> )	0.8	2.7	3.2	3.5	4.3

gases (SO<sub>2</sub>, NO<sub>x</sub> and O<sub>3</sub>), dust concentrations, radiation components (global, diffuse, direct, UV-A and UV-B) and meteorological parameters (*T*, RH, water vapour, wind vector components, speed and direction) were determined during the two steps of each NPF episode: (1) step 1 – formation of the nucleation particles and (2) step 2 – subsequent particle growth. These determinations were performed for the 109 events of type Ia. The resulting database was then subjected to different analysis (Tables 4 and 5; Figs. 8–12).

Table 4 shows the ratios of the mean value of each parameter during the formation (*F*) and growth (*G*) steps to the average value at Izaña for non-event days from 11:00 to 16:00 GMT. The same parameters show high ratios (> 1.2) during the formation and during the growth steps: sulfur dioxide (2.9–2.8), vertical wind component (3.5–4.3) and UV-B (1.4–1.3) radiation. This supports the idea that upward transport of sulfur dioxide (from the boundary layer) and its

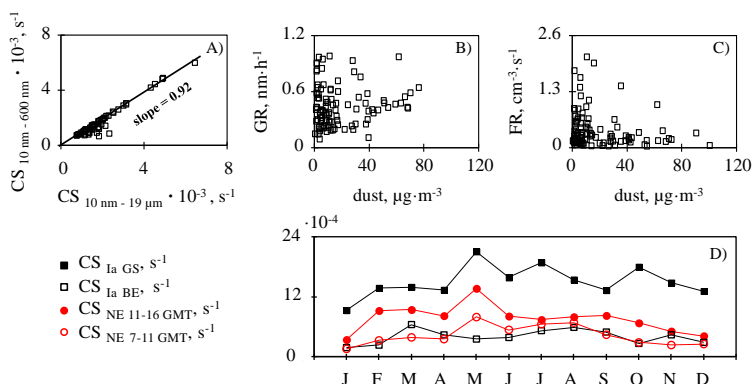


**Fig. 10.** (A)  $CS_{10-600\text{ nm}}$  versus  $CS_{10\text{ nm}-19\text{ }\mu\text{m}}$ , (B–C) Scatter plots of the formation rates (FR) and growth rates (GR) versus dust concentration at Izaña during the NPF events (type Ia), (D) comparative analysis of the CS during NPF events and during non-events. Monthly means of CS during two stages of the NPF event: (i) at the start of the NPF and (ii) during the growth step. Similarly, it is shown at two periods during non-events: (i) 07:00–11:00 GMT (~ start time during NPF) and (ii) 11:00–16:00 GMT (~ typical time of the growth step during NPF).

further photo-oxidation by UV radiation is a key process in the NPF.

Mean values of the study parameters during the formation and growth steps were plotted against wind direction (Fig. 8). Most of the formation step and growth step in the events occur under northern (N–NNE) wind conditions (~ 50 % for *F* and 27 % for *G* steps, respectively) and secondarily under eastern (ENE–E) and western (WNW–W) winds (~ 10 % for both directions; Fig. 8A2 and B2).

The highest FRs and GRs are observed when air blows from the eastern side ( $0-180^\circ$ ), which is the sector associated with the highest  $SO_2$  concentrations (Fig. 8A3 and B3). This precursor also influences the number of nucleation particles formed during the formation step ( $\Delta N_{\text{nuc}}$ ); the highest concentrations are recorded during NE winds (Fig. 8A4).

Different studies in mountain sites show the same behaviour for  $SO_2$  (Boy et al., 2008), radiation (Boulon et al., 2010; Salma et al., 2011; Venzac et al., 2008),  $O_3$  (Hallar et al., 2011) and relative humidity (Boy et al., 2008) when evaluating event and non-event days. In the boundary layer, in the Po Valley (northern Italy), Hamed et al. (2007) observed that temperature, wind speed, solar radiation,  $SO_2$  and  $O_3$  concentrations were on average higher on nucleation days than on non-event days, whereas relative humidity and  $NO_2$  concentration were lower. These conditions are similar to those we observed at Izaña, except for wind speed and ozone (Table 4). At Izaña, a moderate correlation between the concentration of nucleation particles with ozone was observed only in spring, when biogenic emissions tend to increase. Oxidation products of biogenic volatile organic com-

pounds could also take part in the growth processes (Held et al., 2004; Yli-Juuti et al., 2011).

### 3.4.2 Contribution of sulfuric acid to particle growth

The contribution of sulfuric acid to particle growth was estimated for Ia events using the theoretical equations described above. The GR resulting from this sulfuric acid concentration ( $GR_{SA}$ ) is plotted versus the experimental GR ( $GR_E$ ) in Fig. 9a. The whole data set is comprised between two well-defined lines with slopes 0.08 and 1.42. These results show that the sulfuric acid condensation accounts for 8–100 % of the observed GR, depending on the event (Fig. 9a). Time series of monthly mean values of  $GR_E$  and  $GR_{SA}$  are plotted in Fig. 9b. Growth rates of sulfuric acid account for most of the observed growth rates during most of the time. Observe in Fig. 9c how monthly mean values of  $GR_E$  and  $GR_{SA}$  tend to show a high correlation throughout the year. As average,  $GR_{SA}$  accounted for 69 % of  $GR_E$  (Fig. 9c), excluding February and May. In these 2 months,  $GR_{SA}$  accounted for 15 % of  $GR_E$  as average. An interesting behaviour is observed in May, when the highest  $GR_E$  ( $\sim 0.6\text{ nm h}^{-1}$ ) and the lowest contribution of sulfuric acid (13 %) to particle growth were observed (Fig. 9b and c). This strongly suggests a significant involvement of other condensing vapours in this period. Similar conclusions were reached after analysing the particle growth rates in Dome C mount in Antarctica (Järvinen et al., 2013) and in Fichtelgebirge mountains in Germany (Held et al., 2004). A number of studies have shown that oxidation products of monoterpenes may contribute to particle growth (e.g. Held et al., 2004). In Tenerife, these emissions occur in the forest pine that is present between 500 and

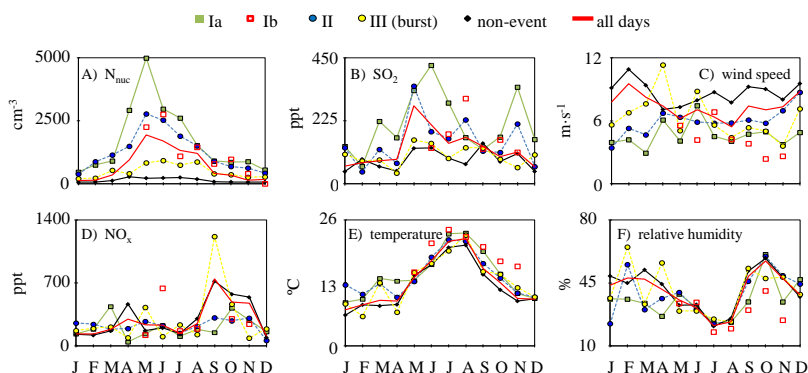


**Fig. 11.** Monthly mean values (calculated with hourly mean values from 11:00 to 16:00 GMT) of a set of parameters during days in which episodes type Ia, Ib, II, III and non-event were registered. Mean values with all days of the months are also included.

2000 m a.s.l. around the island and that affects Izaña during the upward flow diurnal periods.

The variability of the GR depends on the balance between the rate at which condensable vapours are supplied from their source ( $Q$ ) and the rate at which these vapours condense onto pre-existing particles (CS). The larger the degree of CS, the faster new formed nuclei must grow to survive scavenging onto larger pre-existing particles (Kulmala et al., 2004). At Izaña it seems that there is high vapour source rate and low enough CS to allow rather slowly growing nucleation mode to survive to larger sizes (Table 3).

We analysed two specific issues concerning the CS. First, we quantified how the presence of Saharan dust influences the CS. Figure 10a shows the CS calculated for the size range 10–600 nm (SMPS data) versus the CS for the size range 10 nm–12  $\mu\text{m}$  (SMPS + APS data). The contribution of the particles with a geometric diameter 0.7–12  $\mu\text{m}$  (APS range) to the CS is relatively low ( $\sim 8\%$ ). Because of this, the GR vs. CS scatter plot (not shown for the sake of brevity) did not change significantly when the CS included the APS data. This result is consistent with the poor correlation observed between GR and dust concentrations discussed above (Fig. 10b). In contrast, FR shows a significant negative correlation with dust (Fig. 10c). This suggests that Saharan dust may play an important role in scavenging freshly formed nucleation particles. This mechanism could contribute to the observed coating of dust by sulfate in Saharan dust particles emitted in desert regions affected by  $\text{SO}_2$  emissions (Rodríguez et al., 2011).

Second, in order to assess how the condensation of vapours onto pre-existing particles influences NPF, we compared the evolution of CS during NPF events with that during non-events (Fig. 10d). In NPF events, CS at the beginning of the episode is lower than during the growth step. Moreover, CS is

higher during NPF than during non-events in the same period (11:00–16:00 GMT). These results are similar to those observed in other mountain sites such as Jungfrauoch (Boulon et al., 2010) and the Rocky Mountains (Boy et al., 2008). An opposite behaviour has been observed in the continental boundary layer, where condensation onto pre-existing particles and nucleation are competing processes that influence the day-to-day variability in the NPF events (Rodríguez et al., 2005; Hamed et al., 2007). This is not observed in mountain sites due to the low backgrounds of aerosols and vapours.

### 3.4.3 Type Ia versus other type events

The context in which type Ia events occur was compared with that in which the other events (Table 1) occur. For this, the monthly mean value (from 11:00 to 16:00 GMT) of a set of parameters during the different types of events (Ia, Ib, II, III and non-event) was compared with the monthly mean value (from 11:00 to 16:00 GMT) for these parameters (Fig. 11). Some features that differentiate the events are as follows: (a) the highest concentrations of nucleation particles were observed during NPF events (Ia, Ib and II), when  $N_{nuc}$  concentrations are 2–3 times higher than during burst (III) episodes (Fig. 11a), and (b) length of the NPF events seems to be conditioned by  $\text{SO}_2$  availability, which in turn is influenced by wind. Observe how  $\text{SO}_2$  concentrations during events type I (which last at least 4 h) are higher than during events II (which last 2–4 h) and burst episodes (III; Fig. 11b) and how wind speed decreases throughout the sequence of episodes non-event, burst (III) and banana types II and I (Fig. 11c) – a trend opposite to that of  $\text{SO}_2$  (Fig. 11b).

Other features commonly reported for NPF events are also observed at Izaña: (c) except for a few cases, concentrations of  $\text{NO}_x$  tend to be lower during type I banana events

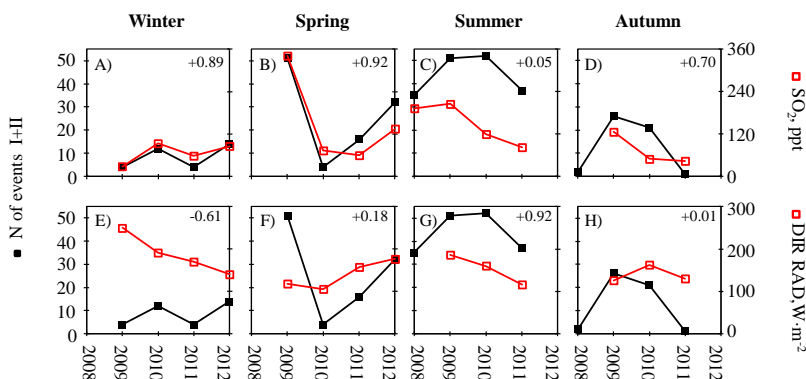


Fig. 12. Number of banana-type events (I + II) and mean values (11:00–16:00 GMT) of  $\text{SO}_2$  and direct radiation per season for the period June 2008–June 2012 at Izaña: winter (Jan–Mar), spring (Apr–Jun), summer (Jul–Sep) and autumn (Oct–Dec).

(Fig. 11d; Boy and Kulmala, 2002; Hamed et al., 2007). (d) Temperature is higher and relative humidity is lower during events type I (Ia + Ib) than monthly mean values and lower than during burst (III) and non-event episodes (Fig. 11e and f; Rodríguez et al., 2005; Hamed et al., 2007). (e) Global, UV-A and UV-B radiation during events type I (banana > 4h) tend to be higher than during the other event types (II, III and non-event; Birmili and Wiedensohler, 2000; Boy and Kulmala, 2002; Hamed et al., 2007; Manninen et al., 2010).

### 3.5 Year-to-year variability

Processes that influence the year-to-year variability of the frequency of each type of episode (Table 1) were studied. For this purpose, the frequency of each type of event was correlated with the reactive gases, condensation sink, sulfuric acid proxy, radiation and meteorological parameters for each season from June 2008 to June 2012. Here we focus just on the key issues for the sake of brevity.

The year-to-year variability in the the frequency of NPF events (I + II) for each season, for the period 2008–2012, showed the highest correlation with  $\text{SO}_2$ . The correlation was higher from autumn to spring ( $r$ : 0.70–0.92) than in summer ( $r$ : 0.05; Fig. 12a–d). This indicates that other processes apart from transport of precursors influence NPF in summertime. In this season, the number of banana-type events (I + II) exhibited a significant correlation with direct radiation (Fig. 12g), and an evident negative correlation with diffuse radiation (not shown in plots). Because diffuse radiation is dominated by Saharan dust at Izaña (García et al., 2014), direct radiation is indicative of clean (dust free) conditions. This indicates that the presence of dust may influence the year-to-year variability in the NPF frequency. This may occur by two processes: first, reducing the amount of radiation reaching the surface (negative forcing) and, second, acting

as a sink of freshly formed nucleation particles and vapours. The number of banana-type NPF events (I + II) also exhibited a significant correlation with UV-B radiation during autumn and winter ( $r$ : +0.9), when they showed their lowest seasonal levels ( $\sim 1 \text{ W m}^{-2}$ ; not shown in plots). This suggests that UV-B radiation (which drives photochemical reactions, leading to oxidation of  $\text{SO}_2$ ) may be an important influencing parameter in autumn–winter, but not in summer because of the persistently high day-to-day levels ( $\sim 2 \text{ W m}^{-2}$ ).

### 3.6 Some considerations about the nucleation mode

The determination of the formation and growth rates is usually performed assuming that the size distribution in the nucleation range (< 25 nm) is constituted by a single mode (Boy et al., 2008; Dal Maso et al., 2005; Salma et al., 2011; Yli-Juuti et al., 2009). In many of the type Ia events we analysed, this hypothesis is supported. However, we detected a significant number of events type Ia in which two nucleation modes were clearly observed. Moreover, the evolution and growth rates of these two modes were in many cases markedly different. Observe in the example shown in Fig. 13 how the nucleation mode 2 (orange arrow) experiences a faster development than the nucleation mode 1 (green arrow).

In a selection of four type Ia events, the growth rates were calculated with three different techniques: (i) directly with the SMPS data (as for data of Figs. 7–8), (ii) after performing a fitting to 3 lognormal distributions (1 nucleation, 1 Aitken and 1 accumulation mode), and (iii) after performing a fitting to 4 lognormal distributions (2 nucleation, 1 Aitken and 1 accumulation mode). GRs obtained from the “1 lognormal mode nucleation fitting” are higher than those obtained directly from the SMPS data (Table 5). Differences in the GR when comparing different techniques were also described by Yli-Juuti et al. (2009). When considering the two nucleation

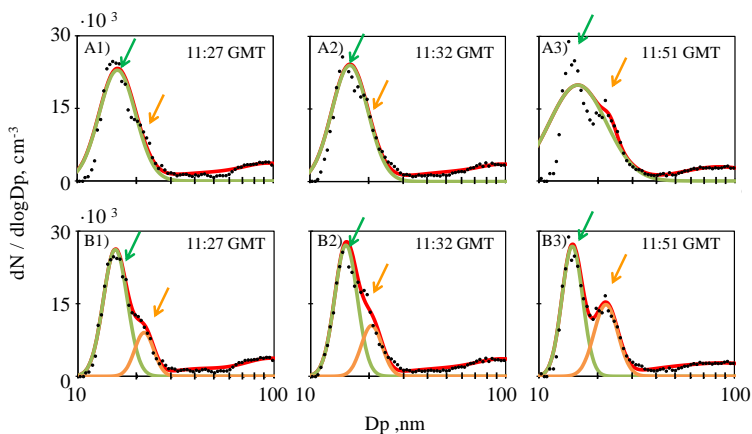


**Fig. 13.** Example of a banana-type Ia event (30 May 2009) in which two nucleation modes were observed (highlighted with green and orange arrows). **(A)** Fitting to 2 lognormal distributions with one nucleation mode (green line). **(B)** Fitting to 3 lognormal distributions with two nucleation modes (green and orange lines). Black dots represent measured data; red line represents the sum of all the fitted modes.

**Table 5.** Mean values of growth rates during four type Ia determined with three methods: (1) SMPS data, (2) fitting to 3 lognormal mode with 1 nucleation mode, and (3) fitting to 4 lognormal mode with 2 nucleation mode.

Day	GR, nm h <sup>-1</sup>	GR, nm h <sup>-1</sup>	GR, nm h <sup>-1</sup>	GR, nm h <sup>-1</sup>
	Method			
	SMPS data	1 nuc. mode fitting	2 nuc. mode fitting (nuc. mode 1)	2 nuc. mode fitting (nuc. mode 2)
30 May 2009	0.98	1.40	0.27	0.58
5 Jul 2009	0.46	1.74	1.01	0.55
16 Aug 2010	0.39	1.40	0.83	0.56
20 Aug 2010	0.90	3.44	0.59	1.59

mode fittings, in some cases the GR of mode 1 is higher than that of mode 2, and the opposite. This illustrates how the two nucleation modes may have markedly different evolution. The second nucleation mode was present in 47 % of 55 events observed from April 2009 to August 2010. A more detailed analysis is needed to describe the context in which these episodes take place.

#### 4 Summary and conclusions

We studied new particle formation (NPF) at high altitude in the subtropical North Atlantic, at the Izaña Global Atmosphere Watch observatory (2373 m a.s.l.; Tenerife, Canary Islands). NPF is associated with the transport of gaseous precursors from the boundary layer by orographic buoyant upward flows that perturb the low free troposphere during

daytime. In the 4-year study period, NPF events took place during 30 % of the days with a clearly marked NPF season (May–August), where monthly mean values of the formation and growth rates exhibited high values, 0.49–0.92 cm<sup>-3</sup> s<sup>-1</sup> and 0.48–0.58 nm h<sup>-1</sup>, respectively. At Izaña, growth rates are significantly lower than those observed in mountain sites located in continental areas. Formation and growth rates are similar to those reported for remote mountains located in oceanic areas (e.g. Mauna Loa, Hawaii). The results of our analysis show that sulfur dioxide accounts for most of the observed particle growth during most of the year (~70 %), except for February and May when other vapours seem to contribute to the particle growth as well. The availability of SO<sub>2</sub> (typical concentrations within the range 60–300 ppt) seems also to be the most influencing parameter in the year-to-year variability in the frequency of NPF events.

Summertime observations, when Izaña is within the Saharan Air Layer, suggest that dust particles may play a significant role acting as coagulation sink of freshly formed nucleation particles. As a novel finding, a set of NPF events in which two nucleation modes may evolve at different rates was identified. Further studies are needed to investigate aerosol dynamical processes involving two nucleation modes.

**Acknowledgements.** For this study the author has received two grants: first, “in-situ aerosol studies” from AEMET and, subsequently, a pre-doctoral fellowship within the training program for research staff of the Canarian Agency for Research, Innovation and Information Society (ACIISI) of the Government of the Canary Islands, co-financed by the European Social Fund. This study was performed within the context of several projects, supported by the Ministry of Economy and Competitiveness of Spain (POLLINDUST, CGL2011-26259), REDMAAS (CGL2011-15008-E) and GRACCIE (CSD2007-00067) and by the European Union (FP7, ACTRIS, grant contract: 262254). Measurements at Izaña observatory are performed within the context of the Global Atmosphere Watch networks with the financial support of AEMET. The excellent work performed by Conchy Bayo, Cándida Hernández, Fernando de Ory, Virgilio Carreño, Rubén del Campo and SIELTEC Canarias is acknowledged.

Edited by: T. Petäjä

## References

- Asmi, A., Collaud Coen, M., Ogren, J. A., Andrews, E., Sheridan, P., Jefferson, A., Weingartner, E., Baltensperger, U., Bukowiecki, N., Lihavainen, H., Kivekäs, N., Asmi, E., Aalto, P. P., Kulmala, M., Wiedensohler, A., Birmili, W., Hamed, A., O’Dowd, C., G Jennings, S., Weller, R., Flentje, H., Fjaeraa, A. M., Fiebig, M., Myhre, C. L., Hallar, A. G., Swietlicki, E., Kristensson, A., and Laj, P.: Aerosol decadal trends – Part 2: In-situ aerosol particle number concentrations at GAW and ACTRIS stations, *Atmos. Chem. Phys.*, 13, 895–916, doi:10.5194/acp-13-895-2013, 2013.
- Birmili, W. and Wiedensohler, A.: New particle formation in the continental boundary layer: Meteorological and gas phase parameter influence, *Geophys. Res. Lett.*, 27, 3325–3328, doi:10.1029/1999GL011221, 2000.
- Boulon, J., Sellegri, K., Venzac, H., Picard, D., Weingartner, E., Wehrle, G., Collaud Coen, M., Büttikofer, R., Flückiger, E., Baltensperger, U., and Laj, P.: New particle formation and ultrafine charged aerosol climatology at a high altitude site in the Alps (Jungfraujoch, 3580 m a.s.l., Switzerland), *Atmos. Chem. Phys.*, 10, 9333–9349, doi:10.5194/acp-10-9333-2010, 2010.
- Boulon, J., Sellegri, K., Hervo, M., Picard, D., Pichon, J.-M., Fréville, P., and Laj, P.: Investigation of nucleation events vertical extent: a long term study at two different altitude sites, *Atmos. Chem. Phys.*, 11, 5625–5639, doi:10.5194/acp-11-5625-2011, 2011.
- Boy, M. and Kulmala, M.: Nucleation events in the continental boundary layer: Influence of physical and meteorological parameters, *Atmos. Chem. Phys.*, 2, 1–16, doi:10.5194/acp-2-1-2002, 2002.
- Boy, M., Karl, T., Turnipseed, A., Mauldin, R. L., Kosciuch, E., Greenberg, J., Rathbone, J., Smith, J., Held, A., Barsanti, K., Wehner, B., Bauer, S., Wiedensohler, A., Bonn, B., Kulmala, M., and Guenther, A.: New particle formation in the Front Range of the Colorado Rocky Mountains, *Atmos. Chem. Phys.*, 8, 1577–1590, doi:10.5194/acp-8-1577-2008, 2008.
- Dal Maso, M., Kulmala, M., Riipinen, I., Wagner, R., Hussein, T., Aalto, P. P., and Lehtinen, K. E. J.: Formation and growth of fresh atmospheric aerosols: eight years of aerosol size distribution data from SMEAR II, Hyytiälä, Finland, *Boreal Environ. Res.*, 10, 323–336, 2005.
- García, R. D.: Aplicación de modelos de transferencia radiativa para el control operativo del programa BSRN (Base-line Surface Radiation Network) del Centro de Investigación Atmosférica de Izaña, PhD Thesis, University of Valladolid at Spain, December, 2011.
- García, R. D., García, O. E., Cuevas, E., Cachorro, V., Romero-Campos, P. M., Ramos, R., and de Frutos, A. M.: Solar radiation measurements compared to simulations at the BSRN Izaña station. Mineral dust radiative forcing and efficiency study, *J. Geophys. Res.*, 119, 179–194, doi:10.1002/2013JD020301, 2014
- Gómez-Moreno, F. J., Alonso, E., Artiñano, B., Juncal Bello, V., Piñero Iglesias, M., López Mahía, P., Pérez, N., Pey, J., Alastuey, A., de la Morena, B. A., García, M. I., Rodríguez, S., Sorribas, M., Titos, G., Lyamani, H., and Alados-Arboledas, L.: The Spanish network on environmental DMAs: the 2012 SMPS+UFP intercomparison campaign and study on particle losses in dryers, *European Aerosol Conference*, Prague, 1–6 September, 2013.
- Hallar, A. G., Lowenthal, D. H., Chirokova, G., Borys, R. D., and Wiedinmyer, C.: Persistent daily new particle formation at a mountain-top location, *Atmos. Environ.*, 45, 4111–4115, 2011.
- Hamed, A., Joutsensaari, J., Mikkonen, S., Sogacheva, L., Dal Maso, M., Kulmala, M., Cavalli, F., Fuzzi, S., Facchini, M. C., Decesari, S., Mircea, M., Lehtinen, K. E. J., and Laaksonen, A.: Nucleation and growth of new particles in Po Valley, Italy, *Atmos. Chem. Phys.*, 7, 355–376, doi:10.5194/acp-7-355-2007, 2007.
- Held, A., Nowak, A., Birmili, W., Wiedensohler, A., Forkel, R., and Klemm, O.: Observations of particle formation and growth in a mountainous forest region in central Europe, *J. Geophys. Res.*, 109, 1–9, doi:10.1029/2004JD005346, 2004.
- Hinds, W. C.: *Aerosol Technology, Properties behaviour and measurements of airborne particles*, Wiley-Interscience, John Wiley & Sons, Inc. Canada, 1999.
- IPCC: *Climate Change 2007, The Physical Science Basis, Contribution of Working Group I to the Fourth Assessment Report of the Intergovernmental Panel on Climate Change*, Cambridge University Press, New York, 2007.
- Järvinen, E., Virkkula, A., Nieminen, T., Aalto, P. P., Asmi, E., Landonelli, C., Busetto, M., Lupi, A., Schioppa, R., Vitale, V., Mazzola, M., Petäjä, T., Kerminen, V.-M., and Kulmala, M.: Seasonal cycle and modal structure of particle number size distribution at Dome C, Antarctica, *Atmos. Chem. Phys.*, 13, 7473–7487, doi:10.5194/acp-13-7473-2013, 2013.
- Kleissl, J., Honrath, R. E., Dziobak, M. P., Tanner, D., Val Martín, M., Owen, R. C., and Helmig, D.: Occurrence of upslope flows at the Pico mountaintop observatory: A case study of orographic

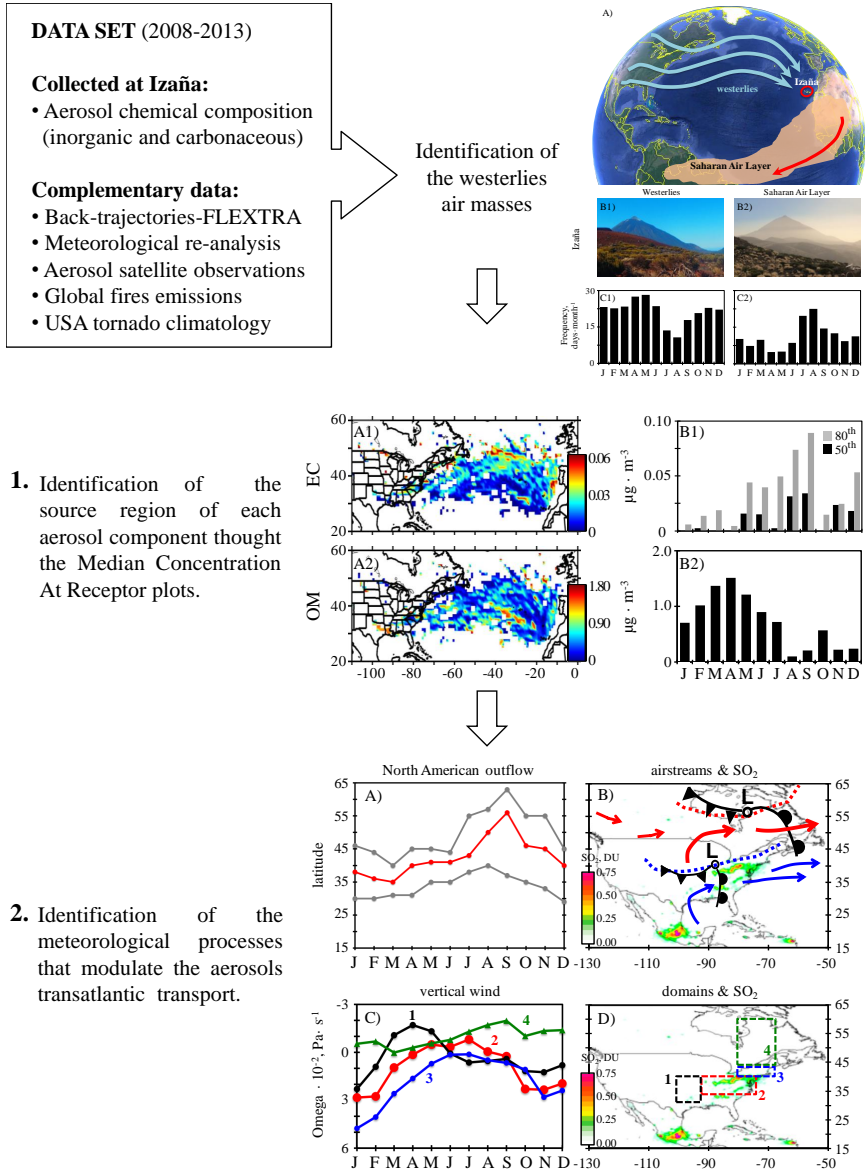
- flows on a small, volcanic island. *J. Geophys. Res.*, 112, D10S35, doi:10.1029/2006JD007565, 2007
- Kulmala, M.: How Particles Nucleate and Grow, *Science*, 302, 100–1001, 2003.
- Kulmala, M. and Kerminen, V. M.: On the formation and growth of Atmospheric nanoparticles, *Atmos. Res.*, 90, 132–150, 2008.
- Kulmala, M., Vehkamäki, H., Petäjä, T., Dal Maso, M., Lauri, A., Kerminen, V.-M., Birmili, W., and McMurry, P. H.: Formation and growth rates of ultrafine atmospheric particles: a review of observations, *J. Aerosol Sci.*, 35, 143–176, doi:10.1016/j.jaerosci.2003.10.003, 2004.
- Kulmala, M., Lehtinen, K. E. J., and Laaksonen, A.: Cluster activation theory as an explanation of the linear dependence between formation rate of 3 nm particles and sulphuric acid concentration, *Atmos. Chem. Phys.*, 6, 787–793, doi:10.5194/acp-6-787-2006, 2006.
- Kulmala, M., Petäjä, T., Nieminen, T., Sipilä, M., Manninen, H. E., Lehtipalo, K., Dal Maso, M., Aalto, P. P., Junninen, H., Paasonen, P., Riipinen, I., Lehtinen, K. E. J., Laaksonen, A., and Kerminen, V.-M.: Measurement of the nucleation of atmospheric aerosol particles, *Nat. Protoc.*, 7, 1651–1667, 2012.
- Kulmala, M., Kontkanen, J., Junninen, H., Lehtipalo, K., Manninen, H. E., Nieminen, T., Petäjä, T., Sipilä, M., Schobesberger, S., Rantala, P., Franchin, A., Jokinen, T., Järvinen, E., Äijälä, M., Kangasluoma, J., Hakala, J., Aalto, P. P., Paasonen, P., Mikkilä, J., Vanhanen, J., Aalto, J., Hakola, H., Makkonen, U., Ruuskanen, T., Mauldin, R. L., Duplissy, J., Vehkamäki, H., Bäck, J., Kortelainen, A., Riipinen, I., Kurtán, T., Johnston, M. V., Smith, J. N., Ehn, M., Mentel, T. F., Lehtinen, K. E. J., Laaksonen, A., Kerminen, V.-M., and Worsnop, D. R.: Direct observations of atmospheric aerosol nucleation, *Science*, 339, 943–946, doi:10.1126/science.1227385, 2013.
- Laakso, L., Anttila, T., Lehtinen, K. E. J., Aalto, P. P., Kulmala, M., Hörrak, U., Paatero, J., Hanke, M., and Arnold, F.: Kinetic nucleation and ions in boreal forest particle formation events, *Atmos. Chem. Phys.*, 4, 2353–2366, doi:10.5194/acp-4-2353-2004, 2004.
- Laaksonen, A., Kulmala, M., O’Dowd, C. D., Joutsensaari, J., Vaatovaara, P., Mikkonen, S., Lehtinen, K. E. J., Sogacheva, L., Dal Maso, M., Aalto, P., Petäjä, T., Sogachev, A., Yoon, Y. J., Lihavainen, H., Nilsson, D., Facchini, M. C., Cavalli, F., Fuzzi, S., Hoffmann, T., Arnold, F., Hanke, M., Sellegri, K., Umann, B., Junkermann, W., Coe, H., Allan, J. D., Alfarra, M. R., Worsnop, D. R., Riekkola, M.-L., Hyötyläinen, T., and Viisanen, Y.: The role of VOC oxidation products in continental new particle formation, *Atmos. Chem. Phys.*, 8, 2657–2665, doi:10.5194/acp-8-2657-2008, 2008.
- Manninen, H. E., Nieminen, T., Asmi, E., Gagné, S., Häkkinen, S., Lehtipalo, K., Aalto, P., Vana, M., Mirme, A., Mirme, S., Hörrak, U., Plass-Dülmer, C., Stange, G., Kiss, G., Hoffer, A., Törö, N., Moerman, M., Henzing, B., de Leeuw, G., Brinkenberg, M., Kouvarakis, G. N., Bougiatioti, A., Mihalopoulos, N., O’Dowd, C., Ceburnis, D., Arneth, A., Svenningsson, B., Swietlicki, E., Tarozzi, L., Decesari, S., Facchini, M. C., Birmili, W., Sonntag, A., Wiedensohler, A., Boulon, J., Sellegri, K., Laj, P., Gysel, M., Bukowiecki, N., Weingartner, E., Wehrle, G., Laaksonen, A., Hamed, A., Joutsensaari, J., Petäjä, T., Kerminen, V.-M., and Kulmala, M.: EUCAARI ion spectrometer measurements at 12 European sites – analysis of new particle formation events, *Atmos. Chem. Phys.*, 10, 7907–7927, doi:10.5194/acp-10-7907-2010, 2010.
- McFiggans, G., Artaxo, P., Baltensperger, U., Coe, H., Facchini, M. C., Feingold, G., Fuzzi, S., Gysel, M., Laaksonen, A., Lohmann, U., Mentel, T. F., Murphy, D. M., O’Dowd, C. D., Snider, J. R., and Weingartner, E.: The effect of physical and chemical aerosol properties on warm cloud droplet activation, *Atmos. Chem. Phys.*, 6, 2593–2649, doi:10.5194/acp-6-2593-2006, 2006.
- Metzger, A., Verheggen, B., Dommen, J., Duplissy, J., Prevot, A. S. H., Weingartner, E., Riipinen, I., Kulmala, M., Spracklen, D. V., Carslaw, K. S., and Baltensperger, U.: Evidence for the role of organics in aerosol particle formation under atmospheric conditions, *P. Natl. Acad. Sci. USA*, 107, 6646–6651, doi:10.1073/pnas.0911330107, 2010.
- Neitola, K., Asmi, E., Komppula, M., Hyvärinen, A.-P., Raatikainen, T., Panwar, T. S., Sharma, V. P., and Lihavainen, H.: New particle formation infrequently observed in Himalayan foothills – why?, *Atmos. Chem. Phys.*, 11, 8447–8458, doi:10.5194/acp-11-8447-2011, 2011.
- Nieminen, T., Lehtinen, K. E. J., and Kulmala, M.: Sub-10 nm particle growth by vapor condensation – effects of vapor molecule size and particle thermal speed, *Atmos. Chem. Phys.*, 10, 9773–9779, doi:10.5194/acp-10-9773-2010, 2010.
- Nishita, C., Osada, K., Kido, M., Matsunaga, K., and Iwasaka, Y.: Nucleation mode particles in upslope valley winds at Mount Norikura, Japan: Implications for the vertical extent of new particle formation events in the lower troposphere, *J. Geophys. Res.*, 113, D06202, doi:10.1029/2007JD009302, 2008.
- Parrish, D. D. and Fehsenfeld, F. C.: Methods for gas-phase measurements of ozone, ozone precursors and aerosol precursors, *Atmos. Environ.*, 34, 1921–1957, 2000.
- Petäjä, T., Mauldin III, R. L., Kosciuch, E., McGrath, J., Nieminen, T., Boy, M., Adamov, A., Kotiaho, T., and Kulmala, M.: Sulfuric acid and OH concentrations in a boreal forest site, *Atmos. Chem. Phys.*, 9, 7435–7448, doi:10.5194/acp-9-7435-2009, 2009.
- Rodríguez, S., Van Dingenen, R., Putaud, J. P., Martins-Dos Santos, S., and Roselli, D.: Nucleation and growth of new particles in the rural atmosphere of Northern Italy – Relationship to air quality monitoring, *Atmos. Environ.*, 39, 6734–6746, 2005.
- Rodríguez, S., González, Y., Cuevas, E., Ramos, R., Romero, P. M., Abreu-Afonso, J., and Redondas, A.: Atmospheric nanoparticle observations in the low free troposphere during upward orographic flows at Izaña Mountain Observatory, *Atmos. Chem. Phys.*, 9, 6319–6335, doi:10.5194/acp-9-6319-2009, 2009.
- Rodríguez, S., Alastuey, A., Alonso-Pérez, S., Querol, X., Cuevas, E., Abreu-Afonso, J., Viana, M., Pérez, N., Pandolfi, M., and de la Rosa, J.: Transport of desert dust mixed with North African industrial pollutants in the subtropical Saharan Air Layer, *Atmos. Chem. Phys.*, 11, 6663–6685, doi:10.5194/acp-11-6663-2011, 2011.
- Salma, I., Borsós, T., Weidinger, T., Aalto, P., Hussein, T., Dal Maso, M., and Kulmala, M.: Production, growth and properties of ultrafine atmospheric aerosol particles in an urban environment, *Atmos. Chem. Phys.*, 11, 1339–1353, doi:10.5194/acp-11-1339-2011, 2011.
- Shaw, G. E.: Aerosols at a mountaintop observatory in Arizona, *J. Geophys. Res.*, 112, D07206, doi:10.1029/2005JD006893, 2007.
- Steinbacher, M., Zellweger, C., Schwarzenbach, B., Bugmann, S., Buchmann, B., Ordóñez, C., Prevot, A. S. H., and Hueglin, C.,

- Nitrogen oxide measurements at rural sites in Switzerland: Bias of conventional measurement techniques, *J. Geophys. Res.*, 112, D11307, doi:10.1029/2006JD007971, 2007.
- Venzac, H., Sellegri, K., and Laj, P.: Nucleation events detected at the high altitude site of the Puy de Dôme research station, France, *Bor. Environ. Res.*, 12, 345–359, 2007.
- Venzac, H., Sellegri, K., Laj, P., Villani, P., Bonasoni, P., Marioni, A., Cristofanelli, P., Calzolari, F., Fuzzi, S., Decesari, S., Facchini, M.-C., Vuillermoz, E., and Verza, G.-P.: High frequency new particle formation in the Himalayas, *P. Natl. Acad. Sci. USA*, 105, 15666–15671, 2008.
- Weber, J. R., McMurry, P. H., Eisele, F. L., and Tanner, D. J.: Measurements of expected nucleation precursors species and 3–500 nm diameter particles at Mauna Loa, Hawaii, *J. Atmos. Sci.*, 52, 2242–2257, 1995.
- Weber, J. R., McMurry, P. H., Mauldin III, R. L., Tanner, D. J., Eisele, F. L., Clarke, A. D., and Kapustin, V. N.: New particle formation in the remote troposphere: a comparison of observations at various sites, *Geophys. Res. Lett.*, 26, 307–310, 1999.
- Yli-Juuti, T., Riipinen, I., Aalto, P. P., Nieminen, T., Maenhaut, W., Janssens, I. A., Claeys, M., Salma, I., Ocskay, R., Hoffer, A., Imre, K., and Kulmala, M.: Characteristics of new particle formation events and cluster ions at K-pusztá, Hungary, *Boreal Environ. Res.*, 14, 683–698, 2009.
- Yli-Juuti, T., Nieminen, T., Hirsikko, A., Aalto, P. P., Asmi, E., Hörrak, U., Manninen, H. E., Patokoski, J., Dal Maso, M., Petäjä, T., Rinne, J., Kulmala, M., and Riipinen, I.: Growth rates of nucleation mode particles in Hyytiälä during 2003–2009: variation with particle size, season, data analysis method and ambient conditions, *Atmos. Chem. Phys.*, 11, 12865–12886, doi:10.5194/acp-11-12865-2011, 2011.



## 4.2 Article 2

Graphical abstract:







## Impact of North America on the aerosol composition in the North Atlantic free troposphere

M. Isabel García<sup>1,2</sup>, Sergio Rodríguez<sup>1,\*</sup>, Andrés Alastuey<sup>3</sup>

5

<sup>1</sup>Izaña Atmospheric Research Centre, AEMET, Associated Unit to CSIC “Studies on Atmospheric Pollution”, Santa Cruz de Tenerife, 38001, Spain

<sup>2</sup>Department of Chemistry (T.U. Analytical Chemistry), Faculty of Science, University of La Laguna, La Laguna, 38206, Spain

10 <sup>3</sup> Institute of Environmental Assessment and Water Research, CSIC, Barcelona, 08034, Spain

*Correspondence to:* Sergio Rodríguez (srodriguez@aemet.es)

**Abstract.** In the AEROATLAN project we study the composition of aerosols collected over ~5 years at Izaña Observatory (located at ~2400 m a.s.l. in Tenerife, the Canary Islands) under the prevailing westerly airflows typical of the North Atlantic free troposphere at subtropical and mid-latitudes. Mass concentrations of sub10- $\mu\text{m}$  aerosols ( $\text{PM}_{10}$ ) carried by westerly winds to Izaña, after transatlantic transport, are typically within the range 1.2 and 4.2  $\mu\text{g}\cdot\text{m}^{-3}$  (20<sup>th</sup> and 80<sup>th</sup> percentiles). The main contributors to background levels of aerosols ( $\text{PM}_{10}$  within the 1<sup>st</sup> - 50<sup>th</sup> percentiles = 0.15 – 2.54  $\mu\text{g}\cdot\text{m}^{-3}$ ) are North American dust (53%), non-sea-salt- $\text{SO}_4^-$  (14%) and organic matter (18%). High  $\text{PM}_{10}$  events (75<sup>th</sup> - 95<sup>th</sup> percentiles  $\approx$  4.0 – 9.0  $\mu\text{g}\cdot\text{m}^{-3}$ ) and are prompted by dust (56%), organic matter (24%) and nss- $\text{SO}_4^-$  (9%). These aerosol components experience a seasonal evolution explained by (i) their spatial distribution in North America and (ii) the seasonal shift of the North American outflow, which migrates from low latitudes in winter (~32°N, January–March) to high latitudes in summer (~52°N, August–September). The westerlies carry maximum loads of nss-sulphate, ammonium and organic matter in spring (March–May), of North American dust from mid-winter to mid-spring (February–May) and of elemental carbon in summer (August–September). Our results suggest that a significant fraction of organic aerosols may be linked to sources other than combustion (e.g. biogenic); further studies are necessary for this topic. The present study evidences how long-term evolution of the aerosol composition in the North Atlantic free troposphere will be influenced by air quality policies and the use of soils (potential dust emitter) in North America.

15  
20  
25

### 1 Introduction

The export of aerosols from their source areas impacts on air quality (Chin et al., 2007) and also on climate related processes (Ramanathan et al., 2001) in downwind receptor regions. Exposure to aerosols – or particulate matter (PM) – and reactive gases in ambient air pollution is associated with ~3.7 million deaths a year<sup>-1</sup>, mostly due to ischaemic heart disease (~40%), stroke (~40%), chronic obstructive pulmonary disease (~11%), lung cancer (~6%) and acute lower respiratory infections in

30

Atmos. Chem. Phys. Discuss., doi:10.5194/acp-2017-60, 2017

Manuscript under review for journal Atmos. Chem. Phys.

Discussion started: 27 February 2017

© Author(s) 2017. CC-BY 3.0 License.



children (~3%) according to the World Health Organization (WHO, 2014). Aerosols are of special interest as they may have an influence on direct radiative transfer and cloud properties by altering the radiative effect and on rain. It is estimated that globally, this influence results in mean radiative forcing due to aerosol-radiation and aerosol-cloud interaction of about  $-0.9 \text{ W}\cdot\text{m}^{-2}$ , with aerosol-radiation contribution of  $-0.35 \text{ W}\cdot\text{m}^{-2}$  as a result of net sulphate contributions ( $-0.4$ ), black carbon ( $+0.4$ ), nitrate ( $-0.11$ ), dust ( $-0.1$ ) and organics ( $-0.12$ ), according to the Intergovernmental Panel on Climate Change (IPCC, 2013; Myhre et al., 2013).

North America is a major source of aerosols and trace gases (Li et al., 2004; Park et al., 2003, 2004). The export of trace gases to the North Atlantic in the so-called North American outflow (Li et al., 2005) is enhanced by mid-latitude cyclones (Dickerson et al., 1995; Merrill and Moody, 1996; Moody et al., 1996). These cyclones frequently form on the lee side of the Rocky Mountains and propagate eastward, with associated cold fronts southeastward across the eastern United States (US; Whittaker and Horn, 1984; Zishka and Smith, 1980). The cyclones occur every 5 days – on average – in summer (Li et al., 2005), although in spring that frequency may be even higher. Four airstreams are associated with mid-latitude cyclones: the warm conveyor belt ahead of the cold front, the cold conveyor belt, the dry airstream subsiding behind the cold front, and the post cold front boundary layer airstream (Cooper et al., 2002a, 2002b). The northeastward ascending airstream represented by the warm conveyor belt prompts the upward transport of pollutants from North America to the free troposphere over the North Atlantic (Eckhardt et al., 2004), where it may connect with the westerly circulation at the north of the Azores High (Li et al., 2005) prompting the transatlantic transport of pollutants; this has been documented for relatively long lifetime (LT) trace gases, such as CO (LT~ 60 days) and O<sub>3</sub> (LT~25 days) (Honrath et al., 2004; Owen et al., 2006). Convection is also an important mechanism for ventilation of the boundary layer; the convective outflow prompts the upward transport of pollutants (Dickerson et al., 1987; Talbot et al., 1998), which may remain over North America for several days prompting ozone production and its subsequent export to the North Atlantic (Li et al., 2005). This mechanism is important in the southeastern United States in summer, as the warm conveyor belt of the mid-latitude cyclones is shifted northward (Li et al., 2005). There are a number of observation-based evidences on the large-scale impact of the CO and O<sub>3</sub> pollution events in the North Atlantic linked to North American fires and pollution export (Parrish et al., 1998; Moody et al., 1996; Honrath et al., 2004; Owen et al., 2006).

Although aerosols have been less studied, some research has found evidence of their export to the Atlantic in the cyclone modulated North American outflow (Li et al., 2005), even if they have a relatively short lifetime (LT~15 days). By ground based and airborne lidar measurements, Ancellet et al. (2016) detected the transatlantic transport of North American biomass burning aerosols and dust to the Mediterranean. At Pico Observatory in the Azores, free troposphere transport of North American black carbon aerosols linked to boreal fires (Val Martin et al., 2006) and sulphate, nitrate, elemental carbon and organic aerosols (such as biomass burning) has been detected (Dzepina et al., 2015). Modelling studies have also shown interest in intercontinental transport of aerosols (Park et al., 2004; Chin et al., 2007).



Previous studies on transatlantic transport of North American aerosols have reported on events detected in intensive campaigns, typically lasting from weeks to a few months. In this study we have used a complementary approach, based on long-term records. We analysed the long-term aerosol chemistry register of the Izaña Observatory – located at ~2400 m a.s.l. on the island of Tenerife – with the aim of identifying the composition, potential sources and origin of the aerosols transported by westerly winds across the North Atlantic. To our knowledge, this is the first study addressing the issue.

## 2 Methods

### 2.1 Sampling site

The Izaña Global Atmospheric Watch (GAW) observatory is located on a mountain ridge (~2400 m.a.s.l.) lying almost permanently above the temperature inversion and marine stratocumulus layer typical of the marine boundary layer (MBL) top in the subtropics. Buoyant upslope winds develop during daylight, with minimum impact on the aerosol mass concentrations (Rodríguez et al., 2009). At night, upslope winds cease and Izaña is basically exposed to the prevailing westerly free troposphere subsiding airflow.

### 2.2 Sampling and chemical composition

This study is based on a long-term record of chemical composition of PM smaller than 10  $\mu\text{m}$  ( $\text{PM}_{10}$ ) and 2.5  $\mu\text{m}$  ( $\text{PM}_{2.5}$ ) aerodynamic diameters at Izaña Observatory. A total of 401  $\text{PM}_{10}$  and 315  $\text{PM}_{2.5}$  samples were collected and chemically analysed from February 2008 to August 2013.

The samples of  $\text{PM}_{10}$  were collected on quartz micro fiber filters (150 mm diameter) pre-heated at 205°C for 5 hours; this procedure removes potentially adsorbed volatile carbon. Aerosol sampling was performed at 30  $\text{m}^3\cdot\text{h}^{-1}$  flow rate overnight (22:00 to 06:00 GMT), under the influence of free troposphere airflows. One  $\text{PM}_x$  sample was collected every 3 days, except in August, when sampling was daily. Concentrations of  $\text{PM}_x$  were determined by gravimetry following the EN-14907 procedure (except that filter conditioning was performed at 30–35% relative humidity instead of 50%). The manual gravimetric method is considered optimal for PM concentrations  $> 10 \mu\text{g}\cdot\text{m}^{-3}$  (EN-14907), so uncertainties are higher below this threshold value (details in section S1 of the supplement). Blank weighting room and blank field filters were collected and weighted as part of the quality assurance / quality control (QA/QC) protocol.

The methods used in the long-term (30-years) aerosol chemical composition record of Izaña Observatory are described in detail in previous articles (Rodríguez et al., 2015). Briefly, in the study period (2008–2013) soluble species were determined by ion chromatography ( $\text{SO}_4^{2-}$ ,  $\text{NO}_3^-$ ,  $\text{Cl}^-$ ; detection limits 0.113, 0.113 and 0.505  $\mu\text{g}\cdot\text{m}^{-3}$ , respectively) and selective electrode ( $\text{NH}_4^+$ ; detection limit 0.056  $\mu\text{g}\cdot\text{m}^{-3}$ ). Elemental composition was determined by Inductively Coupled Plasma Atomic Emission Spectrometry (ICP-AES, IRIS Advantage TJA Solutions, THERMO™) and Inductively Coupled Plasma

Atmos. Chem. Phys. Discuss., doi:10.5194/acp-2017-60, 2017

Manuscript under review for journal Atmos. Chem. Phys.

Discussion started: 27 February 2017

© Author(s) 2017. CC-BY 3.0 License.



Mass Spectrometry (ICP-MS, X Series II, THERMO™) after acid digestion of the samples. Organic and elemental carbon (detection limits 0.8 and 0.032  $\mu\text{g}\cdot\text{m}^{-3}$ , respectively) were analysed by thermal-optical transmittance (TOT, Sunset Laboratory Inc.™) following the EUSAAR2 protocol (Cavalli et al., 2009). Because quartz microfiber filters may adsorb volatile carbon very easily due to the high active surface (Chai et al., 2012), the more unstable part of the organic carbon was discarded based on the results of the field blank filters analysis. Sulphate was split into sea salt sulphate (ss- $\text{SO}_4^-$ ) and non-sea salt sulphate (nss- $\text{SO}_4^-$ ) using the empirical ratio of Na and sulphate ( $\text{SO}_4^-/\text{Na}^+ = 0.25$ ) in seawater (Gravenhorst et al., 1978), which assumes there is no sulfate enrichment due to gas-to-particle conversion of the oxidation of marine  $\text{SO}_2$  (Bonsang et al., 1980). Organic matter (OM) was determined by using the ratio  $\text{OM}/\text{OC} = 1.8$  observed in the North American aerosols collected at Pico Observatory in the Azores (Dzepina et al., 2015). Blank field filters were subject to gravimetry and chemical analysis, and mean values were subtracted from the  $\text{PM}_x$  samples.

The chemical composition data were used for a mass closure of  $\text{PM}_x$  (table 1). The undetermined fraction of PM, i.e. the difference between the gravimetrically determined  $\text{PM}_x$  and the sum of the chemical compounds, increased under low  $\text{PM}_x$  conditions. This has already been observed in previous studies (Ripoll et al., 2015) and is attributed to inaccuracies of the manual gravimetric method under low PM concentrations ( $< 10 \mu\text{g}\cdot\text{m}^{-3}$ ) and to the relatively higher contribution of water not fully removed during filter conditioning.

### 2.3 Meteorology, back-trajectories and MCAR plots

We analyzed meteorological re-analysis data from the National Centre for Environmental Prediction / National Centre for Atmospheric Research (NCEP/NCAR) (Kalnay et al., 1996) to study the processes involved in the export and transatlantic transport of aerosols from North America. The analysis includes geopotential heights, winds and omega (vertical wind) at several standard levels (925, 850 and 700 hPa) and precipitation rates.

Three-dimensional 10-day back-trajectories were computed at 00:00 GMT for Izaña using the meteorological input data from the European Centre for Medium-Range Weather Forecasts (ECMWF) and Lagrangian model FLEXTRA (Stohl et al., 1995; Stohl and Seibert., 1998). These back-trajectories were used as input in a self-developed Matlab script (The Mathworks, Natick, USA) which segregates air masses coming from North America and the North Atlantic, from those from Africa, attending to the latitude and longitude values along the transport path towards Izaña (details in section S2 of the supplement). The frequency of the westerlies and of the Saharan Air Layer at Izaña is shown in Fig. 1C. Samples of  $\text{PM}_{10}$  and  $\text{PM}_{2.5}$  were associated with westerlies and SAL according to the back-trajectories (Fig. S2).

We determined the Median Concentrations At Receptor (MCAR) plots for the main  $\text{PM}_{10}$  chemical component using the method described by Rodríguez et al. (2011). In these MCAR, the typical (median) concentration of each aerosol component recorded at Izaña, when the air mass has passed by each pixel of the study region, is shown. The MCAR plots were



calculated with back-trajectories representative of transatlantic transport from North America. Events linked to (i) back-trajectories from North Africa or (ii) associated with Saharan dust re-circulated over the North Atlantic (exported from North Africa westward and then re-circulated eastward, e.g. as described by Ancellet et al., 2016) were removed; to identify the latter type of events we also used the output forecasts of the BSC-DREAM8b model (Pérez et al., 2006; Basart et al., 2012) storages at the Barcelona Supercomputing Centre website (<http://www.bsc.es/earth-sciences/mineral-dust-forecast-system/bsc-dream8b-forecast/north-africa-europe-and-middle-ea-1>). Similar plots were used to analyse seasonality of the frequency of westerlies reaching Izaña, which is linked to the export of North American pollutants. Monthly Transport Route Frequency (TRF) plots for the period 2008–2013 were calculated in a similar way to the MCAR plots, but instead of the median concentration, the total number of back-trajectories passing by each cell grid is represented.

#### 10 2.4 Complementary data

We used the Global Fire Emissions Database Version 4 including small fires data (GFEDv4.1s; Randerson et al., 2015) to estimate the average burned fraction of each  $0.25^\circ \times 0.25^\circ$  grid cell in North America during the study period (2008–2013). The data set was downloaded from the Oak Ridge National Laboratory Distributed Active Archive Center (ORNL DAAC) for biogeochemical dynamics ([https://daac.ornl.gov/cgi-bin/dsviewer.pl?ds\\_id=1293](https://daac.ornl.gov/cgi-bin/dsviewer.pl?ds_id=1293)). We also made use of Level 3 UV Aerosol Index (AI) data, from the Ozone Monitor Instrument spectrometer onboard satellite Aura (OMI 2008–2013), to study the spatial and temporal variability of dust in North America during the study period (2008–2013). The data set was downloaded from the Giovanni online data system of the NASA Goddard Earth Sciences Data and Information Services Center (GES DISC; <http://disc.sci.gsfc.nasa.gov/>).

### 3 Results and discussion

#### 20 3.1 Chemical characterisation

This study focuses on aerosols transported by the westerlies, i.e. the westerly airstream that flows from North America across the North Atlantic at subtropical and mid-latitudes. Previous studies have shown that the Saharan Air Layer (SAL), i.e. the dusty airstream that expands from North Africa to the Americas, is the most important carrier of aerosols in the tropical and subtropical North Atlantic (Prospero and Carlson, 1972); so first we did a brief comparison of the characteristics of the aerosol composition in these two air streams, with the aim of illustrating the huge differences between them. The frequency of the westerlies and of the Saharan Air Layer at Izaña is shown in Fig. 1C; the westerlies occur with high frequency throughout the year, with a maximum in April–May and a minimum in July–August when Izaña is mostly within the SAL.

Table 1 shows the median chemical composition and mass closure of the  $PM_{10}$  and  $PM_{2.5}$  aerosols in samples collected at Izaña under the SAL and the westerlies (Fig. 1A–B). The transport of particulate pollutants in the SAL had already been



studied by Rodríguez et al. (2011). The SAL impacts on Izaña in July and August, and is linked to the northern shift of the Harmattan – trade winds (Fig. 1A). The summer SAL occurs 1–5 km a.s.l. off North Africa; it is associated with air from the Mediterranean flowing south-westward to the Sahara resulting in the emissions and export of dust to the Atlantic above the marine boundary layer. The westerlies occur throughout the year and are associated with airstreams from North America that, in some cases, may have circulated around the Azores High (Fig. 1A).

Concentrations of bulk  $PM_{10}$  and  $PM_{2.5}$  are ~ 20 and 10 times higher in the SAL than in the westerlies, respectively (table 1). Mass closure of  $PM_x$  accounts for a rather low fraction of the gravimetrically determined  $PM_x$  concentrations under westerly conditions (~ 50–70% of  $PM_x$ , table 1), compared to the SAL (70–90% of  $PM_x$ ). This is attributed to the relatively high inaccuracy of the manual gravimetric method under low  $PM_x$  concentrations described above (see details in section S1 of the supplement). Thus, the sum of the main chemical components ( $\Sigma$  in table 1) is probably a better proxy of the actual bulk  $PM_x$  concentrations in the westerlies than the gravimetric PM concentrations.

In the SAL, the  $PM_{10}$  aerosol population (median of  $\Sigma$  – sum of the main chemical components – ~ 41  $\mu\text{g}\cdot\text{m}^{-3}$ ; table 1) is basically constituted by dust (78%: 36  $\mu\text{g}\cdot\text{m}^{-3}$ ) mixed with organic matter (4.5%: 2.1  $\mu\text{g}\cdot\text{m}^{-3}$ ), sulphate (3.8%: 1.8  $\mu\text{g}\cdot\text{m}^{-3}$ ), nitrate (1.8%: 0.8  $\mu\text{g}\cdot\text{m}^{-3}$ ) and ammonium (0.4%: 0.2  $\mu\text{g}\cdot\text{m}^{-3}$ ). In contrast,  $PM_{10}$  aerosol in the westerlies (median of  $\Sigma$  – sum of the main chemical components – ~ 1.8  $\mu\text{g}\cdot\text{m}^{-3}$ ) is predominantly constituted by dust (44.5%: 1.1  $\mu\text{g}\cdot\text{m}^{-3}$ ), organic matter (12.4%: 0.32  $\mu\text{g}\cdot\text{m}^{-3}$ ), nss- $\text{SO}_4^-$  (9.8%: 0.25  $\mu\text{g}\cdot\text{m}^{-3}$ ) and ammonium (2.2%: 0.06  $\mu\text{g}\cdot\text{m}^{-3}$ ). Nitrate in the SAL mostly occurs in the coarse range as non-ammonium salt coating dust particles (see details in Rodríguez et al. 2011). In the westerlies nitrate concentrations tend to be extremely low; in the few observed nitrate events, it tended to occur in the sub-2.5  $\mu\text{m}$  range, attributed to an ammonium salt. In the SAL, about  $\frac{1}{4}$  of non-sea-salt-sulphate (nss- $\text{SO}_4^-$ ) is present as ammonium sulphate (as- $\text{SO}_4^-$ ) linked to anthropogenic sulphur emissions, with the remaining  $\frac{3}{4}$  being non-ammonium sulphate (na- $\text{SO}_4^-$ ) most probably linked to soil emissions of gypsum / anhydrite soil minerals in beds of Saharan dry lakes (Rodríguez et al., 2011).

Aerosols in the SAL and in the westerlies also exhibit differences in terms of size distribution. PM mass mostly occurs in the sub-2.5 $\mu\text{m}$  in the westerlies and in the coarse 2.5–10  $\mu\text{m}$  range in the SAL (table 1).

### 25 3.2 North American large-scale meteorology and airstreams

The meteorological scenarios that prompt pollutant export events from North America are described in previous studies (Merril and Moody, 1996; Moody et al., 1996; Stohl et al., 2002; Li et al., 2005; Owen et al., 2006); here a complementary view is provided. We analysed how large-scale circulations over North America evolve over the year, more specifically how they may influence on the export of aerosols to the Atlantic. The monthly values of key meteorological fields (geopotential heights, winds and omega at several standard levels, 925, 850 and 700 hPa and precipitation rates, e.g. Fig. 2A) were



determined with the National Center for Environmental Prediction/National Center for Atmospheric Research (NCEP/NCAR) reanalysis data (Kalnay et al., 1996). To facilitate interpretation on how the variability in meteorology may influence the export of aerosols we also plotted (i) the latitudinal range of the westerlies over the eastern coast of North America (observed in the monthly NCEP/NCAR wind fields; Fig. 3A), (ii) the spatial distribution of SO<sub>2</sub> according to Fioletov et al. (2016) (Fig. 3B) and of major aerosol components according to Park et al. (2003, 2004) (Fig. 4) and (iii) the monthly mean values of the omega vertical component of wind in selected domains (Fig. 3C and 3D). Finally, in order to link the export of North American pollutants with transatlantic transport, the Transport Route Frequency (TRF) field was determined for each month based on back-trajectories (Fig. 2B). Figure 2 shows examples for illustrative months (January, April, August and November); additional material is presented in the Supplement (Fig. S3).

10 During January and February, the North Atlantic anticyclone shifts southward, expanding over the Caribbean, resulting in an intense geopotential / pressure gradient (Fig.S2A) and westerly winds over most North America (Fig.2A1). The main stream of the westerlies (which we will refer to as ‘westerly jet’) flows from Western Canada (~55°N) to Eastern US entering the North Atlantic at relatively low latitudes (36–38°N in the 850hPa standard level; Fig. 2A1). We refer to the westerly jet over the eastern coast of North America as ‘North American outflow’, whose latitudinal position over the year is plotted in Fig.

15 3A. The TRF analysis shows that during this period air from Central and Southern US reaches Izaña (Fig. 2B1).

From March to June, the North Atlantic anticyclone progressively intensifies (Fig.S2B) and the western side of its clockwise atmospheric circulation expands from the inner Gulf of Mexico northward to Central and then to Eastern US, resulting in an airstream that we have called ‘the Gulf inflow’, which is observed in the wind fields at the 925, 850 and 700hPa levels (Fig. 2A2). The Gulf inflow is observed from March, when the trade winds building up results in a northward inflow across the coast of Texas, which subsequently turns northeastward over Central US (Arkansas to Tennessee–Indiana) and then eastward resulting in a westerly outflow to the Atlantic by the Eastern coast of North America following the clockwise circulation of the North Atlantic high (Fig. 2B2). The analysis of the (vertical) omega component, at the 925, 850 and 700 hPa levels, shows that upward movement of air occurs in the regions affected by the Gulf inflow of warm and humid air from Texas to Indiana, in such a way that air masses from the continental boundary layer of Central to North-eastern US may be exported

20 in the westerlies to the North Atlantic free troposphere (Fig. S3B). Observe in Fig. 3C how omega decreases to negative values (net upward movements) from March to May in Central US (domain 1 in Fig. 3D) under the influence of the Gulf inflow; the decrease in omega in this season is also observed to the East (domain 2 in Fig. 3D). This is consistent with the fact that the storm season occurs in this period (March to June) between Central US (Northern Texas–Kansas) to the west of the Appalachians (Tennessee–Kentucky–Indiana), as reported by NOAA (section S4 of the supplement). Along the path of

30 the Gulf inflow there are a number of sources of aerosols and their precursors – including coal-fired power plants (Fioletov et al., 2016) – whose emissions may be lifted to the mid-troposphere during convective processes (Dickerson et al., 1987; Talbot et al., 1998), and then exported to the North Atlantic free troposphere by the westerly circulation, which in this period



tends to occur 35–45°N (Fig. 3A). The export of pollutants from Eastern US to the Atlantic is enhanced by eastward moving cyclones, whose tracks typically occur south of 40°N in this season (Cooper et al., 2002a); Fig. 3B shows an illustration of this scenario (Cooper et al., 2002a, 2002b) and the mean SO<sub>2</sub> spatial distribution observed by satellite (Fioletov et al., 2016); a dotted blue line shows the typical eastward track of the cyclones typical in March–April, whereas the blue arrows indicate a simplified scheme of the associated circulation; the satellite detection of SO<sub>2</sub> over the ocean off the coast of Virginia to New Jersey (35–40°N in Fig. 3B) evidences the importance of the export of this aerosol sulphate precursor to the Atlantic. The back-trajectory based TRF analysis shows that air masses from Central US (e.g. domain 1 in Fig. 3D) and Eastern US (e.g. domain 2 in Fig. 3D) are regularly transported to Izaña (Fig. 2B2). This is the season of maximum frequency of westerlies at this observatory (23–27 days·month<sup>-1</sup>; Fig. 1C1) and that has implications for the export of major aerosol components, whose concentrations are high in North-eastern US (Fig. 4).

In July and August, the North Atlantic anticyclone shifts northward (Fig.S2C) resulting in intense trade winds over the Caribbean; the Gulf inflow continues blowing northward across the great plains up to Canada where it connects with the main westerlies jet, whereas southern winds prevail along the Eastern coast of the US (Fig. 2A3). In September, the trade winds, the resulting Gulf inflow and southern winds over the Eastern coast weaken. In this season, the westerlies and the resulting North American outflow shift northward (45–55°N; Fig. 2A3–2B3, Fig.3A); this is consistent with previous studies showing that cyclone tracks and the resulting warm conveyor belts linked to the export of pollutants tend to occur over Canada (Merry and Moody, 1996; Cooper et al., 2002a). This scenario is illustrated in Fig. 3B, where the cyclone track is highlighted by a dotted red line and the circulation by the red arrow. This is consistent with the seasonal evolution of the omega vertical wind component, which shows the lowest (and negative) values in August and September in Eastern Canada (domain 4 in Fig. 3C and Fig. 3D), indicating upward movements of the North American outflow. At Izaña, the westerlies occur with a minimum frequency in July (12 days) and August (9 days; Fig.1C1), the period in which the observatory is frequently within the easterly Saharan Air Layer (Rodríguez et al., 2011, 2015). Observe how the air masses from inner North America have a lower impact at Izaña compared to at other periods (Fig.2B3).

From October to December, the North Atlantic high shifts southward, expanding over Southeastern US (Fig.S1D); the Gulf inflow weakens and the westerly wind band shifts progressively southward prompting the transport of air from Central US to the North Atlantic (Fig. 2A4–2B4).

An overall analysis indicates marked seasonality in the atmospheric circulations with potential implications for the export and transatlantic transport of major aerosol components. The westerlies (Fig. 2A–2B), including the North American outflow (Fig. 3), occur at lower (subtropical) latitudes in winter than in summer (mid latitudes). This seasonal shift is also associated with the upward transport of air, which is important in Central US to Eastern US in March–May (domains 1 and 2 in Fig. 3C and 3D) and shifts northward along Eastern North America through spring and summer (domains 2 to 4 in Fig. 3C and 3D), reaching maximum intensity when the North American outflow occurs over Eastern Canada in August and September



(domains 4 in Fig. 3D). This affects which source regions of North America impact downwind North Atlantic free troposphere; air masses from Southern US are transported across the Atlantic in winter (Fig. 2B1), from Central US in spring (Fig. 2B2) and from Canada in summertime (Fig. 2B3). This is consistent with the seasonal shift of cyclone tracks, westerlies and warm conveyor belt described in previous studies (Stohl, 2001; Cooper et al., 2002a). Of special relevance is the spring, when the westerly jet blows over SO<sub>2</sub> source regions coupled with upward movements able to transport aerosols emitted near ground to altitude above the boundary layer (Fig. 3B).

### 3.3 Transatlantic transport of North American aerosols

We studied the seasonal variability of the sub-10 μm aerosol components under westerly airflow conditions at Izaña and its connection to the transatlantic transport from North America. The chemical composition of 126 samples of PM<sub>10</sub> collected at Izaña (2008–2013) under westerly airflow conditions, whose back-trajectories are plotted in Fig.S1A, were used.

Under westerly airflow conditions, the time series of the aerosol components typically show a low background level and sporadic peak episodes; for example, nss-SO<sub>4</sub><sup>2-</sup> shows a background of 0.05–0.15 μg·m<sup>-3</sup> and peak events 0.5–1.5 μg·m<sup>-3</sup>, organic matter increase from 0.01–0.2 μg·m<sup>-3</sup> background level to 1–2.5 μg·m<sup>-3</sup> peak events, whereas elemental carbon has a background < 0.01 μg·m<sup>-3</sup> and peak events within the range 0.03–0.1 μg·m<sup>-3</sup>. For each aerosol component, we determined the seasonal evolution of the monthly 30<sup>th</sup>, 50<sup>th</sup> and 80<sup>th</sup> percentiles as representative of the background levels, central position of concentration distribution and high concentration episodes, respectively. The 30<sup>th</sup> and 80<sup>th</sup> percentiles plots are presented in the supplement (S5). The Median Concentrations at Receptor (MCAR) plots were determined for the study of the connection of peak events of aerosol components at Izaña with episodes of North American aerosol export.

#### 3.3.1 Sulphate

Figure 5A1 shows the MCAR plot for nss-SO<sub>4</sub><sup>2-</sup>, whereas Fig. 5B1 shows the value of the 50<sup>th</sup> percentile (50<sup>th</sup>P) concentration for each month at Izaña. The monthly 50<sup>th</sup>P of nss-SO<sub>4</sub><sup>2-</sup> shows high levels from March to July (0.28–0.41 μg·m<sup>-3</sup>), with a maximum in March–May (0.33–0.41 μg·m<sup>-3</sup>), and low levels from September to February (0.06–0.24 μg·m<sup>-3</sup>). The March to July period can be considered the high-sulphate concentration season, given that both the monthly background (30<sup>th</sup>P) and median (50<sup>th</sup>P) levels are high in this period (Fig. S5A).

The MCAR plot represents the nss-SO<sub>4</sub><sup>2-</sup> concentration recorded at Izaña (median value, i.e. 50<sup>th</sup>P) when the airflows (tracked by back-trajectories) have passed by each pixel of the study domain (Fig.5A1). Regions with relatively high nss-SO<sub>4</sub><sup>2-</sup> concentrations (0.3–0.5 μg·m<sup>-3</sup> in yellow to red scale) compared to the background (< 0.1 μg·m<sup>-3</sup> in blue) are connected to potential transport routes. The MCAR plot suggests that there are two preferential transport paths. The first route points to the transport of nss-SO<sub>4</sub><sup>2-</sup> from the North-East US at ~40°N; this is consistent with the high SO<sub>2</sub> emissions (Fig. 3B) and high nss-SO<sub>4</sub><sup>2-</sup> concentrations (Fig. 4A) typical of this region (Fig. 3B) associated with coal burning power plants (Mann et al.,



2010; Fioletov et al., 2011, 2016) and the North American outflow (Fig. 3). Because the North American outflow occurs over this region (NE–US) during a great part of the year (Fig. 3), this is probably the most important nss-SO<sub>4</sub><sup>2-</sup> export region to the Atlantic. The correlated seasonal evolution of omega in this region (domain 2 in Fig. 3C and 3D) and nss-SO<sub>4</sub><sup>2-</sup> at Izaña (Fig. 5B1) indicates enhanced upward movements of air from March to July enrich the North Atlantic free troposphere in sulphate aerosols. Maximum nss-SO<sub>4</sub><sup>2-</sup> occurs from March to May (Fig. 5B1), when upward air movements associated with the Gulf inflow (Fig. 3), cyclones (Cooper et al., 2002b) and the occurrence of the North American outflow over this region enhances the export of regional pollutants (Fig. 3A and Fig. 4A). A second transport pathway is associated with transatlantic transport at higher latitudes (50°N) and anticyclonic circulation around the Azores High (Fig. 5A1); this route is associated with the occurrence of the North American outflow over Northern US and Canada, from mid-summer (August) to mid-autumn (November; Fig. 3A1). Observe how the drop in the median (50<sup>th</sup>P: from 0.30 to 0.20 μg·m<sup>-3</sup>; Fig. S5A2) and of the background (30<sup>th</sup>P: from 0.26 to 0.16 μg·m<sup>-3</sup>; Fig. S5A3) nss-SO<sub>4</sub><sup>2-</sup> concentrations from July to August is associated with the northward shift of the main westerly stream and the North American outflow (Fig. 3A1); from August on the westerly jet occurs at higher latitudes, over Canada, in regions depleted in nss-SO<sub>4</sub><sup>2-</sup> compared to NE–US (Fig. 4A), as a result less nss-SO<sub>4</sub><sup>2-</sup> is exported and transported across the Atlantic.

### 15 3.3.2 Nitrate

The MCAR plot and the monthly 50<sup>th</sup>P of NO<sub>3</sub><sup>-</sup> at Izaña are plotted in Fig. 5A2 and 5B2, respectively. Nitrate was present in extremely low concentrations most of the time. Concentrations were < 0.05 μg·m<sup>-3</sup> in 97 samples, and > 0.1 μg·m<sup>-3</sup> in only 21 samples; for this reason the 50<sup>th</sup>P was ~zero for most months (Fig. 5B2). High NO<sub>3</sub><sup>-</sup> concentration events (80<sup>th</sup>P > 0.1 μg·m<sup>-3</sup>) were mostly recorded in winter and early spring (January–April, Fig. 5B2), when high NO<sub>3</sub><sup>-</sup> was within the range 20 0.2–0.8 μg·m<sup>-3</sup>. This is typical behaviour for ammonium nitrate, which mostly forms under low temperature conditions, whereas gaseous nitric acid prevails in warmer environments (Squizzato et al., 2013). The MCAR plot shows transport of NO<sub>3</sub><sup>-</sup> at low latitudes 30–35°N (Fig. 5A2), which is consistent with the circulation of the westerlies (e.g. Fig. 2A1 and Fig. 2B1) and the North American outflow in winter months (e.g. Fig. 3A1), when most of the above-described high NO<sub>3</sub><sup>-</sup> events occur (Fig. 5B2). The highest concentrations of nitrate in North America occur in the Central North region (Fig. 4B); our results suggest that nitrate export events from North America may be associated with NW winds (e.g. as the main stream of the westerlies in winter, Fig. 2A1) over this high nitrate region (Fig. 4B) followed by export at 35–30°N (Fig. 5B1) under geopotential / pressure systems that should be studied in future research. The MCAR plot also suggests a second transport route similar to that observed for nss-SO<sub>4</sub><sup>2-</sup>, i.e. transatlantic transport at high latitudes (50°N) and circulation around the Azores High (Fig. 5B1) which is probably associated with the autumn events (Fig. 5B2), when the North American outflow occurs over Canada (Fig. 3A1). The nitrate concentrations we observe at Izaña are similarly low to those registered by Dzepina et al. (2015) at the Pico free troposphere site in the Azores linked to long range transport from North America; because nitrate may experience negative artefacts during sampling (Schaap et al., 2004; Vecchi et al., 2009), we cannot



discard underestimations and believe that further intercomparison with artefact-free real-time nitrate measurements should be carried out.

### 3.3.3 Ammonium

The MCAR plot and the monthly 50<sup>th</sup>P of NH<sub>4</sub><sup>+</sup> at Izaña are shown in Fig. 5A3 and 5B3, respectively. Median (50<sup>th</sup>P) and 80<sup>th</sup>P concentrations present a maximum in April–May (Fig. 5B3 and Fig. S5C1), as nss-SO<sub>4</sub><sup>=</sup>. The MCAR plot for NH<sub>4</sub><sup>+</sup> shows two main transport pathways which resemble those of nss-SO<sub>4</sub><sup>=</sup>; one transport pathways from North-eastern US at ~40 °N and a second transport route pointing to the occurrence of the North American outflow by Canada and subsequent transatlantic transport at high latitudes and circulation around the Azores High (Fig. 5A3). Because of the prevalent extremely low levels of nitrate, ammonium is attributed to ammonium-sulphate in most events. The transport (north-eastward export) routes we observe for nss-SO<sub>4</sub><sup>=</sup> and NH<sub>4</sub><sup>+</sup> in Eastern US (Alabama–Tennessee–Virginia; Fig. 5A1 and 5A3) are similar to those associated with the passage of spring cyclones and front in the region, prompting the export of pollutants to the Atlantic (Cooper et al., 2002b).

### 3.3.4 Elemental Carbon

Figures 6A1 and 6B1 show the MCAR plot and the monthly 50<sup>th</sup>P and 80<sup>th</sup>P of EC, respectively. The analysis of the monthly 50<sup>th</sup>P and 80<sup>th</sup>P values discloses two relevant periods, associated to high (May–September) and low (January–April) EC events. We associated this seasonal variability of the EC transported by the westerlies to Izaña (i) with the spatial distribution of the EC source regions in North America (Fig. 4D) and (ii) with the seasonal shift of the westerlies (Fig. 2A1–2A4) and the North American outflow (Fig. 3). The highest surface concentrations of EC are estimated to occur in what we have called “EC-rich NE–US regions”, which include large urban areas placed 40–45 °N south of the great lakes to the Atlantic coast (e.g. Chicago, Detroit, New Jersey, Philadelphia and New York; Fig. 4D), linked to fossil fuel combustion (mostly diesel exhaust emissions and coal burning) according to Park et al. (2003).

The season of high EC concentrations at Izaña occurs from May to September, when the westerlies shift northward from 40°N to 55°N (Fig. 3A) affecting the “EC-rich NE–US regions” (40–45°N, Chicago to New York, Fig. 4D). This seasonal shift is associated with a rise of the upward air movements in Eastern US (domains 2 and 3 in Fig. 3C and 3D), including the “EC-rich NE–US regions” (domain 3 in Fig. 3C and 3D), that enhances the export of EC to the North Atlantic free troposphere in the North American outflow. The highest median EC concentrations at Izaña are observed in August and September (~0.03 μg·m<sup>-3</sup>; Fig. 6B1 and Fig. S5D1), when the eastward propagating cyclones over Canada prompt the export of pollutants from these “EC-rich NE–US regions” to the Gulf of Maine and the Atlantic (Merrill and Moody, 1996), in a scenario illustrated in Fig 3B; the lowest values of omega in Eastern Canada (domain 4 in Fig. 3C and 3D) occur in August and September, which indicates a great potential to lift boundary layer air to the North Atlantic free troposphere. This

Atmos. Chem. Phys. Discuss., doi:10.5194/acp-2017-60, 2017  
 Manuscript under review for journal Atmos. Chem. Phys.  
 Discussion started: 27 February 2017  
 © Author(s) 2017. CC-BY 3.0 License.



interpretation is consistent with the MCAR plot for EC, which shows a clear transport pathway (at high latitudes,  $\sim 50^\circ\text{N}$ ) from Canada and these “EC-rich NE–US regions” to the Gulf of Maine and then to the Atlantic with subsequent circulation around the Azores High (Fig. 6A1); this EC transport route is similar to the prevalent transport pathway of August and September (Fig. 2B3).

- 5 Low EC concentrations at Izaña occur between January and April, when the westerlies and the North American outflow occur at low latitudes ( $<40^\circ\text{N}$ ; Fig. 3A), to the south of the EC source regions ( $40\text{--}45^\circ\text{N}$ ; Fig. 4D).

Figure 7 shows the mean burnt fraction (%) of each  $0.25^\circ \times 0.25^\circ$  grid cell associated with fires, which occur mainly in Southeastern US in January–February (Fig. 7A); it then spreads northward from March on over Central US to Southern Canada (Fig. 7B) and over Canada and NW US in June–September (Fig. 7C) and then shifts southward to US (Fig. 7D).

- 10 Boreal fires prompt high EC concentrations in Canada (Park et al., 2005) in NW and North-Central US (Washington, Oregon and Nevada; Park et al., 2003) that can be exported to the Atlantic in the uplifting North American outflow, potentially contributing to the EC records at Izaña in August and September (Fig. 6B1).

### 3.3.5 Organic Matter

- 15 Figures 6A2 and 6B2 show the MCAR plot and the monthly  $50^{\text{th}}$ P of OM. This aerosol component shows very marked seasonal evolution, with high levels from January to July, and a maximum from March to May (Fig. 6B2, Fig. S5E1–E3). This is consistent with the MCAR plot (Fig. 6A2), which shows a transport route from Southeastern US to Izaña at low latitudes ( $30\text{--}40^\circ\text{N}$ ), a common circulation of winter and spring (Fig. 2A1–2A2). From August to December, OM concentrations transported by the westerlies to Izaña are low, associated with the occurrence of the westerlies over North America at high latitudes (Fig. 2A3–2A4).

- 20 The seasonal evolution of OM is very different ( $\sim$ opposite) to that of EC (Fig. 6A2 and 6B2). Air masses transported from Southeastern US to Izaña (January to April) are rich in OM and relatively poor in EC (Fig. 6A2 and 6B2), whereas the air transported from NE US to Izaña (typically from July to September) is poor in OM and rich in EC (Fig. 6A2 and 6B2). This is consistent with the spatial distribution of these aerosol species in the US (Fig. 4D and 4E) and suggests that in Southeastern US there are sources of OM that are not, on the other hand, important in EC, and are most probably biogenic emissions. Globally, biogenic volatile organic carbon emissions (BVOCs), i.e. precursors of secondary OA, are comprised of isoprene ( $\sim 50\%$ ), methanol, ethanol, acetaldehyde, acetone,  $\alpha$ -pinene,  $\beta$ -pinene,  $t$ - $\beta$ -ocimene, limonene, ethene, and propene ( $\sim 30\%$ ), and other compounds (mostly terpenoids;  $\sim 17\%$ ) (Guenther et al., 2012). Biogenic emissions are the principle source of OM in the US, followed by three combustion sources that also emit EC (wildfires, fossil-fuel and bio-fuel) (Park et al., 2003); specifically, in South-eastern US, BVOC emissions are mainly isoprene (81%) and monoterpenes (19%) (Goldstein et al., 2008), with biogenic secondary OA predicted to contribute around 10–20% of  $\text{PM}_{2.5}$  mass (Liao et al.,
- 30



2007). A scenario of biogenic emissions higher in SE–US than in NE–US is consistent with global distribution of the secondary organic aerosols, whose concentrations are usually higher near to the tropics than at mid latitudes (Guenther et al., 2012; Sindelarova et al., 2014). The importance of the spatial variability of the OM and EC sources and the latitudinal shift of the westerlies over Eastern North America is illustrated from July to August, when a drop in OM concentrations (0.85 to  
5 0.20  $\mu\text{g}\cdot\text{m}^{-3}$ ; Fig. 6B2) and an increase in EC concentrations (0.005 to 0.03  $\mu\text{g}\cdot\text{m}^{-3}$ ; Fig. 6B1) is associated with the northern shift of the North American outflow (43° to 50°N; Fig. 3A).

### 3.3.6 Mineral dust

Figures 8A and 8B show the MCAR plot and the monthly 50<sup>th</sup>P of calcium, aluminium and the associated bulk dust concentrations. These aerosol components exhibit high concentrations from February to May (Fig. 8B1–B3; Fig. S5F–S5H).  
10 The MCAR plot shows a pattern of North American dust export at low latitudes (~35°N, through North Carolina) towards the north-east which, once over the Atlantic, follow the anticyclonic circulation around the Azores High to Izaña (Fig. 8A1–A3). We attribute these events to dust emissions in a region that expands from SW Texas northward throughout the High Plains, and subsequent dust export to the Atlantic. Figure 8C shows the Major Dust Activity Frequency (MDAF) detected by satellite; dust activity is observed in SW Texas (Chiguagua–Big Bend Desert) in February, through March to May the  
15 activity expands northward across the High Plains (western Texas to Nebraska); other dust sources with lower potential to impact on the North Atlantic are also observed in western US (Great Basin, Mojave Desert and Colorado Plateau). The High Plains are among the major dust sources in North America, and these sources are considered anthropogenic (linked to agriculture), with maximum activity between February and May (Ginoux et al., 2012). Dust emissions and eastward mobilisation is associated with the intense westerly winds linked to eastward moving cyclones, which also prompt the  
20 upward transport of dust to several kilometres above ground, according to Novlan et al. (2007); this scenario is illustrated in Fig. 8A3, showing how the associated air mass track is consistent with the dust export and transatlantic transport route to Izaña observed in our analysis. During these spring events high dust concentrations (100s of  $\mu\text{g}\cdot\text{m}^{-3}$ ) are lifted to altitudes 6–12 km a.s.l. over Southern US (Talbot et al., 1998). Upward transport of dust is also associated with convective activity in Central US, Colorado and Oklahoma, in May–June (Corr et al., 2016). The correlation we found between the seasonal  
25 evolution of omega in domain 1 (Fig.3C and 3D) and dust at Izaña (Fig.8B3) supports the idea that from February to May westerly winds and the uplifting of air in the High Plains enrich the North American outflow and the westerly jet in the dust aerosols.

### 3.3.7 Sea salt

Sea salt concentrations at Izaña are extremely low, with monthly 50<sup>th</sup>P values 0.07 to 0.22  $\mu\text{g}\cdot\text{m}^{-3}$  between December and  
30 May (Fig. 9). These low concentrations are typical of free troposphere sites; in fact, sea salt at Izaña (average = 0.25  $\mu\text{g}\cdot\text{m}^{-3}$ , median 0.16  $\mu\text{g}\cdot\text{m}^{-3}$ ) is about two orders of magnitude lower than in the marine boundary layer of the Canary Islands

Atmos. Chem. Phys. Discuss., doi:10.5194/acp-2017-60, 2017

Manuscript under review for journal Atmos. Chem. Phys.

Discussion started: 27 February 2017

© Author(s) 2017. CC-BY 3.0 License.



(average  $\sim 11 \mu\text{g}\cdot\text{m}^{-3}$ , Querol et al., 2004). The extremely low concentrations of this marine aerosol at Izaña supports our interpretations, i.e. the aerosols transported by the westerlies to Izaña are mostly linked to emissions and upward transport in continental regions of North America, and not over the ocean.

### 3.3.8 Mass closure of aerosols

- 5 Fig. 10 shows the contribution of each species to bulk  $\text{PM}_{10}$  aerosol mass in samples collected in the westerlies at Izaña; data are classified from the highest to the lowest levels. We considered two approaches: including and excluding mineral dust. When mineral dust is not included (Fig. 10A), the most important contributors to bulk  $\text{PM}_{10}$  are by far  $\text{nss-SO}_4^-$  and OM. In the 1<sup>st</sup>–50<sup>th</sup> percentile range for the sum of aerosol components (a proxy of background levels) - 0.05 to  $1.0 \mu\text{g}\cdot\text{m}^{-3}$  - the most important contributors are  $\text{nss-SO}_4^-$  ( $0.19 \mu\text{g}\cdot\text{m}^{-3}$  on average, accounting for 38% of the sum of chemical species) and OM
- 10 ( $0.14 \mu\text{g}\cdot\text{m}^{-3}$ , 30%). In the 75<sup>th</sup>–95<sup>th</sup> percentile range (a proxy of high load of aerosol events) -  $\sim 2.0$  to  $3.6 \mu\text{g}\cdot\text{m}^{-3}$  - the most important contributors are OM ( $1.43 \mu\text{g}\cdot\text{m}^{-3}$ , 57%) and then  $\text{nss-SO}_4^-$  ( $0.48 \mu\text{g}\cdot\text{m}^{-3}$ , 19%). These results are consistent with previous studies that did not include dust, such as Park et al. (2004, 2005), who focused on the composition of aerosols in the background boundary layer of US, and Dzepina et al. (2015), who studied the aerosols transported from North America to the North Atlantic free troposphere at Pico observatory in the Azores.
- 15 When mineral dust is considered, it becomes the most important contributor to sub- $10\mu\text{m}$  aerosol mass (Fig. 10B). In the 1<sup>st</sup>–50<sup>th</sup> percentile range (a proxy of background levels), bulk  $\text{PM}_{10} = 0.15 - 2.54 \mu\text{g}\cdot\text{m}^{-3}$ , the most important contributors to bulk aerosol mass are dust ( $0.78 \mu\text{g}\cdot\text{m}^{-3}$  on average, accounting for 53% of bulk mass),  $\text{nss-SO}_4^-$  ( $0.21 \mu\text{g}\cdot\text{m}^{-3}$ , 14%), OM ( $0.27 \mu\text{g}\cdot\text{m}^{-3}$ , 18%) and  $\text{NH}_4^+$  ( $0.07 \mu\text{g}\cdot\text{m}^{-3}$ , 5%). In the 75<sup>th</sup>–95<sup>th</sup> percentile range (a proxy of aerosol events), bulk  $\text{PM}_{10} = 3.9-8.9 \mu\text{g}\cdot\text{m}^{-3}$ , the most important contributors to bulk aerosol mass are dust ( $2.8 \mu\text{g}\cdot\text{m}^{-3}$ , 56%) and OM ( $1.23 \mu\text{g}\cdot\text{m}^{-3}$ , 24%)
- 20 followed by  $\text{nss-SO}_4^-$  ( $0.47 \mu\text{g}\cdot\text{m}^{-3}$ , 9%) and  $\text{NH}_4^+$  ( $0.1 \mu\text{g}\cdot\text{m}^{-3}$ , 2%). The lack of previous studies on transatlantic transport of North American dust make the comparison with previous data difficult; it should be highlighted that Ancellet et al. (2016) detected this transatlantic transport in June (out of the seasonal maximum).

Our overall results evidence that dust and organic matter are the most abundant aerosols transported from North America to the North Atlantic free troposphere.

## 25 4 Conclusions

- A  $\sim 5$ -year record of aerosol chemistry at Izaña Observatory (located at  $\sim 2400$  m.a.s.l. in Tenerife, the Canary Islands) was used to study the transatlantic transport of aerosols. This study shows that North America is a major source of aerosols, which are transported by the westerly winds across the North Atlantic free troposphere at subtropical and mid-latitudes. The composition of aerosols carried by the westerlies experiences a marked seasonal evolution which is influenced by (i) the
- 30 spatial distribution of the aerosol sources in North America and (ii) the seasonal variability of the large-scale meteorology in



North America. Of special meteorological relevance is the seasonal shift in the westerly jet and the North American outflow, which migrate from low latitudes in winter (~32°N, January–March) to high latitudes in summer (~52°N, August–September). The export of boundary layer air laden in aerosols to the North Atlantic free troposphere is enhanced by the occurrence of cyclones that move eastward with the westerly atmospheric circulation.

5 We found that the westerlies carry high loads of:

- mineral dust from February to May, associated with dust emissions in a region that expands from SW Texas (Chiguagua–Big Bend Desert) northward through the High Plains (western Texas to Nebraska), and subsequent dust export to the Atlantic associated with eastward moving cyclones, westerly winds and the North American outflow, which in this period migrate from 35°N in February to 40°N in May,
- 10 • non sea-salt-sulphate and ammonium from March to May, when cyclones and the associated outflow occur over North-eastern US, where the highest SO<sub>2</sub> emissions occur in North America,
- organic matter from February to May, when cyclones and the associated outflow occur over regions of Eastern US rich in organic aerosols according to previous studies,
- 15 • elemental carbon in August and September, when cyclones, the westerly jet and the North American outflow occur at high latitudes (50 to 55°N) favouring the export of boundary layer air from the regions where the highest concentrations of elemental carbon occur in North America according to previous studies (Chicago to New York, 40–45°N),

The concentrations of sub10-µm aerosol mass (PM<sub>10</sub>) that reach Izaña Observatory after transatlantic transport typically range between 1.2 and 4.23 µg·m<sup>-3</sup> (20<sup>th</sup> and 80<sup>th</sup> percentiles). The most important contributors to background aerosols (when 20 PM<sub>10</sub> is within the 1<sup>st</sup>–50<sup>th</sup> percentiles = 0.15–2.54 µg·m<sup>-3</sup>) are North American dust (53%), organic matter (18%) and non sea-salt-SO<sub>4</sub><sup>-</sup> (14%). High PM<sub>10</sub> events (75<sup>th</sup>–95<sup>th</sup> percentiles = 3.9–8.9 µg·m<sup>-3</sup>) are prompted by dust (56%), organic matter (24%) and nss-SO<sub>4</sub><sup>-</sup> (9%). Our results suggest that a significant fraction of organic aerosols may be linked to sources other than combustion (e.g. biogenic) and that North American dust may be linked to anthropogenic dust sources linked to the use of soil.

25 The overall results indicate that future long-term evolution of the aerosol composition in the North Atlantic free troposphere will be influenced by air quality policies, with implications for the emissions of aerosol precursors, and the use of potential dust emitter soils in North America. The conversion of natural lands to agriculture and pasturage fields have had a number of environmental implications in North America (Nordstrom et al., 2004, Wu et al., 2007). Research has suggested that this

Atmos. Chem. Phys. Discuss., doi:10.5194/acp-2017-60, 2017  
 Manuscript under review for journal Atmos. Chem. Phys.  
 Discussion started: 27 February 2017  
 © Author(s) 2017. CC-BY 3.0 License.



change of land use may increase (MNP, 2006, Lawler et al., 2014 ) and this would have implications for dust emission, air quality and dust impacts on the North Atlantic free troposphere".

*Acknowledgements:* This study is part of the project AEROATLAN (CGL2015-66299-P), funded by the Ministry of Economy and Competitiveness of Spain and the European Regional Development Fund (ERDF). The long-term records of the GAW aerosol program are also funded by AEMET. M.I. García acknowledges the grant of the Canarian Agency for Research, Innovation and Information Society (ACIISI) co-funded by the European Social Funds. The authors gratefully acknowledge the NOAA/ESRL Physical Sciences Division for the provision of the NCAR/NCEP re-analysis, NILU for providing FLEXTRA back-trajectories based on meteorological data provided from ECMWF (European Centre for Medium Range Weather Forecast), the BSC (Barcelona Supercomputing Centre) for providing DREAM8b model, the Oak Ridge National Laboratory (ORNL) Distributed Active Archive Centre (DAAC) - as part of the NASA Earth Observing System Data and Information System (EOSDIS) - for providing the Global Fire Emissions Database, and the GES-DISC Interactive Online Visualization ANd aNalysis Infrastructure (Giovanni) - as part of the NASA's Goddard Earth Science (GES) Data and Information Service Centre (DISC) - for the OMI AI data set, and the Storm Prediction Centre - as part of the NOAA National Weather service - for providing the Severe Weather Database Files for US tornadoes. We also thank to Juan José Bustos for the calculation of the back-trajectories, Dr. Javier López-Solano for his assistance with the Aerosol Index data processing and Dr. Y.Boose for providing the picture of the Saharan Air Layer conditions. The excellent work performed by the staff of Izaña Observatory (C. Bayo, C. Hernández, F. de Ory, V. Carreño, R. del Campo and SIELTEC Canarias) is appreciated.

*Competing interests:* The authors declare that they have no conflict of interest.



**Gobierno de Canarias**  
 Agencia Canaria  
 de Investigación, Innovación  
 y Sociedad de la Información



European Regional  
 Development Fund

20

## References

25 Ancellet, G., Pelon, J., Totems, J., Chazette, P., Bazureau, A., Sicard, M., Di Iorio, T., Dulac, F., and Mallet, M.: Long-range transport and mixing of aerosol sources during the 2013 North American biomass burning episode: analysis of multiple lidar observations in the western Mediterranean basin, Atmos. Chem. Phys., 16, 4725-4742, doi:10.5194/acp-16-4725-2016, 2016.



- Basart, S., Pérez, C., Nickovic, S., Cuevas, E., Schulz, M., and Baldasano, J. M.: Development and evaluation of BSC-DREAM8b dust regional model over Northern Africa, the Mediterranean and the Middle East regions, *Tellus B*, 64, 18539, doi: 10.3402/tellusb.v64i0.18539, 2012.
- 5 Bonsang, B., Nguyen, B.C., Gaudry, A. and Lambert, G.: Sulfate enrichment in marine aerosols owing to biogenic gaseous sulfur compounds, *J. Geophys. Res. Oc.*, 1978–2012, 85 (C12), 7410–7416, 1980.
- Cavalli, F., Viana, M., Yttri, K. E., Genberg, J. and Putaud, J.-P.: Toward a standardised thermal-optical protocol for measuring atmospheric organic and elemental carbon: the EUSAAR protocol, *Atmos. Meas. Tech. Discuss.*, 2(5), 2321–2345, doi:10.5194/amtd-2-2321-2009, 2009.
- 10 Chai, M., Birch, M. E., and Deye, G.: Organic and elemental carbon filter sets: preparation method and interlaboratory results, *Ann. Occup. Hyg.*, 56, 959–967, 2012.
- Chin, M., Diehl, T., Ginoux, P., and Malm, W.: Intercontinental transport of pollution and dust aerosols: implications for regional air quality, *Atmos. Chem. Phys.*, 7, 5501–5517, doi:10.5194/acp-7-5501-2007, 2007.
- Cooper, O.R., Moody, J. L., Parrish, D. D., Trainer, M., Holloway, J. S., Hübler, G., Fehsenfeld, F. C., and Stohl, A.: Trace gas composition of midlatitude cyclones over the western North Atlantic Ocean: A seasonal comparison of O<sub>3</sub> and CO, *J. Geophys. Res.*, 107, 4057, doi: 10.1029/2001JD000902, 2002a.
- 15 Cooper, O.R., Moody, J. L., Parrish, D. D., Trainer, M., Ryerson, T. B., Holloway, J. S., Hübler, G., Fehsenfeld, F. C. and Evans, M. J.: Trace gas composition of midlatitude cyclones over the western North Atlantic Ocean: A conceptual model. *J. Geophys. Res.*, 107, D7, 4056, 10.1029/2001JD000901, 2002b.
- Corr, C. A., Ziemba, L. D., Scheuer, E., Anderson, B. E., Beyersdorf, A. J., Chen, G., Crosbie, E., Moore, R. H., Shook, M., Thornhill, K. L., Winstead, E., Lawson, R. P., Barth, M. C., Schroeder, J. R., Blake, D. R., Dibb, J. E.: Observational evidence for the convective transport of dust over the Central United States., *J. Geophys. Res. Atmos.*, 121, 1306–1319, doi:10.1002/2015JD023789.
- 20 Dickerson, R. R., Huffman, G. J., Luke, W. T., Nunnermacker, L. J., Pickering, K. E., Leslie, A. C. D., Lindsey, C. G., Slinn, W. G. N., Kelly, T. J., Daum, P. H., Delany, A. C., Greenberg, J. P., Zimmerman, P. R., Boatman, J. F., Ray, J. D., and Stedman, D. H.: Thunderstorms: An important mechanism in the transport of air pollutants, *Science*, 235, 460–464, 1987.
- 25 Dickerson, R. R., Doddridge, B., Kelley, P., and Rhoads, K.: Large scale pollution of the atmosphere over the remote Atlantic Ocean: Evidence from Bermuda, *J. Geophys. Res.*, 100, 8945–8952, 1995.
- Dzepina, K., Mazzoleni, C., Fialho, P., China, S., Zhang, B., Owen, R. C., Helmig, D., Hueber, J., Kumar, S., Perlinger, J. A., Kramer, L. J., Dziobak, M. P., Ampadu, M. T., Olsen, S., Wuebbles, D. J., and Mazzoleni, L. R.: Molecular characterization of free tropospheric aerosol collected at the Pico Mountain Observatory: a case study with a long-range transported biomass burning plume, *Atmos. Chem. Phys.*, 15, 5047–5068, doi:10.5194/acp-15-5047-2015, 2015.
- 30 Eckhardt, S., Stohl, A., Wernli, H., James, P., Forster, C. and Spichtinger, N.: A 15-year climatology of warm conveyor belts, *J. Clim.*, 17(1), 218–237, doi:10.1175/1520-0442(2004)017<0218:AYCOWC>2.0.CO;2, 2004.
- 35 Fioletov, V. E., McLinden, C. A., Krotkov, N. A., Moran, M. D. and Yang, K.: Estimation of SO<sub>2</sub> emissions using OMI retrievals, *Geophys. Res. Lett.*, 38, L21811, doi: 10.1029/2011GL049402, 2011.
- Fioletov, V. E., McLinden, C. A., Krotkov, N., Li, C., Joiner, J., Theys, N., Carn, S., and Moran, M. D.: A global catalogue of large SO<sub>2</sub> sources and emissions derived from the Ozone Monitoring Instrument, *Atmos. Chem. Phys.*, 16, 11497–11519, doi:10.5194/acp-16-11497-2016, 2016.
- 40 Ginoux, P., Prospero, J. M., Gill, T. E., Hsu, N. C. and Zhao, M.: Global-scale attribution of anthropogenic and natural dust sources and their emission rates based on MODIS Deep Blue aerosol products, *Rev. Geophys.*, 50, RG3005, doi:10.1029/2012RG000388, 2012.
- Goldstein, A. H., Koven, C. D., Heald, C. L., and Fung, I. Y.: Biogenic carbon and anthropogenic pollutants combine to form a cooling haze over the southeastern United States, *P. Natl. Acad. Sci. USA*, 106(22), 8835–8840, www.pnas.org/cgi/doi/10.1073/pnas.0904128106, 2009.
- 45 Gravenhorst, G.: Maritime sulfate over the North Atlantic. *Atmos. Environ.*, 12 (1-3, Sulfur Atmosphere), 707-13, 1978.
- Guenther, A. B., Jiang, X., Heald, C. L., Sakulyanontvittaya, T., Duhl, T., Emmons, L. K., and Wang, X.: The Model of Emissions of Gases and Aerosols from Nature version 2.1 (MEGAN2.1): an extended and updated framework for modeling biogenic emissions, *Geosci. Model Dev.*, 5, 1471–1492, doi:10.5194/gmd-5-1471-2012, 2012.

Atmos. Chem. Phys. Discuss., doi:10.5194/acp-2017-60, 2017

Manuscript under review for journal Atmos. Chem. Phys.

Discussion started: 27 February 2017

© Author(s) 2017. CC-BY 3.0 License.



- Honrath, R. E., Owen, R. C., Val Martin, M., Reid, J. S., Lapina, K., Fialho, P., Dziobak, M. P., Kleissl, J., and Westphal, D. L.: Regional and hemispheric impacts of anthropogenic and biomass burning emissions on summertime CO and O<sub>3</sub> in the North Atlantic lower free troposphere, *J. Geophys. Res. Atmos.*, 109, D24310, doi:10.1029/2004JD005147, 2004.
- 5 IPCC, 2013: Climate change 2013: The physical science basis. Contribution of Working Group I to the Fifth Assessment Report of the Intergovernmental Panel on Climate edited by: Stocker, T.F., Qin, D., Plattner, G.K. Tignor, M., Allen, S.K., Boschung, J., Nauels, A., Xia, Y., Bex V., and Midgley P.M. Cambridge University Press, Cambridge, UK and New York, NY, USA, 1535 pp.
- Kalnay, E., Kanamitsu, M., Kistler, R., Collins, W., Deaven, D., Gandin, L., Iredell, M., Saha, S., White, G., Woollen, J., Zhu, Y., Leetmaa, A., Reynolds, R., Chelliah, M., Ebisuzaki, W., Hig-gins, W., Janowiak, J., Mo, K. C., Ropelewski, C., Wang, J., Jenne, R., and Joseph, D.: The NCEP/NCAR 40-Year Reanalysis Project, *B. Am. Meteorol. Soc.*, 77, 437–471, 1996.
- 10 Lawler, J. J., Lewis, D. J., Nelson, E., Plantinga, A. J., Polasky, S., Withey, J. C., Helmers, D. P., Martinuzzi, S., Pennington, D. and Radeloff, V. C.: Projected land-use change impacts on ecosystem services in the United States, *Proc. Natl. Acad. Sci.*, 111(20), 7492–7497, doi:10.1073/pnas.1405557111, 2014.
- 15 Liao, H., Henze, D. K., Seinfeld, J. H., Wu, S. L., and Mickley, L. J.: Biogenic secondary organic aerosol over the United States: Comparison of climatological simulations with observations, *J. Geophys. Res.-Atmos.*, 112, D06201, doi:10.1029/2006JD007813, 2007.
- Li, Q., Jacob, D. J., Munger, J. W., Yantosca, R. M., and Parrish, D. D.: Export of NO<sub>y</sub> from the North American boundary layer: Reconciling aircraft observations and global model budgets, *J. Geophys. Res.*, 109, D02313, doi:10.1029/2003jd004086, 2004.
- 20 Li, Q., Jacob, D., Park, R., Wang, Y., Heald, C., Hudman, R., Yantosca, R., Martin, R., and Evans, M.: North American pollution outflow and the trapping of convectively lifted pollution by upper-level anticyclone, *J. Geophys. Res.*, 110, D10301, doi:10.1029/2004JD005039, 2005.
- Mann, G. W., Carslaw, K. S., Spracklen, D. V., Ridley, D. A., Manktelow, P. T., Chipperfield, M. P., Pickering, S. J., and Johnson, C. E.: Description and evaluation of GLOMAP-mode: a modal global aerosol microphysics model for the UKCA composition-climate model, *Geosci. Model Dev.*, 3, 519–551, doi:10.5194/gmd-3-519-2010, 2010.
- Martinuzzi, S., Radeloff, V. C., Joppa, L. N., Hamilton, C. M., Helmers, D. P., Plantinga, A. J. and Lewis, D. J.: Scenarios of future land use change around United States’ protected areas, *Biol. Conserv.*, 184, 446–455, doi:10.1016/j.biocon.2015.02.015, 2015.
- 30 Merrill, J. T., and Moody, J. L.: Synoptic meteorology and transport during the North Atlantic Regional Experiment (NARE) intensive: Overview, *J. Geophys. Res.*, 101, 28,903–28,921, 1996.
- MNP: Integrated modelling of global environmental change, an overview of IMAGE 2.4., edited by: Bouwman, A. F., Kram, T., and Klein Goldewijk, K., Netherlands Environmental Assessment Agency (MNP), Bilthoven, The Netherlands, 2006.
- 35 Moody, J. L., Davenport, J. C., Merrill, J. T., Oltmans, S. J., Parrish, D. D., Holloway, J. S., Levy II, H., Forbes, G. L., Trainer, M., and Buhr M.: Meteorological mechanisms for transporting O<sub>3</sub> over the western North Atlantic Ocean: A case study for 24–29 August 1993, *J. Geophys. Res.*, 101, 29213–29277, 1996.
- Myhre, G., D. Shindell, F.-M. Bréon, W. Collins, J. Fuglestedt, J. Huang, D. Koch, J.-F. Lamarque, D. Lee, B. Mendoza, T. Nakajima, A. Robock, G. Stephens, T. Takemura and H. Zhang, 2013: Anthropogenic and Natural Radiative Forcing. In: Climate Change 2013: The Physical Science Basis. Contribution of Working Group I to the Fifth Assessment Report of the Intergovernmental Panel on Climate Change [Stocker, T.F., D. Qin, G.-K. Plattner, M. Tignor, S.K. Allen, J. Boschung, A. Nauels, Y. Xia, V. Bex and P.M. Midgley (eds.)]. Cambridge University Press, Cambridge, United Kingdom and New York, NY, USA.
- 40 Nordstrom, K. and Hotta, S.: Wind erosion from cropland solutions in the USA: a review of problems, and prospects, *Geoderma*, 121(3-4), 157–167, doi:10.1016/j.geoderma.2003.11.012z, 2004.
- Novlan, D.J., Hardiman, M., Gill, T.E., 2007. A synoptic climatology of blowing dust events in El Paso, Texas from 1932–2005. In: 16th Conference on Applied Climatology, American Meteorological Society Annual Meeting, January 2007, San Antonio, TX, paper J3.12, 13 pp. [https://ams.confex.com/ams/87ANNUAL/techprogram/paper\\_115842.htm](https://ams.confex.com/ams/87ANNUAL/techprogram/paper_115842.htm).



- Owen, R. C., Cooper, O. R., Stohl, A. and Honrath, R. E.: An analysis of the mechanisms of North American pollutant transport to the central North Atlantic lower free troposphere, *J. Geophys. Res.*, 111(D23), D23S58, doi:10.1029/2006JD007062, 2006.
- 5 Park, R. J., Jacob, D. J., Chin, M., and Martin, R. V.: Sources of carbonaceous aerosols over the United States and implications for natural visibility, *J. Geophys. Res.*, 108(D12), 4355, doi:10.1029/2002JD003190, 2003.
- Park, R. J., Jacob, D., Field, B. D., Yantosca, R., and Chin, M.: Natural and transboundary pollution influences on sulfate-nitrate-ammonium aerosols in the United States: Implications for policy, *J. Geophys. Res.*, 109, D15204, doi:10.1029/2003JD004473, 2004.
- 10 Park, S. S., Harrison, D., Pancras, J. P., and Ondov, J. M.: Highly time-resolved organic and elemental carbon measurements at the Baltimore Supersite in 2002, *J. Geophys. Res.-Atmos.*, 110, D07S06, doi:10.1029/2004jd004610, 2005.
- Parrish, D. D., Holloway, J. S., Trainer, M., Murphy, P. C., Forbers, G. L., and Fehsenfeld, F. C.: Relationships between ozone and carbon monoxide at surface sites in the North Atlantic region, *J. Geophys. Res.*, 103, 13 357–13 376, 1998.
- Perez, C., Nickovic, S., Baldasano, J. M., Sicard, M., Rocadenbosch, F., and Cachorro, V. E.: A long Saharan dust event over the western Mediterranean: Lidar, Sun photometer observations, and regional dust modeling, *J. Geophys. Res.*, 111, D15214, doi:10.1029/2005JD006579, 2006.
- 15 Prospero, J. M. and Carlson, T. N.: Vertical and areal distribution of Saharan dust over the western Equatorial North Atlantic Ocean, *J. Geophys. Res.*, 77, 5255–5265, 1972.
- Querol, X., Alastuey, A., Viana, M. M., Rodríguez, S., Artiñano, B., Salvador, P., Santos, S. G. D., Patier, R. F., Ruiz, C. R., Rosa, J. D. L., Campa, A. S. D. L., Menedez, M., and Gil, J. I.: Speciation and origin of PM<sub>10</sub> and PM<sub>2.5</sub> in Spain, *J. Aerosol Sci.*, 35, 1151–1172, 2004.
- 20 Ramanathan, V., Crutzen, P. J., Kiehl, J. T., and Rosenfeld, D.: Aerosols, climate and the hydrological cycle, *Science*, 294, 2119–2124, 2001.
- Randerson, J.T., G.R. van der Werf, L. Giglio, G.J. Collatz, and P.S. Kasibhatla. 2015. Global Fire Emissions Database, Version 4, (GFEDv4). ORNL DAAC, Oak Ridge, Tennessee, USA. <http://dx.doi.org/10.3334/ORNLDAC/1293>.
- 25 Ripoll, A., Minguillón, M. C., Pey, J., Jimenez, J. L., Day, D. A., Sosedova, Y., Canonaco, F., Prévôt, A. S. H., Querol, X., Alastuey, A.: Long-term real-time chemical characterization of submicron aerosols at Montsec (southern Pyrenees, 1570 m a.s.l.). *Atmos. Chem. Phys.*, 15, 2935–2951, 2015.
- Rodríguez, S., González, Y., Cuevas, E., Ramos, R., Romero, P. M., Abreu-Afonso, J. and Redondas, A.: Atmospheric nanoparticle observations in the low free troposphere during upward orographic flows at Izaña Mountain Observatory, *Atmos. Chem. Phys.*, 9, 6319–6335, doi:10.5194/acpd-9-10913-2009, 2009.
- 30 Rodríguez, S., Alastuey, A., Alonso-Pérez, S., Querol, X., Cuevas, E., Abreu-Afonso, J., Viana, M., Pérez, N., Pandolfi, M., and de la Rosa, J.: Transport of desert dust mixed with North African industrial pollutants in the subtropical Saharan Air Layer, *Atmos. Chem. Phys.*, 11, 6663–6685, doi:10.5194/acp-11-6663-2011, 2011.
- Rodríguez, S., Cuevas, E., Prospero, J. M., Alastuey, A., Querol, X., López-Solano, J., García, M. I. and Alonso-Pérez, S.: Modulation of Saharan dust export by the North African dipole, *Atmos. Chem. Phys.*, 15(13), 7471–7486, doi:10.5194/acp-15-7471-2015, 2015.
- 35 Schaap, M., Spindler, G., Schulz, M., Acker, K., Maenhaut, W., Berner, A., Wiprecht, W., Streit, N., Müller, K., Brüggemann, E., Putaud, J.-P., Puxbaum, H., Baltensperger, U., and ten Brink, H. M.: Artefacts in the sampling of nitrate studied in the “INTERCOMP” campaigns of EUROTRAC-AEROSOL, *Atmos. Environ.*, 38, 6487–6496, 2004.
- 40 Sindelarova, K., Granier, C., Bouarar, I., Guenther, A., Tilmes, S., Stavrou, T., Müller, J.-F., Kuhn, U., Stefani, P., and Knorr, W.: Global data set of biogenic VOC emissions calculated by the MEGAN model over the last 30 years, *Atmos. Chem. Phys.*, 14, 9317–9341, doi:10.5194/acp-14-9317-2014, 2014.
- Squizzato, S., Masiol, M., Brunelli, A., Pistollato, S., Tarabotti, E., Rampazzo, G., and Pavoni, B.: Factors determining the formation of secondary inorganic aerosol: a case study in the Po Valley (Italy), *Atmos. Chem. Phys.*, 13, 1927–1939, doi:10.5194/acp-13-1927-2013, 2013.
- 45 Stohl, A. and Seibert, P.: Accuracy of trajectories as determined from the conservation of meteorological tracers, *Q. J. R. Meteorol. Soc.*, 125, 1465–1484, 1998.
- Stohl, A., Wotawa, G., Seibert, P., and Krump-Kolb, H.: Interpolation errors in wind fields as a function of spatial and temporal resolution and their impact on different types of kinematic trajectories, *J. Appl. Meteor.*, 34, 2149–2165, 1995.
- 50

Atmos. Chem. Phys. Discuss., doi:10.5194/acp-2017-60, 2017

Manuscript under review for journal Atmos. Chem. Phys.

Discussion started: 27 February 2017

© Author(s) 2017. CC-BY 3.0 License.



- Stohl, A.: A one-year Lagrangian “climatology” of airstreams in the Northern Hemisphere troposphere and lowermost stratosphere, *J. Geophys. Res.*, 106, 7263–7279, 2001.
- Stohl, A.: On the pathways and timescales of intercontinental air pollution transport, *J. Geophys. Res.*, 107(D23), 4684, doi:10.1029/2001JD001396, 2002.
- 5 Talbot, R. W., Dibb, J. E., and Loomis, M. B.: Influence of vertical transport on free tropospheric aerosols over the central USA in springtime, *Geophys. Res. Lett.*, 25, 1367–1370, 1998.
- Val Martín, M., Honrath, R. E., Owen, R. C., Pfister, G., Fialho, P., and Barata, F.: Significant enhancements of nitrogen oxides, black carbon, and ozone in the North Atlantic lower free troposphere resulting from North American boreal wildfires, *J. Geophys. Res.*, 111, D23S60, doi:10.1029/2006JD007530, 2006
- 10 Vecchi, R., Valli, G., Fermo, P., D’Alessandro, A., Piazzalunga, A., and Bernardoni, V.: Organic and inorganic sampling artefacts assessment, *Atmos. Environ.*, 43(10), 1713–1720, 2009.
- Whittaker, K. M., and Horn L. H.: Northern hemisphere extra-tropical cyclone activity for four mid-season months, *J. Climatol.*, 4, 297 – 310, 1984.
- WHO, World Health Organization, 2014. Burden of disease from ambient and household air pollution. [http://www.who.int/phe/health\\_topics/outdoorair/databases/en/](http://www.who.int/phe/health_topics/outdoorair/databases/en/) last accessed, 23-feb-2016.
- 15 Wu, J. and Cho, S.H.: The effect of local land use regulations on urban development in the Western United States, *Reg. Sci. Urban Econ.*, 37(1), 69–86, doi:10.1016/j.regsciurbeco.2006.06.008, 2007.
- Wu, S., Mickley, L. J., Kaplan, J. O., and Jacob, D. J.: Impacts of changes in land use and land cover on atmospheric chemistry and air quality over the 21st century, *Atmos. Chem. Phys.*, 12, 1597–1609, doi:10.5194/acp-12-1597-2012, 2012.
- 20 Zishka, K. M., and Smith, P. J.: The climatology of cyclones and anticyclones over North America and surrounding ocean environs for January and July, 1950–1977, *Mon. Weather Rev.*, 108, 387–401, 1980.

25



**Table 1.** Mass closure and median concentrations of PM<sub>10</sub> and PM<sub>2.5</sub> components in samples collected when Izaña was (i) within the Saharan Air Layer (SAL) and (ii) within the westerlies (WES). Only days when PM<sub>10</sub> and PM<sub>2.5</sub> were sampled simultaneously were taken into account. The percentage of the corresponding parameter with respect to the PM is shown.

	Saharan Air Layer				westerlies			
	PM <sub>10</sub>	%	PM <sub>2.5</sub>	%	PM <sub>10</sub>	%	PM <sub>2.5</sub>	%
NS	146		146		96		96	
<b>mass closure</b>								
PM, µg·m <sup>-3</sup>	46.42		21.27		2.54		2.19	
Σ, µg·m <sup>-3</sup>	40.87	<b>88</b>	15.59	<b>73</b>	1.78	<b>70</b>	1.05	<b>48</b>
undetermined, µg·m <sup>-3</sup>	5.55	<b>12</b>	5.68	<b>27</b>	0.75	<b>30</b>	1.14	<b>52</b>
<b>median concentrations</b>								
dust, µg·m <sup>-3</sup>	36.07	<b>77.7</b>	13.18	<b>62.0</b>	1.13	<b>44.5</b>	0.50	<b>22.8</b>
sea salt, µg·m <sup>-3</sup>	< 0.01	<b>~0</b>	< 0.01	<b>~0</b>	0.01	<b>0.5</b>	0.01	<b>0.5</b>
EC, µg·m <sup>-3</sup>	< 0.01	<b>~0</b>	< 0.01	<b>~0</b>	0.02	<b>0.6</b>	0.01	<b>0.3</b>
OM, µg·m <sup>-3</sup>	2.07	<b>4.5</b>	1.00	<b>4.7</b>	0.32	<b>12.4</b>	0.26	<b>11.7</b>
NH <sub>4</sub> <sup>+</sup> , µg·m <sup>-3</sup>	0.18	<b>0.4</b>	0.17	<b>0.8</b>	0.06	<b>2.2</b>	0.06	<b>2.7</b>
NO <sub>3</sub> <sup>-</sup> , µg·m <sup>-3</sup>	0.82	<b>1.8</b>	0.17	<b>0.8</b>	< 0.01	<b>~0</b>	< 0.01	<b>~0</b>
SO <sub>4</sub> <sup>=</sup> , µg·m <sup>-3</sup>	1.73	<b>3.8</b>	1.06	<b>5.0</b>	0.25	<b>10.0</b>	0.22	<b>10.0</b>
<b>sulphate speciation</b>								
ss-SO <sub>4</sub> <sup>=</sup> , µg·m <sup>-3</sup>	< 0.01	<b>0</b>	< 0.01	<b>0</b>	< 0.01	<b>0</b>	< 0.01	<b>0.1</b>
nss-SO <sub>4</sub> <sup>=</sup> , µg·m <sup>-3</sup>	1.72	<b>3.7</b>	1.05	<b>4.9</b>	0.25	<b>9.8</b>	0.22	<b>10.0</b>
a-SO <sub>4</sub> <sup>=</sup> , µg·m <sup>-3</sup>	0.48	<b>1.0</b>	0.45	<b>2.2</b>	nd	<b>nd</b>	nd	<b>nd</b>
na-SO <sub>4</sub> <sup>=</sup> , µg·m <sup>-3</sup>	1.22	<b>2.6</b>	0.55	<b>2.6</b>	nd	<b>nd</b>	nd	<b>nd</b>

**NS:** number of samples. **PM:** Particulate matter obtained with the gravimetric method. **Σ:** summation of the major chemical species (dust + sea salt + EC + OM + NH<sub>4</sub><sup>+</sup> + NO<sub>3</sub><sup>-</sup> + SO<sub>4</sub><sup>=</sup>). **nd:** not determined.

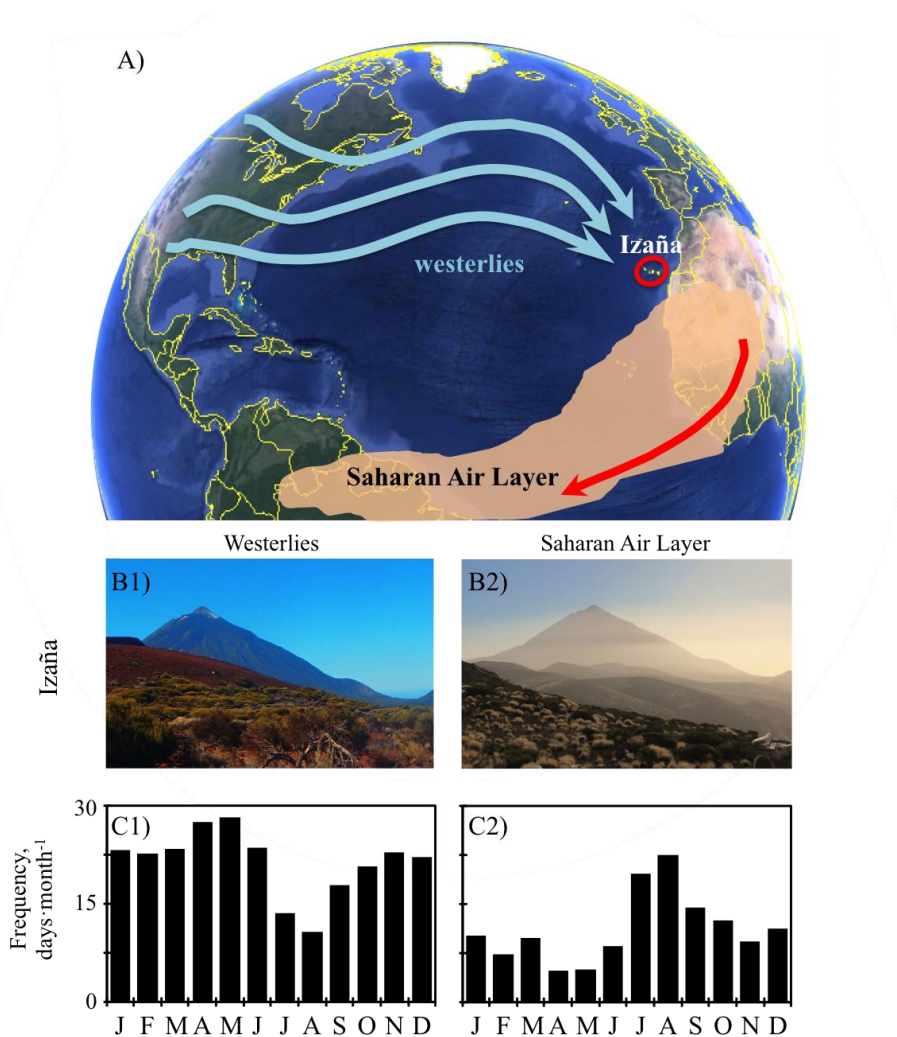


**Figure 1.** (A) Location of the Izaña Observatory with an illustration of the Saharan Air Layer and the westerlies. (B) View from the Izaña Observatory to the west under the westerly and Saharan Air Layer conditions. (C) Monthly frequency (number of days per month) of westerly and Saharan Air Layer at Izaña based on backtrajectories.

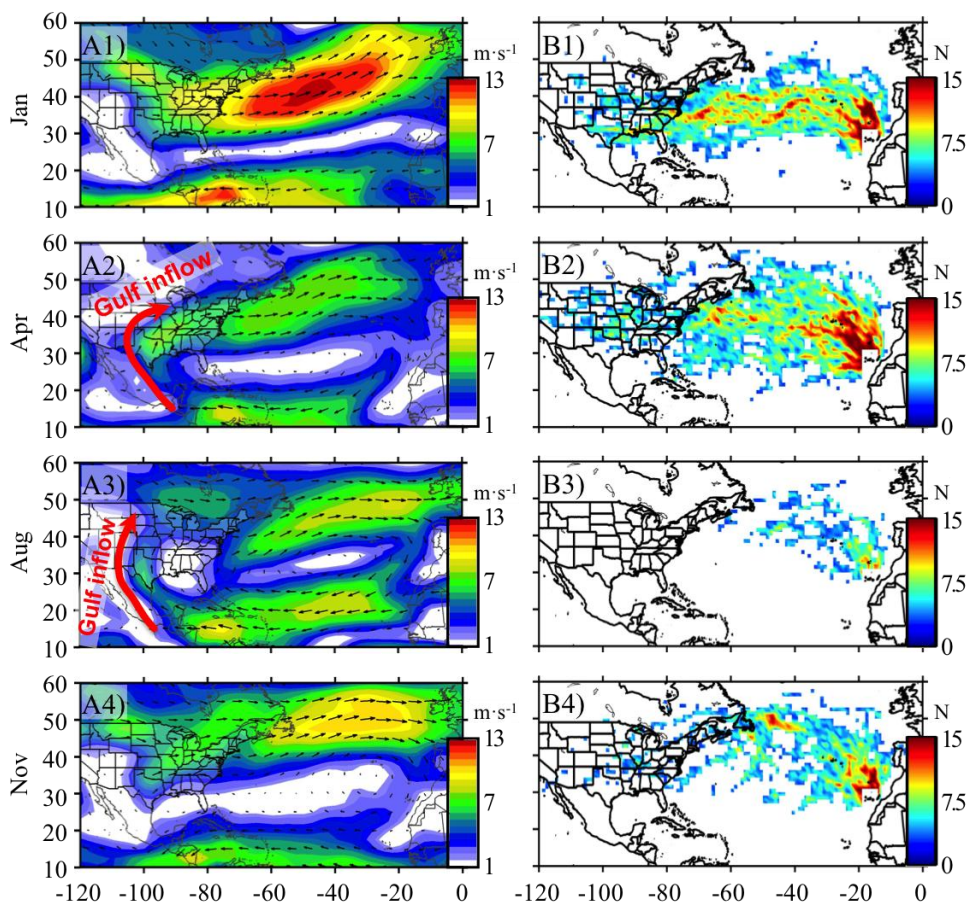


**Figure 2.** (A) Wind vector at 850 mb and (B) Transport Route Frequency (TRF) for January (Jan), April (Apr), August (Aug) and November (Nov) of the period 2008–2013. The Gulf inflow is highlighted.

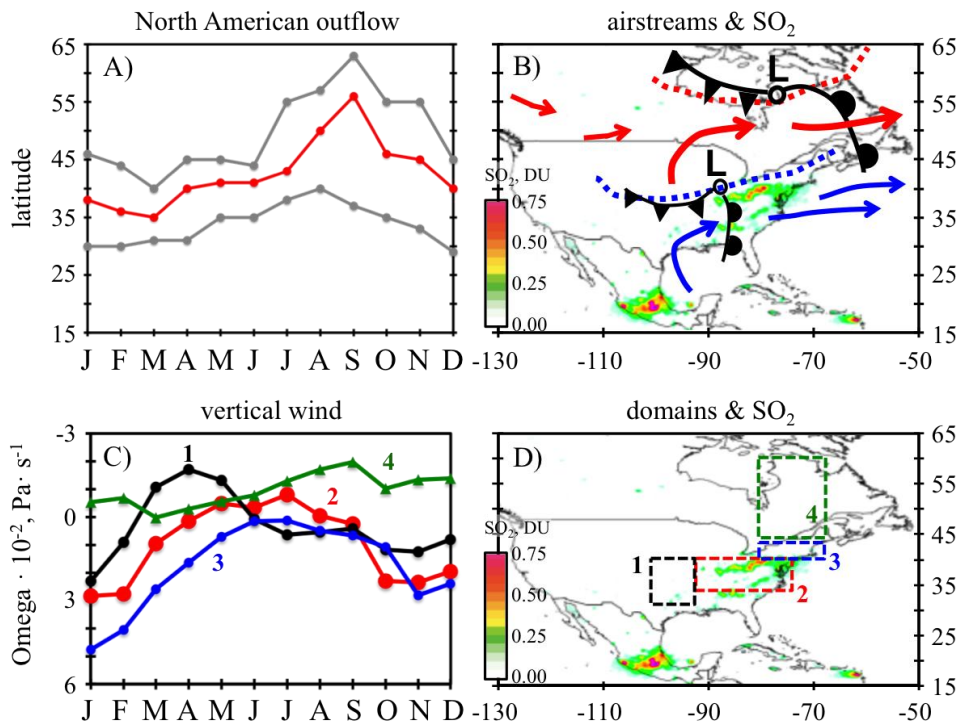


**Figure 3.** (A) Latitudinal ranges at which the westerlies occurs over the Eastern coast of North America. Grey circles: maximum and minimum latitude of the outflow. Red circles: centre of the outflow (B) Meteorological scenarios associated with export of pollutants (according to Cooper et al., 2002a, 2002b, Merry and Moody, 1996) and circulations (blue: Jan-May, red: Jul-Aug) illustrated over mean  $\text{SO}_2$  values observed by satellite by Fioletov et al., (2016) -Copyright by Author(s) 2016. CC Attribution 3.0 License-. (C) Monthly average values of the omega vertical wind component at the 850hPa level (negative values indicate upward movements) illustrated in plot (D). (D) Domains 1 (32–40° N, 90–100° W), 2 (35–40° N, 75–90° W), 3 (40–43° N, 70–80° W) and 4 (46–60° N, 70–80° W).

Atmos. Chem. Phys. Discuss., doi:10.5194/acp-2017-60, 2017  
Manuscript under review for journal Atmos. Chem. Phys.  
Discussion started: 27 February 2017  
© Author(s) 2017. CC-BY 3.0 License.

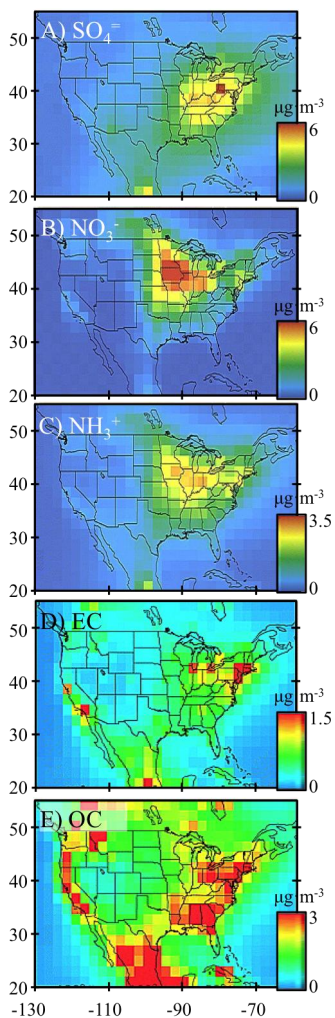


**Figure 4.** Mean surface concentrations of the (A)  $\text{SO}_4^{2-}$ , (B)  $\text{NO}_3^-$ , (C)  $\text{NH}_3^+$ , (D) EC and (E) OC in North America obtained in previous studies by GEOS-CHEM modelling validated with the observations in the network IMPROVE (Park et al. 2003, 2004, Copyright by the American Geophysical Union).

5

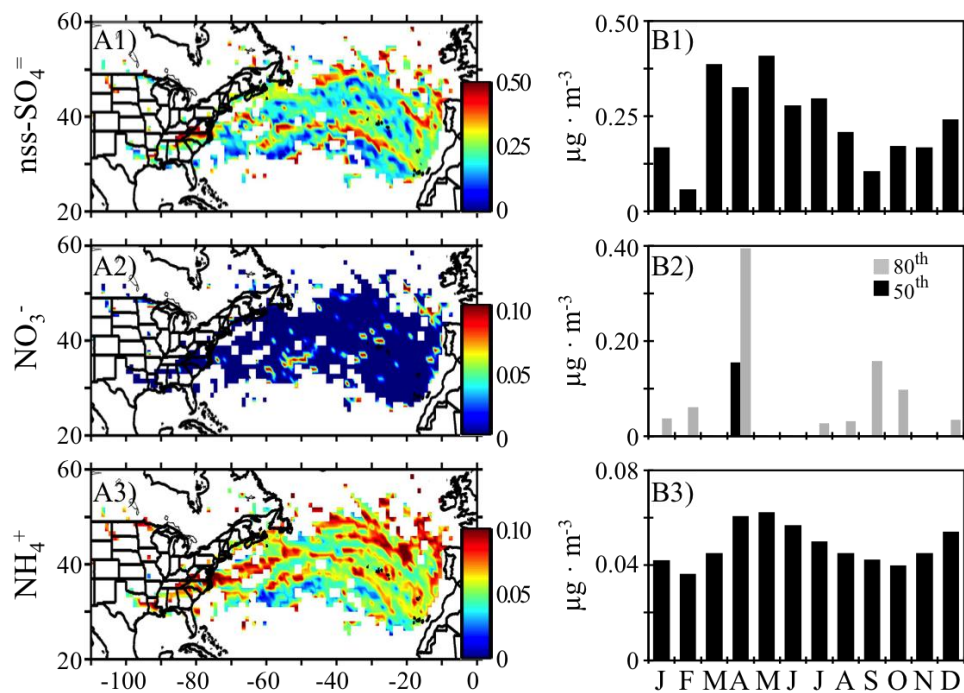


**Figure 5.** (A) Median Concentration At Receptor (MCAR) plots and (B) Monthly median distribution for nss-SO<sub>4</sub><sup>=</sup>, NO<sub>3</sub><sup>-</sup>, and NH<sub>4</sub><sup>+</sup> for the study period. Percentiles 50 and 80 are shown for NO<sub>3</sub><sup>-</sup>. The MCAR plots maximum concentration tick label includes concentration higher than this upper limit.

5

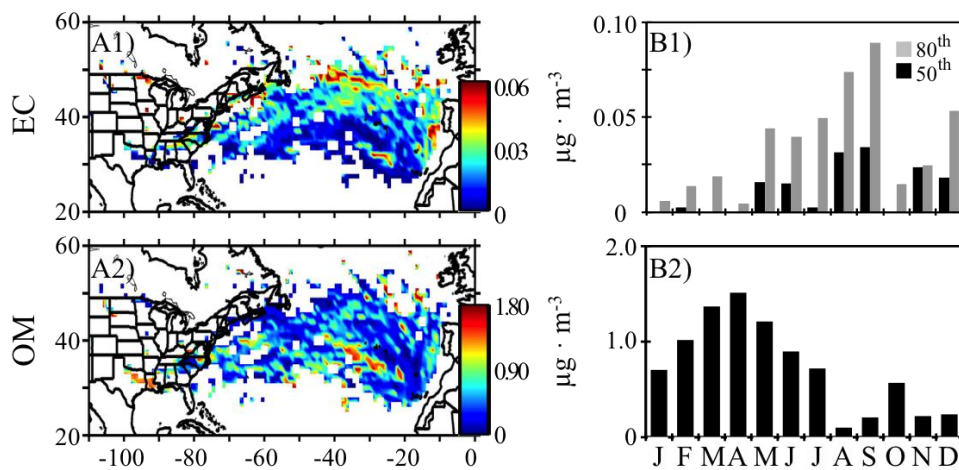


**Figure 6.** (A) Median Concentration At Receptor (MCAR) plots and (B) Monthly median distribution for elemental carbon (EC) and organic matter (OM) for the study period. Percentiles 50 and 80 are shown for EC. The MCAR plots maximum concentration tick label includes concentration higher than this upper limit.

5

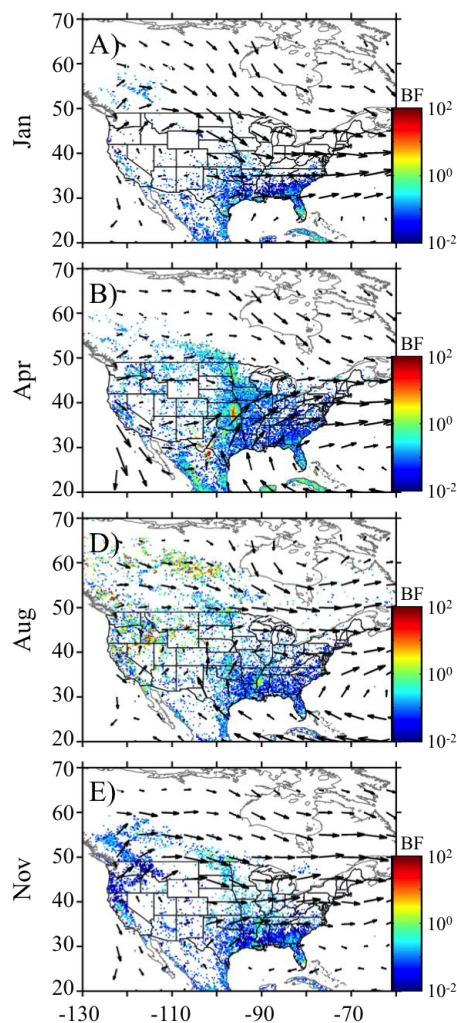


**Figure 7.** Burned fraction (BF) – of each  $0.25^\circ \times 0.25^\circ$  grid cell – and vector wind at 850 mb averaged from 2008 to 2013 for (A) January, (B) April, (C) August and (D) November. The Global Fire Emissions Database Version 4 including small fires data (GFEDv4.1s; Randerson et al., 2015) was downloaded from the Oak Ridge National Laboratory Distributed Active  
 5 Archive Centre (ORNL DAAC) for biogeochemical dynamics ([https://daac.ornl.gov/cgi-bin/dsviewer.pl?ds\\_id=1293](https://daac.ornl.gov/cgi-bin/dsviewer.pl?ds_id=1293)).

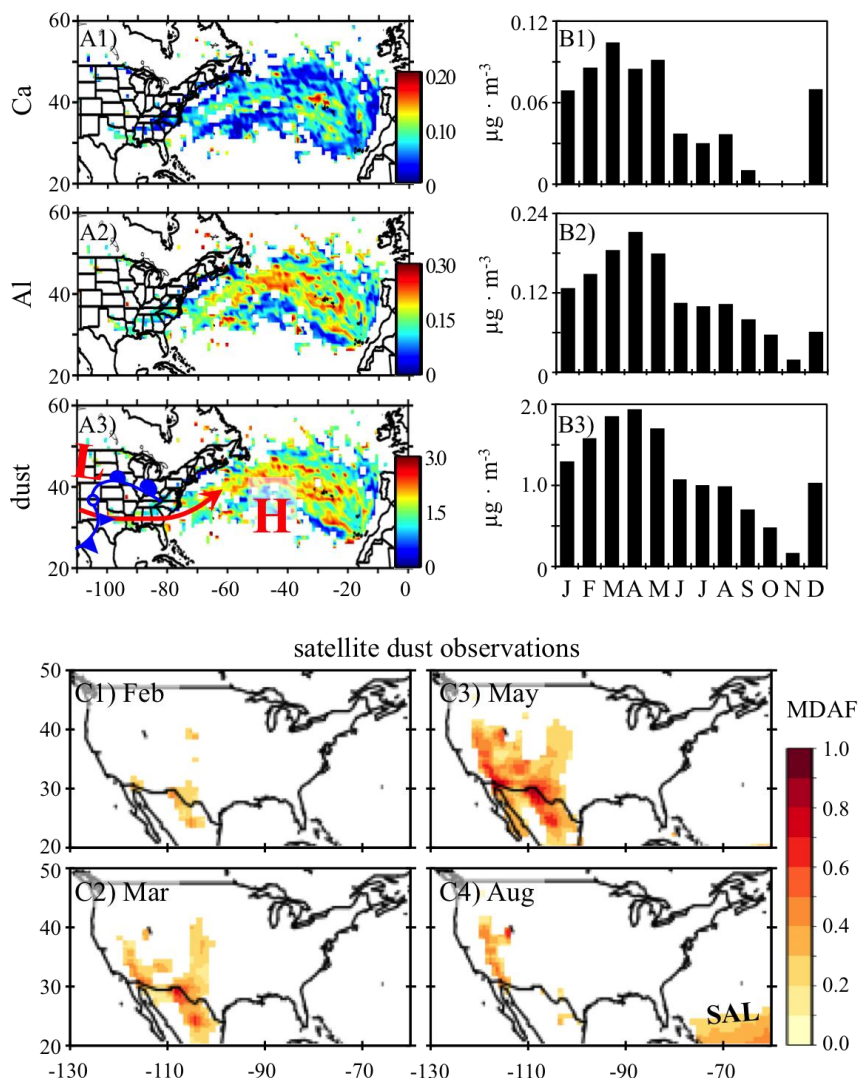


**Figure 8.** (A) Median Concentration At Receptor (MCAR) plots and (B) monthly median distribution for calcium (Ca), aluminium (Al) and dust, and (C) Mean 2008-2013 Aerosol index averaged (data source: <http://disc.sci.gsfc.nasa.gov/>). The MCAR plots maximum concentration tick label includes concentration higher than this upper limit.

Atmos. Chem. Phys. Discuss., doi:10.5194/acp-2017-60, 2017  
Manuscript under review for journal Atmos. Chem. Phys.  
Discussion started: 27 February 2017  
© Author(s) 2017. CC-BY 3.0 License.

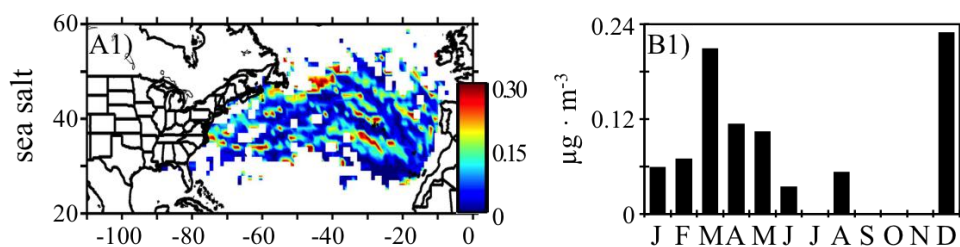


**Figure 9.** (A) Median Concentration At Receptor (MCAR) plots and (B) Monthly median distribution for sea salt for the study period. The MCAR plots maximum concentration tick label includes concentration higher than this upper limit.

5

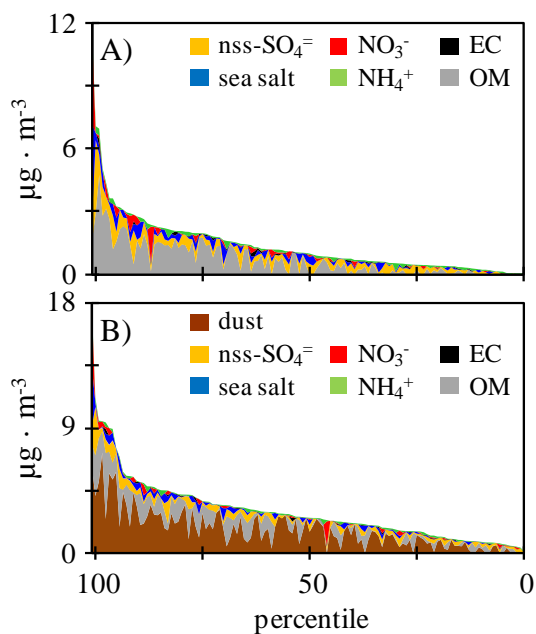


**Figure 10.** Contribution of each aerosol specie to bulk PM<sub>10</sub> in samples collected at Izaña under westerly airflow conditions; data classified from the highest to the lowest levels. **(A)** Considering mayor components except dust. **(B)** Considering all mayor components including mineral dust.



*Supplement of*

**Impact of North America on the aerosol composition in the  
North Atlantic Free troposphere**

**M. I. García et al.**

Correspondence to: Sergio Rodríguez (*srodriguezg@aemet.es*)

### S1. Uncertainty of the gravimetric method

Concentrations of  $PM_x$  were determined by gravimetry following the EN-14907 procedure (except that filter conditioning was performed at 30–35 % relative humidity instead of 50 %). The combined standard uncertainty ( $uc$ ), associated to a specific  $PM_x$  concentration, is expressed as the combination of the individual sources of uncertainty identified in EN-14907; by multiplying  $uc$  by the coverage factor  $k=2$ , the expanded uncertainty ( $U$ ) is obtained.  $U$  implies that there is a 95 % probability that the true value lies within  $\pm U$  of the measured value and it was calculated for individual samples, with the Izaña sampling conditions (sampling time: 8 h; sampler flow:  $30\text{ m}^3\cdot\text{h}^{-1}$ ), as represented in Fig. S1. The expanded uncertainty associated for  $PM_x < 10\ \mu\text{g}\cdot\text{m}^{-3}$  is  $\pm 5\ \mu\text{g}\cdot\text{m}^{-3}$ .  $U$  (%) will depend on the sample mass, with  $U > 50\%$  for  $PM_x < 10\ \mu\text{g}\cdot\text{m}^{-3}$ .

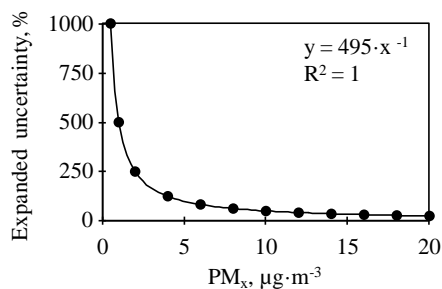


Figure S1: Expanded uncertainty ( $U$ ) of the gravimetric method for individual  $PM_x$  samples as described in EN-14907.

The European standard procedure sets the relative humidity (for filter conditioning and during weighing) to 50 % to avoid the effect of water absorption by the filter material, and therefore in the filter mass. The conditioning to 30–35 % used in the long-term program of Izaña is suitable for the low relative humidity of the ambient air and is consistent with the measurements of other aerosol properties (optical properties and number size distribution) that are performed after conditioning the aerosol sample at relative humidity lower than 40 % according to GAW standardization.

### S2. Westerlies and Saharan air Layer

Westerlies (WES) and Saharan Air Layer (SAL) air masses were separated attending to the back-trajectories computed with FLEXTRA. A self-developed software, programmed in MATLAB 7.4 (The Mathworks, Natick, USA), scanned the latitude and longitude points for each day classifying samples as WES or SAL. This sorting depended on if the air

masses passed over Africa or came from North America and the Atlantic Ocean. After the classification, we used the output of the Barcelona Supercomputing Centre-DREAM8b – atmospheric dust forecast system – in order to verify that the westerlies associated back-trajectories were not Saharan dust re-circulated events. From the total of the 401  $PM_{10}$  samples, 126 were collected under the westerlies (Fig. S2A), 177 under the SAL (Fig. S2B) and 98 were Saharan dust re-circulated events (Fig. S2C). Figure S1A shows the back-trajectories used as input for the Median Concentrations At Receptor (MCAR) plots of the  $PM_{10}$  samples collected under the westerlies influence.

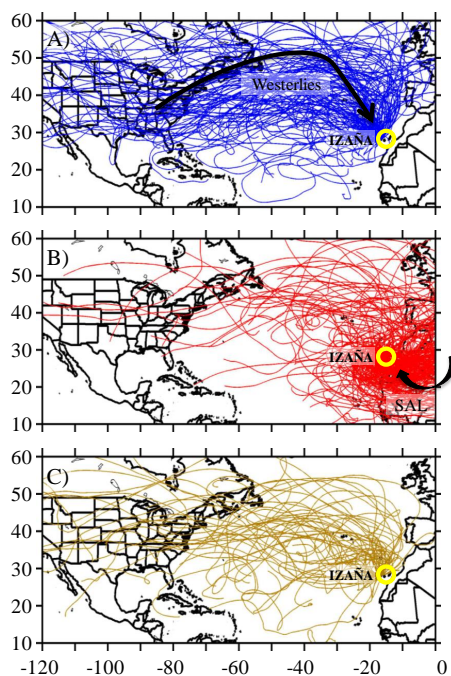


Figure S2: 10 days back-trajectories from 2008 to 2013 of the chemically analyzed samples collected under (A) the westerlies, (B) the Saharan Air Layer and (C) Saharan dust re-circulated over the North Atlantic conditions.

### S3. Meteorological scenario

Monthly values of key meteorological fields – geopotential heights, winds and omega (at 925, 850 and 700 hPa standard levels) and precipitations rates – were determined with the National Centre for Environmental Prediction/National

Centre for Atmospheric Research (NCEP/NCAR) reanalysis data. Figure S3 shows the averaged (2008–2013) geopotential height at 850 hPa for the most representative months (January, May, August and November) in order to illustrate the latitudinal shift in the North Atlantic anticyclone.

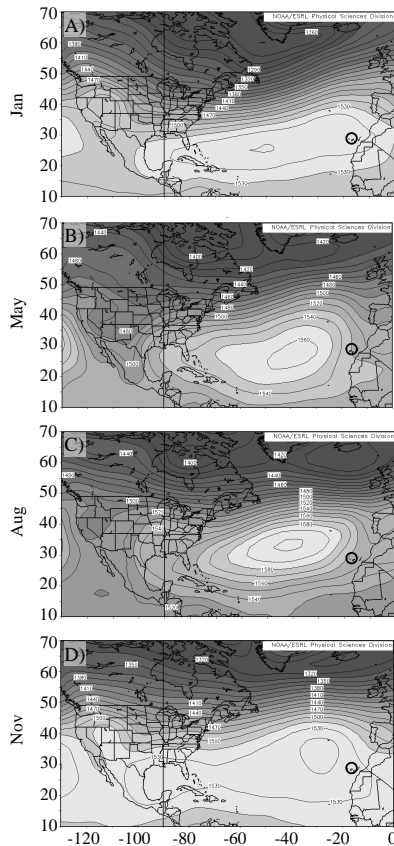


Figure S3: Geopotential Height at 850 mb averaged from 2008 to 2013 for (A) January, (B) May, (C) August and (D) November. The location of Izaña is highlighted (black circle).

#### S4. North America storm season

The records of tornado climatology provided by the National Weather Service (National Oceanic and Atmospheric Administration, NOAA) show that North America is affected by a ‘tornado season’, which usually occurs from spring to early summer (March to July). The regional

frequency of the tornados is related to the progression of the warm season, moving north from spring to summer (<http://www.ncdc.noaa.gov/climate-information/extreme-events/us-tornado-climatology>) (Fig. S4A). In early spring, tornados affects to Gulf States – such as Mississippi and Louisiana – and then moves northward affecting Kansas, Nebraska, and the Tennessee Valley region during late spring. Into summer, most of ‘Tornado Alley’ – south central United States – is active, and then shifts back southward into the late autumn. Tornados, the most violent of atmospheric convective storms, significantly influence the vertical distribution of aerosols by transporting them from the boundary layer to the troposphere (Barth et al., 2015). Ginoux et al. (2012) identified the Great Plains – located between the east of the Rocky Mountains and the Mississippi River – as the largest dust source in United States with a main anthropogenic origin. The maximum monthly average of tornadoes occurrence, from Southern (Texas, Oklahoma, New Mexico) to Central (Kansas, Colorado) plains, is from April to June (Fig. S4B) – during the study period (2008–2013) – according with the maximum recorded high dust concentrations at Izaña.

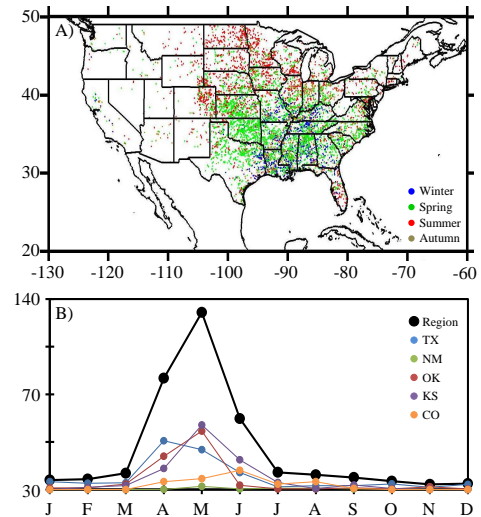


Figure S4: (A) Tornadoes which took place in U.S.A during the study period (2008–2013). The starting point is represented by colours depending on the season of occurrence. (B) Monthly average number of tornadoes during the study period (2008–2013) in the selected States and the whole Region (TX, NM, OK, KS and CO). TX: Texas; OK: Oklahoma; NM: New Mexico; KS: Kansas; CO: Colorado. Data source: <http://www.spc.noaa.gov/wcm/index.html>data.

## 4 M.I García et al.: Supplement of ‘Impact of North America on the aerosol composition in the North Atlantic FT’

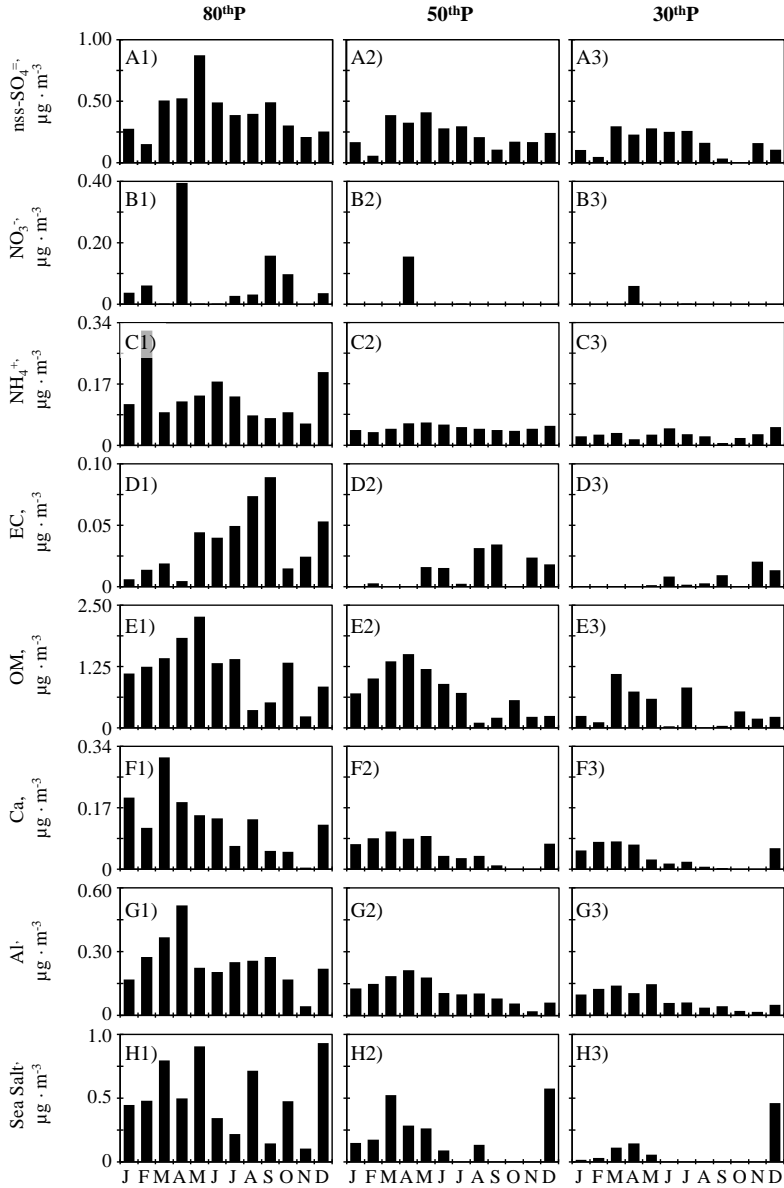


Figure S5: Monthly distribution of the percentiles 80, 50 and 30 for the concentrations of (A)  $\text{nss-SO}_4^{2-}$ , (B)  $\text{NO}_3^-$ , (C)  $\text{NH}_4^+$ , (D) EC, (E) OM, (F) Ca, (G) Al and (H) sea salt, from Jan 2008 to Aug 2013.

### S5. Percentiles of the inorganic compounds concentration

To explain the seasonal evolution of the background (30<sup>th</sup>P), median (50<sup>th</sup>P) and high (80<sup>th</sup>P) concentration events, monthly distribution for the aerosol components concentrations are shown in Fig. S5. The aerosol background (30<sup>th</sup>P) composition changes significantly throughout the year, although  $\text{nss-SO}_4^-$ ,  $\text{NH}_4^+$  and Al are always part of the total bulk. The remaining chemical species exhibit certain seasonality. Two seasons – associated to the latitudinal ranges of the North American outflow and the spatial distribution of the source regions – can be well differentiated: (i) Jan-May ( $\sim 35\text{--}40^\circ\text{N}$ ) and Jun-Dec ( $\sim 40\text{--}55^\circ\text{N}$ ). The first season is characterized by an increase of the concentrations of most chemical species ( $\text{nss-SO}_4^-$ ,  $\text{NH}_4^+$ , OM, Ca, Al and dust), whereas the second season is mainly associated to an increase in the concentration of EC.

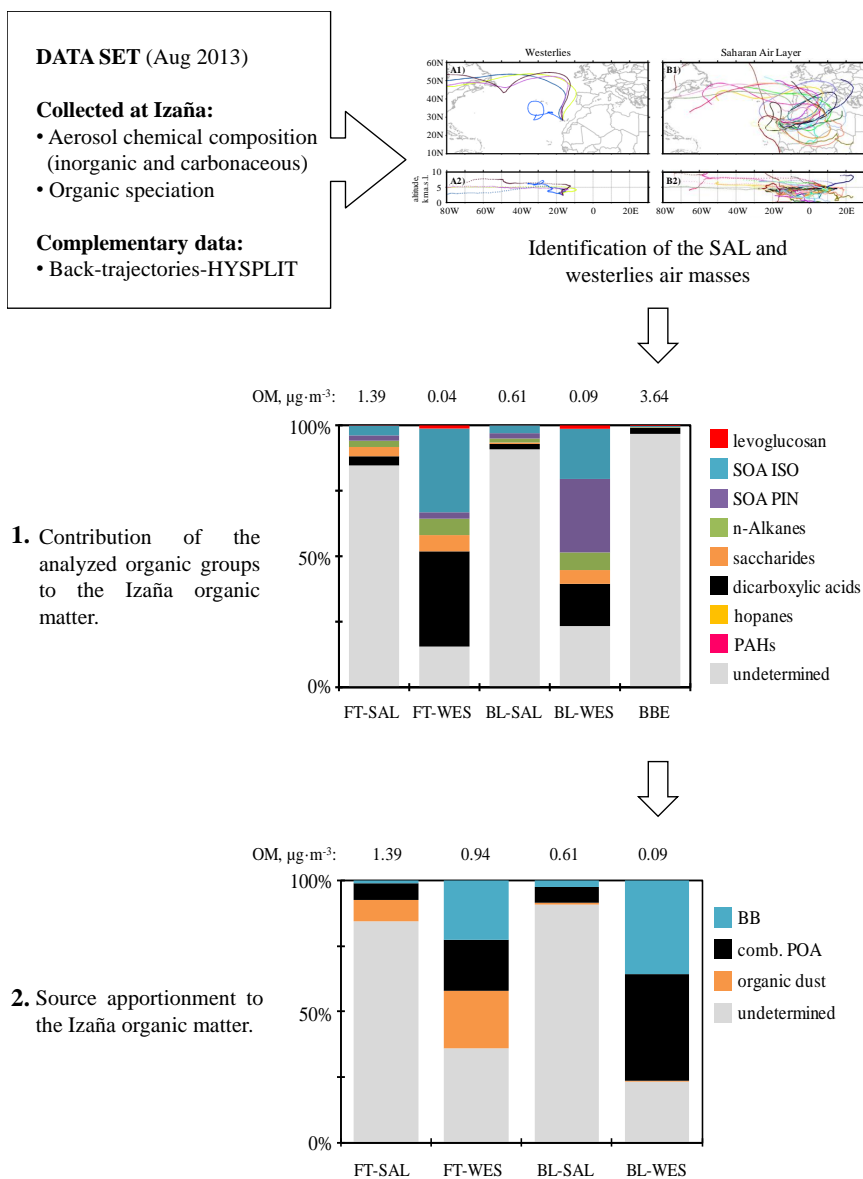
### Supporting References

Barth, M. C., Cantrell, C. A., Brune, W. H., Rutledge, S. A., Crawford, J. H., Huntrieser, H., Carey, L. D., acGorman, D., Weisman, M., Pickering, K. E., Bruning, E., Anderson, B., Apel, E., Biggerstaff, M., Campos, T., CampuzanoJost, P., Cohen, R., Crouse, J., Day, D. A., Diskin, G., Flocke, F., Fried, A., Garland, C., Heikes, B., Honomichi, S., Hornbrook, R., Huey, L. G., Jimenez, J., Lang, T., Lichtenstern, M., Mikoviny, T., Nault, B., OSullivan, D., Pan, L., Peischl, J., Pollack, I., Richter, D., Riemer, D., Ryerson, T., Schlager, H., St. Clair, J., Walega, J., Weibring, P., Weinheimer, A., Wennberg, P., Wisthaler, A., Wooldridge, P., and Zeigler, C.: The Deep Convective clouds and Chemistry (DC3) Field Campaign, *B. Am. Meteorol. Soc.*, 96, 1281–1309, doi:10.1175/BAMS-D-13-00290.1, 2015.



## 4.3 Article 3

Graphical abstract:







## Speciation of organic aerosols in the Saharan Air Layer and in the free troposphere westerlies

M. Isabel García<sup>1,2</sup>, Barend L. van Drooge<sup>3</sup>, Sergio Rodríguez<sup>1</sup> and Andrés Alastuey<sup>3</sup>

- 5 <sup>1</sup> Izaña Atmospheric Research Centre, AEMET, Associated Unit to CSIC “Studies on Atmospheric Pollution”, Santa Cruz de Tenerife, 38001, Spain  
<sup>2</sup> Department of Chemistry (T.U. Analytical Chemistry), Faculty of Science, University of La Laguna, La Laguna, 38206, Spain  
<sup>3</sup> Institute of Environmental Assessment and Water Research, CSIC, Barcelona, 08034, Spain
- 10 *Correspondence to:* Sergio Rodríguez (srodriguezg@aemet.es)

**Abstract.** We focused this research on the composition of the organic aerosols transported in the two main airflows of the subtropical North Atlantic free troposphere: (i) the Saharan Air Layer – the warm, dry and dusty airstream that expands from North Africa to the Americas at subtropical and tropical latitudes – and (ii) the westerlies – which flows from North America through the North Atlantic at mid and subtropical latitudes –. We determined the inorganic compounds (secondary inorganic species and elemental composition), elemental carbon and the organic fraction (bulk organic carbon and organic speciation) present in the aerosol collected at Izaña Observatory, ~2400 m a.s.l. in Tenerife Island. The concentrations of all inorganic and almost all organic compounds were higher in the Saharan Air Layer than in the westerlies, with bulk organic matter concentrations within the range 0.02–4.0  $\mu\text{g}\cdot\text{m}^{-3}$ . In the Saharan Air Layer, the total aerosol population was by far dominated by dust (93% of bulk mass), which was mixed with secondary inorganic pollutants (<5%) and organic matter (~1.5%). The chemical speciation of the organic aerosols (levoglucosan, dicarboxylic acids, saccharides, n-alkanes, hopanes, polycyclic aromatic hydrocarbons and those formed after oxidation of  $\alpha$ -pinene and isoprene, determined by gas-chromatography coupled to mass-spectrometry) accounted for a 15% of the bulk organic matter (determined by the thermo-optical transmission technique); the most abundant organic compounds were saccharides (associated with surface soils), secondary organic aerosols linked to oxidation of biogenic isoprene (SOA ISO) and dicarboxylic acids (linked to several primary sources and SOA). When the Saharan Air Layer shifted southward, Izaña was within the westerlies stream and the organic matter accounted for ~28% of bulk mass of the aerosol cocktail. In the westerlies, the determined organic aerosol species accounted for 64% of the bulk organic matter, being SOA ISO and dicarboxylic acids the most abundant; the highest concentration of organic matter (3.6  $\mu\text{g}\cdot\text{m}^{-3}$ ) and of some organic species (e.g. levoglucosan and some dicarboxylic acids) were associated with biomass burning linked to a fire in North America. In the Saharan Air Layer, the correlation found between SOA ISO and nitrate suggests a large-scale impact of the enhancement in the formation of secondary organic aerosols due to interaction with anthropogenic  $\text{NO}_x$  emissions.

15  
20  
25  
30

Atmos. Chem. Phys. Discuss., doi:10.5194/acp-2017-108, 2017  
Manuscript under review for journal Atmos. Chem. Phys.  
Discussion started: 27 February 2017  
© Author(s) 2017. CC-BY 3.0 License.



## 1 Introduction

Atmospheric aerosols, or particulate matter, influence on processes affecting climate, on continental and marine ecosystems, and on human health. The magnitude of these effects depends on the aerosols composition, which may include secondary inorganic species (e.g. sulphate, nitrate, ammonium and sea salt), mineral dust, elemental carbon and a number organic species constituting the so-called organic aerosols (OA) (IPCC, 2013). OA account for an important fraction of particulate matter, ranging from ~20% (continental mid-latitudes) to ~90% (tropical forested areas) (Kanakidou et al., 2005). As other aerosol components, OA also contributes to (i) light scattering and absorption (Kirchstetter and Novakov, 2004), (ii) cloud formation providing cloud condensation and ice nuclei (Sun and Ariya, 2005), and (iii) heterogeneous chemical reactions in the atmosphere (Kanakidou et al., 2005).

Principal sources of Primary OA (POA) include vegetation, fossil fuel combustion, biomass burning, biological aerosols and particles from soils. Precursors of Secondary OA (SOA) include natural and anthropogenic sources (Volkamer, et al., 2006; Gouw and Jimenez, 2009); emissions of biogenic volatile organic compounds (VOCs) significantly contribute to the global budget of SOA (Guenter et al., 2012). An important factor influencing SOA formation are reactive nitrogen species, specifically  $\text{NO}_x$  and  $\text{NO}_3$  (Presto et al., 2005; Ng et al., 2007, 2008) interacting with VOCs in gas-phase, likely having an impact in global OA levels as indicated by modelling (Pye et al., 2010) and experimental work (Surratt et al., 2006). In remote environments, VOCs enhance condensational growth of new particles which can enter to the free troposphere (FT) by means of elevated mounts (García et al., 2014). These tropospheric aerosols are subject to much greater lifetimes and wind speed than in the planetary boundary layer (BL), favouring long-range atmospheric transport and aerosol impacts (Winker et al., 2013). The aged and processed long-range transported OA is of particular interest, as is spatially representative of the remote background conditions having important implications for global air quality and climate.

The most extended technique to quantify the amount of bulk organic and elemental carbon in the atmospheric aerosols is the thermo-oxidant combustion and optical detection (Birch and Cary, 1996; Cavalli et al., 2010; Karanasiou et al., 2015). This is a useful method for mass closure, but does not provide information on OA speciation and consequently on OA sources and properties related to impacts. Alternatively, gas-chromatography coupled to mass-spectrometry analysis of aerosol samples allows the speciation of the organic compounds and the quantification of many of those identified as tracers for distinguish sources and processes contributing to the budget of OA (Bauer et al. 2008; Mazurek et al. 1989; Claeys et al., 2007; Hallquist et al., 2009; Howsam and Jones 1998; Iinuma et al., 2007; Kawamura and Kaplan, 1987; Medeiros and Simoneit 2007; Narukawa et al., 1999; Rogge et al., 1993; Shauer et al. 2002; Simoneit et al. 1991; Simoneit et al. 2004a; Simoneit, 2002; Szmigielski et al., 2007). A number of studies have focused on OA speciation in urban areas (Alier et al., 2013; Kawamura and Kaplan, 1987; Puxbaum et al., 2007; Schauer et al., 1996; Simoneit et al., 1991; Van Drooge and Grimald, 2015) compared to remote environments. Studies in the free troposphere are scarce (Simoneit et al. 2004b; Fu et al., 2008,

Atmos. Chem. Phys. Discuss., doi:10.5194/acp-2017-108, 2017  
Manuscript under review for journal Atmos. Chem. Phys.  
Discussion started: 27 February 2017  
© Author(s) 2017. CC-BY 3.0 License.



2014; Wang et al., 2009; van Drooge et al., 2010; Meng et al., 2014), even if they are of interest due to the long-range transport potential linked to the high wind speeds above the boundary layer.

In this study we focused on the OA transported from inner Sahara over the North Atlantic in the so-called Saharan Air Layer (SAL; Prospero and Carlson, 1972). In summertime, the continental BL depth grows up to 5 km a.s.l. over the Sahara (Cuesta et al., 2009) and the prevailing easterly winds prompt the export of the warm Saharan air to the North Atlantic above the cool NNE trade winds that blows in the marine boundary layer. This results in the development of the SAL – a warm, dry and stable air stream that expands from North African coast, at altitudes 2 to 5 km a.s.l., to the Americas (Prospero and Carlson, 1972; Tsamalis et al., 2013) –. Because of the high stability associated with the warm air above the cool marine air, the SAL acts as a band conveyor that transport continental Saharan dusty air – originally placed near ground – over the North Atlantic; in addition to dust, other substances such as pollutants, vegetation debris or microorganisms are carried mixed with dust.

OA in the SAL has received little attention, even if its impacts are of interest. Anthropogenic bioaccumulative and toxic organic compounds (including organochlorine and organophosphate pesticides, polycyclic aromatic hydrocarbons, polychlorinated biphenyl) are transported from Western Sahara to the Caribbean within the SAL (Garrison et al., 2013). Viruses, bacteria, fungal and pollens also travels mixed with dust across the Atlantic (Griffin et al., 2007; Izquierdo et al., 2011). Field measurements in the SAL at Izaña Observatory found dust being the major ice nuclei at temperatures colder than  $-30^{\circ}\text{C}$  (Boose et al., 2016), whereas the observed ice nuclei at  $-8^{\circ}\text{C}$  points to a role of OA as ice nuclei at warm temperatures (Conen et al., 2015).

In this study we primarily focused on the origin of OA in the SAL. We collected in-situ aerosol samples directly into the high-altitude SAL at Izaña Observatory, located at  $\sim 2400$  m a.s.l. in Tenerife Island. The profile of the organic species was used for a source apportionment of the bulk organic matter. The results were compared with a similar data set obtained during the same campaign under the westerlies (WES) airflow that regularly brings air from North America across the North Atlantic. The observed differences illustrate the diversity of OA sources over the North Atlantic free troposphere.

## 2 Methodology

### 2.1 Sampling site

Sample collection was performed at the Izaña Global Atmospheric Watch (GAW) Observatory in Tenerife island (Fig. 1;  $16^{\circ}29'58''\text{W}$ ,  $28^{\circ}18'32''\text{N}$ ). The site is located on a mountaintop (2373 m a.s.l), surrounded by a pine forest (limited between  $\sim 500$ – $2300$  m). The Observatory remains almost permanently above the temperature inversion layer associated to the trade winds, which separates the moist marine BL from the dry FT avoiding vertical mixing before sunrise. Sunlight during

Atmos. Chem. Phys. Discuss., doi:10.5194/acp-2017-108, 2017  
Manuscript under review for journal Atmos. Chem. Phys.  
Discussion started: 27 February 2017  
© Author(s) 2017. CC-BY 3.0 License.



daytime activate thermal convection, developing an orographic thermal-buoyant upslope winds, that transport species emitted in the BL by biogenic and anthropogenic sources (see details in Rodríguez et al., 2009).

## 2.2 Sampling

Samples were collected within the annual aerosols summer campaign of the Izaña Observatory in August 2013. Particulate Matter (PM) was collected on pre-heated (at 205°C) quartz filters (Pall Science 150 mm diameter) on high volume air samplers (Hi-Vol; MCZ) at a flow rate of  $30 \text{ m}^3 \cdot \text{h}^{-1}$ . 30 samples of total particulate matter ( $\text{PM}_{\text{T}}$ ) were collected daily during nighttime (22:00–6:00 GMT; FT) and 12 samples of particulate matter smaller than  $2.5 \mu\text{m}$  ( $\text{PM}_{2.5}$ ) in non-consecutive days during daytime (10:00–16:00 GMT; BL). Field blanks were collected weekly and treated like the samples regarding preparation, transport and storage, as part of the quality assurance / quality control (QA/QC) protocol.

## 10 2.3 Chemical Analysis

### 2.3.1 Organics

One quarter of the filter sample was used for the organic compounds speciation by gas-chromatography coupled to mass-spectrometry (GC-MS). A detailed description of the analytical method is given elsewhere (Fontal et al. 2015, van Drooge and Grimalt 2015). Briefly, filters were spiked with deuterated standards of acids, anhydro-saccharides, alkanes, and PAHs, and extracted ultrasonically in a mixture of dichloromethane and methanol. Extracts were filtered and concentrated until 0.5 mL. For the analysis of polar compounds, i.e. acids and saccharides, a 25  $\mu\text{L}$  aliquot of the extract was evaporated until dryness, and 25  $\mu\text{L}$  of bis-(trimethylsilyl)-trifluoroacetamide (BSFTA) + trimethylchlorosilane (99:1) (Supelco, Bellefonte, PA, USA) and 10  $\mu\text{l}$  of pyridine (Merck, Darmstadt, Germany) were added and left overnight to derivatize the polar compounds to their trimethylsilyl esters and ethers in order to analyse them by GC-MS. The remaining extract was used for the analysis of polycyclic aromatic hydrocarbons (PAH), n-alkanes and hopanes, and was clean-up by adsorption column chromatography, packed with 1 g of aluminium oxide (Merck, Germany). The analytes were eluted with 10 ml of hexane: dichloromethane (1:2 (v/v), Merck, Germany), which was collected and concentrated to 1 ml by rotovap and to 25  $\mu\text{l}$  under a gentle nitrogen stream for quantification by GC-MS (Thermo Trace GC Ultra – DSQ II). The MS detector was operated in full scan ( $m/z$  from 50 to 650) and electron impact (70 eV) ionization mode for the polar compounds. The sample extracts for the analysis of non-polar species was performed in SIM mode for the corresponding ions of the compounds. Organic species were identified by their GC retention time and characteristic ions in the MS (see section S1 of the supplement).

### 2.3.2 OC and EC

Organic and elemental carbon (OC and EC) were analysed by thermal-optical transmittance (TOT, Sunset Laboratory Inc. <sup>TM</sup>) by using the EUSAAR2 protocol (Cavalli et al., 2010). The method provided four OC fractions (OC1, OC2, OC3 and



OC4), from which the more volatile were discarded based on the results of the field blank filters analysis. Organic Matter (OM) was determined by using the ratio  $OM/OC = 1.8$  for remote places (Pitchford et al. 2007; Dzepina et al. 2015).

### 2.3.3 Inorganics

The methodology used for the inorganic speciation is described in detail in Rodríguez et al. (2015). Briefly, soluble species were determined by ion chromatography ( $SO_4^{2-}$ ,  $NO_3^-$ ,  $Cl^-$ ) and selective electrode ( $NH_4^+$ ) after water leaching a fraction of filter. Elemental composition was determined by Inductively Coupled Plasma Atomic Emission Spectrometry (ICP-AES, IRIS Advantage TJA Solutions, THERMO™) and Inductively Coupled Plasma Mass Spectrometry (ICP-MS, X Series II, THERMO™) after acid digestion of the sample. Mineral dust was calculated as the sum of  $Al_2O_3 + SiO_2 + Fe + CaCO_3 + K + Na + Mg + P + Ti + Sr$  (see details in Rodríguez et al., 2011, 2015) and normalized so Al accounts for 8% of the dust mass (see details in Pérez et al., 2016).  $SO_4^{2-}$  was split in non-sea salt sulphate (nss- $SO_4^{2-}$ ) and sea salt sulphate (ss- $SO_4^{2-} = SO_4^{2-} -$  ss- $SO_4^{2-}$ ) through the relation between marine Na and  $SO_4^{2-}$ . Blank field filters were subject to gravimetric and chemical analysis and mean values subtracted to the  $PM_x$  samples.

### 2.4 Meteorology

The air mass origin and transport was tracked by means of backward trajectory analysis. Calculations were performed with the HYbrid Single-Particle Lagrangian Integrated Trajectory Model (HYSPLIT, <http://ready.arl.noaa.gov/HYSPLIT.php>; Draxler and Rolph, 2003; Draxler and Hess, 1998; Stein et al., 2015) developed by the National Oceanic and Atmospheric Administration (NOAA). HYSPLIT was run with the National Centre for Environmental Prediction's (NCEP) Global Data Assimilation System (GDAS, 1 degree) data set. Ten days back-trajectories arriving at 2400 m a.s.l were computed daily (00 UTC) for August 2013.

### 20 2.5 Data treatment

In order to observe the similarities and differences among the chemical composition of the samples, the experimental organic compound data were merged for evaluation with Multivariate Curve Resolution Alternating Least Squares (MCR-ALS). The joint dataset was imported into MATLAB 7.4 (The Mathworks, Natick, USA) for subsequent calculations using MATLAB PLS 5.8 Toolbox (Eigenvector Research Inc, Masson WA, USA) (Jaumot et al. 2005). The MCR-ALS method decomposes the data matrix using an Alternating Least Squares algorithm under a set of constraints such as non-negativity, unimodality, closure, trilinearity or selectivity (Tauler et al., 1995a, b). The MCR-ALS method had been applied successfully in a previous study on organic aerosol in urban and rural areas (Alier et al. 2013; Van Drooge and Grimalt 2015). The explained variance by the different components is similar to a PCA, but not orthogonal. Since the natural sources in the environment are rarely orthogonal, the MCR-ALS method provides more realistic descriptions of the components than the orthogonal

Atmos. Chem. Phys. Discuss., doi:10.5194/acp-2017-108, 2017  
Manuscript under review for journal Atmos. Chem. Phys.  
Discussion started: 27 February 2017  
© Author(s) 2017. CC-BY 3.0 License.



database decomposition methods. Multilinear regression tools were applied to quantify the contribution of the identified sources to the total OM.

### 3 Results and Discussion

We collected aerosol samples in four different airflows: 2 FT airflows and other 2 airstreams potentially mixed with BL air. Samples collected at night ( $PM_T$ ) are representative of the two FT airflows that prevail in this region: the WES and the SAL. As already described, the WES flow from North America across the North Atlantic at mid-latitudes, with their southern edge shifting to the subtropics in winter, and flow over Canada (Merry and Moody, 1996) reaching Izaña after circulation around the Azores high in summer (see backtrajectories of the samples collected from 26Aug to 30Aug – with "ddmm" referred to ending sampling day – in Fig.1A). The SAL expands from North Africa to the Americas at subtropical latitudes in summertime (see backtrajectories associated during the study period in Fig. 1B), season in which the Izaña Observatory is mostly within this dusty airstream and the presence of the WES is associated with southern shifts of the SAL.

Samples collected during daylight ( $PM_{2.5}$ ) are representative of the FT potentially mixed with BL air, more specifically the BL-SAL mixing and BL-WES mixing. The presence of BL air is associated with the development of buoyant upslope winds caused by the heating of terrain, which typically results in increases of primary gaseous pollutants and new particle formation at Izaña (García et al, 2014; Rodríguez et al., 2009).

Thus, in this study we differentiate between 4 scenarios:  $PM_T$  (FT, nighttime) within (i) the SAL (FT-SAL) and (ii) the WES (FT-WES), and  $PM_{2.5}$  (BL, daytime) within (iii) the SAL (BL-SAL) and (iv) the WES (BL-WES).

#### 3.1 Major Components

Table 1 shows the composition of the aerosol samples collected at Izaña. Concentrations of aerosol major components are the same order to those found in previous studies (Maring et al., 2000; Rodríguez et al., 2011). All species present much higher concentrations within the SAL than within the WES. Some species shows slightly higher concentrations during the day linked to the upslope winds and boundary layer air.

#### 3.2 Organic molecular tracers

In the next sections, organic speciation results are described. Table 2 shows the average concentrations of the 40 organic compounds analysed in this study under the different scenarios (SAL and WES) for  $PM_T$  and  $PM_{2.5}$ . In order to improve the insight on the origin and sources of some FT organic aerosol, correlations among the organic groups and the major species are evaluated (Table 3).



### 3.2.1 Levoglucosan

Levoglucosan (1,6-anhydro- $\beta$ -D-glucopyranose) is emitted during biomass burning as a consequence of the thermal alteration of cellulose and hemi-cellulose present in vegetation (Simoneit, 2002). It is considered a particle-phase marker for the identification of wood combustion because of its source specific emission, but its atmospheric stability is still a matter of discussion. Experiments carried out by Hennigan et al. (2010) and Hoffmann et al. (2010) showed that levoglucosan reacts with gas-phase hydroxyl radicals (OH), especially under high relative humidity conditions. However, studies performed by Fraser and Lakshmanan (2000) demonstrated no degradation of levoglucosan under acidic conditions over a period of 10 days.

Levoglucosan daily values measured at Izaña within the FT and the BL were  $< 1.5 \text{ ng}\cdot\text{m}^{-3}$  for all samples, except on 28Aug when  $\sim 9 \text{ ng}\cdot\text{m}^{-3}$  was measured. Hysplit back-trajectories and the Atmospheric Infrared Sounder (AIRS) satellite images (NASA) indicate the North America origin of the air masses, where several wildfires – as the Rim Fire – were affecting western USA 10 days before the arriving of the air mass towards Izaña (detailed information not provided for sake of brevity). We detected a long-range transport biomass burning plume within the FT from the fires originated in North America. Other studies performed at Pico Mountain Observatory (Azores, 2225 m a.s.l.) have also detected the impact of other biomass burning plumes by means of the levoglucosan detection (Dzepina et al, 2015). These results give support to the atmospheric stability of levoglucosan, for the specific conditions of the atmospheric long-range transport. Due to the particular composition of this biomass burning event (BBE), we will discuss this sample separately (Table 2) and the sample will not be included when describing the general composition of the samples collected at night under conditions of the westerlies (FT-WES; Table 2). Levoglucosan concentration, measured at Izaña during the BBE ( $9.3 \text{ ng}\cdot\text{m}^{-3}$ ), is similar to the average levels detected in the marine BL on the Azores in the North Atlantic ( $5.2 \text{ ng}\cdot\text{m}^{-3}$ ) or at free tropospheric site in the European continent ( $7.8 \text{ ng}\cdot\text{m}^{-3}$ ), but much lower than those found in sites under influence of local BB or continental sites in winter ( $653\text{--}1290 \text{ ng}\cdot\text{m}^{-3}$ ) (Puxbaum et al. 2007).

### 3.2.2 Dicarboxylic acids

Dicarboxylic acids can be emitted in small quantities from several natural and anthropogenic primary sources such as vegetation, meat cooking and motor exhaust emissions (Kawamura and Kaplan, 1987, Narukawa et al., 1999), although atmospheric photochemical transformation of volatile and semi-volatile organic compounds is considered to be an important source for the presence of these aged compounds in the atmosphere (Alier et al. 2013, Jang and McDow, 1997; Kleindienst et al. 2012; Paulot et al. 2011). This oxidative degradation of VOCs by tropospheric oxidants may be responsible for the similar mean  $\Sigma$ dicarboxylic acids concentrations within the FT (SAL:  $14.4 \text{ ng}\cdot\text{m}^{-3}$ ; WES:  $16.7 \text{ ng}\cdot\text{m}^{-3}$ ) and the BL (SAL:  $11.1 \text{ ng}\cdot\text{m}^{-3}$ ; WES:  $12.9 \text{ ng}\cdot\text{m}^{-3}$ ) at Izaña.

Atmos. Chem. Phys. Discuss., doi:10.5194/acp-2017-108, 2017  
 Manuscript under review for journal Atmos. Chem. Phys.  
 Discussion started: 27 February 2017  
 © Author(s) 2017. CC-BY 3.0 License.



Succinic (suc) and phthalic (pth) acids were the most abundant dicarboxylic acids (Table 2) with FT and BL average values (suc: 6.5–3.7 and pth: 3.2–2.8  $\text{ng}\cdot\text{m}^{-3}$  for the FT-BL) much lower than this found for  $\text{PM}_{2.5}$  in the FT Mount Tai (suc: 30; Wang et al., 2009), similar to those observed in  $\text{PM}_T$  in the Himalayas (4276 m a.s.l.) (suc: 13.7 and pth: 9.5  $\text{ng}\cdot\text{m}^{-3}$ ; Cong et al., 2015), but higher than those detected for  $\text{PM}_T$  in the North Pacific remote marine (suc: 2.8 and pth: 0.66  $\text{ng}\cdot\text{m}^{-3}$ ; Kawamura and Sakaguchi., 1999). Malic acid within the BL (the third most abundant poly-acid at Izaña; Table 2) might have a photochemical origin via OH oxidation of the surrounding biogenic compounds transported by the day-time upslope winds. The Izaña Observatory is surrounded downhill by a forest ring – an important source of biogenic volatile organic compounds (BVOCs) – which contributes significantly to the measured concentrations at Izaña. Oxidation of these biogenic precursors may also provide important amounts of  $\text{C}_7$ – $\text{C}_9$  dicarboxylic acids.

10 High concentrations of dicarboxylic acids have been reported in plumes from BB (Narukawa et al., 1999; Gao et al., 2003), which is in agreement with the observed values for the long-range transport BBE (82  $\text{ng}\cdot\text{m}^{-3}$ ). Concentrations of succinic, glutaric and malic acids were high ( $\sim 33$   $\text{ng}\cdot\text{m}^{-3}$ ,  $\sim 7$   $\text{ng}\cdot\text{m}^{-3}$  and  $\sim 32$   $\text{ng}\cdot\text{m}^{-3}$ , respectively; Table 2), compared to the rest of the period, surely as a consequence of the lofted concentration emitted in the open fire and long-range transport photochemical aging processes.

### 15 3.2.3 Saccharides

Primary saccharides and polyols are tracer compounds of surface soils (Medeiros and Simoneit 2007; Simoneit et al. 2004a), related to plant tissue and microorganisms. Glucose ( $\alpha$ ,  $\beta$ ), fructose and sucrose are important constituents of OM in soils (Simoneit et al. 2004a), whereas mannitol is related to airborne fungal spores (Bauer et al. 2008). They are completely water-soluble, contributing to water soluble organic carbon (WSOC) in aerosols (Simoneit et al. 2004a). Wind erosion and up

20 whirling of soil dust emit these compounds to the atmosphere (Simoneit et al. 2004a).

The average concentration of the saccharides exhibits a marked difference within the FT- $\text{PM}_T$  (23.5  $\text{ng}\cdot\text{m}^{-3}$ ) and the BL- $\text{PM}_{2.5}$  (3.5  $\text{ng}\cdot\text{m}^{-3}$ ). Previous studies have shown that some organic compounds are strongly particle size dependent (Yttri et al., 2007; Van Drooge and Grimalt, 2015), with special emphasis in sugars and sugar alcohols which are present mostly in very large particles (Graham et al., 2003; Mochida et al., 2003). This size-segregation is clearly seen for the  $\text{PM}_{2.5}$  samples

25 collected within the BL, that cut off an important fraction of the coarse organic soil dust aerosol, showing similar concentrations under SAL and WES influence (BL-SAL = 3.3  $\text{ng}\cdot\text{m}^{-3}$ ; BL-WES = 4.0  $\text{ng}\cdot\text{m}^{-3}$ ). A different scenario takes place with the  $\text{PM}_T$  samples, for which concentrations rise one order of magnitude from SAL influence to clean conditions (FT-SAL = 27  $\text{ng}\cdot\text{m}^{-3}$ ; FT-WES = 2.5  $\text{ng}\cdot\text{m}^{-3}$ ) linked to Saharan dust contribution. The average saccharides levels in the FT-SAL are higher than these observed in a natural forest area in tropical India (12.78  $\text{ng}\cdot\text{m}^{-3}$ ; Fu et al., 2010) and a rural

30 background in Norway (10.4  $\text{ng}\cdot\text{m}^{-3}$ ; Yttri et al., 2007), but very similar to the average concentrations measured in the FT over central china (28.1  $\text{ng}\cdot\text{m}^{-3}$ ; Fu et al., 2014).



Glucose ( $\alpha+\beta$ ) was the predominant saccharide within the SAL, with mean FT concentration of  $\sim 10 \text{ ng}\cdot\text{m}^{-3}$  (Table 2); both isomers showed a good correlation ( $R^2=0.998$ ) consistent with their relation in the soil (Simoneit et al. 2004a). Under the WES airflows, glucose ( $\alpha+\beta$ ), sucrose and mannitol were slightly higher during the day (BL; Table 2), suggesting that there might be some soil contribution of transported terrestrial OM by land breeze. This load is more evident in the sucrose (FT-  
5 WES =  $0.3 \text{ ng}\cdot\text{m}^{-3}$ ; BL-WES =  $1.3 \text{ ng}\cdot\text{m}^{-3}$ ; Table 2), which is a predominant sugar in the phloem of plants playing a key role in developing flowers (Bialeski et al., 1995) and has been suggested as a tracer for airborne pollen grains (Fu et al., 2012).

### 3.2.4 n-Alkanes

n-Alkanes, or aliphatic hydrocarbons, are a result of biogenic and anthropogenic emissions such as plant waxes and fossil fuel combustion products (Mazurek et al. 1989; Simoneit et al. 1991; Shauer et al. 2002). In the present study n-alkanes from  
10  $n_{C_{24}}$  to  $n_{C_{34}}$  were quantified, with total n-alkanes mean concentrations ( $\sim 8 \text{ ng}\cdot\text{m}^{-3}$  in the FT and in the BL) much lower than this measured in the tropical Indian summer ( $126 \text{ ng}\cdot\text{m}^{-3}$ ; Fu et al., 2010), but similar to this found in rural Spain during the warm period ( $12 \text{ ng}\cdot\text{m}^{-3}$ ; Van Drooge and Grimalt, 2015).

Information about the possible source can be provided by the carbon number maximum ( $C_{\text{max}}$ ). In general,  $n_{C_{27}}$ ,  $n_{C_{29}}$  and  $n_{C_{31}}$  are related to waxes from terrestrial higher plants, whereas low-molecular-weight alkanes ( $C_{22}\text{--}C_{25}$ ) are more associated  
15 to combustion sources (Mazurek et al. 1989). At Izaña, the most abundant n-alkanes within the FT-SAL were  $n_{C_{27}}$ ,  $n_{C_{29}}$  and  $n_{C_{31}}$  ( $\sim 1.0 \text{ ng}\cdot\text{m}^{-3}$ ,  $\sim 1.4 \text{ ng}\cdot\text{m}^{-3}$  and  $\sim 1.8 \text{ ng}\cdot\text{m}^{-3}$  respectively; Table 2) reflecting a vegetative source as previously described for Saharan dust samples measured in the North Atlantic (Simoneit et al., 1977), whereas within the BL  $n_{C_{24}\text{--}n_{C_{25}}}$  presented the higher concentrations (Table 2) linked to anthropogenic emissions carried by the upslope winds. Another indicator that can be used to show the type of source is the carbon preference index ( $\text{CPI} = \frac{\sum \text{odd n-alkanes}}{\sum \text{even n-alkanes}}$ ) with  $\text{CPI} >$   
20 1 related to biogenic origin and  $\text{CPI} \approx 1$  to combustion processes (Mazurek et al. 1989; Simoneit, 2002). In this study, CPI values ranged from 0.9 to 6.3 with average values for the FT-SAL ( $\sim 2$ ) higher than for the BL ( $\sim 1.7$ ) and the FT-WES ( $\sim 1.2$ ), reflecting the larger influence of vegetation within the FT-SAL and the predominance of combustion contribution within the BL and FT-WES samples. Although the vegetative source dominates in the FT, there is a significant correlation between n-alkanes and  $\text{NO}_3^-$  ( $r = 0.8$ ,  $p < 0.01$ ; Table 3), mostly due to its anthropogenic fraction ( $C_{24}\text{--}C_{25}$ ).

### 25 3.2.5 Hopanes

Hopanes ( $17\alpha(\text{H}),21\beta(\text{H})$ -29-norhopane and  $17\alpha(\text{H}),21\beta(\text{H})$ -hopane) are linked to mineral oil and related to unburned lubricating residues from primary vehicles emissions (Rogge et al., 1993; Schauer et al., 1996, 2002).  $\sum$ Hopanes mean concentrations were  $0.13$  and  $0.08 \text{ ng}\cdot\text{m}^{-3}$  within the FT and BL respectively, values much higher than the  $7\cdot 10^{-4} \text{ ng}\cdot\text{m}^{-3}$   
30 surrounding region are minimal. Under the WES airflows, hopanes concentrations were slightly higher during the day,

Atmos. Chem. Phys. Discuss., doi:10.5194/acp-2017-108, 2017  
 Manuscript under review for journal Atmos. Chem. Phys.  
 Discussion started: 27 February 2017  
 © Author(s) 2017. CC-BY 3.0 License.

Atmospheric  
 Chemistry  
 and Physics  
 Discussions

Open Access  
 EGU



suggesting influence of pollution transported within the BL, related to motorized vehicle emissions. The quantified hopane and norhopane showed very good linear correlations ( $R^2=0.95$ ), pointing to the same emission sources.

A strong correlation is observed in the FT between hopanes and  $\text{NO}_3^-$  ( $r=0.8$ ,  $p<0.01$ ; Table 3) suggesting that most of  $\text{NO}_3^-$  in the FT has its origin in on-road vehicle emissions instead of the industry. Anthropogenic sources of  $\text{NO}_x$  (the major  $\text{NO}_3^-$  precursor) include fossil fuel emitted from agriculture, power plants, industry and transport. The latter one covers almost a 50% of the nitrogen oxides emissions (<http://www.eea.europa.eu/data-and-maps/indicators/eea-32-nitrogen-oxides-nox-emissions-1/assessment.2010-08-19.0140149032-3>), with on-road transport in 2010 being the highest (25.2  $\text{Tg}\cdot\text{year}^{-1}$ ) compared to non-road (10.1  $\text{Tg}\cdot\text{year}^{-1}$ ), shipping (16.2  $\text{Tg}\cdot\text{year}^{-1}$ ), aviation (3.0  $\text{Tg}\cdot\text{year}^{-1}$ ) or rail (1.6  $\text{Tg}\cdot\text{year}^{-1}$ ) (Yan et al., 2014).

### 10 3.2.6 Polycyclic aromatic hydrocarbons

Polycyclic aromatic hydrocarbons (PAH) are organic pollutants generated during incomplete combustion of organic material natural (e.g. forest fires, volcanic activity) and anthropogenic (e.g. fossil fuels combustion, coke production) sources (Howsam and Jones 1998; Iinuma et al., 2007; Rogge et al., 1993; Schauer et al., 1996, 2002). PAHs are composed of two or more fused aromatic rings and some of them have carcinogenicity, genotoxicity, and potential endocrine disruptiveness, affecting human health. At Izaña mean values of the total PAHs exhibited higher values in the BL (24  $\text{pg}\cdot\text{m}^{-3}$ ) than in the FT (16.3  $\text{pg}\cdot\text{m}^{-3}$ ), reflecting the contribution of the upslope winds as described for other organic compounds.

Similar PAHs concentrations were previously found by van Drooge et al. (2010) who measured an average PAHs concentration of 33.1  $\text{pg}\cdot\text{m}^{-3}$  at Izaña. In general, all individual PAHs decreased its concentration except benz(a)anthracene that increased by a factor of 1.5 and 1.35 with respect to the mean concentrations of the FT and BL correspondingly. Much higher concentrations have been reported in other remote FT locations as Mt. Tai (1534 m a.s.l.) where  $\sim 9 \text{ ng}\cdot\text{m}^{-3}$  were measured (Fu et al., 2008). In the FT there is a strong correlation between PAHs and EC ( $r=0.7$ ,  $p<0.01$ ; Table 3), which points to the incomplete combustion of fossil fuels (Frenklach., 2000).

During the detected North America wildfire event (28Aug), PAHs concentration was 9.4  $\text{pg}\cdot\text{m}^{-3}$ , which is much lower than levels measured in Thailand for  $\text{PM}_{\text{T}}$  samples during BBEs in the dry season (1150 to 4140  $\text{pg}\cdot\text{m}^{-3}$ ; Chuesaard et al., 2014). The concentrations of PAHs measured in the sample corresponding to the fire event were not higher than those observed in the other samples, which may be due to photochemical transformations of PAH in the atmosphere during long-range transport.

### 3.2.7 Tracers of $\alpha$ -pinene oxidation (SOA PIN)



Vegetation emit large quantities of biogenic volatile organic compounds (BVOCs) into the atmosphere compared to anthropogenic VOCs (Guenther et al., 2006, 2012; Lamarque et al., 2010), particularly monoterpenes and isoprene. The most abundant volatile monoterpene, emitted mainly by coniferous trees (i.e. *Pinus canariensis*) is  $\alpha$ -pinene (Andreani-Aksoyoglu and Keller, 1995; Rinne et al., 2009; Smolander et al., 2014) and the tracers related to its photochemical oxidation (SOA PIN) are *cis*-pinonic acid, 3-hydroxyglutaric acid (3-HGA) and 3-methyl-1,2,3-butanetricarboxylic acid (MBTCA) (Claeys et al., 2007; Szmigielski et al., 2007).

SOA PIN organic tracers were not detected in all samples, with values in the FT influenced by a couple of extreme points that increased their average concentration. SOA PIN exhibited the lowest concentration in the FT-WES ( $1.2 \text{ ng}\cdot\text{m}^{-3}$ ) with a predominance of *cis*-pinonic acid (Table 2). Aircraft measurements in the FT over central China (Fu et al., 2014) recorded higher concentrations of 3-HGA ( $8.5 \text{ ng}\cdot\text{m}^{-3}$ ) and MBTCA ( $1.9 \text{ ng}\cdot\text{m}^{-3}$ ) than measure in the present study (Table 2). Further generation oxidation products (3-HGA and MBTCA) were higher in the BL ( $0.51$  and  $0.24 \text{ ng}\cdot\text{m}^{-3}$  correspondingly; Table 2), with a significant correlation ( $R^2 = 0.81$ ) that points to a same precursor. Monoterpenes reacts relatively fast, with atmospheric lifetimes ranging from minutes to hours (Saxton et al., 2007), resulting in  $\alpha$ -pinene emitted in the ring forest that reacts along its upward transport to the Observatory. Daytime emissions of gaseous  $\alpha$ -pinene at Izaña were measured by Fisher et al. (1998) with concentration in the range of  $0.011$ – $0.102$  ppbv (mean:  $0.028$  ppbv), supporting the evidence of its origin close to the Observatory during the day.

### 3.2.8 Tracers of isoprene oxidation (SOA ISO)

It is estimated that about a half of the total global BVOCs emission is due to isoprene ( $535 \text{ Tg}\cdot\text{y}^{-1}$ ; Guenther et al., 2012), making it the largest BVOC emitted from land vegetation (Guenther et al., 2006). Isoprene emission is limited to a number of species in the plant kingdom, contrary to many other BVOCs that are emitted from most plants (Guenther et al., 2012). Secondary products of isoprene oxidation (SOA ISO) evaluated in the present study are 2-methylglyceric acid (2-MGA), 2-methylthreitol (2-MT1) and 2-methylerythritol (2-MT2) (Claeys et al., 2004; Hallquist et al., 2009).

Analogous FT concentrations of 2-methylthreitol and 2-methylerythritol were measured in the present study under the SAL ( $7.3$  and  $16.8 \text{ ng}\cdot\text{m}^{-3}$ ; Table 2) and over the central China FT ( $8$  and  $17 \text{ ng}\cdot\text{m}^{-3}$ ; Fu et al., 2014), one of the most important source regions of isoprene emission in the world during summertime (Guenther et al., 1995). Similar SOA ISO concentrations were found in the BL within the SAL and the WES ( $\sim 17$  and  $\sim 16 \text{ ng}\cdot\text{m}^{-3}$  respectively) revealing the emission and following ascending transport of biogenic or anthropogenic compounds, as found in previous studies performed at Izaña, which observed emissions of isoprene during daytime associated to anthropogenic compounds (Salisbury et al., 2006). A significant correlation among 2-MT1 and 2-MT2 was found for individual values ( $R^2 = 0.94$ ) as previously observed in other studies (Ion et al., 2005; El Haddad et al., 2011), but with a mass concentration ratio 2-MT1 vs. 2-MT2 (slope from linear

Atmos. Chem. Phys. Discuss., doi:10.5194/acp-2017-108, 2017  
 Manuscript under review for journal Atmos. Chem. Phys.  
 Discussion started: 27 February 2017  
 © Author(s) 2017. CC-BY 3.0 License.



regression=2.3) slightly lower than this found by El Haddad et al. (2011). This correlation between the two diastereoisomers indicates a same origin though the same photo-oxidation process.

The highest concentration of SOA ISO was measured under the FT-SAL (~28 ng·m<sup>-3</sup>), associated to Saharan dust, as was observed for SOA PIN (~33 ng·m<sup>-3</sup>). However, global estimations of isoprene and  $\alpha$ -pinene emissions and sources show they are diverse and not equally distributed in the globe (Luo et al., 2010; Guenther et al., 2012; Sindelarova et al., 2014). Correlation between total concentration of SOA ISO and total concentration of SOA PIN (Fig. 2) exhibits two distinct trends in the FT that might be associated to different global sources of the precursor volatile compounds, although the trajectories of the sampled air mass does not distinguish clearly between different origins. Some species with a high isoprene emission potential have been identified in central and western Africa, but quantification of isoprene emissions are largely unverified for West Africa (Saxton et al., 2007). Several evaluations of isoprene and  $\alpha$ -pinene global emissions (Luo et al., 2010; Guenther et al., 2012; Sindelarova et al., 2014) confine the North Africa sources to a small belt over the northern part of Morocco, Algeria and Tunes, whereas Europe is pointed as a potential source. Some episodes, for which SOA PIN and SOA ISO were measured, do not have a trajectory over this African belt – based on the Hysplit model – , suggesting that air masses from Europe can also incorporate gaseous precursors and oxidized species previous to its pass over Africa and Izaña in the Atlantic Ocean.

Rodríguez et al. (2011) previously reported high concentrations of SO<sub>4</sub><sup>2-</sup>, NO<sub>3</sub><sup>-</sup> and NH<sub>4</sub><sup>+</sup> for air masses arriving to Izaña from the Atlantic coast of Morocco, Eastern Algeria, Northern Algeria and Tunisia. Industrial states with sources of gaseous precursors (SO<sub>x</sub>, NO<sub>x</sub> and NH<sub>3</sub>) of these aerosol compounds were identified. Although African emissions seem to be responsible of the pollutants arriving to the North Atlantic FT, Europe could also contribute with an amount of pollutants that should not be neglected as evidenced by the concentration of SOA PIN and SOA ISO arriving to Izaña. These species could play a key role in secondary organic aerosol formation, as some studies point to the influence of anthropogenic emission on secondary organic aerosol formation (El Haddad et al., 2011; Hoyle et al., 2011). SOA ISO seems to depend strongly on the conditions (NO<sub>x</sub> concentrations and aerosol acidity) used to oxidize isoprene (Surratt et al., 2006; 2007). We found the relation among SOA ISO and NO<sub>3</sub><sup>-</sup> within the FT-SAL (Fig.3) present three tendencies which might be associated to the ratio isoprene:NO<sub>x</sub> in the source.

Significant correlations in the FT between biogenic secondary organic compounds and NO<sub>3</sub><sup>-</sup> ( $r$  SOA PIN–NO<sub>3</sub><sup>-</sup> = 0.6,  $p < 0.01$ ; Table 3) and nss-SO<sub>4</sub><sup>2-</sup> ( $r$  SOA ISO–nss-SO<sub>4</sub><sup>2-</sup> = 0.6,  $p < 0.01$ ; Table 3), point to its formation from the oxidation of their gaseous precursors NO<sub>x</sub> and SO<sub>2</sub> respectively. Dust transformation in the FT is also evidenced by its highly significant correlation with SOA PIN ( $r$  = 0.7,  $p < 0.01$ ; Table 3) as well as both saccharides ( $r$  = 0.6,  $p < 0.01$ ) and hopanes ( $r$  = 0.9,  $p < 0.01$ ) showing that natural and anthropogenic substances might be mixed after aging processes.

### 3.2.9 Determined fraction of OM



Bulk organic carbon (OC) determined for every single day (thermo-optical transmittance method) at Izaña during this study was within the range 0.01–2.20  $\mu\text{g}\cdot\text{m}^{-3}$ , which is of the order to that found in other FT studies (e.g. 1.4  $\mu\text{g}\cdot\text{m}^{-3}$  at Qomolangma, Mt. Everest, 4276 m a.s.l. by Cong et al., 2015 and 4  $\mu\text{g}\cdot\text{m}^{-3}$  at NW Pacific, 2–6.5 km column by Heald et al., 2005). FT-PM<sub>T</sub> OC under SAL conditions (0.77  $\mu\text{g}\cdot\text{m}^{-3}$ ) was higher than under WES (0.52  $\mu\text{g}\cdot\text{m}^{-3}$ , including the BBE) events. Figure 4 shows the mass closure (sum of the organic species determined by speciation) of bulk organic matter OM (determined as OC·1.8); this mass closure accounts for 2 to 100 % of the OM for every single day, depending on the sample and the airflows.

Concentrations of OM were much higher in the FT-SAL (1.39  $\mu\text{g}\cdot\text{m}^{-3}$ ) than under FT-WES (0.04  $\mu\text{g}\cdot\text{m}^{-3}$  without the BBE; 0.94  $\mu\text{g}\cdot\text{m}^{-3}$  including the BBE) conditions. The selected tracers (levoglucosan, SOA ISO, SOA PIN, n-Alkanes, saccharides, dicarboxylic acids, hopanes and PAHs) represents as average:

- (i) a 15% of the OM (Fig. 4), under FT-SAL conditions (when mean OM was 1.39  $\mu\text{g}\cdot\text{m}^{-3}$ ). This determined fraction is mainly composed by SOA ISO (30%), saccharides (27%) and dicarboxylic acids (18%).
- (ii) a 84% of the OM (Fig. 4), in the FT-WES airflows without the BBE (when mean OM was 0.04  $\mu\text{g}\cdot\text{m}^{-3}$ ). This determined fraction is constituted by dicarboxylic acids (44%; mainly succinic and phthalic, indicating aged aerosols after the long-range atmospheric transport), and SOA ISO (34%) with a minor presence of saccharides (8%). Biogenic SOA represent an important fraction of the OM at Izaña (~40%), as seen in other remote high altitude regions (Xu et al. 2015).
- (iii) a 3% of the OM (Fig. 4) in the FT-WES during the BBE (when mean OM was 3.64  $\mu\text{g}\cdot\text{m}^{-3}$ ). The determined fraction of OM for 28Aug (3%) contained a 68% of dicarboxylic acids (mostly succinic and malic acids) and an 8% of the BB tracer levoglucosan. This sample has the OM profile with the highest contribution of aged SOA (di-acids), formed during the long-range atmospheric transport, and the lowest contributions of SOA PIN (4%) and SOA ISO (12%), which could indicate the further oxidation of these products under the BBE air masses conditions.
- (iv) a 64% of the OM in the FT-WES including the BBE (when mean OM was 0.94  $\mu\text{g}\cdot\text{m}^{-3}$ ). This determined fraction is constituted mainly by dicarboxylic acids (50%), and SOA ISO (28%).

The determined OM composition within the BL (PM<sub>2.5</sub>; BL-FT: 9% of the OM and BL-WES: 77% of the OM; Fig. 4) remains almost the same under both airflows, but with higher concentrations of SOA ISO and n-alkanes under the SAL. However, due to the PM<sub>2.5</sub> cut-off of the collected particles, the influence of the dust-associated organic compound is probably not well represented since these products are situated in the coarse fraction of the PM.

### 3.3 Sources of OM

Atmos. Chem. Phys. Discuss., doi:10.5194/acp-2017-108, 2017  
Manuscript under review for journal Atmos. Chem. Phys.  
Discussion started: 27 February 2017  
© Author(s) 2017. CC-BY 3.0 License.



We used receptor modelling for apportioning OM between the OA sources traced by the species included in the speciation performed in this study. This analysis is complementary to the mass closure performed above (Fig.4). The loading factors obtained in the MCR-ALS were used to identify OA sources (Fig.5A1–5C1), whereas the score factors were used as independent variables in the Multilinear Regression Analysis (MLRA) to apportion the determined fraction of OM between the identified sources. Three components (sources) were identified (Fig. 5), which accounted by 81% of the total variance. MCR-ALS method was also applied only to PM<sub>7</sub> samples to verify the influence of PM<sub>2.5</sub> in the final results; no significant differences were observed as shown in Fig. S1 of the supplement.

### 3.3.1 Biomass Burning (BB)

The major component (accounting for 63% of the total variance) is associated with levoglucosan, dicarboxylic acids, phthalic acid, SOA PIN, C<sub>24</sub>–C<sub>28</sub> alkanes and hopanes and PAHs to a lesser extent (Fig. 5A). This factor represents biomass burning aerosols (BB). The peak event in the score factor observed the 28Aug (Fig. 5A2) is associated with the episode of levoglucosan linked to the long-range transport of BB from North America. SOA PIN indicates photochemical oxidation of biogenic volatile organic compounds during the wild fire. The presence of short-chain dicarboxylic acids, along with important amounts of malic acid, suggests the effective oxidation of organic species to shorter di-acids chains during long-range atmospheric transport. PAH contribution in this component is low, despite potential emissions of PAHs during biomass burning. The low PAH contributions could be the result of photochemical degradation during long-range transport, which on their term could be related to the presence of higher contributions of phthalic acid in this component. BB in the FT is significantly associated to the OM ( $r\text{-FT} = 0.40$ ,  $p < 0.05$ ; Table S1) and EC ( $r\text{-FT} = 0.65$ ,  $p < 0.01$ ; Table S1) concentrations.

### 3.3.2 Combustion POA

The second component (accounting for 21% of the total variance) is associated with long-chain dicarboxylic acids, SOA ISO, C<sub>24</sub> – C<sub>29</sub> n-alkanes and PAHs (Fig. 5B). This factor is related to the primary organic aerosols linked to combustion sources. This is the component that best represents the variability of PM<sub>2.5</sub> samples collected during daylight, when the BL may reach Izaña under the slope wind regime. High loadings of suberic (C<sub>8</sub>) and azelaic acids (C<sub>9</sub>) indicate the presence of oxidized compounds in the early stage of photochemical transformation processes, such as the ozonolysis of oleic acid (Moise and Rudich, 2002). Organic species supporting the anthropogenic contribution are lower-molecular-weight n-alkanes (C<sub>24</sub> – C<sub>25</sub>) and PAHs (from incomplete combustion processes). FT aerosol is also described by this component with the exception of low-molecular-weight alkanes (C<sub>24</sub>–C<sub>25</sub>) which is the main feature of the BL samples. The component is significantly representative of the measured EC for all samples, and highly representative for the BL, as shown by its Pearson correlation coefficient ( $r\text{-All} = 0.36$  and  $r\text{-BL} = 0.71$ ,  $p < 0.05$ ; Table S1).

Atmos. Chem. Phys. Discuss., doi:10.5194/acp-2017-108, 2017  
Manuscript under review for journal Atmos. Chem. Phys.  
Discussion started: 27 February 2017  
© Author(s) 2017. CC-BY 3.0 License.



### 3.3.3 Organic dust

The third component, accounting for 16% of the total variance, is composed by short-chain dicarboxylic acids, SOA ISO, saccharides, C<sub>26</sub>–C<sub>34</sub> alkanes, hopanes, and PAHs to a lesser extent (Fig. 5C). This component, identified as organic dust, is associated with soil re-suspension as evidenced by the saccharides and mannitol high loadings. The predominant presence of the soil OM related compounds, those from fungi and terrestrial higher plants (C<sub>27</sub>, C<sub>29</sub> and C<sub>31</sub>), suggest fresh and primary OA. Notwithstanding, glutaric, adipic and pimelic acids indicate oxidation products, suggesting the aging of the samples. As a consequence of this aging, natural and anthropogenic markers are mixed in this component. The biogenic influence is indicated by the presence of soil related markers and oxidation products from isoprene (2MGA, 2MT-1 and 2MT-2), whereas the anthropogenic influence is well defined by the presence of hopanes (primary vehicle emissions) and high molecular weight PAH (products of incomplete combustion). The scores of this component display the highest correlation with dust (r-All = 0.84, p < 0.01; Table S1) and OM (r-All = 0.64, p < 0.01; Table S1) concentrations for all samples. Although this component is not relevant for the BL-PM<sub>2.5</sub> samples – because of part of the compounds are present in the larger particle size fractions – the correlation with dust (r-BL = 0.73, p < 0.01; Table S1) and OM (r-BL = 0.75, p < 0.01; Table S1) are highly significant due to the mixing of dust with the anthropogenic compounds.

### 3.3.4 Source apportionment of OM in the SAL and the westerlies

The source apportionment of OM was performed by the multilinear regression technique described above. The difference between the bulk OM (determined by thermo-optical method) and the sum of the organic species (determined with the speciation) was labelled as undetermined fraction. Figure 6 shows the time series of the daily contribution of each source to the determined OM and Fig. 7 shows the average source contribution to total OM in the aerosol samples collected in the different airstreams. The correlation between the sum of the three components scores and the OM within the FT (OM r-FT = 0.63; Table S1) indicates that the identified sources might describe, not only the determined fraction of the OM but also the total OM. This significant correlation is not seen for the BL (OM r-BL = 0.33; Table S1), where there could be additional sources.

In the FT-SAL airflow, most of OM was undermined (~85, Fig.7). The three identified sources, i.e. the organic dust, combustion POA and biomass burning, accounts for 8%, 6% and 1% of the bulk OM, respectively (62%, 34% and 4% of the determined OM, respectively). The presence of biogenic SOA products mixed with combustion POA was also found in previous studies which suggested that biogenic SOA formation may be more efficient in polluted atmospheres (Gouw and Jiménez., 2009 and references therein).

In the FT-WES, the undermined fraction accounts for ~36% of the OM (Fig.7). The contribution of the three identified sources, i.e. the organic dust, combustion POA and biomass burning, is 22%, 19% and 23% to the bulk OM, respectively

Atmos. Chem. Phys. Discuss., doi:10.5194/acp-2017-108, 2017  
Manuscript under review for journal Atmos. Chem. Phys.  
Discussion started: 27 February 2017  
© Author(s) 2017. CC-BY 3.0 License.



(28%, 23% and 49% to the determined OM, respectively). Yttri et al. (2007) proposed biomass burning as a source of saccharides in the OA and Fraser and Lakshmanan (2000) found that some saccharides resist degradation in the atmosphere over a period of 10 days, being able to be transported over long distances; this may be the source of the organic fraction of dust we detected in the FT-WES.

- 5 For the BL samples, the dust related component is not well represented (Fig. 6), because the coarse fraction was not sampled here. On the other hand, combustion POA explains a 6 and 41 % (Table S2) of the bulk OM for the SAL and WES, respectively. Background regional fires also affect the BL as described by the BB component, which represent a 2 and 36 % (Table S2) of the bulk OM for the SAL and WES, respectively.

#### 4 Conclusions

- 10 The present study is focused on the organic aerosol composition within the two main airflows of the subtropical North Atlantic free troposphere: (i) the Saharan Air Layer – the warm, dry and dusty airstream that expands from North Africa to the Americas at subtropical and tropical latitudes – and (ii) the westerlies – which flows from North America through the North Atlantic at mid and subtropical latitudes –. Atmospheric particulate matter was analysed on secondary inorganic species, elemental composition, elemental and organic carbon and 40 organic tracer species (levoglucosan, dicarboxylic acids, saccharides, n-alkanes, hopanes, polycyclic aromatic hydrocarbons and those formed after oxidation of  $\alpha$ -pinene and isoprene) in order to distinguish possible sources for the organic aerosol. The organic particulate aerosol speciation and its subsequent source apportionment was performed for 42 filter samples collected in summer at the Izaña Observatory (~2400 m a.s.l.) in Tenerife, Spain.

- 20 The levels of all inorganic and almost all organic tracers were generally higher under the Saharan Air Layer influence in comparison to the pristine conditions of the Westerlies and the differences in the composition of the determined organic matter under these two air masses were important.

- In the Saharan Air Layer, the aerosol composition was dominated by dust (93%), secondary inorganic pollutants (<5%) and organic matter (~1.5%). The organic compounds (determined by gas-chromatography coupled to mass-spectrometry) accounted for a 15% of the bulk organic matter and were related to soils (saccharides), biogenic secondary organic aerosols linked to isoprene oxidation (SOA ISO) and natural and anthropogenic primary sources such as vegetation and motor exhaust emissions (dicarboxylic acids).

In the Westerlies, the organic matter represented a higher fraction of the total aerosol bulk (~28%) and the determined organic compounds accounted for an 64% of the organic matter with dicarboxylic acids and SOA ISO being the most abundant. In this airstream, a long-range atmospheric transport of a biomass burning plume from North America was

Atmos. Chem. Phys. Discuss., doi:10.5194/acp-2017-108, 2017  
 Manuscript under review for journal Atmos. Chem. Phys.  
 Discussion started: 27 February 2017  
 © Author(s) 2017. CC-BY 3.0 License.



detected (with organic matter representing a 53% of the total aerosol bulk), supporting the atmospheric stability of levoglucosan over transport and time under certain conditions.

- Three sources of organic aerosol, which contribute to the organic matter composition in this part of the North Atlantic, could be resolved in multivariate analysis: one biomass burning-related, one primary combustion-related and one organic dust-related. In the Saharan Air Layer, the organic matter comes from organic dust (8% of the bulk OM; 63% of the determined OM) and combustion (6% of the bulk OM; 34% of the determined OM) sources, whereas under the westerlies comes from organic dust (22% of the bulk OM; 28% of the determined OM), biomass burning (23% of the bulk OM; 49% of the determined OM) and combustion (19% of the bulk OM; 23% of the determined OM) sources, showing that the free troposphere is highly influenced by combustion and biomass burning compounds.
- 10 A comprehensive knowledge of the organic aerosol chemistry is of high importance for assessing anthropogenic influences and evaluating the effect of radiative forcing. The work presented here offers new insights into the organic composition of the North Atlantic free troposphere as well as the trans-boundary origin of some compounds. Further studies are needed to understand the main mechanisms by which the aerosol is lofted into the free troposphere and transported over long distances.

- Acknowledgements:* This study was performed within the context of the projects AEROATLAN (CGL2015-66299-P; MINECO/FEDER) and TEAPARTICLE (CGL2011-29621), supported by the Ministry of Economy and Competitiveness of Spain and the European Regional Development Fund (ERDF). The authors acknowledge the NOAA Air Resources Laboratory (ARL) for the provision of the HYSPLIT back-trajectories used in this publication. The excellent work performed by the staff of the Atmospheric Research Centre (C. Bayo, C. Hernández, F. de Ory, V. Carreño, R. del Campo and SIELTEC Canarias) and of the Institute of Environmental Assessment and Water Research (R. Chalor, D. Fanjul, and B. Hortelano) is appreciated. M. I. García acknowledges the grant of the Canarian Agency for Research, Innovation and Information Society (ACIISI) co-funded by the European Social Funds. Measurements at Izaña observatory are performed within the context Global Atmospheric Watch networks with the financial support of the State Meteorological Agency of Spain (AEMET).
- 15
- 20

- 25 *Competing interests:* The authors declare that they have no conflict of interest.



European Regional  
 Development Fund



**Gobierno de Canarias**  
 Agencia Canaria  
 de Investigación, Innovación  
 y Sociedad de la Información



Unión Europea  
 Fondo Social Europeo

Atmos. Chem. Phys. Discuss., doi:10.5194/acp-2017-108, 2017  
 Manuscript under review for journal Atmos. Chem. Phys.  
 Discussion started: 27 February 2017  
 © Author(s) 2017. CC-BY 3.0 License.



## References

- Alier, M., van Drooge, B. L., Dall'Osto, M., Querol, X., Grimalt, J. O. and Tauler, R.: Source apportionment of submicron organic aerosol at an urban background and a road site in Barcelona (Spain) during SAPUSS, *Atmos. Chem. Phys.*, 13(20), 10353–10371, doi:10.5194/acp-13-10353-2013, 2013.
- Andreani-aksoyoglu, S. and Keller, J.: Estimates of monoterpene and isoprene emissions from the forests in Switzerland, *J. Atmos. Chem.*, 20(1), 71–87, doi:10.1007/BF01099919, 1995.
- Bauer, H., Claeys, M., Vermeylen, R., Schueller, E., Weinke, G., Berger, A. and Puxbaum, H.: Arabitol and mannitol as tracers for the quantification of airborne fungal spores, *Atmos. Environ.*, 42(3), 588–593, doi:10.1016/j.atmosenv.2007.10.013, 2008.
- Bielecki, R.: Onset of phloem export from senescent petals of daylily, *Plant Physiol.*, 109, 557–565, 1995.
- Birch, M. E. and Cary, R. A.: Elemental carbon-based method for monitoring occupational exposures to particulate diesel exhaust, *Aerosol Sci. Technol.*, 25, 221–241, 1996.
- Boose, Y., Sierau, B., García, M. I., Rodríguez, S., Alastuey, A., Linke, C., Schnaiter, M., Kupiszewski, P., Kanji, Z. A., and Lohmann, U.: Ice nucleating particles in the Saharan Air Layer, *Atmos. Chem. Phys.*, 16, 9067–9087, doi:10.5194/acp-16-9067-2016, 2016.
- Cavalli, F., Viana, M., Yttri, K. E., Genberg, J., and Putaud, J.-P.: Toward a standardised thermal-optical protocol for measuring atmospheric organic and elemental carbon: the EUSAAR protocol, *Atmos. Meas. Tech.*, 3, 79–89, doi:10.5194/amt-3-79-2010, 2010.
- Chuesaard, T., Chetianukornkul, T., Kameda, T., Hayakawa, K. and Toriba, A.: Influence of Biomass Burning on the Levels of Atmospheric Polycyclic Aromatic Hydrocarbons and Their Nitro Derivatives in Chiang Mai, Thailand. *Aerosol Air Qual. Res.* 14: 1247–1257, 2014.
- Claeys, M., Graham, B., Vas, G., Wang, W., Vermeylen, R., Pashynska, V., Cafmeyer, J., Guyon, P., Andreae, M. O., Artaxo, P. and Maenhaut, W.: Formation of secondary organic aerosols through photooxidation of isoprene., *Science*, 303(5661), 1173–1176, doi:10.1126/science.1092805, 2004.
- Claeys, M., Szmigielski, R., Kourtchev, I., Van der Veken, Pi., Vermeylen, R., Maenhaut, W., Jaoui, M., Kleindienst, T., Lewandowski, M., Offenberg, J., and Edney, E.: Hydroxydicarboxylic Acids: Markers for Secondary Organic Aerosol from the Photooxidation of  $\alpha$ -Pinene, *Environ. Sci. Technol.*, 41, 1628–1634, 2007.
- Conen, F., Rodríguez, S., Hüglin, C., Henne, S., Herrmann, E., Bukowiecki, N., and Alewell, C.: Atmospheric ice nuclei at the high-altitude observatory Jungfraujoch, Switzerland, *Tellus, Ser. B*, 67, 1–10, doi:10.3402/tellusb.v67.25014, 2015.
- Cong, Z., Kang, S., Kawamura, K., Liu, B., Wan, X., Wang, Z., Gao, S. and Fu, P.: Carbonaceous aerosols on the south edge of the Tibetan Plateau: concentrations, seasonality and sources, *Atmos. Chem. Phys.*, 15(3), 1573–1584, doi:10.5194/acp-15-1573-2015, 2015.
- Cuesta, J., Marsham, J. H., Parker, D. J., and Flamant, C.: Dynamical mechanisms controlling the vertical redistribution of dust and the thermodynamic structure of the West Saharan atmospheric boundary layer during summer, *Atmos. Sci. Lett.*, 10, 34–42, doi:10.1002/asl.207, 2009.
- Draxler, R. R., and Hess, G. D.: Description of the HYSPLIT 4 modeling system. NOAA Tech.Memo. ERL ARL-224, NOAA Air Resources Laboratory, Silver Spring, MD, 1997.
- Draxler, R.R. and Rolph, G.D., 2003. HYSPLIT (HYbrid Single-Particle Lagrangian Integrated Trajectory) Model access via NOAA ARL READY Website (<http://www.arl.noaa.gov/ready/hysplit4.html>). NOAA Air Resources Laboratory, Silver Spring, MD.
- Dzepina, K., Mazzoleni, C., Fialho, P., China, S., Zhang, B., Owen, R. C., Helmig, D., Hueber, J., Kumar, S., Perlinger, J. A., Kramer, L. J., Dziobak, M. P., Ampadu, M. T., Olsen, S., Wuebbles, D. J. and Mazzoleni, L. R.: Molecular characterization of free tropospheric aerosol collected at the Pico Mountain Observatory: a case study with a long-range transported biomass burning plume, *Atmos. Chem. Phys.*, 15(9), 5047–5068, doi:10.5194/acp-15-5047-2015, 2015.
- El Haddad, I., Marchand, N., Temime-Roussel, B., Wortham, H., Piot, C., Besombes, J.-L., Baduel, C., Voisin, D., Armengaud, A., and Jaffrezo, J.-L.: Insights into the secondary fraction of the organic aerosol in a Mediterranean urban area: Marseille, *Atmos. Chem. Phys.*, 11, 2059–2079, doi:10.5194/acp-11-2059-2011, 2011.



- Fischer, H., Nikitas, C., Parchatka, U., Zenker, T., Harris, G. W., Matuska, P., Schmitt, R., Mihelcic, D., Muesgen, P., Paetz, H.-W., Schultz, M. and Volz-Thomas, A.: Trace gas measurements during the Oxidizing Capacity of the Tropospheric Atmosphere campaign 1993 at Izaña, *J. Geophys. Res.*, 103(D11), 13505, doi:10.1029/97JD01497, 1998.
- Fontal, M., van Drooge, B. L., Lopez, J. F., Fernández, P., and Grimalt, J. O.: Broad spectrum analysis of polar and apolar organic compounds in submicron atmospheric particles, *J. Chromatogr. A*, 1404, 28–38, 2015.
- Fraser, M. P. and Lakshmanan, K.: Using levoglucosan as a molecular marker for the long-range transport of biomass combustion aerosols, *Environ. Sci. Technol.*, 34(21), 4560–4564, doi:10.1021/es991229i, 2000.
- Frenklach, M.: Reaction mechanism of soot formation in flames, *Phys. Chem. Chem. Phys.*, 4(11), 2028–2037, doi:10.1039/b110045a, 2002.
- Fu, P., Kawamura, K., Okuzawa, K., Aggarwal, S. G., Wang, G., Kanaya, Y. and Wang, Z.: Organic molecular compositions and temporal variations of summertime mountain aerosols over Mt. Tai, North China Plain, *J. Geophys. Res.*, 113(D19), D19107, doi:10.1029/2008JD009900, 2008.
- Fu, P. Q., Kawamura, K., Pavuluri, C. M., Swaminathan, T. and Chen, J.: Molecular characterization of urban organic aerosol in tropical India: contributions of primary emissions and secondary photooxidation, *Atmos. Chem. Phys.*, 10(6), 2663–2689, doi:10.5194/acp-10-2663-2010, 2010.
- Fu, P., Kawamura, K., Kobayashi, M. and Simoneit, B. R. T.: Seasonal variations of sugars in atmospheric particulate matter from Gosan, Jeju Island: Significant contributions of airborne pollen and Asian dust in spring, *Atmos. Environ.*, 55, 234–239, doi:10.1016/j.atmosenv.2012.02.061, 2012.
- Fu, P. Q., Kawamura, K., Cheng, Y. F., Hatakeyama, S., Takami, A., Li, H. and Wang, W.: Aircraft measurements of polar organic tracer compounds in tropospheric particles (PM<sub>10</sub>) over central China, *Atmos. Chem. Phys.*, 14(8), 4185–4199, doi:10.5194/acp-14-4185-2014, 2014.
- Gao, S., Hegg, D. A., Hobbs, P. V., Kirchstetter, T. W., Magi, B. I. and Sadilek, M.: Water-soluble organic components in aerosols associated with savanna fires in southern Africa: Identification, evolution, and distribution, *J. Geophys. Res. Atmos.*, 108(D13), n/a–n/a, doi:10.1029/2002JD002324, 2003.
- García, M. I., Rodríguez, S., González, Y. and García, R. D.: Climatology of new particle formation at Izaña mountain GAW observatory in the subtropical North Atlantic, *Atmos. Chem. Phys.*, 14(8), 3865–3881, doi:10.5194/acp-14-3865-2014, 2014.
- Garrison, V. H., Majewski, M. S., Foreman, W. T., Genualdi, S. A., Mohammed, A., and Massey Simonich, S. L.: Persistent organic contaminants in Saharan dust air masses in West Africa, Cape Verde and the eastern Caribbean, *Sci. Total Environ.*, 468–469, 530–543, 2013.
- Gouw, J. D. E. and Jimenez, J. L.: Organic Aerosols in the Earth's Atmosphere, 43(20), 7614–7618, 2009.
- Graham, B., Guyon, P., Taylor, P. E., Artaxo, P., Maenhaut, W., Glovsky, M. M., Flagan, R. C., and Andreae, M. O.: Organic compounds present in the natural Amazonian aerosol: characterization by gas chromatography-mass spectrometry, *J. Geophys. Res.*, 108(D24), 4766, doi:10.1029/2003JD003990, 2003.
- Griffin, D.: Atmospheric movement of microorganisms in clouds of desert dust and implications for human health, *Clin. Microbiol. Rev.*, 20, 459–477, doi:10.1128/CMR.00039-06, 2007.
- Guenther, A., Hewitt, C. N., Erickson, D., Fall, R., Geron, C., Graedel, T., Harley, P., Klinger, L., Lerdau, M., McKay, W. A., Pierce, T., Scholes, B., Steinbrecher, R., Tallamraju, R., Taylor, J., and Zimmerman, P.: A global-model of natural volatile organic-compound emissions, *J. Geophys. Res.*, 100, 8873–8892, 1995.
- Guenther, A. B., Jiang, X., Heald, C. L., Sakulyanontvittaya, T., Duhl, T., Emmons, L. K., and Wang, X.: The Model of Emissions of Gases and Aerosols from Nature version 2.1 (MEGAN2.1): an extended and updated framework for modeling biogenic emissions, *Geosci. Model Dev.*, 5, 1471–1492, doi:10.5194/gmd-5-1471-2012, 2012.
- Guenther, A., Karl, T., Harley, P., Wiedinmyer, C., Palmer, P. I., and Geron, C.: Estimates of global terrestrial isoprene emissions using MEGAN (Model of Emissions of Gases and Aerosols from Nature), *Atmos. Chem. Phys.*, 6, 3181–3210, doi:10.5194/acp-6-3181-2006, 2006.
- Hallquist, M., Wenger, J. C., Baltensperger, U., Rudich, Y., Simpson, D., Claeys, M., Dommen, J., Donahue, N. M., George, C., Goldstein, a. H., Hamilton, J. F., Herrmann, H., Hoffmann, T., Iinuma, Y., Jang, M., Jenkin, M. E., Jimenez, J. L., Kiendler-Scharr, A., Maenhaut, W., McFiggans, G., Mentel, T. F., Monod, A., Prévôt, a. S. H., Seinfeld, J. H., Surratt, J. D., Szmigielski, R. and Wildt, J.: The formation, properties and impact of secondary organic aerosol: current and emerging issues, *Atmos. Chem. Phys.*, 9(14), 5155–5236, doi:10.5194/acp-9-5155-2009, 2009.

Atmos. Chem. Phys. Discuss., doi:10.5194/acp-2017-108, 2017  
 Manuscript under review for journal Atmos. Chem. Phys.  
 Discussion started: 27 February 2017  
 © Author(s) 2017. CC-BY 3.0 License.



- Heald, C. L., Jacob, D. J., Park, R. J., Russell, L. M., Huebert, B. J., Seinfeld, J. H., Liao, H. and Weber, R. J.: A large organic aerosol source in the free troposphere missing from current models, *Geophys. Res. Lett.*, 32(18), 1–4, doi:10.1029/2005GL023831, 2005.
- Hennigan, C. J., Sullivan, A. P., Collett, J. L. and Robinson, A. L.: Levoglucosan stability in biomass burning particles exposed to hydroxyl radicals, *Geophys. Res. Lett.*, 37(9), n/a–n/a, doi:10.1029/2010GL043088, 2010.
- Hoffmann, D.; Tilgner, A.; Iinuma, Y.; Herrmann, H. Atmospheric Stability of Levoglucosan: A Detailed Laboratory and Modeling Study. *Environ. Sci. Technol.* 44, 694–699, 2010.
- Howsam, M. and Jones, K.: Sources of PAHs in the environment, *Handb. Environ. Chem.*, 3, 137–174, doi:10.1007/978-3-540-49697-7\_4, 1998.
- Hoyle, C. R., Boy, M., Donahue, N. M., Fry, J. L., Glasius, M., Guenther, A., Hallar, A. G., Huff Hartz, K., Petters, M. D., Petäjä, T., Rosenoern, T., and Sullivan, A. P.: A review of the anthropogenic influence on biogenic secondary organic aerosol, *Atmos. Chem. Phys.*, 11, 321–343, doi:10.5194/acp-11-321-2011, 2011.
- Iinuma, Y., Brüggemann, E., Gnauk, T., Müller, K., Andreae, M. O., Helas, G., Parmar, R. and Herrmann, H.: Source characterization of biomass burning particles: The combustion of selected European conifers, African hardwood, savanna grass, and German and Indonesian peat, *J. Geophys. Res.*, 112(D8), D08209, doi:10.1029/2006JD007120, 2007.
- IPCC, 2013: Climate change 2013: The physical science basis. Contribution of Working Group I to the Fifth Assessment Report of the Intergovernmental Panel on Climate edited by: Stocker, T.F., Qin, D., Plattner, G.K. Tignor, M. , Allen, S.K. , Boschung, J. , Nauels, A. , Xia, Y. , Bex V. , and Midgley P.M. Cambridge University Press, Cambridge, UK and New York, NY, USA, 1535 pp.
- Ion, A. C., Vermeylen, R., Kourtschev, I., Cafmeyer, J., Chi, X., Gelencsér, A., Maenhaut, W. and Claeys, M.: Polar organic compounds in rural PM<sub>2.5</sub> aerosols from K-pusztá, Hungary, during a 2003 summer field campaign: Sources and diel variations, *Atmos. Chem. Phys.*, 5(7), 1805–1814, doi:10.5194/acp-5-1805-2005, 2005.
- Izquierdo, R., Belmonte, J., Avila, A., Alarcón, M., Cuevas, E., and Alonso-Pérez, S.: Source areas and long-range transport of pollen from continental land to Tenerife (Canary Islands), *Int. J. Biometeorol.*, 55, 67–85, doi: 10.1007/s00484-010-0309-1, 2011.
- Jang, M. and Medow, S. R.: Products of benz[a]anthracene photodegradation in the presence of known organic constituents of atmospheric aerosols, *Environ. Sci. Technol.*, 31(4), 1046–1053, doi:10.1021/es960559s, 1997.
- Jaumot, J., Gargallo, R., de Juan, A. and Tauler, R.: A graphical user-friendly interface for MCR-ALS: a new tool for multivariate curve resolution in MATLAB, *Chemom. Intell. Lab. Syst.*, 76(1), 101–110, doi:10.1016/j.chemolab.2004.12.007, 2005.
- Kanakidou, M., Seinfeld, J. H., Pandis, S. N., Barnes, I., Dentener, F. J., Facchini, M. C., Van Dingenen, R., Ervens, B., Nenes, A., Nielsen, C. J., Swietlicki, E., Putaud, J. P., Balkanski, Y., Fuzzi, S., Horth, J., Moortgat, G. K., Winterhalter, R., Myhre, C. E. L., Tsigaridis, K., Vignati, E., Stephanou, E. G., and Wilson, J.: Organic aerosol and global climate modelling: a review, *Atmos. Chem. Phys.*, 5, 1053–1123, doi:10.5194/acp-5-1053-2005, 2005.
- Karanasiou, A., Minguillón, M. C., Viana, M., Alastuey, A., Putaud, J.-P., Maenhaut, W., Panteliadis, P., Močnik, G., Favez, O., and Kuhlbusch, T. A. J.: Thermal-optical analysis for the measurement of elemental carbon (EC) and organic carbon (OC) in ambient air a literature review, *Atmos. Meas. Tech. Discuss.*, 8, 9649–9712, doi:10.5194/amtd-8-9649-2015, 2015.
- Kawamura, K. and Kaplan, I. R.: Motor Exhaust Emissions as a Primary Source for Dicarboxylic Acids in Los Angeles Ambient Air, *Environ. Sci. Technol.*, 21(1), 105–110, doi:10.1021/es00155a014, 1987.
- Kawamura, K. and Sakaguchi, F.: Molecular distributions of water soluble dicarboxylic acids in marine aerosols over the Pacific Ocean including tropics, *J. Geophys. Res. Atmos.*, 104, 3501–3509, 1999.
- Kirchstetter, T. Novakov, W., T., and Hobbs, P. V.: Evidence that the spectral dependence of light absorption by aerosols is affected by organic carbon. *J. Geophys. Res.*, 109, D21208, doi:10.1029/2004JD004999, 2004.
- Kleindienst, T. E., Jaoui, M., Lewandowski, M., Offenberg, J. H. and Docherty, K. S.: The formation of SOA and chemical tracer compounds from the photooxidation of naphthalene and its methyl analogs in the presence and absence of nitrogen oxides, *Atmos. Chem. Phys.*, 12(18), 8711–8726, doi:10.5194/acp-12-8711-2012, 2012.
- Lamarque, J.-F., Bond, T. C., Eyring, V., Granier, C., Heil, A., Klimont, Z., Lee, D., Liousse, C., Mieville, A., Owen, B., Schultz, M. G., Shindell, D., Smith, S. J., Stehfest, E., Van Aardenne, J., Cooper, O. R., Kainuma, M., Mahowald, N.,



- McConnell, J. R., Naik, V., Riahi, K. and van Vuuren, D. P.: Historical (1850–2000) gridded anthropogenic and biomass burning emissions of reactive gases and aerosols: methodology and application, *Atmos. Chem. Phys.*, 10(15), 7017–7039, doi:10.5194/acp-10-7017-2010, 2010.
- Luo, G. and Yu, F.: A numerical evaluation of global oceanic emissions of  $\alpha$ -pinene and isoprene, *Atmos. Chem. Phys.*, 10, 2007–2015, doi:10.5194/acp-10-2007-2010, 2010.
- Maring, H., Savoie, D. L., Izaguirre, M. A., McCormick, C., Arimoto, R., Prospero, J. M. and Pilinis, C.: Aerosol physical and optical properties and their relationship to aerosol composition in the free troposphere at Izaña, Tenerife, Canary Islands, during July 1995, *J. Geophys. Res. Atmos.*, 105(D11), 14677–14700, doi:10.1029/2000JD900106, 2000.
- Mazurek, M. A., Cass, G. R. and Simoneit, B. R. T.: Interpretation of High-Resolution Gas Chromatography and High-Resolution Gas Chromatography / Mass Spectrometry Data Acquired from Atmospheric Organic Aerosol Samples, *Aerosol Sci. Technol.*, 10(2), 408–420, doi:10.1080/02786828908959280, 1989.
- Medeiros, P. M. and Simoneit, B. R. T.: Analysis of sugars in environmental samples by gas chromatography-mass spectrometry, *J. Chromatogr. A*, 1141(2), 271–278, doi:10.1016/j.chroma.2006.12.017, 2007.
- Meng, J., Wang, G., Li, J., Cheng, C., Ren, Y., Huang, Y., Cheng, Y., Cao, J., and Zhang, T.: Seasonal characteristics of oxalic acid and related SOA in the free troposphere of Mt. Hua, central China: implications for sources and formation mechanisms, *Sci Total Environ*, 493, 1088–1097, 2014.
- Merrill, J. T., and Moody J. L.: Synoptic meteorology and transport during the North Atlantic Regional Experiment (NARE) intensive: Overview, *J. Geophys. Res.*, 101, 28, 903–28,921, 1996.
- Mochida, M., Kawamura, K., Umemoto, N., Kobayashi, M., Matsunaga, S., Lim, H. J., Turpin, B. J., Bates, T. S. and Simoneit, B. R. T.: Spatial distributions of oxygenated organic compounds (dicarboxylic acids, fatty acids, and levoglucosan) in marine aerosols over the western Pacific and off the coast of East Asia: Continental outflow of organic aerosols during the ACE-Asia campaign, *J. Geophys. Res.*, 108(D23), 8638, doi:10.1029/2002JD003249, 2003.
- Moise, T. and Rudich, Y.: Reactive Uptake of Ozone by Aerosol-Associated Unsaturated Fatty Acids: Kinetics, Mechanism, and Products, *J. Phys. Chem. A*, 106, 669–6476, 2002.
- Narukawa, M., Kawamura, K., Takeuchi, N., and Nakajima, T.: Distribution of dicarboxylic acids and carbon isotopic compositions in aerosols from 1997 Indonesian forest fires, *Geophys. Res. Lett.*, 26, 3101–3104, 1999.
- Ng, N. L., Chhabra, P. S., Chan, A. W. H., Surratt, J. D., Kroll, J. H., Kwan, A. J., McCabe, D. C., Wennberg, P. O., Sorooshian, A., Murphy, S. M., Dalleska, N. F., Flagan, R. C., and Seinfeld, J. H.: Effect of NO<sub>x</sub> level on secondary organic aerosol (SOA) formation from the photooxidation of terpenes, *Atmos. Chem. Phys.*, 7, 5159–5174, doi:10.5194/acp-7-5159-2007, 2007.
- Ng, N. L., Kwan, A. J., Surratt, J. D., Chan, A. W. H., Chhabra, P. S., Sorooshian, A., Pye, H. O. T., Crouse, J. D., Wennberg, P. O., Flagan, R. C., and Seinfeld, J. H.: Secondary organic aerosol (SOA) formation from reaction of isoprene with nitrate radicals (NO<sub>3</sub>), *Atmos. Chem. Phys.*, 8, 4117–4140, doi:10.5194/acp-8-4117-2008, 2008.
- Paulot, F., Wunch, D., Crouse, J. D., Toon, G. C., Millet, D. B., Decarlo, P. F., Vigouroux, C., Deutscher, N. M., Abad, G. G., Notholt, J., Warneke, T., Hannigan, J. W., Warneke, C., De Gouw, J. A., Dunlea, E. J., De Mazière, M., Griffith, D. W. T., Bernath, P., Jimenez, J. L. and Wennberg, P. O.: Importance of secondary sources in the atmospheric budgets of formic and acetic acids, *Atmos. Chem. Phys.*, 11(5), 1989–2013, doi:10.5194/acp-11-1989-2011, 2011.
- Pérez García-Pando, C., Perlwitz, J. P., Miller, R. L., and Rodriguez, S.: Predicting the mineral composition of dust aerosols: Insights from chemical composition measurements at the Izaña Observatory, *Geophys. Res. Lett.*, 2016.
- Pitchford, M., Maim, W., Schichtel, B., Kumar, N., Lowenthal, D. and Hand, J.: Revised algorithm for estimating light extinction from IMPROVE particle speciation data., *J. Air Waste Manag. Assoc.*, 57(January 2015), 1326–1336, doi:10.3155/1047-3289.57.11.1326, 2007.
- Presto, A. A., Hartz, K. E. H., and Donahue, N. M.: Secondary organic aerosol production from terpene ozonolysis. 2. Effect of NO<sub>x</sub> concentration, *Environ. Sci. Technol.*, 39, 7046–7054, doi: 10.1021/Es050400s, 2005.
- Prospero, J. M. and Carlson, T. N.: Vertical and areal distribution of Saharan dust over the western Equatorial North Atlantic Ocean, *J. Geophys. Res.*, 77, 5255–5265, 1972.
- Puxbaum, H., Caseiro, A., Sánchez-Ochoa, A., Kasper-Giebl, A., Cleays, M., Gelencsér, A., Legrand, M., Preunkert, S., and Pio, C.: Levoglucosan levels at background sites in Europe for assessing the impact of biomass combustion on the European aerosol background, *J. Geophys. Res.*, 112, D23S05, doi:10.1029/2006JD008114, 2007.

Atmos. Chem. Phys. Discuss., doi:10.5194/acp-2017-108, 2017  
 Manuscript under review for journal Atmos. Chem. Phys.  
 Discussion started: 27 February 2017  
 © Author(s) 2017. CC-BY 3.0 License.

Atmospheric  
 Chemistry  
 and Physics  
 Discussions

Open Access  




- Pye, H. O. T., Chan, A. W. H., Barkley, M. P., and Seinfeld, J. H.: Global modeling of organic aerosol: the importance of reactive nitrogen (NO<sub>x</sub> and NO<sub>3</sub>), *Atmos. Chem. Phys.*, 10, 11261–11276, doi:10.5194/acp-10-11261-2010, 2010.
- Rinne, J., Bäck, J. and Hakola, H.: Biogenic volatile organic compound emissions from the Eurasian taiga: Current knowledge and future directions, *Boreal Environ. Res.*, 14(4), 807–826 [online] Available from: <http://www.scopus.com/inward/record.url?eid=2-s2.0-69949092124&partnerID=40&md5=64765c400b7ae11f40cb879cfffbc7515>, 2009.
- Rodríguez, S., González, Y., Cuevas, E., Ramos, R., Romero, P. M., Abreu-Afonso, J. and Redondas, A.: Atmospheric nanoparticle observations in the low free troposphere during upward orographic flows at Izaña Mountain Observatory, *Atmos. Chem. Phys.*, 9(17), 6319–6335, doi:10.5194/acp-9-6319-2009, 2009.
- Rodríguez, S., Alastuey, A., Alonso-Pérez, S., Querol, X., Cuevas, E., Abreu-Afonso, J., Viana, M., Pérez, N., Pandolfi, M. and De La Rosa, J.: Transport of desert dust mixed with North African industrial pollutants in the subtropical Saharan Air Layer, *Atmos. Chem. Phys.*, 11(13), 6663–6685, doi:10.5194/acp-11-6663-2011, 2011.
- Rodríguez, S., Cuevas, E., Prospero, J. M., Alastuey, A., Querol, X., López-Solano, J., García, M. I. and Alonso-Pérez, S.: Modulation of Saharan dust export by the North African dipole, *Atmos. Chem. Phys.*, 15(13), 7471–7486, doi:10.5194/acp-15-7471-2015, 2015.
- Rogge, W. F., Hildemann, L. M., Mazurek, M. a., Cass, G. R. and Simoneit, B. R. T.: Sources of fine organic aerosol. 2. Noncatalyst and catalyst-equipped automobiles and heavy-duty diesel trucks, *Environ. Sci. Technol.*, 27(4), 636–651, doi:10.1021/es00041a007, 1993.
- Salisbury, G.; Williams, J.; Gros, V.; Bartenbach, S.; Xu, X.; Fischer, H.; Kormann, R.; de Reus, M.; Zoellner, M.: Assessing the effect of a Saharan dust storm on oxygenated organic compounds at Izaña, Tenerife (July–August 2002), *J. Geophys. Res. Atmos.*, 111, , D2230, doi:10.1029/2005JD006840, 2006.
- Saxton, J. E., Lewis, A. C., Kettlewell, J. H., Ozel, M. Z., Gogus, F., Boni, Y., Korogone, S. O. U. and Serca, D.: Isoprene and monoterpene measurements in a secondary forest in northern Benin, *Atmos. Chem. Phys.*, 7(15), 4095–4106, doi:10.5194/acp-7-4095-2007, 2007.
- Schauer, J., Rogge, W., Hildemann, L., Mazurek, M., Cass, G. and Simoneit, B.: Source apportionment of airborne particulate matter using organic compounds as tracers, *Atmos. Environ.*, 41, 241–259, doi:10.1016/j.atmosenv.2007.10.069, 1996.
- Schauer, J. J., Kleeman, M. J., Cass, G. R. and Simoneit, B. R. T.: Measurement of emissions from air pollution sources. 5. C1–C32 organic compounds from gasoline-powered motor vehicles., *Environ. Sci. Technol.*, 36(6), 1169–1180, doi:10.1021/es0108077, 2002.
- Simoneit, B. R. T.: Organic matter in eolian dusts over the Atlantic Ocean, *Mar. Chem.*, 5, 443–464, 1977.
- Simoneit, B. R. T., Sheng, G., Chen, X., Fu, J., Zhang, J. and Xu, Y.: Molecular marker study of extractable organic matter in aerosols from urban areas of China, *Atmos. Environ. Part A, Gen. Top.*, 25(10), 2111–2129, doi:10.1016/0960-1686(91)90088-O, 1991.
- Simoneit, B. R. T.: Biomass burning - A review of organic tracers for smoke from incomplete combustion, *Appl. Geochemistry*, 17(3), 129–162, doi:10.1016/S0883-2927(01)00061-0, 2002.
- Simoneit, B. R. T., Elias, V. O., Kobayashi, M., Kawamura, K., Rushdi, A. I., Medeiros, P. M., Rogge, W. F. and Didyk, B. M.: Sugars: dominant water-soluble organic compounds in soils and characterization as tracers in atmospheric particulate matter., *Environ. Sci. Technol.*, 38(22), 5939–5949, doi:10.1021/es0403099, 2004a.
- Simoneit, B. R. T., Kobayashi, M., Mochida, M., Kawamura, K. and Huebert, B. J.: Aerosol particles collected on aircraft flights over the northwestern Pacific region during the ACE-Asia campaign: Composition and major sources of the organic compounds, *J. Geophys. Res. D Atmos.*, 109(19), D19S09, doi:10.1029/2004JD004565, 2004b.
- Sindelarova, K., Granier, C., Bouarar, I., Guenther, A., Tilmes, S., Stavrou, T., Müller, J.-F., Kuhn, U., Stefani, P., and Knorr, W.: Global data set of biogenic VOC emissions calculated by the MEGAN model over the last 30 years, *Atmos. Chem. Phys.*, 14, 9317–9341, doi:10.5194/acp-14-9317-2014, 2014.
- Smolander, S., He, Q., Mogensen, D., Zhou, L., Bäck, J., Ruuskanen, T., Noe, S., Guenther, A., Aaltonen, H., Kulmala, M. and Boy, M.: Comparing three vegetation monoterpene emission models to measured gas concentrations with a model of meteorology, air chemistry and chemical transport, *Biogeosciences*, 11(19), 5425–5443, doi:10.5194/bg-11-5425-2014, 2014.

Atmos. Chem. Phys. Discuss., doi:10.5194/acp-2017-108, 2017

Manuscript under review for journal Atmos. Chem. Phys.

Discussion started: 27 February 2017

© Author(s) 2017. CC-BY 3.0 License.



- Stein, A. F., Draxler, R. R., Rolph, G. D., Stunder, B. J. B., Cohen, M. D. and Ngan, F.: NOAA's HYSPLIT Atmospheric Transport and Dispersion Modeling System, *Bull. Am. Meteorol. Soc.*, 96(12), 2059–2077, doi:10.1175/BAMS-D-14-00110.1, 2015.
- Sun, J., and Ariya, P. A.: Atmospheric organic and bio-aerosols as cloud condensation nuclei (CCN): A review, *Atmos. Environ.*, 40, 795–820, doi:10.1016/j.atmosenv.2005.05.052, 2006.
- Surratt, J. D., Murphy, S. M., Kroll, J. H., Ng, N. L., Hildebrandt, L., Sorooshian, A., Szmigielski, R., Vermeylen, R., Maenhaut, W., Claeys, M., Flagan, R. C., and Seinfeld, J. H.: Chemical Composition of Secondary Organic Aerosol Formed from the Photooxidation of Isoprene, *J. Phys. Chem. A*, 110, 9665–9690, doi:10.1021/jp061734m, 2006.
- Surratt, J. D., Lewandowski, M., Offenberg, J. H., Jaoui, M., Kleindienst, T. E., Edney, E. O. and Seinfeld, J. H.: Effect of acidity on secondary organic aerosol formation from isoprene, *Environ. Sci. Technol.*, 41(15), 5363–5369, doi:10.1021/es0704176, 2007.
- Szmigielski, R., Surratt, J. D., Gómez-González, Y., Van der Veken, P., Kourtchev, I., Vermeylen, R., Blockhuys, F., Jaoui, M., Kleindienst, T. E., Lewandowski, M., Offenberg, J. H., Edney, E. O., Seinfeld, J. H., Maenhaut, W., and Claeys, M.: 3-Methyl-1,2,3-butanetricarboxylic acid: an atmospheric tracer for terpene secondary organic aerosol, *Geophys. Res. Lett.*, 34, L24811, doi:10.1029/2007GL031338, 2007.
- Tauler, R.: Multivariate curve resolution applied to second order data, *Chemometr. Intell. Lab.*, 30, 133–146, 1995a.
- Tauler, R., Smilde, A., and Kowalski, B.: Selectivity, local rank, 3-way data-analysis and ambiguity in multivariate curve resolution, *J. Chemometr.*, 9, 31–58, 1995b.
- Tsamalis, C., Chédin, A., Pelon, J., and Capelle, V.: The seasonal vertical distribution of the Saharan Air Layer and its modulation by the wind, *Atmos. Chem. Phys.*, 13, 11235–11257, doi:10.5194/acp-13-11235-2013, 2013.
- Van Drooge, B. L., Fernández, P., Grimalt, J. O., Stuchlík, E., Torres García, C. J. and Cuevas, E.: Atmospheric polycyclic aromatic hydrocarbons in remote European and Atlantic sites located above the boundary mixing layer., *Environ. Sci. Pollut. Res. Int.*, 17(6), 1207–16, doi:10.1007/s11356-010-0296-0, 2010.
- Van Drooge, B.L., Grimalt, J.O.: Particle size-resolved source apportionment of primary and secondary organic tracer compounds at urban and rural locations in Spain, *Atmos. Chem. Phys.*, 15, 7735–7752, 2015.
- Volkamer, R., Jimenez, J. L., San Martini, F., Dzepina, K., Zhang, Q., Salcedo, D., Molina, L. T., Worsnop, D. R., and Molina, M. J.: Secondary organic aerosol formation from anthropogenic air pollution: rapid and higher than expected, *Geophys. es. Lett.*, 33, L17811, doi:10.1029/2006GL026899, 2006.
- Von Schneidmesser, E., Schauer, J. J., Hagler, G. S. W. and Bergin, M. H.: Concentrations and sources of carbonaceous aerosol in the atmosphere of Summit, Greenland, *Atmos. Environ.*, 43(27), 4155–4162, doi:10.1016/j.atmosenv.2009.05.043, 2009.
- Wang, G. H., Kawamura, K., Umemoto, N., Xie, M. J., Hu, S. Y., and Wang, Z. F.: Water-soluble organic compounds in PM<sub>2.5</sub> and size-segregated aerosols over Mount Tai in North China Plain, *J. Geophys. Res.-Atmos.*, 114, D19208, doi:10.1029/2008JD011390, 2009.
- Winker, D. M., Tackett, J. L., Getzewich, B. J., Liu, Z., Vaughan, M. A., and Rogers, R. R.: The global 3-D distribution of tropospheric aerosols as characterized by CALIOP, *Atmos. Chem. Phys.*, 13, 3345–3361, doi:10.5194/acp-13-3345-2013, 2013.
- Xu, J. Z., Zhang, Q., Wang, Z. B., Yu, G. M., Ge, X. L. and Qin, X.: Chemical composition and size distribution of summertime PM<sub>2.5</sub> at a high altitude remote location in the northeast of the Qinghai-Xizang (Tibet) Plateau: Insights into aerosol sources and processing in free troposphere, *Atmos. Chem. Phys.*, 15(9), 5069–5081, doi:10.5194/acp-15-5069-2015, 2015.
- Yan, F., Winijkul, E., Streets, D. G., Lu, Z., Bond, T. C., and Zhang, Y.: Global emission projections for the transportation sector using dynamic technology modeling, *Atmos. Chem. Phys.*, 14, 5709–5733, doi:10.5194/acp-14-5709-2014, 2014.
- Yttri, K. E., Dye, C. and Kiss, G.: Ambient aerosol concentrations of sugars and sugar-alcohols at four different sites in Norway, *Atmos. Chem. Phys. Discuss.*, 7(2), 5769–5803, doi:10.5194/acpd-7-5769-2007, 2007.

Atmos. Chem. Phys. Discuss., doi:10.5194/acp-2017-108, 2017  
 Manuscript under review for journal Atmos. Chem. Phys.  
 Discussion started: 27 February 2017  
 © Author(s) 2017. CC-BY 3.0 License.



**Table 1.** Average concentration of the chemical major compounds for (i) FT-PM<sub>T</sub> and BL-PM<sub>2.5</sub> having into account all samples, (ii) FT-PM<sub>T</sub> and BL-PM<sub>2.5</sub> collected within the Saharan air layer (SAL), (iii) FT-PM<sub>T</sub> and BL-PM<sub>2.5</sub> collected within the Westerlies (WES) without the FT-PM<sub>T</sub> biomass burning event and (iv) FT-PM<sub>T</sub> biomass burning event (BBE).

5

	FT-PM <sub>T</sub> ALL	BL-PM <sub>2.5</sub> ALL	FT-PM <sub>T</sub> SAL	FT-PM <sub>T</sub> WES	BL-PM <sub>2.5</sub> SAL	BL-PM <sub>2.5</sub> WES	FT-PM <sub>T</sub> BBE
∑ CC, μg·m <sup>-3</sup>	78.98	13.70	92.74	2.16	17.07	4.70	6.84
Dust, μg·m <sup>-3</sup>	73.61	11.18	86.71	1.51	14.10	3.39	1.66
Sea Salt, μg·m <sup>-3</sup>	0.53	0.36	0.59	0.27	0.25	0.66	< 0.01
OM, μg·m <sup>-3</sup>	1.32	0.47	1.39	0.04	0.61	0.09	3.64
EC, μg·m <sup>-3</sup>	0.04	0.07	0.03	< 0.01	0.08	0.05	0.29
NO <sub>3</sub> <sup>-</sup> , μg·m <sup>-3</sup>	0.73	0.08	0.87	< 0.01	0.11	< 0.01	< 0.01
NH <sub>4</sub> <sup>+</sup> , μg·m <sup>-3</sup>	0.33	0.25	0.35	0.14	0.32	0.07	0.54
nss-SO <sub>4</sub> <sup>-</sup> , μg·m <sup>-3</sup>	2.42	1.28	2.80	0.19	1.61	0.43	0.71
ss-SO <sub>4</sub> <sup>-</sup> , μg·m <sup>-3</sup>	0.02	0.01	0.02	0.01	0.01	0.03	< 0.01

∑CC: sum chemical composition; OM: organic matter; EC: elemental carbon; nss-SO<sub>4</sub><sup>-</sup>: non sea salt sulphate; ss-SO<sub>4</sub><sup>-</sup>: sea salt sulphate.

10



**Table 2.** Average concentration of the selected organic species for (i) FT-PM<sub>T</sub> and BL-PM<sub>2.5</sub> having into account all samples, (ii) FT-PM<sub>T</sub> and BL-PM<sub>2.5</sub> collected within the Saharan air layer (SAL), (iii) FT-PM<sub>T</sub> and BL-PM<sub>2.5</sub> collected within the Westerlies (WES) without the FT-PM<sub>T</sub> biomass burning event and (iv) FT-PM<sub>T</sub> biomass burning event (BBE).

	FT-PM <sub>T</sub> ALL	BL-PM <sub>2.5</sub> ALL	FT-PM <sub>T</sub> SAL	FT-PM <sub>T</sub> WES	BL-PM <sub>2.5</sub> SAL	BL-PM <sub>2.5</sub> WES	FT-PM <sub>T</sub> BBE
<b>Levogluconan</b>							
Levogluconan, ng·m <sup>-3</sup>	0.75	0.53	0.41	0.40	0.34	1.04	9.33
<b>Dicarboxylic acids</b>							
Succinic, ng·m <sup>-3</sup>	6.51	3.70	5.70	3.52	4.03	2.80	33.35
Glutaric, ng·m <sup>-3</sup>	1.97	0.83	1.90	0.74	0.85	0.77	7.23
Adipic, ng·m <sup>-3</sup>	1.43	0.69	1.53	0.62	0.72	0.60	1.71
Pimelic, ng·m <sup>-3</sup>	0.83	0.35	0.92	0.37	0.33	0.39	0.17
Suberic, ng·m <sup>-3</sup>	0.48	0.30	0.50	0.29	0.29	0.31	0.39
Azelic, ng·m <sup>-3</sup>	0.88	0.79	0.93	0.57	0.78	0.82	0.71
Malic, ng·m <sup>-3</sup>	2.01	2.15	0.75	1.20	1.67	3.43	32.21
Phthalic, ng·m <sup>-3</sup>	3.18	2.77	2.19	9.43	2.38	3.80	6.21
<b>Saccharides</b>							
α-glucose, ng·m <sup>-3</sup>	9.26	0.90	10.79	0.62	0.90	0.89	1.65
β-glucose, ng·m <sup>-3</sup>	9.13	1.00	10.63	0.61	1.01	0.98	1.65
Fructose, ng·m <sup>-3</sup>	2.02	1.01	2.23	0.95	1.10	0.76	0.69
Sucrose, ng·m <sup>-3</sup>	2.72	0.47	3.18	0.27	0.18	1.26	0.01
Mannitol, ng·m <sup>-3</sup>	0.35	0.12	0.40	0.08	0.12	0.12	0.07
<b>n-Alkanes</b>							
nC24, ng·m <sup>-3</sup>	0.72	1.63	0.75	0.48	1.87	0.97	1.01
nC25, ng·m <sup>-3</sup>	0.93	2.93	0.95	0.40	3.26	2.05	2.09
nC26, ng·m <sup>-3</sup>	0.60	0.64	0.65	0.26	0.69	0.49	0.54
nC27, ng·m <sup>-3</sup>	0.89	0.95	0.98	0.24	0.94	0.98	0.76
nC28, ng·m <sup>-3</sup>	0.37	0.32	0.39	0.17	0.38	0.17	0.36
nC29, ng·m <sup>-3</sup>	1.18	0.42	1.34	0.25	0.48	0.25	0.63
nC30, ng·m <sup>-3</sup>	0.45	0.14	0.51	0.07	0.16	0.10	0.18
nC31, ng·m <sup>-3</sup>	1.55	0.31	1.77	0.37	0.33	0.25	0.29
nC32, ng·m <sup>-3</sup>	0.39	0.10	0.45	0.05	0.11	0.06	0.08
nC33, ng·m <sup>-3</sup>	0.48	0.10	0.55	0.06	0.12	0.06	0.13
nC34, ng·m <sup>-3</sup>	0.29	0.05	0.34	0.02	0.05	0.04	0.01
<b>Hopanes</b>							
Hopane, ng·m <sup>-3</sup>	0.06	0.02	0.07	0.01	0.03	0.01	0.03
nor-Hopane, ng·m <sup>-3</sup>	0.07	0.05	0.08	0.02	0.07	0.02	0.03
<b>PAHs</b>							
B [a] A, pg·m <sup>-3</sup>	1.48	1.48	1.58	0.80	1.61	1.13	1.37
Chr, pg·m <sup>-3</sup>	4.27	4.37	4.63	1.92	5.12	2.39	3.38
B [b+j+k] F, pg·m <sup>-3</sup>	3.67	5.74	4.20	0.66	6.69	3.21	1.13
B [e] P, pg·m <sup>-3</sup>	1.36	1.94	1.50	0.47	2.22	1.20	0.83
B [a] P, pg·m <sup>-3</sup>	0.78	1.21	0.89	0.18	1.25	1.08	0.29
In[123cd] P, pg·m <sup>-3</sup>	1.47	2.33	1.65	0.46	2.18	2.74	0.56
B [ghi] Per, pg·m <sup>-3</sup>	3.29	6.94	3.56	1.73	6.37	8.46	1.84
<b>SOA PIN</b>							
Cis-Pinonic, ng·m <sup>-3</sup>	27.83	15.24	32.72	0.89	13.23	20.59	1.00
3-HGA, ng·m <sup>-3</sup>	0.21	0.51	0.09	0.24	0.39	0.81	2.88
MBTCA, ng·m <sup>-3</sup>	0.03	0.24	0.01	0.05	0.13	0.54	0.27
<b>SOA ISO</b>							
2MGA, ng·m <sup>-3</sup>	4.22	2.38	4.46	1.63	2.65	1.65	6.56
2MT-1, ng·m <sup>-3</sup>	6.64	4.94	7.27	3.40	5.16	4.33	2.40
2MT-2, ng·m <sup>-3</sup>	15.45	9.53	16.79	8.95	9.24	10.31	5.53

**B[a]A:** benz[a]anthracene; **Chr:** chrysene; **B[b+j+k]F:** benzo[b+k]fluoranthene; **B[e]P:** benzo[e]pyrene; **B[a]P:** benzo[a]pyrene; **In[123cd]P:** indeno[1,2,3-cd]pyrene; **B[ghi]Per:** benzo[ghi]perylene; **3-HGA:** 3-hydroxyglutaric acid; **MBTCA:** 3-methyl-1,2,3-butanetricarboxylic acid; **2MGA:** 2-methylglyceric acid; **2MT-1:** 2-methylthreitol; **2MT-2:** 2-methylerythritol.

5

10

Atmos. Chem. Phys. Discuss., doi:10.5194/acp-2017-108, 2017  
 Manuscript under review for journal Atmos. Chem. Phys.  
 Discussion started: 27 February 2017  
 © Author(s) 2017. CC-BY 3.0 License.



**Table 3.** Pearson correlation coefficients matrix of the organic and inorganic compounds within the free troposphere ( $PM_{10}$ ). Highly statistically significant correlations ( $p$ -value  $< 0.01$ ) are highlighted. BBE was excluded in this analysis.

	Levogluco- saccharan	Dicarboxylic acids	Saccharides	n-Alkanes	Hopanes	PAHs	SOA PIN	SOA ISO	Dust	Sea Salt	OM	EC	$NO_3^-$	$NH_4^+$	$nss-SO_4^{2-}$	$ss-SO_4^{2-}$	
Levogluco- saccharan	1.0																
Dicarboxylic acids	0.0	1.0															
Saccharides	0.0	0.4	1.0														
n-Alkanes	0.1	0.5	<b>0.5</b>	1.0													
Hopanes	0.0	<b>0.6</b>	<b>0.7</b>	<b>0.8</b>	1.0												
PAHs	0.3	0.3	0.2	0.3	0.3	1.0											
SOA PIN	-0.1	0.2	0.3	<b>0.6</b>	0.5	0.1	1.0										
SOA ISO	0.2	0.3	0.2	0.3	0.3	<b>0.6</b>	0.4	1.0									
Dust	0.0	<b>0.7</b>	<b>0.6</b>	<b>0.7</b>	<b>0.9</b>	0.2	<b>0.7</b>	0.2	1.0								
Sea Salt	<b>0.6</b>	-0.1	-0.2	-0.1	-0.3	0.4	0.1	0.2	-0.2	1.0							
OM	-0.1	0.3	0.3	<b>0.7</b>	<b>0.8</b>	0.2	<b>0.8</b>	0.4	<b>0.9</b>	0.0	1.0						
EC	0.2	0.1	-0.1	-0.1	-0.2	<b>0.7</b>	-0.2	0.3	-0.3	0.3	-0.2	1.0					
$NO_3^-$	0.0	0.4	<b>0.7</b>	<b>0.8</b>	<b>0.8</b>	0.5	<b>0.6</b>	0.4	<b>0.8</b>	-0.1	<b>0.8</b>	0.0	1.0				
$NH_4^+$	0.1	0.1	0.2	0.2	0.3	<b>0.6</b>	-0.1	0.3	0.2	0.0	0.2	0.5	0.5	1.0			
$nss-SO_4^{2-}$	0.1	0.2	<b>0.6</b>	0.5	<b>0.6</b>	0.5	0.5	<b>0.6</b>	0.5	0.1	<b>0.6</b>	0.1	<b>0.8</b>	<b>0.7</b>	1.0		
$ss-SO_4^{2-}$	<b>0.6</b>	0.0	-0.2	0.0	-0.2	0.4	0.1	0.2	-0.2	<b>1.0</b>	0.0	0.3	0.0	0.0	0.0	1.0	

OM: organic matter; EC: elemental carbon;  $nss-SO_4^{2-}$ : non sea salt sulphate;  $ss-SO_4^{2-}$ : sea salt sulphate.

5

Atmos. Chem. Phys. Discuss., doi:10.5194/acp-2017-108, 2017  
Manuscript under review for journal Atmos. Chem. Phys.  
Discussion started: 27 February 2017  
© Author(s) 2017. CC-BY 3.0 License.

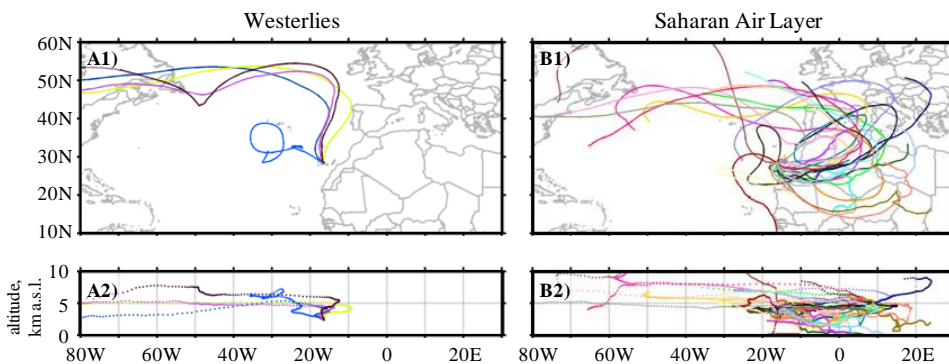


**Figure 1:** Ten-day back-trajectories based on HYSPLIT model for the samples collected within the (A) Westerlies (26Aug–30Aug) and (B) the Saharan Air Layer (01Aug–25Aug and 31Aug–01Sep); with “ddmm” referred to ending sampling day.

Atmos. Chem. Phys. Discuss., doi:10.5194/acp-2017-108, 2017  
 Manuscript under review for journal Atmos. Chem. Phys.  
 Discussion started: 27 February 2017  
 © Author(s) 2017. CC-BY 3.0 License.

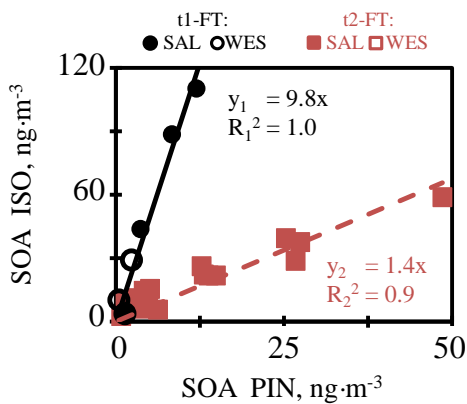


**Figure 2:** Scatter plot between total concentration of SOA ISO and total concentration of SOA PIN within the FT ( $PM_T$  collected during the night). Two tendencies can be distinguished: tendency-1 (t1; circles) and tendency-2 (t2; squares). Filled markers correspond to measurements within the SAL and open markers to measurements within the WES.

5

Atmos. Chem. Phys. Discuss., doi:10.5194/acp-2017-108, 2017  
Manuscript under review for journal Atmos. Chem. Phys.  
Discussion started: 27 February 2017  
© Author(s) 2017. CC-BY 3.0 License.

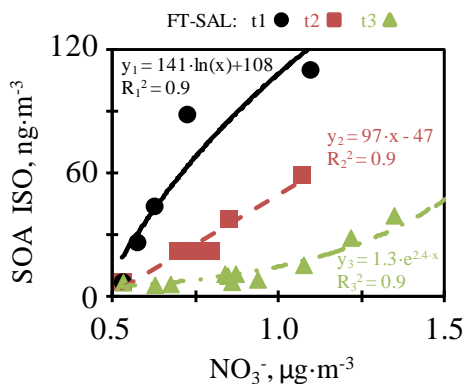


**Figure 3:** Scatter plot between SOA ISO and nitrate within the SAL under FT conditions (FT-PM<sub>T</sub> samples collected during the night).  
5 Three tendencies can be distinguished: tendency-1 (t1; circles), tendency-2 (t2; squares) and tendency-3 (t3; triangles). Westerlies were excluded when calculating the regression coefficients as values were under the detection limit.

Atmos. Chem. Phys. Discuss., doi:10.5194/acp-2017-108, 2017  
 Manuscript under review for journal Atmos. Chem. Phys.  
 Discussion started: 27 February 2017  
 © Author(s) 2017. CC-BY 3.0 License.

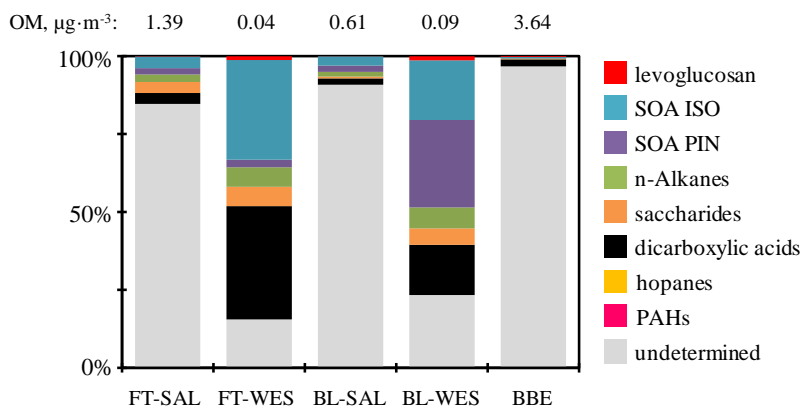


**Figure 4:** Contribution of the eight analysed organic groups to the Izaña OM composition within the FT and the BL under the SAL (FT-SAL and BL-SAL) and the WES (FT-WES, BL-WES, BBE). Average total OM for each air mass is on top. FT-PM<sub>7</sub> samples were collected during the night (22–6 GMT) and BL-PM<sub>2.5</sub> samples were collected during the day (10–16 GMT).

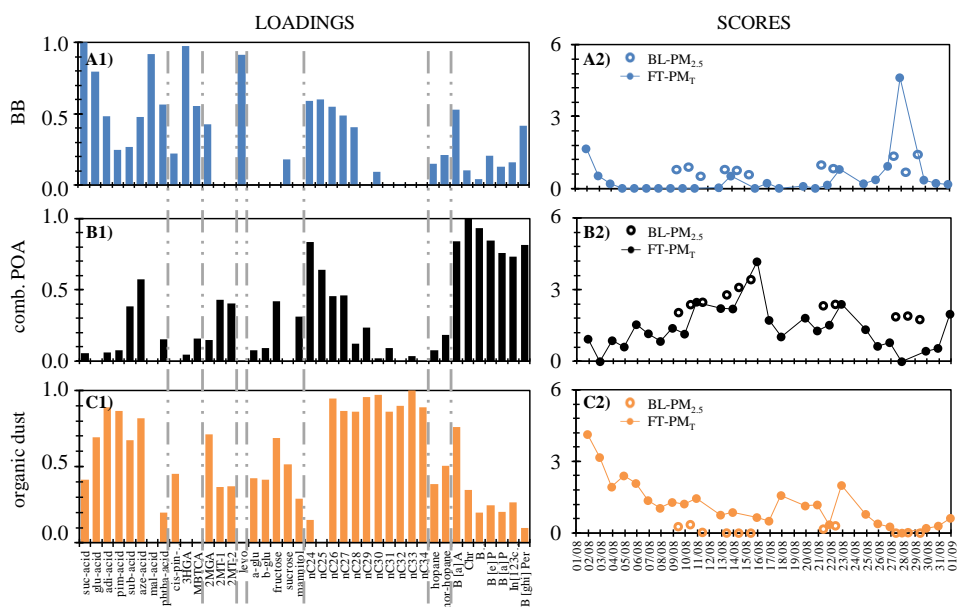


**Figure 5:** FT-PM<sub>T</sub> (night) and BL-PM<sub>2.5</sub> (day) loadings and scores of the three components from MCR-ALS resolved profiles. Filled markers correspond to FT-PM<sub>T</sub> and open markers to BL-PM<sub>2.5</sub>. Grey lines separate the compounds belonging to the different organic groups: dicarboxylic acids, SOA PIN, SOA ISO, levoglucosan, saccharides, n-alkanes, hopanes and PAHs (from left to right).

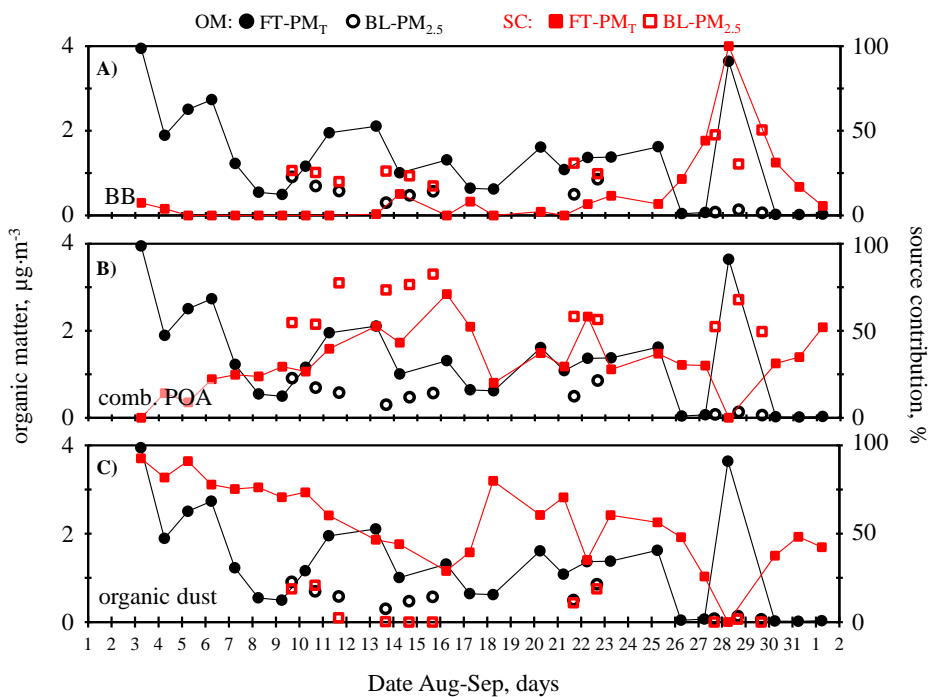


**Figure 6:** Time series of the total organic matter (OM; circle markers) and the source contribution (SC; square markers) to the determined organic matter for the FT- $\text{PM}_T$  (filled markers) and the BL- $\text{PM}_{2.5}$  samples (open markers). Sources: (A) biomass burning (BB), (B) combustion (comb.) POA and (C) organic dust.

5

Atmos. Chem. Phys. Discuss., doi:10.5194/acp-2017-108, 2017  
Manuscript under review for journal Atmos. Chem. Phys.  
Discussion started: 27 February 2017  
© Author(s) 2017. CC-BY 3.0 License.

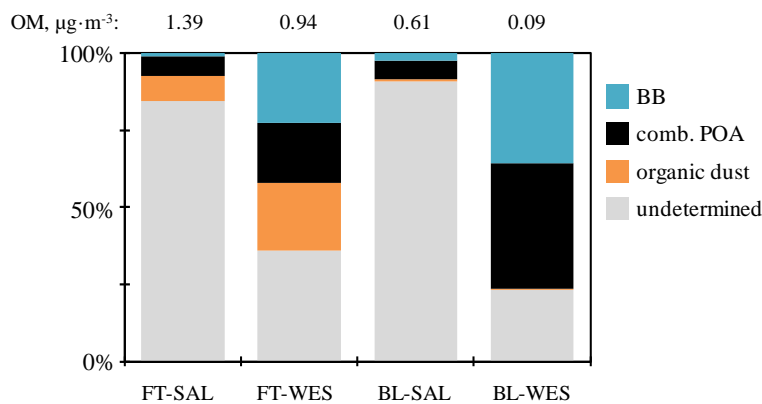


**Figure 7:** Contribution of the identified organic aerosol sources to the total organic matter within the FT and the BL under the SAL (FT-SAL and BL-SAL) and the WES (FT-WES, BL-WES, BBE). Average total OM for each air mass is on top. FT-PM<sub>T</sub> samples were collected during the night (22–6 GMT) and BL-PM<sub>2.5</sub> samples were collected during the day (10–16 GMT).



*Supplement of*

**Speciation of organic aerosols in the Saharan Air Layer  
and in the free troposphere westerlies**

**M. I. García et al.**

Correspondence to: Sergio Rodríguez ([srodriguezg@aemet.es](mailto:srodriguezg@aemet.es))

### S1. Organic compounds

Organic species were identified by their GC retention time and characteristic ions in the MS. Retention time was compared to those of the standards or with literature and NIST library and literature data (Claeys et al., 2007; Kourtchev et al., 2005; Clements and Seinfeld, 2007; Medeiros and Simoneit 2007; Fontal et al. 2015). The organic species analyzed and their characteristic ions are: succinic acid ( $m/z$  247), glutaric acid ( $m/z$  261), adipic acid ( $m/z$  275), pimelic acid ( $m/z$  289), suberic acid ( $m/z$  303), azelaic acid ( $m/z$  317), malic acid ( $m/z$  233), phthalic acid ( $m/z$  295), cis-pinonic acid ( $m/z$  171), 3-hydroxyglutaric acid (3-HGA;  $m/z$  349), 3-methyl-1,2,3-butanetricarboxylic acid (MBTCA;  $m/z$  405), 2-methylglyceric acid (2-MGA;  $m/z$  219), 2-methylthreitol (2-MT1) and 2-methylerythritol (2-MT2;  $m/z$  219); levoglucosan ( $m/z$  204),  $\alpha$ - and  $\beta$ -glucose ( $m/z$  204), man-

nitol ( $m/z$  319) and sucrose ( $m/z$  361); benzo[a]anthracene ( $m/z$  228), chrysene ( $m/z$  228), benzo[b+k]fluoranthene ( $m/z$  252), benzo[e]pyrene ( $m/z$  252), benzo[a]pyrene ( $m/z$  252), indeno[1,2,3-cd]pyrene ( $m/z$  276), benzo[ghi]perylene ( $m/z$  276); 17(H) $\alpha$ ,21(H) $\beta$ -29-Norhopane and 17(H) $\alpha$ ,21(H) $\beta$ -hopane ( $m/z$  191); n-alkanes ( $m/z$  71). The limits of quantification (LOQ) in the applied methodologies were  $0.02 \text{ ng}\cdot\text{m}^{-3}$  for the saccharides,  $0.01 \text{ ng}\cdot\text{m}^{-3}$  for the acids and  $0.002 \text{ ng}\cdot\text{m}^{-3}$  for PAHs, hopanes and n-alkanes. The concentrations were corrected by the recoveries of the above mentioned surrogates. The recoveries of the surrogate standards were higher than 60%. The field blanks concentrations of the reported compounds were between 1 and 30% of the sample concentration. Organic compounds, such as carboxylic acids are not reported due to higher blank concentrations. No corrections for the blank concentrations were applied on the sample concentrations.

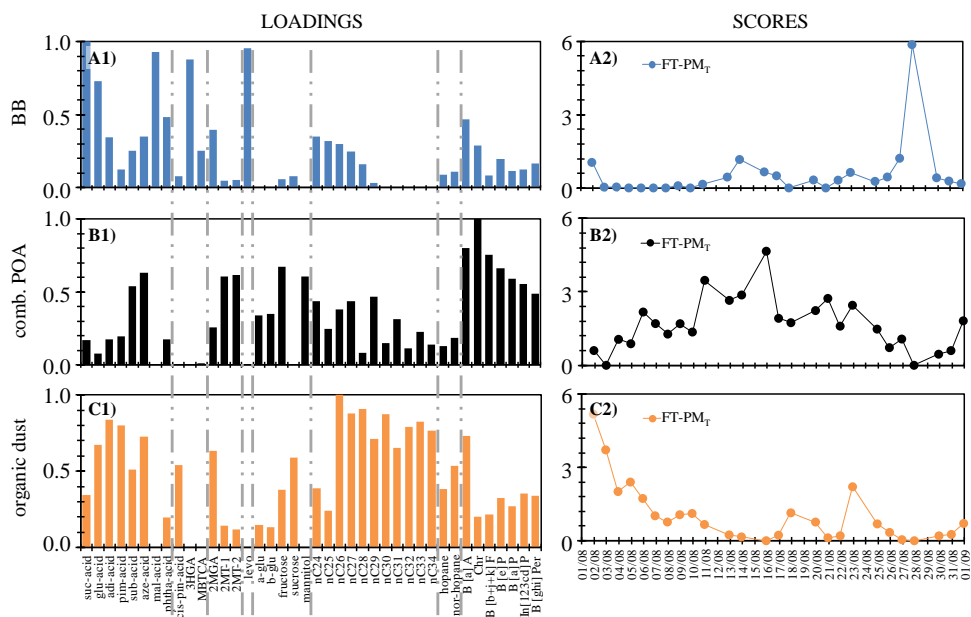


Figure S1:  $\text{PM}_T$  samples loadings and scores of the three components from MCR-ALS resolved profiles. Grey lines separate the compounds belonging to the different organic groups: dicarboxylic acids, SOA PIN, SOA ISO, levoglucosan, saccharides, n-alkanes, hopanes and PAHs (from left to right). FT-PMT samples were collected during the night (22 to 06 GMT). **BB**: biomass burning; **comb. POA**: Primary organic aerosol from combustion.

## S2. Sources of organic aerosol

Multivariate Curve Resolution (MCR-ALS) was applied to identify potential contribution sources to the OM. In order to evaluate possible changes in the sources profiles whether the method was applied to the free troposphere (FT-PMT) and boundary layer (BL-PM<sub>2.5</sub>) samples separately, we performed MCR-ALS only for the FT-PMT samples. Figure S1 shows the sources profiles, which did not vary greatly from those obtain when having both sample sets (FT-PMT and BL-PM<sub>2.5</sub>) into account. The main differences are seen in the n-alkanes and saccharides distributions, between combustion POA (Fig. S1B1) and organic dust (Fig. S1C1), as combustion POA is not affected by BL-PM<sub>2.5</sub>.

## S3. Evaluation of the MCR-ALS results

**Table S1.** Pearson correlation coefficients of the components scores and organic matter, elemental carbon and dust. Statistically significant correlations ( $p$ -value  $< 0.05$ ) are highlighted. FT-PMT samples were collected during the night (22 to 06 GMT) and BL-PM<sub>2.5</sub> samples were collected during the day (10 to 16 GMT).

	BB	Com. POA	Organic dust	$\Sigma$ SS
All				
dust	0.05	-0.27	0.84	0.53
OM	0.20	-0.28	0.64	0.44
EC	0.57	0.36	-0.38	0.51
FT-PMT				
dust	0.14	-0.13	0.84	0.63
OM	0.40	-0.12	0.55	0.63
EC	0.65	0.24	-0.38	0.49
BL-PM <sub>2.5</sub>				
dust	-0.08	-0.08	0.73	0.10
OM	-0.56	0.36	0.75	0.33
EC	-0.10	0.71	-0.50	0.67

**BB:** biomass burning; **comb. POA:** Primary organic aerosol from combustion;  **$\Sigma$ SS:** sum scores of the three components; **OM:** organic matter; **EC:** elemental carbon.

Scores obtained from the Multivariate Curve Resolution (MCR-ALS) applying non-negativity constraints, for both FT-PMT and BL-PM<sub>2.5</sub>, were correlated with dust, organic matter (OM) and elemental carbon (EC). The correlation was done for all-samples, FT-samples and BL-samples, to

verify there was a statistical relationship between the selected sources and the above mentioned variables. Overall, the correlation of the components sum with the total OM ( $r$ -All=0.44,  $p < 0.01$ ; Table 1S) and EC ( $r$ -All=0.51,  $p < 0.01$ ; Table 1S) concentrations is significant for all samples. The correlation holds for the FT (OM  $r$ -FT=0.63 and EC  $r$ -FT=0.49,  $p < 0.05$ ; Table 1S) and BL (EC  $r$ -BL=0.67,  $p < 0.05$ ; Table S1) separately, revealing that the identified sources might describe, not only the determined fraction of the OM but also the total OM.

## S4. Sources contribution

To evaluate the contribution of each source to the determined OM, a multilinear regression analysis ( $r^2=0.84$ ) was performed with the scores – obtained in the MCR-ALS – as independent variables and the sum of the organic tracer compounds as the dependent variable. Average source contribution to the determined OM was calculated for the four studied air masses. The biomass burning event is enclosed in the free troposphere under the Westerlies influence (FT-WES).

**Table S2.** Contribution of the three identified sources to the OM fraction for the studied air masses: free troposphere under the SAL (FT-SAL) and WES (FT-WES) influence and BL under the SAL (BL-SAL) and the WES (BL-WES) influence. FT-PMT samples were collected during the night (22 to 06 GMT) and BL-PM<sub>2.5</sub> samples were collected during the day (10 to 16 GMT).

	BB, %	Com. POA, %	Organic dust, %	Undetermined, %
FT-SAL	1.1	6.1	8.2	84.6
FT-WES	22.5	19.4	22.2	35.8
BL-SAL	2.3	6.1	0.8	90.8
BL-WES	35.7	40.8	0.2	23.4

**BB:** biomass burning; **comb. POA:** Primary organic aerosol from combustion.

## Supporting References

- Kourtchev, I., Ruuskanen, T., Maenhaut, W., Kulmala, M. and Claeys, M.: Observation of 2-methyltetrols and related photo-oxidation products of isoprene in boreal forest aerosols from Hyytiel, Finland, *Atmos. Chem. Phys. Discuss.*, 5(3), 29472971, doi:10.5194/acpd-5-2947-2005, 2005.
- Clements, A. L. and Seinfeld, J. H.: Detection and quantification of 2-methyltetrols in ambient aerosol in the southeastern United States, *Atmos. Environ.*, 41(9), 18251830, doi:10.1016/j.atmosenv.2006.10.056, 2007.



## CHAPTER

# 5

# Discussion

The results of this study provide new insights on the processes that contribute to the variability of the aerosols composition in the North Atlantic free troposphere. This variability is linked to (i) the spatial distribution of the continental aerosol sources, (ii) the seasonal shift of meteorological processes involved in the export and transatlantic transport of aerosols and (iii) the atmospheric processes affecting the aerosol composition.

## **Meteorology**

The tools developed in this study have allowed investigating the aerosol composition in the main two airflows of the North Atlantic free troposphere: the westerlies and the Saharan Air Layer. The westerlies flow from North America across the North Atlantic at subtropical and mid-latitudes, whereas airstreams from the Mediterranean flow to North Africa and then to the North Atlantic resulting in the Saharan Air Layer airstream. This conceptual model is extremely useful for understanding the long-term variability of the composition of the atmosphere. The role of the Saharan Air Layer as a carrier of not only desert dust, but also compounds from Europe (e.g. sulphate, Prospero et al., 1995; Gangoiti et al., 2006; Kallos et al., 1998, 2007), the Mediterranean basin (e.g. water vapour, González et al., 2016) and North Africa (e.g. sulphate, nitrate, fungi and other biogenic material, Griffin et al., 2003; Rodríguez et al., 2011; Izquierdo et al., 2011) to the Americas has been discussed in previous studies.

The present study shows novel results on how the large scale meteorology over North America influences on the aerosol composition in the North Atlantic remote free troposphere. Preceding studies showed that the export, from North America to the North Atlantic, of boundary layer air enriched in carbon monoxide and other reactive gases (such as ozone) is a regular phenomenon, prompted by the air streams – specially the warm conveyor belt (Eckhardt et al., 2004) – linked to mid-latitudes cyclones (Dickerson et al., 1995; Merrill and Moody, 1996; Moody et al., 1996) and convective processes (Dickerson et al., 1987; Talbot et al., 1998); the results of the present study are consistent with these previous investigations.

This thesis has shown that the export and transatlantic transport of aerosols is also a regular phenomenon. This study even has demonstrated how the latitudinal migration of the westerly jet from low-latitudes in winter ( $\sim 32^\circ\text{N}$  January–March) to high-latitudes in summer ( $\sim 52^\circ\text{N}$ , August–September), coupled with the spatial distribution of the aerosol sources, induces a seasonal variability in the composition of the aerosol in the westerlies, which carry maximum loads of North American dust from mid-winter to mid-spring (February–May), of non-sea-salt-sulphate, ammonium and organic matter in spring (March–May) and of elemental carbon in summer (August–September). This implies that the seasonal evolution of the aerosol composition is significantly influenced by the large-scale meteorology and that the long-term evolution of the aerosol composition in the remote downwind free troposphere will be influenced, not only by the emission rate, but also by the long-term evolution of air streams, a topic that should be subject of future studies.

The results of the present research also support the idea that upward movements linked to convection in inner continental areas and further advections, coupled with subsidence over the oceans, plays a key role on the intercontinental transport of pollutants (e.g. from North America to Europe). In North America, these processes prompt (i) the emissions and upward transport of dust from Central–Southern United States ( $30\text{--}35^\circ\text{N}$ ) to the Atlantic from ending-winter to mid-spring, (ii) the upward transport of sulphate and its precursors from North-eastern United States ( $30\text{--}40^\circ\text{N}$ ) to the Atlantic in spring, and (iii) the upward transport and advection of elemental carbon from the North Eastern edge of United States ( $\sim 45^\circ\text{N}$ ) to the Atlantic in summer. In this study, a conceptual model for understanding how the variability of the large-scale meteorology over North America influences on the export of aerosols, and their composition after transatlantic transport, has been proposed for the first time.

### Aerosol composition in the westerlies

This study has provided novel results on the composition of aerosols linked to transatlantic transport from North America in the westerlies.

The export of North American aerosols to the Atlantic was identified in a few previous studies based on rather short-term studies: (i) at Pico Observatory in the Azores, Val Martin et al. (2006) identified events of black carbon particles, CO and  $\text{NO}_x$  linked to boreal fires of Canada during August 2004, (ii) also at Pico Observatory, Dzepina et al. (2015) identified, from June to September 2012, organic aerosols and elemental carbon linked to wildfires in North-western North America, (iii) by remote sensing techniques, Ancellet et al. (2016) identified the transport of biomass burning aerosols and dust from North America across the North Atlantic in June 2013. In this study, a complementary approach is used based on long-term records. The 5 years observations of aerosol chemistry used in this study have allowed obtaining, for the first time, the climatology of aerosol composition in the North Atlantic free troposphere. The amount of aerosols that reaches Izaña after long-range transport typically ranges between 1.2 and  $4.2 \mu\text{g}\cdot\text{m}^{-3}$  (20<sup>th</sup> and 80<sup>th</sup> percentiles of bulk  $\text{PM}_{10}$ ). The bulk sub- $10 \mu\text{m}$  aerosol mass is dominated by North American dust, organic matter and non-sea-salt-sulphate, which contributes with a 53 %, 18 % and 14 % under aerosol background concentration conditions ( $\text{PM}_{10}$  within the 1<sup>st</sup>–50<sup>th</sup> percentiles =  $0.15\text{--}2.54 \mu\text{g}\cdot\text{m}^{-3}$ ) and with a 56 %, 24 % and 9 % under high aerosol concentration conditions ( $\text{PM}_{10}$  within the 1<sup>st</sup>–50<sup>th</sup> percentiles =  $4.0\text{--}9.0 \mu\text{g}\cdot\text{m}^{-3}$ ). Dzepina et al. (2015), who did not determined the dust amount in their aerosol samples, concluded that organic aerosols, sulphate and nitrate

---

dominated the aerosol mass.

The transatlantic transport of North American dust has been observed from February to May in the present study, associated with dust emissions in a region that expands from South-western Texas northward throughout the High Plains, and subsequent dust export to the Atlantic (linked to eastward moving cyclones, westerly winds and the North American outflow, which in this period migrate from 35°N in February to 40°N in May). Dust emissions in the High Plains are attributed to the change in the use of soils due to agriculture activities (Ginoux et al., 2012). It has been pointed that conversion of land from natural vegetation to agriculture or pasturage could adversely affect surface levels of mineral dust by modifying surface sediments and soil moisture; as a result, the frequency and amount of airborne dust increase (Nordstrom et al., 2004). This practise, of agricultural land-use, is expected to increase over United States in the period 2000–2050 (MNP, 2006), mainly related to changes in population, economic developments and energy crops demands (i.e. biofuels). Regulating land management can reduce the production, emission and transport of this anthropogenic dust. Another feature influenced by human activities is the land-cover (i.e. include grass, asphalt, trees, bare ground), which is indeed closely related to land-use.

Organic matter has been identified as the second most abundant aerosol component, especially from February to May, when cyclones and the associated outflow occur over regions of Eastern United States rich in organic aerosols according to previous studies (Park et al. 2003). Biogenic emissions are the principal source of organic matter in the United States, followed by three combustion sources that also emit elemental carbon (i.e. wildfires, fossil-fuel and bio-fuel) (Park et al., 2003). South-eastern United States dominates the emissions of biogenic volatile organic compounds (Lee et al., 2010 and references there in), which are mainly isoprene (81 %) and monoterpenes (19 %) (Goldstein et al., 2008). This scenario of higher biogenic emissions in South-eastern than in North-eastern United States is consistent with global distribution of the secondary organic aerosols, whose concentrations are usually higher near the tropics than at mid-latitudes (Guenther et al., 2012; Sindelarova et al., 2014). The present thesis has also resolved ~64 % of the organic aerosol transported in the westerlies in summer. The most abundant organic compounds are (i) secondary organic aerosols from isoprene oxidation (i.e. 2-methylglyceric acid, 2-methylthreitol and 2-methylerythritol) and (ii) dicarboxylic acids (mainly succinic and phthalic, indicating aged aerosols after the long-range atmospheric transport); saccharides (i.e.  $\alpha,\beta$ -glucose, fructose, sucrose and mannitol) are found but in minor presence. High concentrations of organic matter and of some organic species (e.g. levoglucosan, succinic and malic acids) have been associated with a North America fire; this sample had the highest contribution of aged organic aerosols (diacids formed during the long-range atmospheric transport) and the lowest contributions of secondary organic aerosols from oxidation of isoprene and  $\alpha$ -pinene (further oxidized under the biomass burning air). These organic aerosols, transported by the westerlies, would be affected by changes in land-cover and climate change. Changes in land-cover are expected to decrease the biogenic volatile organic compounds (e.g. isoprene and monoterpenes) (Wu et al., 2012), which are important precursors of secondary organic aerosols as described above. Climate change is already affecting forest in Canada (which represents one-quarter of global boreal forests, Mouillot and Field, 2005) by increasing the frequency and severity of fires (Flannigan et al., 2009). In addition, in Western United States the number of large fires per year increased in the period 1984–2011, mainly related to an increase in drought severity (Dennison et al., 2014). These facts may have an impact on the organic matter concentrations

in the North Atlantic.

None-sea-salt-sulphate and ammonium concentrations have been found to be high from March to May, linked to cyclones and the associated outflow over North-eastern United States, where the highest SO<sub>2</sub> and NH<sub>3</sub> emissions in North America are produced. These emissions are linked to coal burning power plants (Mann et al., 2010; Fioletov et al., 2011, 2016), livestock and fertilizers (Park et al., 2003; Mann et al., 2010; Fioletov et al., 2011, 2016), respectively. United States is the second coal producer in the World, with this energy source responsible of ~50% of its electricity production (Heinberg, 2009); most of coal resources are located in Eastern United States, with three states (Pennsylvania, Kentucky and West Virginia) producing ~52% of the higher-quality coal (Heinberg, 2009). The air quality policies implemented in the United States in 1970s to reduce emissions of air pollutants (through the federal law to control air pollution: The Clean Air Act), resulted in a decrease of SO<sub>2</sub> emissions by a 90% in the period 1980–2016 (U.S. EPA 2016); this trend has been confirmed by several studies (e.g. 2000–2010, Klimont et al., 2013; 1990–2016, Maas et al., 2016). Concretely, Hand et al. (2012) observed a drop off in the annual SO<sub>2</sub> emissions from power plants (1990–2010); this decline, in the period 2001–2010, and the decline of sulphate concentration, occurred at a similar rate pointing to a linear relationship between SO<sub>2</sub> emissions and sulphate concentrations (Hand et al., 2012). Modelling simulations performed by Xing et al. (2015) successfully reproduced the above named SO<sub>2</sub> decreasing tendency over 1990–2010. Long-term monitoring of atmospheric aerosols allows understanding the effectiveness of historical implementation of legislation on the variability of the emissions, which will be affected by the human-derived activities and the implemented legislation to control them.

Elemental carbon, according to the present study, experiences a significant transatlantic transport in summertime, when the meteorological conditions – discussed above – enhance the export from the northeast extreme of the United States. This result is consistent with those of Park et al. (2003), who estimated that the highest surface concentrations occurs in the large urban areas from Chicago to New York (40–45°N), according to emissions inventories and modelling. Major sources of elemental carbon in the United States are those associated with fossil fuel combustion (i.e. diesel exhaust emissions and coal burning, Park et al., 2003; Bond et al., 2004), wild and controlled burning of vegetation (Bond et al., 2004), and wood stoves and other biofuels to a lesser extent (Bond et al., 2004). The analysis of the transport pathways of elemental carbon based on median concentration at receptor plots, performed in the present research, could not identify the impact of fires. However, the speciation of organic aerosols in the samples collected in the westerlies has evidenced the impact of this source. Simple methods for distinguishing the contributions of fires and of fossil fuel combustions on elemental carbon need to be developed in futures studies. Many authors have observed a decreasing trend in elemental carbon emissions in the States of New Mexico (1989–1995; Junker et al., 2004), California (1963–2000; Kirchstetter et al., 2008) and New York (1835–2005; Husain et al., 2008); observations performed by Murphy et al. (2011), at national parks and other remote sites in the United States, reported a decrease over 25% of the average concentration of elemental carbon (1990–2004), with this percentage being much larger in winter than in summer. Xing et al., (2015) also confirmed by modelling simulation the decreasing tendency over the period 1990–2010. Future trends in the concentration of the elemental carbon in the North Atlantic would be linked to the emissions controls of human-derived activities and climate change affecting the frequency and severity of wildfires.

---

These overall results indicate that aerosol impacts in the North Atlantic free troposphere will be influenced not only by the air quality policies, but also for the consequences of climate change and long-term management of soils.

### **Organic aerosols in the Saharan Air Layer**

This study provides novel results on the composition and sources of organic aerosols exported to the Atlantic Ocean in the Saharan Air Layer. In summertime, organic aerosols are mixed with dust in the Saharan Air Layer, even if dust emissions occur in areas where not significant sources of organic aerosols, other than soil, are expected.

Previous studies observed that the Saharan Air Layer carries biogenic materials such as pollen (Izquierdo et al., 2011), viruses, bacteria and fungal (Griffin et al., 2001), anthropogenic bio-accumulative and toxic organic compounds (e.g. organochlorine and organophosphate pesticides, polycyclic aromatic hydrocarbons and polychlorinated biphenyl) (Risebrough et al., 1968; Prospero and Seba, 1972; Van Drooge et al., 2001, 2010; Garrison et al., 2014). These studies focused on specific groups of organic species and not in a whole characterization of the organic matter. Moreover, the presence of organic aerosols has been attributed as the source of ice nuclei at warm temperatures ( $-8^{\circ}\text{C}$ ) observed in the summer Saharan Air Layer at Izaña (Conen et al., 2015).

Studies on the organic aerosols have mostly focused in the winter dry season, when the Saharan Air Layer expands at low latitudes ( $<15^{\circ}\text{N}$ ; Tsamalis et al., 2013) to the tropical North Atlantic (Capes et al., 2008). In winter dust is mainly emitted in sub-Sahara and Sahel region ( $<20^{\circ}\text{N}$ ) and subsequently mixed with biomass burning emissions. Previous research identified that the organic aerosol species are linked to fossil fuel and biomass (Formenti et al., 2003; Hand et al., 2010; Kandler et al., 2011; Salvador et al., 2016). In addition, Simoneit et al. (1977) also observed n-alkanes, n-carboxylic acids and n-fatty alcohols associated with higher plants, Garrison et al. (2014) persistent organic contaminants probably linked to agriculture, numerous small fires, vehicle exhaust, unpaved roads, small garden plots, and industry, and Gonçalves et al. (2014) n-alkanols related to biogenic contributions of microbial or epicuticular plants.

The results of this study show that the organic aerosols mixed with dust – mostly emitted in inner subtropical Sahara ( $20\text{--}30^{\circ}\text{N}$ ) – in the summer Saharan Air Layer are associated with (i) primary compounds of surface soils (i.e. saccharides such as  $\alpha,\beta$ -glucose, fructose, sucrose and mannitol) and terrestrial higher plants (i.e. nC27, nC29 and nC31 n-alkanes), which were essentially associated with the coarse fraction, (ii) secondary organic aerosols linked to oxidation of biogenic isoprene (i.e. 2-methylglyceric acid, 2-methylthreitol and 2-methylerythritol) and  $\alpha$ -pinene (i.e. cis-pinonic acid, 3-hydroxyglutaric acid and 3-methyl-1,2,3-butanetricarboxylic acid), (iii) primary vehicles emissions (i.e.  $17\alpha(\text{H}),21\beta(\text{H})$ -29-norhopane and  $17\alpha(\text{H}),21\beta(\text{H})$ -hopane), and (iv) toxic organic compounds (i.e. polycyclic aromatic hydrocarbons), although these latter compounds appeared generally in very low concentrations ( $<5\text{ pg}\cdot\text{m}^{-3}$ ). The mixture of organics from different sources along the atmospheric transport is likely occurring, but the presence of substantial higher concentrations of saccharides and odd numbered alkanes in combination with biogenic secondary organic aerosols in the Saharan Air Layer points to a dominating biogenic contribution to organic matter. Nevertheless, the mixture of anthropogenic and biogenic source emissions may lead to synergistic aerosol processing. Of special relevance is the correlation found between ni-

trate and secondary organic aerosols linked to oxidation of biogenic isoprene, which suggests a large-scale impact, of the enhancement in the formation of secondary organic aerosols due to interaction with anthropogenic nitric oxides emissions, as a result of the synoptic scale of the Saharan Air Layer.

## Processes

Results of this study have also allowed understanding some of the microphysical processes influencing on the aerosol composition and aerosol properties in the North Atlantic free troposphere.

The climatology of the new particle formation events at Izaña shows that these events occur with a frequency of  $\sim 30\%$  of the days $\cdot$ y $^{-1}$ ; they have a seasonality with a maximum frequency from May to August. Monthly mean values of the formation and growth rates were within the ranges of 0.20–0.92 cm $^{-3}\cdot$ s $^{-1}$  and 0.26–0.58 nm $\cdot$ h $^{-1}$ , respectively. Formation rates are of the same magnitude as those found in other high-mountain sites (e.g. 0.9 cm $^{-3}\cdot$ s $^{-1}$  at Jungfraujoch–Switzerland, Manninen et al., 2010; 0.5 cm $^{-3}\cdot$ s $^{-1}$  at Mauna Loa–Hawaii, Weber et al., et al., 1999). Growth rates are significantly lower than those observed in mountain sites located in continental areas (e.g. 6.0 nm $\cdot$ h $^{-1}$  at Jungfraujoch–Switzerland, Boulon et al., 2010; Manninen et al., 2010; 6.2 nm $\cdot$ h $^{-1}$  at Puy de Dôme–France, Boulon et al., 2011) – probably because of the lower concentrations of the gas phase precursor –, but similar to those reported for remote mountains located in oceanic areas (e.g. 0.4 nm $\cdot$ h $^{-1}$  at Mauna Loa–Hawaii, Weber et al., 1995).

According to the Izaña data records analysed in this study, the year-to-year variability of the frequency of new particle formation events is correlated with mean concentrations of sulphur dioxide. This is consistent with the idea that sulphuric acid plays a key role in the formation (e.g. Coffman and Hegg, 1995; Nilsson and Kulmala, 1998) and growth of the clusters as condensing gas together with other organic species (e.g. Laaksonen et al., 2008; Kulmala et al., 2013). Moreover, this also points that sulphur dioxide may significantly influence the number of new particles in the ambient air, which has implications on climate, since about half of the cloud condensation nuclei are originated by new particle formation processes (Merikanto et al., 2009). Asmi et al. (2013) analysed a decadal record (2001–2010) of the number of particles at remote-background observatories across Europe, North America, Antarctica and Pacific Ocean islands, finding a decreasing trend in most of sites linked to a decrease in anthropogenic emissions of primary particles, SO $_2$  or some co-emitted species. The results of the present thesis support that sulphur-modulated new particle formation may have played a significant role.

An exhaustive research on the role of some biogenic organic species on new particle formation (e.g. Marti et al., 1997; Zhang et al., 2004; Laaksonen et al., 2008; Kulmala et al., 2013; Patoulias et al., 2015) and secondary organic aerosol formation (e.g. Gouw et al., 2009; Hallquist et al., 2009; Jimenez et al., 2009) has been conducted in the last decade, more especially how organic gases emitted by vegetation (e.g. isoprene, terpenes such as  $\alpha$ -pinene and sesquiterpenes) are oxidized and converted to aerosols (e.g. Carlton et al., 2009; Ehn et al., 2014). The organic speciation performed in this study has shown that concentrations of the oxidation products of biogenic volatile organic compounds (i.e. isoprene and  $\alpha$ -pinene) at Izaña are higher during daylight than at night (seen under the clean condition of the westerlies), as a result of the biogenic emissions from the boundary layer

---

carried by the diurnal upslope winds. This is consistent with previous studies at Izaña, that observed short-lived gaseous species  $\alpha$ -pinene (Fisher et al., 1998) and isoprene (Salisbury et al., 2006) during daytime linked to the emissions of the surrounding ring forest. Bianchi et al., (2016) studied new particle formation in the interface of the free troposphere and the boundary layer, concluding that these events may occur 1–2 days after the free troposphere air entered in contact with the planetary boundary layer, the time needed for the oxidation of organic compounds to form highly oxygenated molecules. The overall results support the idea that anthropogenic (i.e.  $\text{SO}_2$ ) and biogenic (e.g. isoprene and  $\alpha$ -pinene) emissions interact, resulting in new particle formation observed in rather short-time scales during upslope winds in this study.

The interaction of biogenic with anthropogenic emissions may also occur with nitrogenous compounds, more specifically the reaction of nitrogen oxides (whose emissions are dominated by vehicle exhaust and other combustion sources) and biogenic volatile organic compounds, to enhance the secondary organic aerosol formation (Surratt et al., 2006, 2007; El Haddad et al., 2011; Hoyle et al., 2011). As already cited above, the correlation observed in this study between nitrate and oxidation products of isoprene, in the Saharan Air Layer, suggests a large-scale impact of this process. The interaction between nitric oxides and biogenic volatile organic compounds may potentially occur over the Mediterranean and North Africa resulting in secondary organic aerosols that are spread over the North Atlantic to the Americas.

This study also has found an interaction between dust and the freshly formed new particles in the Saharan Air Layer. More specifically, the negative correlation observed between the formation rates of new particles and low-polluted dust suggest that this latter aerosol type acts as a coagulation sink of new particles. Opposite results have been found in highly-polluted dust plumes, where new particle formation and growth was promoted as a consequence of dust-induced heterogeneous photochemical processes (e.g. the photodecomposition of coated nitrate releasing  $\text{NO}_3$  radical to oxidize volatile organic carbons; Nie et al., 2014). These interactions may lead to the so-called ‘dust processing’, a set of processes – including acid process – that may change some of the physicochemical properties of dust which are relevant for some climate processes (Baker and Croot, 2010; Shi et al., 2012). Because new particles are rather rich in sulphuric acid–sulphate, the internal mixing of dust with these components may be prompted, resulting also in ‘dust processing’. In the present study, this interaction has been observed at Izaña Observatory; however, these processes may also occur in inner Sahara before dust export. In a study performed by the Izaña in-situ aerosols group, Rodríguez et al. (2011) found high concentrations of ammonium sulphate and nitrate mixed with dust in the Saharan Air Layer when air had previously flown over industrial areas of North Africa. In a more recent study, lead by the same group (and in which this PhD candidate has also participated), Ravelo et al. (2016) found an enhancement in the solubility of the iron present in sub-micron dust particles due to the mixing of dust with sulphate. This increase in iron-dust solubility has important implications on climate related processes, since soluble iron is considered a phytoplankton fertilizer and may consequently influence on the ocean-atmospheric  $\text{CO}_2$  exchanges (e.g. Martin and Fitzwater, 1990; De Baar et al., 2005; Schulz et al., 2012).

The influence of dust deposition on marine biogeochemistry and on atmospheric-ocean  $\text{CO}_2$  exchanges, and the modification of dust properties by atmospheric processing are nowadays hotspot topics on climate research (e.g. GESAMP, 2011; Shao et al., 2011; Schulz et al., 2012; Abdelkader et al., 2017).



CHAPTER

# 6

## Conclusions

The present thesis has lead to the following conclusions:

- **The studies of aerosols and other atmospheric constituents in the North Atlantic free troposphere should differentiate between measurements performed within the westerlies and the Saharan Air Layer.**

The composition of the westerlies is sensitive to emissions in North America, whereas the Saharan Air Layer is sensitive to emissions in North Africa, the Mediterranean and Europe. This differentiation is of special interest in future studies on long-term chemical variability of the atmosphere.

- **Aerosols emitted in the boundary layer of North America are regularly exported to the North Atlantic free troposphere, where they experience transatlantic transport in the westerlies.**

As far as known, this study has presented the first climatology of the composition of the aerosols transported by the westerlies across the North Atlantic.

- **The composition of the aerosols in the westerlies experience a marked seasonal evolution that is influenced by (i) the spatial distribution of their sources in North America, and (ii) the seasonal shift of the westerly jet and the associated eastward moving cyclones.**

The westerlies carry maximum loads of:

- (i) mineral dust from February to May, associated with the occurrence of the westerly jet at rather low latitudes ( $35^{\circ}$ – $40^{\circ}$ N), dust emissions in a region that extends from Southwest Texas to the High Plains, and subsequent dust export to the Atlantic,

- (ii) none-sea-salt-sulphate and ammonium from March to May, linked to the presence of the westerly jet and to the export of polluted air from Northeastern United States, where the highest SO<sub>2</sub> emissions in North America occur,
  - (iii) organic matter from February to May, associated with the westerly jet and export from regions of Eastern United States rich in organic aerosols,
  - (iv) elemental carbon in August and September, associated with the occurrence of the westerly jet at rather high latitudes (50°–55°N) and the consequent export from the regions (Chicago to New York) where the highest concentrations of elemental carbon occur in North America.
- **Dust is a major component of the aerosols transported from North America across the North Atlantic free troposphere.**
- Mass concentrations of sub-10 μm aerosols that reach the Izaña Observatory, after transatlantic transport, typically range between 1.2 and 4.2 μg·m<sup>-3</sup> (20<sup>th</sup> and 80<sup>th</sup> percentiles). The main contributors to background levels (1<sup>st</sup>–50<sup>th</sup> percentiles = 0.15–2.54 μg·m<sup>-3</sup>) are North American dust (53 %), non-sea-salt-SO<sub>4</sub><sup>2-</sup> (14 %) and organic matter (18 %), whereas aerosol composition during high PM<sub>10</sub> events (75<sup>th</sup>–95<sup>th</sup> percentiles = 3.9–8.9 μg·m<sup>-3</sup>) is dominated by North American dust (56 %), organic matter (24 %) and nss-SO<sub>4</sub><sup>2-</sup> (9 %).
- **The main sources of organic aerosols in the subtropical North Atlantic free troposphere in summertime are: biomass burning, fossil fuel combustion and soil dust.**
    - **About the half of the organic matter in the North Atlantic has a natural origin.**  
The comprehensive characterization of the organic aerosols obtained in this study has shown that:
      - (i) in the Saharan Air Layer, the determined 15 % of the total organic matter is formed by secondary organic aerosols from the isoprene oxidation (29 %), saccharides (27 %), dicarboxylic acids (18 %), secondary organic aerosols from the α-pinene oxidation (13 %), n-alkanes (12 %), levoglucosan (0.6 %), hopanes (0.2 %) and polycyclic aromatic hydrocarbons (0.03 %),
      - (ii) in the westerlies, the determined 64 % of the total organic matter is formed by dicarboxylic acids (50 %), secondary organic aerosols from the isoprene oxidation (28 %), saccharides (7 %), n-alkanes (7 %), levoglucosan (3 %), secondary organic aerosols from the α-pinene oxidation (3 %), hopanes (0.1 %) and polycyclic aromatic hydrocarbons (0.02 %).
    - **The main sources of organic aerosols in the Saharan Air Layer are soil dust and fossil fuel combustion.**  
These sources account for 8 % and 6 % of the bulk organic matter and for 63 %

---

and 34 % of the determined fraction of the organic matter, respectively.

- **The main sources of organic aerosols in the westerlies are biomass burning, fossil fuel combustion and soil dust.**

These sources account for 23 %, 19 % and 22 % of the bulk organic matter and 49 %, 23 % and 28 % of the determined fraction of the organic matter, respectively.

- **The enhancement in the formation of secondary organic aerosols due to interaction with anthropogenic NO<sub>x</sub> emissions exerts a large-scale impact.**

The correlation between secondary organic aerosol from the oxidation of isoprene and nitrate, within the Saharan Air Layer, might be associated with the ratio isoprene:NO<sub>x</sub> in the source; secondary organic aerosol from the oxidation of isoprene depend strongly on the conditions (NO<sub>x</sub> concentrations and aerosol acidity) during the oxidation process.

- **Levoglucosan is a stable biomass burning tracer under certain atmospheric conditions.**

- **New particle formation is a frequent source of aerosols above Tenerife.**

- New particle formation is observed during periods of upslope winds that bring gaseous precursors from the boundary layer to the interface with the low free troposphere.
- New particle formation occurs a 30 % of the days as average. There is a clearly marked new particle formation season (May–August), when monthly mean values of the formation and growth rates are within the range 0.49–0.92 cm<sup>-3</sup>·s<sup>-1</sup> and 0.48–0.58 nm·h<sup>-1</sup>, respectively.
- Sulphuric acid plays a key role as gas precursor, contributing with ~70 % to the observed growth rate. Organic species, such as oxidation products of biogenic volatile organic compounds, probably also contribute.
- Sulphur dioxide influences the long-term interannual variability in the frequency of new particle formation at Izaña.
- The presence of dust influence on new particle formation, acting as coagulation sink of freshly formed nucleation particles.



CHAPTER

# 7

## Future Prospects

The research developed in the present thesis can be continued by means of the following tasks:

1. Identification of the transport routes, sources and seasonal evolution of the trace elements transported in the westerlies.
2. Description of the size distribution of the aerosol population transported in the westerlies.
3. Segregation of natural and anthropogenic source regions of the organic aerosol transported by the westerlies.
4. Determination of the seasonal contribution of natural and anthropogenic sources to the organic matter transported in the westerlies.
5. Identification and quantification of the organic species contribution to new particle formation.
6. Quantification of the change in dust properties, relevant to climate, during transatlantic transport.



CHAPTER

# A

## Annex I

### Introduction

In parallel to the development of the final part of the present thesis, the PhD candidate started a new research focused on studying the change in the microphysical properties of dust during transatlantic transport. This section presents preliminary results of this research.

The Saharan Air Layer expands from the North African coast, as far as the Caribbean Sea, Central America, and the Gulf of Mexico. During this transatlantic transport, dust undergoes heterogeneous reactions on its surface as a consequence of the condensation of atmospheric acids (e.g. nitric acid), acidic gases (e.g. sulphur dioxide) and pollutants (e.g. ammonium sulphate). This chemical aging, or atmospheric processing, changes the dust original physicochemical properties (e.g. light scattering efficiency, Li et al., 2009; cloud scavenging efficiency, Lance et al., 2013; iron solubility, Ravelo et al., 2016; ice nuclei availability, Boose et al., 2016), having implications on how dust minerals influence on climate-related processes.

This research has been developed in collaboration with the University of Miami. To this end, additional research carried in a four-month stay performed at the Rosenstiel School of Marine and Atmospheric Science (University of Miami, U.S.A.) has focused on the Saharan dust export from North Africa across the Canary Islands and the subsequent changes in dust properties during its transatlantic transport to the Caribbean.

The **objective** is to assess to what extent are the changes in the physicochemical properties of dust affecting climate-related processes during the transatlantic transport.

## Methodology

The research is centred on the summertime season, when dust emissions and impacts throughout the North Atlantic are at a maximum strength. During July and August 2015, filter samples of aerosols were collected every day at Izaña Observatory (2367 m a.s.l., Tenerife) off North African coast, at Barbados (~ 50 m a.s.l.) in the eastern Caribbean, and at Miami (~ 25 m a.s.l.) in the eastern coast of the United States. Samples at Izaña were gathered within the high altitude Saharan Air Layer; they are representative of the fresh dust recently exported from the Sahara. In contrast, samples collected at Barbados and Miami are representative of aged dust, after about a week of transport across the Atlantic.

Filter samples (Whatman-41 cellulose filters) were analyzed to obtain bulk dust concentrations by means of the ashed-filter method (Prospero et al., 1999), soluble ions ( $\text{Ca}^{2+}$ ,  $\text{K}^+$ ,  $\text{Na}^+$  and  $\text{Li}^+$ ) by flame photometry, and elemental composition (Al and Ca) by proton-induced X-ray emission (PIXE) analysis. Briefly, one quarter of each filter was extracted with 20 ml of deionised water (10+5+5 ml) in a centrifuge (3x10 min) to remove soluble ions. The extract was kept in totally dried vials for its subsequent analysis by atomic absorption spectroscopy. The extracted filter was placed in a crucible into an oven for 8 h at 500°C. After reaching room temperature, crucibles were introduced in a desiccator for 24 h and weighed with and without sample. The ash residue (less blank) is assumed to be mineral dust. The remaining extract, with the soluble ions, was analyzed by flame photometry. A portion of each filter (~ 173 cm<sup>2</sup>) was sent to the National Institute of Nuclear Physics (INFN, Italy) for the PIXE analysis.

These data have been complemented and interpreted by using meteorological NCEP/NCAR re-analysis data (<https://www.esrl.noaa.gov>), output of the model forecast Skiron (<http://forecast.uoa.gr/dustindx.php>), and satellite observations (Aerosol Optical Depth from the Moderate Resolution Imaging Spectroradiometer, <https://modis.gsfc.nasa.gov/> and Ultra Violet Aerosol Index from the Ozone Monitor Instrument Spectrometer, <http://disc.sci.gsfc.nasa.gov/>). Some preliminary results are presented below.

## Preliminary results: El Niño 2015

In a first stage, the climatological context of dust export and transport (July–August 2015) has been identified. The interannual variability in summer dust export is connected to variability in large-scale meteorology in North Africa, more specifically to the variability in the North African Dipole Intensity (NAFDI; Rodríguez et al., 2015), i.e. the difference of geopotential height anomalies averaged over the subtropics (30–32°N) and the tropics (10–13°N) close to the Atlantic coast (at 5–8°W). Summers with high NAFDI values (e.g. > +0.8) are associated with strong Harmattan winds, northern shifts of the SAL and enhanced dust export to the subtropics resulting in high dust impacts at subtropical latitudes including Izaña. In contrast, low NAFDI (e.g. < -1.0) summers are associated with a weakness in the Harmattan and southern shifts of the SAL, resulting in low dust impacts at Izaña and at subtropical latitudes. Variations in the NAFDI are connected to variations in winds over western North Africa and monsoon rainfall (affecting the Sahel region), pointing to a connection between Saharan dust export and climate variability in the last decades (Rodríguez et al., 2015). In addition, during intense El Niño-summer, the NAFDI weakens and the northern edge of the SAL shifts southward (e.g. 1897, 1997 and 2009), resulting in low dust summer at Izaña

attributed to the weakness of Harmattan winds at the north of the ITCZ.

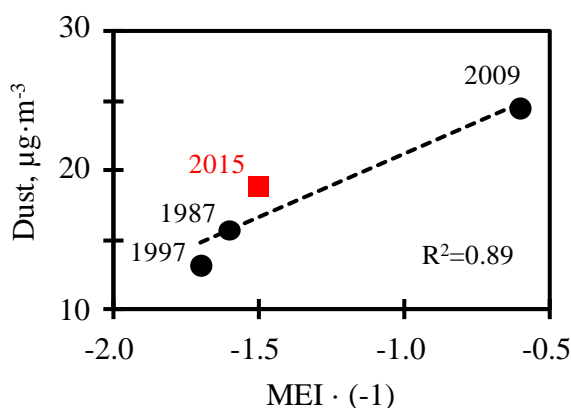


**Figure 16:** Summer mean dust at Izaña(August) vs. MEI(-1) – Multivariate ENSO Index – averaged for Jul–Aug–Sep for Intense El Niño Events (1987, 1997, 2009 and 2015).

El Niño-2015 has been considered a strong event based in the analysis of the Southern Oscillation Index time series for the period 1876–2015 (Varotsos et al., 2016). Winds in the Subtropical Saharan Stripe (SSS, where Harmattan winds result in Saharan dust emissions) typically weaken during El Niño events, resulting in low dust summer in Izaña. Despite the higher intensity of El Niño-2015 in summertime, dust at Izaña was higher than in some previous El Niño events (dust-2015 =  $18.9 \mu\text{g}\cdot\text{m}^{-3}$ ; dust-1987 =  $15.7 \mu\text{g}\cdot\text{m}^{-3}$ ; dust-1997 =  $13.2 \mu\text{g}\cdot\text{m}^{-3}$ ). This is consistent with the Multivariate El NiñoSouthern Oscillation (ENSO) Index (MEI; Fig. 16) and with winds in the SSS, which were not as low as in previous El Niño episodes (Rodríguez et al., 2015).

It worth to **highlight** that:

The preliminary results of this study are consistent with the idea (originally detected by this research group, Rodríguez et al., 2015) that ENSO has an important influence on dust export. This research will allow assessing the sensitivity of dust export from North Africa to climate variability related large-scale changes of meteorology.

### **Preliminary results: meteorology**

In order to assess the degree of comparability of dust samples collected across the North Atlantic, the export and transatlantic transport of dust was studied. Results shows that dust events may be tracked from North Africa across the North Atlantic.

Daily bulk dust concentrations at Izaña, Barbados and Miami (July–August 2015; Fig. 17) have allowed identifying that dust export frequently occurred by ‘pulse’ events prompted by intensification of winds in the SSS. Satellite observations, meteorological fields and dust modelling show that these dust export ‘pulses’ can be tracked across the North Atlantic to Barbados and Miami. These pulses are modulated by the variability of the North African Dipole Index by mechanism described by Cuevas et al. (2016). The transatlantic transport may last about a week to Barbados and more than a week to Miami. Figure 17 shows as

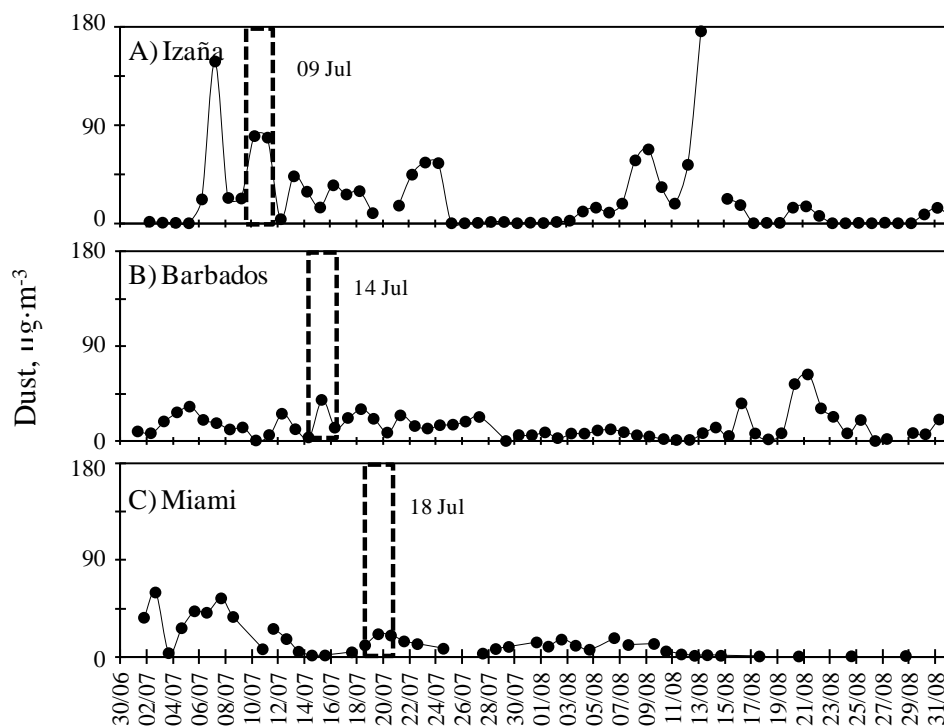


**Figure 17:** Summer 2015 (Jul–Aug) total dust concentrations at (A) Izaña, (B) Barbados and (C) Miami. ‘Dust impact’ days of the dust episode that started on 09 July at Izaña and finished on 18 July at Miami, are highlighted.

example one of these events: dust exported impacted at Izaña the 09 of July (Fig. 17A and Fig. 18 column left for satellite, modelling and meteorology), at Barbados the 14 of July (Fig. 17B and Fig. 18 column centre for satellite, modelling and meteorology) and at Miami the 18 of July (Fig. 17C and Fig. 18 column centre for satellite, modelling and meteorology).

During transatlantic transport the properties of the dust particles population may change, as previously described; coarse dust particles will deposit whereas smaller dust particles may experience aging processes (including acid processing, in cloud processing and changes in surface properties due to oxidation or exposure to sunlight), that may increase dust solubility. The identification of the dust pulses will allow, in a third stage of the research, assessing how size distribution, dust composition and dust mixing with pollutants may change during transatlantic transport.

These preliminary results allow to **highlight** that:

Dust events tend to occur as pulses that can be tracked across the North Atlantic. The methodology used here allows to track these events across the North Atlantic and to properly compare the properties of dust samples collected across the different sites.

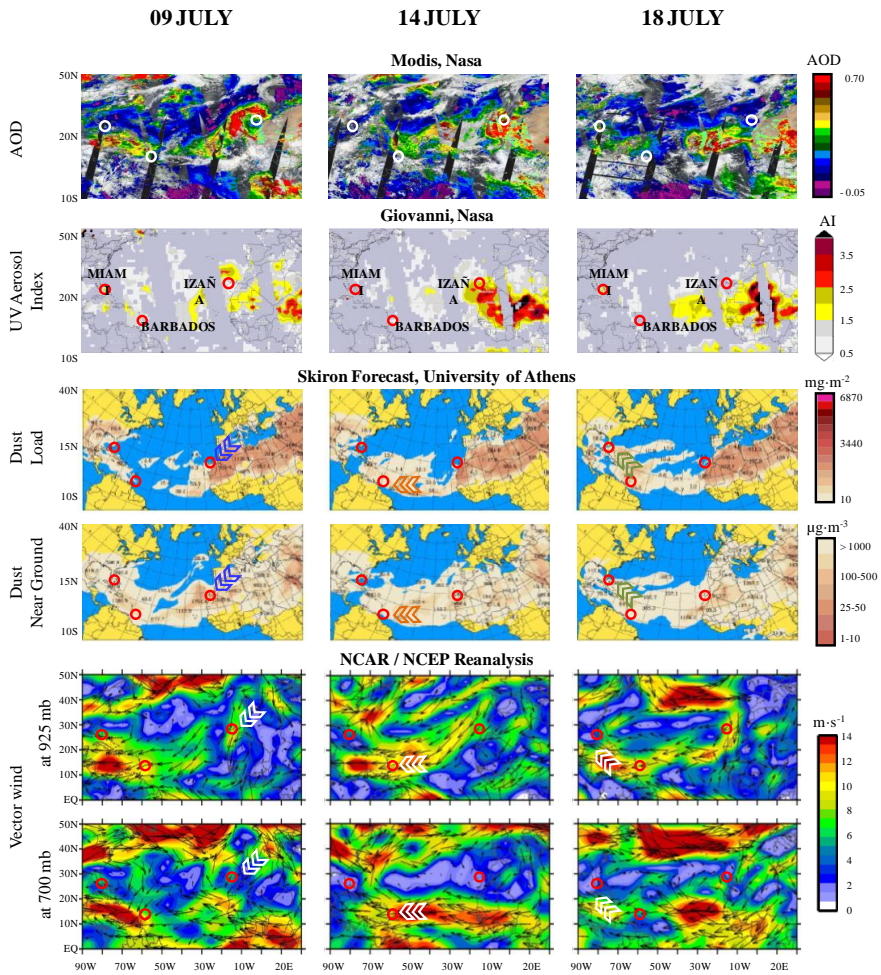


**Figure 18:** Tracking of the dust episode that started on 09 July at Izaña and finished on 18 July at Miami. Only days of ‘dust impact’ in each station are shown for the sake of brevity. **Sources:** <https://worldview.earthdata.nasa.gov/> (Modis), <http://giovanni.gsfc.nasa.gov/giovanni/> (Giovanni), <http://forecast.uoa.gr/dustindx.php> (Skiron forecast) and <http://www.cpc.ncep.noaa.gov/> (NCAR / NCEP).

### Preliminary results: Calcium solubility

Mineral components of dust includes illite, hematite, kaolinite, smectite, quartz, feldspars, calcite and gypsum, whose global distributions are presented in Scanza et al., 2015. The most abundant elements in the above named minerals are Silicon, Aluminium and Calcium (Zhang et al., 2015), with the latter one involved in dust aging as a consequence of the reaction of Ca bearing minerals (e.g. calcite) with acids (e.g. nitric or sulphuric acids), which results in the neutralization product calcium-nitrate (Laskin et al., 2005; Gibson et al., 2006; Karydis et al., 2016). Calcium might serve as a proxy for the overall dust processing during its transatlantic transport. By comparing the variation of the ratio of soluble calcium (Ca-sol) to mineral calcium (Ca-min) and dust at Izaña, Barbados and Miami, the degree to which Ca-min is transformed during transatlantic transport by atmospheric processing will be asses. These ratios have been calculated for three identified and tracked episodes during July–August 2015 (Table 2).

**Table 2:** Ratio soluble calcium to mineral calcium (Ratio-1) and soluble calcium to dust concentration (Ratio-2) at Izaña, Barbados and Miami for three identified dust pulses.

	Izaña Ratio-1	Barbados Ratio-1	Miami Ratio-1	Izaña Ratio-2	Barbados Ratio-2	Miami Ratio-2
Pulse-1	0.08	0.32	0.52	0.003	0.036	0.040
Pulse-2	0.10	0.19	0.22	0.005	0.017	0.018
Pulse-3	0.11	0.50	0.40	0.004	0.036	0.017

A first approach has evidenced how the ratios Ca-sol/Ca-min and Ca-sol/dust increases during transatlantic transport. It clearly shows that Ca present in dust becomes more soluble during the transatlantic transport. Next steps will include a deeper meteorological and chemical analysis of the samples tracked by each pulses, and probably the study of other chemical compounds which have not been analysed yet.

These preliminary results allow to **highlight** that:

Calcium tends to be more soluble during the transatlantic transport. This supports the importance of dust aging during transatlantic transport. Further steps should include other properties relevant for climate related processes.

# References

- Abdelkader, M., Metzger, S., Steil, B., Klingmüller, K., Tost, H., Pozzer, A., Stenchikov, G., Barrie, L., and Lelieveld, J.: Sensitivity of transatlantic dust transport to chemical aging and related atmospheric processes, *Atmos. Chem. Phys.*, 17, 3799–3821, doi:10.5194/acp-17-3799-2017, 2017.
- Abel, X., Jaenicke, R., Junge, C., Kanter, H. Rodríguez Garcia Prieto, P., and Seiler, W.: Luftchemische Studien am Observatorium Izana (Teneriffa). *Meteorolog. Rundschau*, 22, 158-167, 1969.
- Abouchami, W., Nätke, K., Kumar, A., Galer, S. J. G., Jochum, K. P., Williams, E., Horbe, A. M. C., Rosa, J. W. C., Balsam, W., Adams, D., Mezger, K., and Andreae, M. O.: Geochemical and isotopic characterization of the Bodélé Depression dust source and implications for transatlantic dust transport to the Amazon Basin, *Earth Planet. Sci. Lett.*, 380, 112–123, doi:10.1016/j.epsl.2013.08.028, 2013.
- Adams, A. M., Prospero, J. M. and Zhang, C.: CALIPSO-Derived three-dimensional structure of aerosol over the atlantic basin and adjacent continents, *J. Clim.*, 25 (19), 6862–6879, doi:10.1175/JCLI-D-11-00672.1, 2012.
- Alastuey, A., Querol, X., Castillo, S., Escudero, M., Avila, A., Cuevas, E., Torres, C., Romero, P. M., Exposito, F., García, O., Diaz, J. P., Van Dingenen, R. and Putaud, J. P.: Characterisation of TSP and PM<sub>2.5</sub> at Izaña and Sta. Cruz de Tenerife (Canary Islands, Spain) during a Saharan Dust Episode (July 2002), *Atmos. Environ.*, 39 (26), 4715–4728, doi:10.1016/j.atmosenv.2005.04.018, 2005.
- Alier, M., van Drooge, B. L., Dall’Osto, M., Querol, X., Grimalt, J. O. and Tauler, R.: Source apportionment of submicron organic aerosol at an urban background and a road site in Barcelona (Spain) during SAPUSS, *Atmos. Chem. Phys.*, 13 (20), 10353–10371, doi:10.5194/acp-13-10353-2013, 2013.
- Almeida-Silva, M., Almeida, S. M., Freitas, M. C., Pio, C. a, Nunes, T. and Cardoso, J.: Impact of Sahara dust transport on Cape Verde atmospheric element particles., *J. Toxicol. Environ. Health. A*, 76 (4–5), 240–51, doi:10.1080/15287394.2013.757200, 2013.
- Ancellet, G., Pelon, J., Totems, J., Chazette, P., Bazureau, A., Sicard, M., Di Iorio, T., Dulac, F., and Mallet, M.: Long-range transport and mixing of aerosol sources during the 2013 North American biomass burning episode: analysis of multiple lidar observations in the western Mediterranean basin, *Atmos. Chem. Phys.*, 16, 4725–4742, doi:10.5194/acp-16-4725-2016, 2016.
- Andronache, C., Donner, L. J., Seman, C. J. and Hemler, R. S.: A study of the impact of the Intertropical Convergence Zone on aerosols during INDOEX, *J. Geophys. Res. Atmos.*, 107 (19), 45–53, doi:10.1029/2001JD900248, 2002.

- Arimoto, R., Duce, R. A., Ray, B. J., Ellis Jr., W. G., Cullen, J. D. and Merrill, J. T.: Trace elements in the atmosphere over the North Atlantic, *J. Geophys. Res.*, 100 (D1), 1199–1213, doi:10.1029/94JD02618, 1995.
- Asmi, A., Collaud Coen, M., Ogren, J. A., Andrews, E., Sheridan, P., Jefferson, A., Weingartner, E., Baltensperger, U., Bukowiecki, N., Lihavainen, H., Kivekäs, N., Asmi, E., Aalto, P. P., Kulmala, M., Wiedensohler, A., Birmili, W., Hamed, A., O'Dowd, C., G Jennings, S., Weller, R., Flentje, H., Fjaeraa, A. M., Fiebig, M., Myhre, C. L., Hallar, A. G., Swietlicki, E., Kristensson, A., and Laj, P.: Aerosol decadal trends – Part 2: In-situ aerosol particle number concentrations at GAW and ACTRIS stations, *Atmos. Chem. Phys.*, 13, 895–916, doi:10.5194/acp-13-895-2013, 2013.
- Baker, A. R. and Croot, P. L.: Atmospheric and marine controls on aerosol iron solubility in seawater, *Mar. Chem.*, 120 (1–4), 4–13, doi:10.1016/j.marchem.2008.09.003, 2010.
- Basart, S., Pérez, C., Nickovic, S., Cuevas, E. and Baldasano, J.M.: Development and evaluation of the BSC-DREAM8b dust regional model over Northern Africa, the Mediterranean and the Middle East. *Tellus B*, 64, 1–23, doi: 10.3402/tellusb.v64i0.18539, 2012.
- Bauer, S. E., Koch, D., Unger, N., Metzger, S. M., Shindell, D. T., and Streets, D. G.: Nitrate aerosols today and in 2030: a global simulation including aerosols and tropospheric ozone, *Atmos. Chem. Phys.*, 7, 5043–5059, doi:10.5194/acp-7-5043-2007, 2007.
- Ben-Ami, Y., Koren, I., Rudich, Y., Artaxo, P., Martin, S. T., and Andreae, M. O.: Transport of North African dust from the Bodélé depression to the Amazon Basin: a case study, *Atmos. Chem. Phys.*, 10, 7533–7544, doi:10.5194/acp-10-7533-2010, 2010.
- Bianchi, F., Tröstl, J., Junninen, H., Frege, C., Henne, S., Hoyle, C. R., Molteni, U., Herrmann, E., Adamov, A., Bukowiecki, N., Chen, X., Duplissy, J., Gysel, M., Hutterli, M., Kangasluoma, J., Kontkanen, J., Kürten, A., Manninen, H. E., Münch, S., Peräkylä, O., Petäjä, T., Rondo, L., Williamson, C., Weingartner, E., Curtius, J., Worsnop, D. R., Kulmala, M., Dommen, J. and Baltensperger, U.: New particle formation in the free troposphere: A question of chemistry and timing, *Science* (80), 352 (6289), 1109–1112, doi:10.1126/science.aad5456, 2016.
- Blanchard, D. C.: The production, distribution and bacterial enrichment of the sea-salt aerosol, in: *Air-Sea Exchange of Gases and Particles*, edited by: Liss, P. S. and Slinn, W. G. N., Reidel, Boston, USA, 407–454, doi: 10.1007/978-94-009-7169-1\_7, 1983.
- Bond, T. C., Streets, D. G., Yarber, K. F., Nelson, S. M., Woo, J. H., and Klimont, Z.: A technology-based global inventory of Black and Organic Carbon emissions from Combustion, *J. Geophys. Res.*, 109, D14203, doi:10.1029/2003JD003697, 2004.
- Boose, Y., Sierau, B., García, M. I., Rodríguez, S., Alastuey, A., Linke, C., Schnaiter, M., Kupiszewski, P., Kanji, Z. A., and Lohmann, U.: Ice nucleating particles in the Saharan Air Layer, *Atmos. Chem. Phys.*, 16, 9067–9087, doi:10.5194/acp-16-9067-2016, 2016.
- Boulon, J., Sellegri, K., Venzac, H., Picard, D., Weingartner, E., Wehrle, G., Collaud Coen, M., Bütikofer, R., Flückiger, E., Baltensperger, U., and Laj, P.: New particle formation and ultrafine charged aerosol climatology at a high altitude site in the Alps (Jungfrauoch, 3580 m a.s.l., Switzerland), *Atmos. Chem. Phys.*, 10, 9333–9349, doi:10.5194/acp-10-9333-2010, 2010.
- Boulon, J., Sellegri, K., Hervo, M., Picard, D., Pichon, J. M., Fréville, P., and Laj, P.: Investigation of nucleation events vertical extent: a long term study at two different altitude sites, *Atmos. Chem. Phys.*, 11, 5625–5639, doi:10.5194/acp-11-5625-2011, 2011.
- Boy, M., Karl, T., Turnipseed, A., Mauldin, R. L., Kosciuch, E., Greenberg, J., Rathbone, J., Smith, J., Held, A., Barsanti, K., Wehner, B., Bauer, S., Wiedensohler, A., Bonn,

## REFERENCES

---

- B., Kulmala, M., and Guenther, A.: New particle formation in the Front Range of the Colorado Rocky Mountains, *Atmos. Chem. Phys.*, 8, 1577–1590, doi:10.5194/acp-8-1577-2008, 2008.
- Capes, G., Johnson, B., McFiggans, G., Williams, P. I., Haywood, J., and Coe, H.: Aging of biomass burning aerosols over West Africa: Aircraft measurements of chemical composition, microphysical properties, and emission ratios, *J. Geophys. Res.*, 113, D00C15, doi:10.1029/2008JD009845, 2008.
- Carlton, A. G., Wiedinmyer, C., and Kroll, J. H.: A review of Secondary Organic Aerosol (SOA) formation from isoprene, *Atmos. Chem. Phys.*, 9, 4987–5005, doi:10.5194/acp-9-4987-2009, 2009.
- Cavalli, F., Viana, M., Yttri, K. E., Genberg, J., and Putaud, J. P.: Toward a standardised thermal-optical protocol for measuring atmospheric organic and elemental carbon: the EUSAAR protocol, *Atmos. Meas. Tech.*, 3, 79–89, doi:10.5194/amt-3-79-2010, 2010.
- Chai, M., Birch, M. E. and Deye, G.: Organic and elemental carbon filter sets: Preparation method and interlaboratory results, *Ann. Occup. Hyg.*, 56 (8), 959–967, doi:10.1093/annhyg/mes029, 2012.
- Chiapello, I., Moulin, C., and Prospero, J. M.: Understanding the long-term variability of African dust transport across the Atlantic as recorded in both Barbados surface concentrations and large-scale Total Ozone Mapping Spectrometer (TOMS) optical thickness, *J. Geophys. Res.*, 110, D18S10, doi:10.1029/2004JD005132, 2005.
- Chin, M., Ginoux, P., Kinne, S., Torres, O., Holben, B. N., Duncan, B. N., Martin, R. V., Logan, J. a., Higurashi, A. and Nakajima, T.: Tropospheric Aerosol Optical Thickness from the GOCART Model and Comparisons with Satellite and Sun Photometer Measurements, *J. Atmos. Sci.*, 59 (3), 461–483, doi:10.1175/1520-0469(2002)059<0461:TAOTFT>2.0.CO;2, 2002.
- Chooari, O. A., Zawar-Reza, P. and Sturman, A.: The global distribution of mineral dust and its impacts on the climate system: A review, *Atmos. Res.*, 138 (1–2), 152–165, doi:10.1016/j.atmosres.2013.11.007, 2014.
- Chung, S. H. and Seinfeld, J. H.: Global distribution and climate forcing of carbonaceous aerosols, *J. Geophys. Res.*, 107 (D19), 4407, doi:10.1029/2001JD001397, 2002.
- Claeys, M., Szmigielski, R., Kourtchev, I., Van der Veken, Pi., Vermeylen, R., Maenhaut, W., Jaoui, M., Kleindienst, T., Lewandowski, M., Offenberg, J., and Edney, E.: Hydroxycarboxylic Acids: Markers for Secondary Organic Aerosol from the Photooxidation of  $\alpha$ -Pinene, *Environ. Sci. Technol.*, 41, 1628–1634, doi: 10.1021/es0620181, 2007.
- Clarisse, L., Coheur, P. F., Prata, F., Hadji-Lazaro, J., Hurtmans, D., and Clerbaux, C.: A unified approach to infrared aerosol remote sensing and type specification, *Atmos. Chem. Phys.*, 13, 2195–2221, doi:10.5194/acp-13-2195-2013, 2013.
- Clements, A. L. and Seinfeld, J. H.: Detection and quantification of 2-methyltetrols in ambient aerosol in the southeastern United States, *Atmos. Environ.*, 41 (9), 1825–1830, doi:10.1016/j.atmosenv.2006.10.056, 2007.
- Coffman, D. J. and Hegg, D. A.: A preliminary study of the effect of ammonia on particle nucleation in the MBL, *J. Geophys. Res.*, 100, 7147–7160, doi: 10.1029/94JD03253, 1995.
- Conen, F., Rodríguez, S., Hüglin, C., Henne, S., Herrmann, E., Bukowiecki, N., and Alewell, C.: Atmospheric ice nuclei at the high-altitude observatory Jungfraujoch, Switzerland, *Tellus B*, 67, 1–10, doi:10.3402/tellusb.v67.25014, 2015.
- Cooper, O.R., Moody, J. L., Parrish, D. D., Trainer, M., Holloway, J. S., Hübler, G., Fehsen-

- feld, F. C., and Stohl, A.: Trace gas composition of midlatitude cyclones over the western North Atlantic Ocean: A seasonal comparison of O<sub>3</sub> and CO, *J. Geophys. Res.*, 107, 4057, doi: 10.1029/2001JD000902, 2002a.
- Cooper, O.R., Moody, J. L., Parrish, D. D., Trainer, M., Ryerson, T. B., Holloway, J. S., Hübler, G., Fehsenfeld, F. C. and Evans, M. J.: Trace gas composition of midlatitude cyclones over the western North Atlantic Ocean: A conceptual model. *J. Geophys. Res.*, 107, D7, 4056, doi: 10.1029/2001JD000901, 2002b.
- Cuevas, E., Gómez-Peláez, Á. J., Rodríguez, S., Terradellas, E., Basart, S., García, R. D., García, O. E., and Alonso-Pérez, S.: Pivotal role of the North African Dipole Intensity (NAFDI) on alternate Saharan dust export over the North Atlantic and the Mediterranean, and relationship with the Saharan Heat Low and mid-latitude Rossby waves, *Atmos. Chem. Phys. Discuss.*, doi:10.5194/acp-2016-287, 2016.
- Dal Maso, M., Kulmala M., Riipinen, I., Wagner, R., Hussein, T., Aalto, P. P., and Lehtinen, K. E. J.: Formation and growth of freshatmospheric aerosols: eight years of aerosol size distribution data from SMEAR II, Hyytiälä, Finland, *Boreal Environ. Res.*, 10, 323–336, 2005.
- Dal Maso, M., Hyvärinen, A., Komppula, M., Tunved, P., Kerminen, V. M., Lihavainen, H., Viisanen, Y., Hansson, H. C. and Kulmala, M.: Annual and interannual variation in boreal forest aerosol particle number and volume concentration and their connection to particle formation, *Tellus, Ser. B Chem. Phys. Meteorol.*, 60 (4), 495–508, doi:10.1111/j.1600-0889.2008.00366.x, 2008.
- Darwin, C.: An account of the Fine Dust which often falls on Vessels in the Atlantic Ocean., *Q. J. Geol. Soc.*, 2 (1–2), 26–30, doi:10.1144/GSL.JGS.1846.002.01-02.09, 1846.
- Davidson, C. I., Phalen, R. F. and Solomon, P. A.: Airborne Particulate Matter and Human Health: A Review, *Aerosol Sci. Technol.*, 39 (8), 737–749, doi:10.1080/02786820500191348, 2005.
- De Baar, H. J. W., Boyd, P. W., Coale, K. H., Landry, M. R., Tsuda, A., Assmy, P., Bakker, D. C. E., Bozec, Y., Barber, R. T., Brzezinski, M. A., Buesseler, K. O., Boye, M., Croot, P. L., Gervais, F., Gorbunov, M. Y., Harrison, P. J., Hiscock, W. T., Laan, P., Lancelot, C., Law, C. S., Lévassieur, M., Marchetti, A., Millero, F. J., Nishioka, J., Nojiri, Y., van Oijen, T., Riebesell, U., Rijkenberg, M. J. A., Saito, H., Takeda, S., Timmermans, K. R., Veldhuis, M. J. W., Waite, A. M. and Wong, C. S.: Synthesis of iron fertilization experiments: From the iron age in the age of enlightenment, *J. Geophys. Res.*, 110 (C9), 1–24, doi:C09s16\rf10.1029/2004jc002601, 2005.
- Delany, a. C., Claire Delany, A., Parkin, D. W., Griffin, J. J., Goldberg, E. D. and Reimann, B. E. F.: Airborne dust collected at Barbados, *Geochim. Cosmochim. Acta*, 31 (5), 885–909, doi:10.1016/S0016-7037(67)80037-1, 1967.
- Dennison, P. E., Brewer, S. C., Arnold, J. D. and Moritz, M. A.: Large wildfire trends in the western United States, 1984–2011, *Geophys. Res. Lett.*, 41 (8), 2928–2933, doi:10.1002/2014GL059576, 2014.
- Dentener, F. J., Carmichael, G. R., Zang, Y., Lelieveld, J., and Crutzen, P. J.: Role of mineral aerosol as a reactive surface in the global troposphere, *J. Geophys. Res.*, 101, 22 869–22 889, doi: 10.1029/96JD01818, 1996.
- Dentener, F., Kinne, S., Bond, T., Boucher, O., Cofala, J., Generoso, S., Ginoux, P., Gong, S., Hoelzemann, J. J., Ito, A., Marelli, L., Penner, J. E., Putaud, J. P., Textor, C., Schulz, M., van der Werf, G. R., and Wilson, J.: Emissions of primary aerosol and precursor gases in the years 2000 and 1750 prescribed data-sets for AeroCom, *Atmos. Chem. Phys.*, 6,

## REFERENCES

---

- 4321–4344, doi:10.5194/acp-6-4321-2006, 2006.
- Dickerson, R. R., Huffman, G. J., Luke, W. T., Nunnermacker, L. J., Pickering, K. E., Leslie, A. C. D., Lindsey, C. G., Slinn, W. G. N., Kelly, T. J., Daum, P. H., Delany, A. C., Greenberg, J. P., Zimmerman, P. R., Boatman, J. F., Ray, J. D., and Stedman, D. H.: Thunderstorms: An important mechanism in the transport of air pollutants, *Science*, 235, 460–464, doi: 10.1126/science.235.4787.460, 1987.
- Dickerson, R. R., Doddridge, B., Kelley, P., and Rhoads, K.: Large scale pollution of the atmosphere over the remote Atlantic Ocean: Evidence from Bermuda, *J. Geophys. Res.*, 100, 8945–8952, doi: 10.1029/95JD00073, 1995.
- Dominguez-Rodríguez, A., Abreu-González, P., Rodríguez, S., Avanzas, P., Juárez-Prera R.A: Short-term effects of air pollution, markers of endothelial activation, and coagulation to predict major adverse cardiovascular events in patients with acute coronary syndrome: insights from AIRACOS study, *Biomarkers*, 24, 1–5, doi:10.3109/1354750X.2016.1160430, 2016.
- Draxler, R. R., and Hess, G. D.: Description of the HYSPLIT 4 modeling system, NOAA Tech. Memo. ERL ARL-224, NOAA Air Resources Laboratory, Silver Spring, M. D., 1998.
- Draxler, R. R. and Rolph, G. D.: HYSPLIT (HYbrid Single-Particle Lagrangian Integrated Trajectory) Model access via NOAA ARL READY Website (<http://www.arl.noaa.gov/ready/hysplit4.html>). NOAA Air Resources Laboratory, Silver Spring, M.D., 2003.
- Dunn, M. J., Jimenez, J. L., Baumgardner, D., Castro, T., McMurry, P. H., and Smith, J. N.: Measurements of Mexico City nanoparticle size distributions: observations of new particle formation and growth, *Geophys. Res. Lett.*, 31, L10102, doi:10.1029/2004GL019483, 2004.
- Dzepina, K., Mazzoleni, C., Fialho, P., China, S., Zhang, B., Owen, R. C., Helmig, D., Hueber, J., Kumar, S., Perlinger, J. A., Kramer, L. J., Dziobak, M. P., Ampadu, M. T., Olsen, S., Wuebbles, D. J., and Mazzoleni, L. R.: Molecular characterization of free tropospheric aerosol collected at the Pico Mountain Observatory: a case study with a long-range transported biomass burning plume, *Atmos. Chem. Phys.*, 15, 5047–5068, doi:10.5194/acp-15-5047-2015, 2015.
- Eckhardt, S., Stohl, A., Wernli, H., James, P., Forster, C. and Spichtinger, N.: A 15-year climatology of warm conveyor belts, *J. Clim.*, 17(1), 218–237, doi:10.1175/1520-0442(2004)017<0218:AYCOWC>2.0.CO;2, 2004.
- Ehn, M., Thornton, J. A., Kleist, E., Sipila, M., Junninen, H., Pullinen, I., Springer, M., Rubach, F., Tillmann, R., Lee, B., Lopez-Hilfiker, F., Andres, S., Acir, I. H., Rissanen, M., Jokinen, T., Schobesberger, S., Kangasluoma, J., Kontkanen, J., Nieminen, T., Kurten, T., Nielsen, L. B., Jorgensen, S., Kjaergaard, H. G., Canagaratna, M., Dal Maso, M., Berndt, T., Petaja, T., Wahner, A., Kerminen, V. M., Kulmala, M., Worsnop, D. R., Wildt, J. and Mentel, T. F.: A large source of low-volatility secondary organic aerosol, *Nature*, 506 (7489), 476–479, doi:10.1038/Nature13032, 2014.
- El Haddad, I., Marchand, N., Temime-Roussel, B., Wortham, H., Piot, C., Besombes, J. L., Baduel, C., Voisin, D., Armengaud, A., and Jaffrezo, J. L.: Insights into the secondary fraction of the organic aerosol in a Mediterranean urban area: Marseille, *Atmos. Chem. Phys.*, 11, 2059–2079, doi:10.5194/acp-11-2059-2011, 2011.
- Engelstaedter, S. and Washington, R.: Atmospheric controls on the annual cycle of North African dust, *J. Geophys. Res.*, 112, D17111, doi: 10.1029/2006JD007195, 2007.
- Fairall, C. W., Davidson, K. L. and Schacher, G. E.: An analysis of the surface production

- of sea-salt aerosols, *Tellus B*, 35 B (1), 31–39, doi:10.1111/j.1600-0889.1983.tb00005.x, 1983.
- Finlayson-Pitts, B. J. and Pitts, J. N.: Chemistry of the Upper and Lower Atmosphere: Theory, Experiments, and Applications, Academic press., 1999.
- Fioletov, V. E., McLinden, C. A., Krotkov, N. A., Moran, M. D. and Yang, K.: Estimation of SO<sub>2</sub> emissions using OMI retrievals, *Geophys. Res. Lett.*, 38, L21811, doi:10.1029/2011GL049402, 2011.
- Fioletov, V. E., McLinden, C. A., Krotkov, N., Li, C., Joiner, J., Theys, N., Carn, S., and Moran, M. D.: A global catalogue of large SO<sub>2</sub> sources and emissions derived from the Ozone Monitoring Instrument, *Atmos. Chem. Phys.*, 16, 11497–11519, doi:10.5194/acp-16-11497-2016, 2016.
- Fischer, H., Nikitas, C., Parchatka, U., Zenker, T., Harris, G. W., Matuska, P., Schmitt, R., Mihelcic, D., Muesgen, P., Paetz, H. W., Schultz, M. and Volz-Thomas, A.: Trace gas measurements during the Oxidizing Capacity of the Tropospheric Atmosphere campaign 1993 at Izaña, *J. Geophys. Res.*, 103 (D11), 13505, doi:10.1029/97JD01497, 1998.
- Flannigan, M. D., Krawchuk, M. A., de Groot, W. J., Wotton, M. B. and Gowman, L. M.: Implications of changing climate for global wildland fire, *Int. J. Wildl. Fire*, 18 (5), 483–507, doi:10.1071/WF08187, 2009.
- Fomba, K. W., Müller, K., van Pinxteren, D., Poulain, L., van Pinxteren, M., and Herrmann, H.: Long-term chemical characterization of tropical and marine aerosols at the Cape Verde Atmospheric Observatory (CVAO) from 2007 to 2011, *Atmos. Chem. Phys.*, 14, 8883–8904, doi:10.5194/acp-14-8883-2014, 2014.
- Fontal, M., van Drooge, B. L., Lopez, J. F., Fernández, P., and Grimalt, J. O.: Broad spectrum analysis of polar and apolar organic compounds in submicron atmospheric particles, *J. Chromatogr. A*, 1404, 28–38, doi:10.1016/j.chroma.2015.05.042, 2015.
- Formenti, P., Elbert, W., Maenhaut, W., Haywood, J. and Andreae, M. O.: Chemical composition of mineral dust aerosol during the Saharan Dust Experiment (SHADE) airborne campaign in the Cape Verde region, September 2000, *J. Geophys. Res.*, 108 (D18), 8576, doi:10.1029/2002JD002648, 2003.
- Freney, E., Karine, S., Eija, A., Clemence, R., Aurelien, C., Jean-Luc, B., Aurelie, C., Maxime, H., Nadege, M., Laeticia, B. and David, P.: Experimental evidence of the feeding of the free troposphere with aerosol particles from the mixing layer, *Aerosol Air Qual. Res.*, 16 (3), 702–716, doi:10.4209/aaqr.2015.03.0164, 2016.
- Fuchs, N. A.: On the stationary charge distribution on aerosol particles in a bipolar ionic atmosphere, *Geofis. Pura e Appl.*, 56 (1), 185–193, doi:10.1007/BF01993343, 1963.
- Fuchs, N. A. and Sutugin, A. G.: Highly dispersed aerosols, in: *Topics in current aerosol research (Part 2)*, edited by: Hidy, G. M., and Brock, J. R., Pergamon, New York, ISBN: 978-0-08-016809-8, 1971.
- Gangoiti, G., Alonso, L., Navazo, M., Antonio Garcia, J. and Millán, M. M.: North African soil dust and European pollution transport to America during the warm season: Hidden links shown by a passive tracer simulation, *J. Geophys. Res. Atmos.*, 111 (10), 1–24, doi:10.1029/2005JD005941, 2006.
- Ganzeveld, L. N., van Aardenne, J. A., Butler, T. M., Lawrence, M. G., Metzger, S. M., Stier, P., Zimmermann, P., and Lelieveld, J.: Technical Note: Anthropogenic and natural offline emissions and the online Emissions and dry DEPosition submodel EMDEP of the Modular Earth Submodel system (MESSy), *Atmos. Chem. Phys. Discuss.*, 6, 5457–5483, doi:10.5194/acpd-6-5457-2006, 2006.

## REFERENCES

---

- García, R. D.: Aplicación de modelos de transferencia radiativa para el control operativo del programa BSRN (Base-line Surface Radiation Network) del Centro de Investigación Atmosférica de Izaña, PhD Thesis, University of Valladolid at Spain, December, 2011.
- Garrido, A., Jimenez-Guerrero, P., and Ratola, N.: Levels, trends and health concerns of atmospheric PAHs in Europe, *Atmos. Environ.*, 99, 474–484, doi: doi.org/10.1016/j.atmosenv.2014.10.011, 2014.
- Garrison, V. H., Majewski, M. S., Foreman, W. T., Genualdi, S. A., Mohammed, A., and Massey Simonich, S. L.: Persistent organic contaminants in Saharan dust air masses in West Africa, Cape Verde and the eastern Caribbean, *Sci. Total Environ.*, 468–469, 530–543, doi: 10.1016/j.scitotenv.2013.08.076, 2014.
- GESAMP (IMO/FAO/UNESCO-IOC/UNIDO/WMO/IAEA/UN/UNEP Joint Group of Experts on the Scientific Aspects of Marine Environmental Protection). Workshop on Modelling and Observing the Impacts of Dust Transport/Deposition on Marine productivity, Sliema, Malta, 7–9 March 2011, Prepared by Robert A. Duce and Prof. Peter Liss, 50 pp, November 2011, 2011.
- Gibson, E., Hudson, P., and Grassian, V.: Physicochemical properties of nitrate aerosols: implications for the atmosphere, *J. Phys. Chem. A*, 110, 11785–11799, doi: 10.1021/jp063821k, 2006.
- Gieré, R. and Querol, X.: Solid particulate matter in the atmosphere, *Elements*, 6 (4), 215–222, doi:10.2113/gselements.6.4.215, 2010.
- Ginoux, P., Prospero, J. M., Torres, O., and Chin, M.: Long-term simulation of global dust distribution with the GOCART model: Correlation with North Atlantic Oscillation, *Environ. Modell. Softw.*, 19, 113–128, doi: 10.1016/S1364-8152(03)00114-2, 2004.
- Ginoux, P., Prospero, J. M., Gill, T. E., Hsu, N. C., and Zhao, M.: Global-scale attribution of anthropogenic and natural dust sources and their emission rates based on MODIS Deep Blue aerosol products, *Rev. Geophys.*, 50, RG3005, doi:10.1029/2012RG000388, 2012.
- Goff, J. A. and Gratch, S.: Thermodynamic properties of moist air, *Trans. Am. Soc. Heat. Vent. Eng.*, 51, 125–158, 1945.
- Goldstein, A. H. and Galbally, I. E.: Known and unexplored organic constituents in the earth's atmosphere, *Environ. Sci. Technol.*, 41, 1514–1521, doi: 10.1021/es072476p, 2007.
- Gómez-Moreno, F. J., Sorribas, M., Alonso, E., Artíñano, B., Juncal, V., Piñeiro, M., López, P., Pérez, N., Pey, J., Alastuey, A., García, M. I., Rodríguez, S., Titos, G., Lyamani, H., Alados-Arboledas, L., De la Morena, B. A.: Intercomparaciones de la Red Española de DMAs Ambientales (REDMAAS) en la estación de sondeos atmosféricos del INTA en el Arenosillo, pp. 9–58, Instituto Nacional de Técnica Aeroespacial (INTA), 01/09/2013, ISBN: 978-84-938932-1-7, 2013.
- Gonçalves, C., Alves, C., Nunes, T., Rocha, S., Cardoso, J., Cerqueira, M., Pio, C., Almeida, S. M., Hillamo, R. and Teinilä, K.: Organic characterisation of PM<sub>10</sub> in Cape Verde under Saharan dust influxes, *Atmos. Environ.*, 89 (D5), 425–432, doi:10.1016/j.atmosenv.2014.02.025, 2014.
- González, Y., Schneider, M., Dyroff, C., Rodríguez, S., Christner, E., García, O. E., Cuevas, E., Bustos, J. J., Ramos, R., Guirado-Fuentes, C., Barthlott, S., Wiegeler, A., and Sepúlveda, E.: Detecting moisture transport pathways to the subtropical North Atlantic free troposphere using paired H<sub>2</sub>O- $\delta$ D in situ measurements, *Atmos. Chem. Phys.*, 16, 4251–4269, doi:10.5194/acp-16-4251-2016, 2016.
- Gouw, J. D. E. and Jimenez, J. L.: Organic Aerosols in the Earth's Atmosphere, 43 (20), 7614–7618, doi: 10.1021/es9006004, 2009.

- Gravenhorst, G. : Maritime sulfate over the North Atlantic, *Atmos. Environ.*, 12 (1–3, Sulfur Atmosphere), 707–13, doi: doi.org/10.1016/0004-6981(78)90251-2, 1978.
- Griffin, D. W., Garrison, V. H., Herman, J. R. and Shinn, E. A.: African desert dust in the Caribbean atmosphere: Microbiology and public health, *Aerob. (Bologna)*, 17 (3), 203–213, doi:10.1023/A:1011868218901, 2001.
- Griffin, D. W., Kellogg, C. A., Garrison, V. H., Lisle, J. T., Borden, T. C. and Shinn, E. A.: Atmospheric microbiology in the northern Caribbean during African dust events, *Aerob. (Bologna)*, 19 (3–4), 143–157, doi:10.1023/B:AERO.0000006530.32845.8d, 2003.
- Grigas, T., Ovadnevaite, J., Ceburnis, D., Moran, E., McGovern, F. M., Jennings, S. G. and O’Dowd, C.: Sophisticated Clean Air Strategies Required to Mitigate Against Particulate Organic Pollution, *Sci. Rep.*, 7 (21), 44737, doi:10.1038/srep44737, 2017.
- Guenther, A. B., Jiang, X., Heald, C. L., Sakulyanontvittaya, T., Duhl, T., Emmons, L. K., and Wang, X.: The Model of Emissions of Gases and Aerosols from Nature version 2.1 (MEGAN2.1): an extended and updated framework for modeling biogenic emissions, *Geosci. Model Dev.*, 5, 1471–1492, doi:10.5194/gmd-5-1471-2012, 2012.
- Hallar, A. G., Lowenthal, D. H., Chirokova, G., Borys, R. D., and Wiedinmyer, C.: Persistent daily new particle formation at a mountain-top location, *Atmos. Environ.*, 45, 4111–4115, doi: 10.1016/j.atmosenv.2011.04.044, 2011.
- Hallquist, M., Wenger, J. C., Baltensperger, U., Rudich, Y., Simpson, D., Claeys, M., Dommen, J., Donahue, N. M., George, C., Goldstein, a. H., Hamilton, J. F., Herrmann, H., Hoffmann, T., Iinuma, Y., Jang, M., Jenkin, M. E., Jimenez, J. L., Kiendler-Scharr, A., Maenhaut, W., McFiggans, G., Mentel, T. F., Monod, A., Prévôt, a. S. H., Seinfeld, J. H., Surratt, J. D., Szmigielski, R. and Wildt, J.: The formation, properties and impact of secondary organic aerosol: current and emerging issues, *Atmos. Chem. Phys.*, 9 (14), 5155–5236, doi:10.5194/acp-9-5155-2009, 2009.
- Hamed, A., Joutsensaari, J., Mikkonen, S., Sogacheva, L., Dal Maso, M., Kulmala, M., Cavalli, F., Fuzzi, S., Facchini, M. C., Decesari, S., Mircea, M., Lehtinen, K. E. J., and Laaksonen, A.: Nucleation and growth of new particles in Po Valley, Italy, *Atmos. Chem. Phys.*, 7, 355–376, doi:10.5194/acp-7-355-2007, 2007.
- Hand, V. L., Capes, G., Vaughan, D. J., Formenti, P., Haywood, J. M. and Coe, H.: Evidence of internal mixing of African dust and biomass burning particles by individual particle analysis using electron beam techniques, *J. Geophys. Res. Atmos.*, 115(13), 14802–14807, doi:10.1029/2009JD012938, 2010.
- Hand, J. L., Schichtel, B. A., Malm, W. C., and Pitchford, M. L.: Particulate sulfate ion concentration and SO<sub>2</sub> emission trends in the United States from the early 1990s through 2010, *Atmos. Chem. Phys.*, 12, 10353–10365, doi:10.5194/acp-12-10353-2012, 2012.
- Heinberg, R.: *Blackout: coal, climate and the last energy crisis*, New Society Publishers, 2009.
- Heinold, B., Tegen, I., Bauer, S. and Wendisch, M.: Regional modelling of Saharan dust biomass-burning smoke: Part 2: Direct radiative forcing atmospheric dynamic response, *Tellus, Ser. B Chem. Phys. Meteorol.*, 63 (4), 800–813, doi:10.1111/j.1600-0889.2011.00574.x, 2011.
- Henze, D. K., Seinfeld, J. H., Ng, N. L., Kroll, J. H., Fu, T. M., Jacob, D. J., and Heald, C. L.: Global modeling of secondary organic aerosol formation from aromatic hydrocarbons: high- vs. low-yield pathways, *Atmos. Chem. Phys.*, 8, 2405–2420, doi:10.5194/acp-8-2405-2008, 2008.
- Hinds, W. C.: *Aerosol Technology: Properties, Behaviour and Measurement of Airborne*

## REFERENCES

---

- Particles, 2nd Edn., John Wiley, New York, 1999.
- Hoffmann, T., O'Dowd, C. D., and Seinfeld, J. H.: Iodine oxide homogeneous nucleation: an explanation for coastal new particle production, *Geophys. Res. Lett.*, 28, 1949–1952, doi: 10.1029/2000GL012399, 2001.
- Holland, H. D., *The Chemistry of the Atmosphere and Oceans*, 154, John Wiley, New York, 1978.
- Honrath, R. E., Owen, R. C., Val Martin, M., Reid, J. S., Lapina, K., Fialho, P., Dziobak, M. P., Kleissl, J., and Westphal, D. L.: Regional and hemispheric impacts of anthropogenic and biomass burning emissions on summertime CO and O<sub>3</sub> in the North Atlantic lower free troposphere, *J. Geophys. Res. Atmos.*, 109, D24310, doi:10.1029/2004JD005147, 2004.
- Hoyle, C. R., Boy, M., Donahue, N. M., Fry, J. L., Glasius, M., Guenther, A., Hallar, A. G., Huff Hartz, K., Petters, M. D., Petäjä, T., Rosenoern, T., and Sullivan, A. P.: A review of the anthropogenic influence on biogenic secondary organic aerosol, *Atmos. Chem. Phys.*, 11, 321–343, doi:10.5194/acp-11-321-2011, 2011.
- Huang, J., Zhang, C. and Prospero, J. M.: Aerosol-induced large-scale variability in precipitation over the tropical Atlantic, *J. Clim.*, 22 (19), 4970–4988, doi:10.1175/2009JCLI2531.1, 2009.
- Huang, J., Zhang, C. and Prospero, J. M.: African dust outbreaks: A satellite perspective of temporal and spatial variability over the tropical Atlantic Ocean, *J. Geophys. Res.*, 115 (D5), D05202, doi:10.1029/2009JD012516, 2010.
- Huang, J. P., Liu, J. J., Chen, B., and Nasiri, S. L.: Detection of anthropogenic dust using CALIPSO lidar measurements, *Atmos. Chem. Phys.*, 15, 11653–11665, doi:10.5194/acp-15-11653-2015, 2015.
- Huneeus, N., Schulz, M., Balkanski, Y., Griesfeller, J., Prospero, J., Kinne, S., Bauer, S., Boucher, O., Chin, M., Dentener, F., Diehl, T., Easter, R., Fillmore, D., Ghan, S., Ginoux, P., Grini, A., Horowitz, L., Koch, D., Krol, M. C., Landing, W., Liu, X., Mahowald, N., Miller, R., Morcrette, J. J., Myhre, G., Penner, J., Perlwitz, J., Stier, P., Takemura, T., and Zender, C. S.: Global dust model intercomparison in AeroCom phase I, *Atmos. Chem. Phys.*, 11, 7781–7816, doi:10.5194/acp-11-7781-2011, 2011.
- Husain, L., Khan, A. J., Ahmed, T., Swami, K., Bari, A., and Webber, J. S.: Trends in atmospheric elemental carbon concentrations from 1835 to 2005, *J. Geophys. Res.*, 113, D13102, doi:10.1029/2007JD009398, 2008.
- IPCC, 2013: *Climate change 2013: The physical science basis. Contribution of Working Group I to the Fifth Assessment Report of the Intergovernmental Panel on Climate* edited by: Stocker, T. F., Qin, D., Plattner, G. K. Tignor, M. , Allen, S. K. , Boschung, J. , Nauels, A. , Xia, Y. , Bex V. , and Midgley P.M. Cambridge University Press, Cambridge, UK and New York, NY, USA, 1535 pp, 2013.
- Izquierdo, R., Belmonte, J., Avila, A., Alarcón, M., Cuevas, E. and Alonso-Pérez, S.: Source areas and long-range transport of pollen from continental land to Tenerife (Canary Islands), *Int. J. Biometeorol.*, 55 (1), 67–85, doi:10.1007/s00484-010-0309-1, 2011.
- Jacobson, M. Z.: Isolating nitrated and aromatic aerosols and nitrated aromatic gases as sources of ultraviolet light absorption, *J. Geophys. Res.*, 104 (D3), 3527, doi:10.1029/1998JD100054, 1999.
- Jaeglé, L., Quinn, P. K., Bates, T. S., Alexander, B., and Lin, J. T.: Global distribution of sea salt aerosols: new constraints from in situ and remote sensing observations, *Atmos. Chem. Phys.*, 11, 3137–3157, doi:10.5194/acp-11-3137-2011, 2011.

- Jaenicke, R.: Abundance of cellular material and proteins in the atmosphere., *Science*, 308 (5718), 73, doi:10.1126/science.1106335, 2005.
- Järvinen, E., Virkkula, A., Nieminen, T., Aalto, P. P., Asmi, E., Lanconelli, C., Busetto, M., Lupi, A., Schioppa, R., Vitale, V., Mazzola, M., Petäjä, T., Kerminen, V. M., and Kulmala, M.: Seasonal cycle and modal structure of particle number size distribution at Dome C, Antarctica, *Atmos. Chem. Phys.*, 13, 7473–7487, doi:10.5194/acp-13-7473-2013, 2013.
- Jaumot, J., Gargallo, R., de Juan, A. and Tauler, R.: A graphical user-friendly interface for MCR-ALS: a new tool for multivariate curve resolution in MATLAB, *Chemom. Intell. Lab. Syst.*, 76 (1), 101–110, doi:10.1016/j.chemolab.2004.12.007, 2005.
- Jeong, M. J. and Li, Z.: Quality, compatibility, and synergy analyses of global aerosol products derived from the advanced very high resolution radiometer and Total Ozone Mapping Spectrometer, *J. Geophys. Res. D Atmos.*, 110 (10), 1–18, doi:10.1029/2004JD004647, 2005.
- Jimenez, J. L., Canagaratna, M. R., Donahue, N. M., Prevot, a. S. H., Zhang, Q., Kroll, J. H., DeCarlo, P. F., Allan, J. D., Coe, H., Ng, N. L., Aiken, a. C., Docherty, K. S., Ulbrich, I. M., Grieshop, A. P., Robinson, a. L., Duplissy, J., Smith, J. D., Wilson, K. R., Lanz, V. a., Hueglin, C., Sun, Y. L., Tian, J., Laaksonen, A., Raatikainen, T., Rautiainen, J., Vaattovaara, P., Ehn, M., Kulmala, M., Tomlinson, J. M., Collins, D. R., Cubison, M. J., Dunlea, J., Huffman, J. A., Onasch, T. B., Alfarra, M. R., Williams, P. I., Bower, K., Kondo, Y., Schneider, J., Drewnick, F., Borrmann, S., Weimer, S., Demerjian, K., Salcedo, D., Cottrell, L., Griffin, R., Takami, A., Miyoshi, T., Hatakeyama, S., Shimono, A., Sun, J. Y., Zhang, Y. M., Dzepina, K., Kimmel, J. R., Sueper, D., Jayne, J. T., Herndon, S. C., Trimborn, a. M., Williams, L. R., Wood, E. C., Middlebrook, A. M., Kolb, C. E., Baltensperger, U., Worsnop, D. R., Dunlea, E. J., Huffman, J. A., Onasch, T. B., Alfarra, M. R., Williams, P. I., Bower, K., Kondo, Y., Schneider, J., Drewnick, F., Borrmann, S., Weimer, S., Demerjian, K., Salcedo, D., Cottrell, L., Griffin, R., Takami, A., Miyoshi, T., Hatakeyama, S., Shimono, A., Sun, J. Y., Zhang, Y. M., Dzepina, K., Kimmel, J. R., Sueper, D., Jayne, J. T., Herndon, S. C., Trimborn, a. M., Williams, L. R., Wood, E. C., Middlebrook, A. M., Kolb, C. E., Baltensperger, U., Worsnop, D. R., Dunlea, J., Huffman, J. A., et al.: Evolution of Organic Aerosols in the Atmosphere, *Science* (80), 326 (5959), 1525–1529, doi:10.1126/science.1180353, 2009.
- Junge, C. E.: Recent investigation in air chemistry, *Tellus*, 8, 127–139, doi:10.3402/tellusa.v8i2.8971, 1956.
- Junker, C., Sheahan, J. N., Jennings, S. G., O'Brien, P., Hinds, B. D., Martinez-Twary, E., Hansen, A. D. A., White, C., Garvery, D. M., and Pinnick, R. G.: Measurement and analysis of aerosol and black carbon in the southwestern United States and Panama and their dependence on air mass origin, *J. Geophys. Res.*, 103, D13201, doi: 10.1029/2003JD004066, 2004.
- Kallos, G., Kotroni, V., Lagouvardos, K. and Papadopoulos, A.: On the long-range transport of air pollutants from Europe to Africa, *Geophys. Res. Lett.*, 25 (5), 619–622, doi:10.1029/97GL03317, 1998.
- Kallos, G., Astitha, M., Katsafados, P. and Spyrou, C.: Long-range transport of anthropogenically and naturally produced particulate matter in the Mediterranean and North Atlantic: Current state of knowledge, *J. Appl. Meteorol. Climatol.*, 46 (8), 1230–1251, doi:10.1175/JAM2530.1, 2007.
- Kalnay, E., Kanamitsu, M., Kistler, R., Collins, W., Deaven, D., Gandin, L., Iredell, M., Saha, S., White, G., Woollen, J., Zhu, Y., Chelliah, M., Ebisuzaki, W., Higgins, W., Janowiak,

## REFERENCES

---

- J., Mo, K. C., Ropelewski, C., Wang, J., Leetmaa, A., Reynolds, R., Jenne, R. and Joseph, D.: The NCEP/NCAR 40-year reanalysis project, *Bull. Am. Meteorol. Soc.*, 77 (3), 437–471, doi:10.1175/1520-0477(1996)077<0437:TNYRP>2.0.CO;2, 1996.
- Kanakidou, M., Seinfeld, J. H., Pandis, S. N., Barnes, I., Dentener, F. J., Facchini, M. C., Van Dingenen, R., Ervens, B., Nenes, A., Nielsen, C. J., Swietlicki, E., Putaud, J. P., Balkanski, Y., Fuzzi, S., Horth, J., Moortgat, G. K., Winterhalter, R., Myhre, C. E. L., Tsigaridis, K., Vignati, E., Stephanou, E. G. and Wilson, J.: Organic aerosol and global climate modelling: a review, *Atmos. Chem. Phys.*, 5, 1053–1123, doi:10.5194/acp-5-1053-2005, 2005.
- Kandler, K., Lieke, K., Benker, N., Emmel, C., Küpper, M., Müller-Ebert, D., Ebert, M., Scheuvs, D., Schladitz, A., Schütz, L. and Weinbruch, S.: Electron microscopy of particles collected at Praia, Cape Verde, during the Saharan Mineral Dust Experiment: Particle chemistry, shape, mixing state and complex refractive index, *Tellus, Ser. B Chem. Phys. Meteorol.*, 63 (4), 475–496, doi:10.1111/j.1600-0889.2011.00550.x, 2011.
- Karydis, V. A., Tsimpidi, A. P., Pozzer, A., Astitha, M., and Lelieveld, J.: Effects of mineral dust on global atmospheric nitrate concentrations, *Atmos. Chem. Phys.*, 16, 1491–1509, doi:10.5194/acp-16-1491-2016, 2016.
- Kaufman, Y. J., Boucher, O., Tanre, D., Chin, M., Remer, L. A., and Takemura, T.: Aerosol anthropogenic component estimated from satellite data, *Geophys. Res. Lett.*, 32, L17804, doi:10.1029/2005GL023125, 2005.
- Kirchstetter, T. A., Aguiar, J., Tonse, S., Fairley, D., and Novakov, T., Black carbon concentrations and diesel vehicle emission factors derived from coefficient of haze measurements in California: 1967–2003, *Atmos. Environ.*, 42, 480–491, 2008.
- Kistler, R., Kalnay, E., Collins, W., Saha, S., White, G., Woollen, J., Chelliah, M., Ebisuzaki, W., Kanamitsu, M., Kousky, V., Van derDool, H., Jenne, R., and Fiorino, M.: The NCEP-NCAR 50-year reanalysis: Monthly means CD-ROM and documentation, *Bull. Am. Met. Soc.*, 82, 247–267, 2001.
- Klein, T., Karlsson, P.E., Andersson, S., Engardt, M., Sjöberg, K.: Assessing and improving the Swedish forecast and information capabilities for ground-level ozone. Report Meteorology and Climatology, No114, Swedish Meteorological and Hydrological Institute, 2011.
- Klimont, Z., Smith, S. J. and Cofala, J.: The last decade of global anthropogenic sulfur dioxide: 2000–2011 emissions, *Environ. Res. Lett.*, 8 (1), 014003, doi:10.1088/1748-9326/8/1/014003, 2013.
- Koren, I., Kaufman, Y. J., Washington, R., Todd, M. C., Rudich, Y., Martins, J. V. and Rosenfeld, D.: The Bodélé depression: a single spot in the Sahara that provides most of the mineral dust to the Amazon forest, *Environ. Res. Lett.*, 1 (1), 014005, doi:10.1088/1748-9326/1/1/014005, 2006.
- Korhonen, P., Laaksonen, A., Viisanen, Y., McGraw, R., and Seinfeld, J. H.: Ternary nucleation of H<sub>2</sub>SO<sub>4</sub>, NH<sub>3</sub>, and H<sub>2</sub>O in the atmosphere, *J. Geophys. Res.*, 104, 26349–26353, doi: 10.1029/1999JD900784, 1999.
- Kourtchev, I., Ruuskanen, T., Maenhaut, W., Kulmala, M. and Claeys, M.: Observation of 2-methyltetrols and related photo-oxidation products of isoprene in boreal forest aerosols from Hyytiälä, Finland, *Atmos. Chem. Phys. Discuss.*, 5 (3), 2947–2971, doi:10.5194/acpd-5-2947-2005, 2005.
- Kristiansen, N. I., Stohl, A., Olivie, D. J. L., Croft, B., Søvde, O. A., Klein, H., Christoudias, T., Kunkel, D., Leadbetter, S. J., Lee, Y. H., Zhang, K., Tsigaridis, K., Bergman, T.,

- Evangelidou, N., Wang, H., Ma, P. L., Easter, R. C., Rasch, P. J., Liu, X., Pitari, G., Di Genova, G., Zhao, S. Y., Balkanski, Y., Bauer, S. E., Faluvegi, G. S., Kokkola, H., Martin, R. V., Pierce, J. R., Schulz, M., Shindell, D., Tost, H., and Zhang, H.: Evaluation of observed and modelled aerosol lifetimes using radioactive tracers of opportunity and an ensemble of 19 global models, *Atmos. Chem. Phys.*, 16, 3525–3561, doi:10.5194/acp-16-3525-2016, 2016.
- Kulmala, M., Korhonen, P., Napari, I., Karlsson, A., Berresheim, H., and O’Dowd, C. D.: Aerosol formation during PARFORCE: ternary nucleation of H<sub>2</sub>SO<sub>4</sub>, NH<sub>3</sub>, and H<sub>2</sub>O, *J. Geophys. Res.*, 107, 8111, doi:10.1029/2001JD000900, 2002.
- Kulmala, M.: How Particles Nucleate and Grow, *Science*, 302, 100–1001, doi: 10.1126/science.1090848, 2003.
- Kulmala, M., Vehkamäki, H., Petäjä, T., Dal Maso, M., Lauri, A., Kerminen, V. M., Birmili, W. and McMurry, P. H.: Formation and growth rates of ultrafine atmospheric particles: A review of observations, *J. Aerosol Sci.*, 35 (2), 143–176, doi:10.1016/j.jaerosci.2003.10.003, 2004.
- Kulmala, M., Lehtinen, K. E. J., and Laaksonen, A.: Cluster activation theory as an explanation of the linear dependence between formation rate of 3 nm particles and sulphuric acid concentration, *Atmos. Chem. Phys.*, 6, 787–793, doi:10.5194/acp-6-787-2006, 2006.
- Kulmala, M., Petäjä, T., Nieminen, T., Sipilä, M., Manninen, H. E., Lehtipalo, K., Dal Maso, M., Aalto, P. P., Junninen, H., Paasonen, P., Riipinen, I., Lehtinen, K. E. J., Laaksonen, A. and Kerminen, V. M.: Measurement of the nucleation of atmospheric aerosol particles, *Nat. Protoc.*, 7 (9), 1651–1667, doi:10.1038/nprot.2012.091, 2012.
- Kulmala, M., Kontkanen, J., Junninen, H., Lehtipalo, K., Manninen, H. E., Nieminen, T., Petäjä, T., Sipilä, M., Schobesberger, S., Rantala, P., Franchin, A., Jokinen, T., Järvinen, E., Äijälä, M., Kangasluoma, J., Hakala, J., Aalto, P. P., Paasonen, P., Mikkilä, J., Vanhanen, J., Aalto, J., Hakola, H., Makkonen, U., Ruuskanen, T., Mauldin, R. L., Duplissy, J., Vehkamäki, H., Bäck, J., Kortelainen, A., Riipinen, I., Kurtén, T., Johnston, M. V., Smith, J. N., Ehn, M., Mentel, T. F., Lehtinen, K. E. J., Laaksonen, A., Kerminen, V. M., and Worsnop, D. R.: Direct Observations of Atmospheric Aerosol Nucleation, *Science*, 339, 943–946, doi:10.1126/science.1227385, 2013.
- Laakso, L., Makela, J. M., Pirjola, L., and Kulmala, M.: Model studies on ion – induced nucleation in the atmosphere, *J. Geophys. Res.*, 107, 4427, doi:10.1029/2002JD002140, 2002.
- Laakso, L., Anttila, T., Lehtinen, K. E. J., Aalto, P. P., Kulmala, M., Hörrak, U., Paatero, J., Hanke, M., and Arnold, F.: Kinetic nucleation and ions in boreal forest particle formation events, *Atmos. Chem. Phys.*, 4, 2353–2366, doi:10.5194/acp-4-2353-2004, 2004.
- Laaksonen, A., Kulmala, M., O’Dowd, C. D., Joutsensaari, J., Vaattovaara, P., Mikkonen, S., Lehtinen, K. E. J., Sogacheva, L., Dal Maso, M., Aalto, P., Petäjä, T., Sogachev, A., Yoon, Y. J., Lihavainen, H., Nilsson, D., Facchini, M. C., Cavalli, F., Fuzzi, S., Hoffmann, T., Arnold, F., Hanke, M., Sellegri, K., Umann, B., Junkermann, W., Coe, H., Allan, J. D., Alfarra, M. R., Worsnop, D. R., Riekkola, M. L., Hyötyläinen, T., and Viisanen, Y.: The role of VOC oxidation products in continental new particle formation, *Atmos. Chem. Phys.*, 8, 2657–2665, doi: 10.5194/acp-8-2657-2008, 2008.
- Lance, S., Raatikainen, T., Onasch, T. B., Worsnop, D. R., Yu, X., Alexander, M. L., Stolzenburg, M. R., McMurry, P. H., Smith, J. N., and Nenes, A.: Aerosol mixing state, hygroscopic growth and cloud activation efficiency during MIRAGE 2006, *Atmos. Chem. Phys.*, 13, 5049–5062, doi:10.5194/acp-13-5049-2013, 2013.

## REFERENCES

---

- Laskin, A., Wietsma, T. W., Krueger, B. J., and Grassian, V. H.: Heterogeneous chemistry of individual mineral dust particles with nitric acid: A combined CCSEM/EDX, ESEM, and ICP-MS study, *J. Geophys. Res. Atmos.*, 110, D10208, doi:10.1029/2004JD005206, 2005.
- Lee, Y., Lee, H., Kim, M., Choi, C. Y., and Kim, J.: Characteristics of particle formation events in the coastal region of Korea in 2005, *Atmos. Environ.*, 42, 3729–3739, doi:10.1016/j.atmosenv.2007.12.064, 2008.
- Lee, K. H., Li, Z., Kim, Y. J. and Kokhanovsky, A.: Atmospheric aerosol monitoring from satellite observations: A history of three decades, *Atmos. and Bio. Environ. Monit.*, 13–38, 2009.
- Lee, S., Wang, Y. and Russell, A. G.: Assessment of Secondary Organic Carbon in the Southeastern United States: A Review, *J. Air Waste Manage. Assoc.*, 60 (11), 1282–1292, doi:10.3155/1047-3289.60.11.1282, 2010.
- Lehtinen, K. E. J., Dal Maso, M., Kulmala, M. and Kerminen, V. M.: Estimating nucleation rates from apparent particle formation rates and vice versa: Revised formulation of the Kerminen-Kulmala equation, *J. Aerosol Sci.*, 38 (9), 988–994, doi:10.1016/j.jaerosci.2007.06.009, 2007.
- Levy, H.: The Aeroce Project, in: *Tropospheric Ozone*, vol. 104, 365–370, Springer Netherlands, Dordrecht., 1988.
- Li, Q., Jacob, D., Park, R., Wang, Y., Heald, C., Hudman, R., Yantosca, R., Martin, R., and Evans, M.: North American pollution outflow and the trapping of convectively lifted pollution by upper-level anticyclone, *J. Geophys. Res.*, 110, D10301, doi:10.1029/2004JD005039, 2005.
- Li, W. J. and Shao, L. Y.: Observation of nitrate coatings on atmospheric mineral dust particles, *Atmos. Chem. Phys.*, 9, 1863–1871, doi:10.5194/acp-9-1863-2009, 2009.
- Li, Z., Zhao, X., Kahn, R., Mishchenko, M., Remer, L., Lee, K. H., Wang, M., Laszlo, I., Nakajima, T., and Maring, H.: Uncertainties in satellite remote sensing of aerosols and impact on monitoring its long-term trend: a review and perspective, *Ann. Geophys.*, 27, 2755–2770, doi:10.5194/angeo-27-2755-2009, 2009.
- Liu, Y., Cain, J. P., Wang, H., and Laskin, A.: Kinetic Study of Heterogeneous Reaction of Deliquesced NaCl Particles with Gaseous HNO<sub>3</sub> using Particle-on-Substrate Stagnation Flow Reactor Approach, *J. Phys. Chem. A*, 111, 10026–10043, doi:10.1021/jp072005p, 2007.
- Maas, R. and Grennfelt, P.: *Towards Cleaner Air, Scientific Assessment Report 2016*, EMEP Steering Body and Working Group on Effects of the Convention on Long-Range Transboundary Air Pollution, Oslo. xx+50pp, 2016.
- Madonna, F., Amodeo, A., D’Amico, G. and Pappalardo, G.: A study on the use of radar and lidar for characterizing ultragraining aerosol, *J. Geophys. Res. Atmos.*, 118 (17), 10056–10071, doi:10.1002/jgrd.50789, 2013.
- Mahajan, A. S., Fadnavis, S., Thomas, M. A., Pozzoli, L., Gupta, S., Royer, S. J., Saiz-Lopez, A. and Simó, R.: Quantifying the impacts of an updated global dimethyl sulfide climatology on cloud microphysics and aerosol radiative forcing, *J. Geophys. Res. Atmos.*, 120 (6), 2524–2536, doi:10.1002/2014JD022687, 2015.
- Mann, G. W., Carslaw, K. S., Spracklen, D. V., Ridley, D. A., Manktelow, P. T., Chipperfield, M. P., Pickering, S. J., and Johnson, C. E.: Description and evaluation of GLOMAP-mode: a modal global aerosol microphysics model for the UKCA composition-climate model, *Geosci. Model Dev.*, 3, 519–551, doi:10.5194/gmd-3-519-2010, 2010.

- Manninen, H. E., Nieminen, T., Asmi, E., Gagné, S., Häkkinen, S., Lehtipalo, K., Aalto, P., Vana, M., Mirme, A., Mirme, S., Hörrak, U., Plass-Dülmer, C., Stange, G., Kiss, G., Hoffer, A., Törö, N., Moerman, M., Henzing, B., de Leeuw, G., Brinkenberg, M., Kouvarakis, G. N., Bougiatioti, A., Mihalopoulos, N., O'Dowd, C., Ceburnis, D., Arneth, A., Svenningsson, B., Swietlicki, E., Tarozzi, L., Decesari, S., Facchini, M. C., Birmili, W., Sonntag, A., Wiedensohler, A., Boulon, J., Sellegri, K., Laj, P., Gysel, M., Bukowiecki, N., Weingartner, E., Wehrle, G., Laaksonen, A., Hamed, A., Joutsensaari, J., Petäjä, T., Kerminen, V. M., and Kulmala, M.: EUCAARI ion spectrometer measurements at 12 European sites – analysis of new particle formation events, *Atmos. Chem. Phys.*, 10, 7907–7927, doi:10.5194/acp-10-7907-2010, 2010.
- Martin, J. H., Fitzwater, S. E. and Gordon, R. M.: Iron deficiency limits phytoplankton growth in Antarctic waters, *Global Biogeochem. Cycles*, 4 (1), 5–12, doi:10.1029/GB004i001p00005, 1990.
- Marti, J. J., Weber, R. J., McMurry, P. H., Eisele, F., Tanner, D., and Jefferson, A.: New particle formation at a remote continental site, assessing the contributions of SO<sub>2</sub> and organic precursors, *J. Geophys. Res.*, 102, 6331–6339, doi: 10.1029/96JD02545, 1997.
- McMurry, P. H., Kuang, C. A., Smith, J. N., Zhao, J., and Eisele, F.: *Atmospheric New Particle Formation: Physical and Chemical Measurements*, Aerosol Measurement, John Wiley Sons, Inc., 681–695, 2011.
- Medeiros, P. M. and Simoneit, B. R. T.: Analysis of sugars in environmental samples by gas chromatography-mass spectrometry, *J. Chromatogr. A*, 1141 (2), 271–278, doi:10.1016/j.chroma.2006.12.017, 2007.
- Merikanto, J., Spracklen, D. V., Mann, G. W., Pickering, S. J., and Carslaw, K. S.: Impact of nucleation on global CCN, *Atmos. Chem. Phys.*, 9, 8601–8616, doi:10.5194/acp-9-8601-2009, 2009.
- Merrill, J. T., and Moody, J. L.: Synoptic meteorology and transport during the North Atlantic Regional Experiment (NARE) intensive: Overview, *J. Geophys. Res.*, 101, 28, 903–28, 921, doi: 10.1029/96JD00097, 1996.
- Metzger, A., Verheggen, B., Dommen, J., Duplissy, J., Prevot, A. S. H., Weingartner, E., Riipinen, I., Kulmala, M., Spracklen, D. V., Carslaw, K. S., and Baltensperger, U.: Evidence for the role of organics in aerosol particle formation under atmospheric conditions, *P. Natl. Acad. Sci. USA*, 107, 6646–6651, doi:10.1073/pnas.0911330107, 2010.
- MNP: Integrated modelling of global environmental change, an overview of IMAGE 2.4., edited by: Bouwman, A. F., Kram, T., and Klein Goldewijk, K., Netherlands Environmental Assessment Agency (MNP), Bilthoven, The Netherlands, 2006.
- Monahan, E. C., Spiel, D. E., and Davidson, K. L.: A model of marine aerosol generation via whitecaps and wave disruption, in: *Oceanic Whitecaps*, edited by: Monahan, E. C. and Mac Niocaill, G. D., Reidel Publishing Company, 167–174, 1986.
- Moody, J. L., Davenport, J. C., Merrill, J. T., Oltmans, S. J., Parrish, D. D., Holloway, J. S., Levy II, H., Forbes, G. L., Trainer, M., and Buhr M.: Meteorological mechanisms for transporting O<sub>3</sub> over the western North Atlantic Ocean: A case study for 24–29 August 1993, *J. Geophys. Res.*, 101, 29213–29277, doi: 10.1029/96JD00885, 1996.
- Mouillot, F. and Field, C. B.: Fire history and the global carbon budget: A 1°x1° fire history reconstruction for the 20th century, *Glob. Chang. Biol.*, 11 (3), 398–420, doi:10.1111/j.1365-2486.2005.00920.x, 2005.
- Murphy, D. M., Chow, J. C., Leibensperger, E. M., Malm, W. C., Pitchford, M., Schichtel, B. A., Watson, J. G., and White, W. H.: Decreases in elemental carbon and fine particle

## REFERENCES

---

- mass in the United States, *Atmos. Chem. Phys.*, 11, 4679–4686, doi:10.5194/acp-11-4679-2011, 2011.
- Myhre, G., D. Shindell, F. M. Bréon, W. Collins, J. Fuglestedt, J. Huang, D. Koch, J. F. Lamarque, D. Lee, B. Mendoza, T. Nakajima, A. Robock, G. Stephens, T. Takemura and H. Zhang, 2013: Anthropogenic and Natural Radiative Forcing, in: *Climate Change 2013: The Physical Science Basis. Contribution of Working Group I to the Fifth Assessment Report of the Intergovernmental Panel on Climate Change*, edited by: Stocker, T. F., D. Qin, G. K. Plattner, M. Tignor, S.K. Allen, J. Boschung, A. Nauels, Y. Xia, V. Bex and P.M. Midgley, Cambridge University Press, Cambridge, United Kingdom and New York, NY, USA, 2013.
- Napari, I., Noppel, M., Vehkamäki, H., and Kulmala, M.: Parameterization of ternary nucleation rates for H<sub>2</sub>SO<sub>4</sub>-NH<sub>3</sub>-H<sub>2</sub>O vapors, *J. Geophys. Res.*, 107, 4381, doi:10.1029/2002JD002132, 2002.
- Nie, W., Ding, A., Wang, T., Kerminen, V. M., George, C., Xue, L., Wang, W., Zhang, Q., Petäjä, T., Qi, X., Gao, X., Wang, X., Yang, X., Fu, C. and Kulmala, M.: Polluted dust promotes new particle formation and growth., *Sci. Rep.*, 4 (2), 6634, doi:10.1038/srep06634, 2014.
- Nieminen, T., Lehtinen, K. E. J., and Kulmala, M.: Sub-10 nm particle growth by vapor condensation – effects of vapor molecule size and particle thermal speed, *Atmos. Chem. Phys.* 10, 9773–9779, doi:10.5194/acp-10-9773-2010, 2010.
- Nilsson, E. D. and Kulmala, M.: The potential for atmospheric mixing processes to enhance the binary nucleation rate, *J. Geophys. Res.*, 103, 1381–1389, doi: 10.1029/97JD02629, 1998.
- Nishita, C., Osada, K., Kido, M., Matsunaga, K., and Iwasaka, Y.: Nucleation mode particles in upslope valley winds at Mount Norikura, Japan: Implications for the vertical extent of new particle formation events in the lower troposphere, *J. Geophys. Res.*, 113, D06202, doi:10.1029/2007JD009302, 2008.
- Nordstrom, K. and Hotta, S.: Wind erosion from cropland solutions in the USA: a review of problems, and prospects, *Geoderma*, 121 (3–4), 157–167, doi:10.1016/j.geoderma.2003.11.012z, 2004.
- Owen, R. C., Cooper, O. R., Stohl, A. and Honrath, R. E.: An analysis of the mechanisms of North American pollutant transport to the central North Atlantic lower free troposphere, *J. Geophys. Res.*, 111 (D23), D23S58, doi:10.1029/2006JD007062, 2006.
- Park, R. J., Jacob, D. J., Chin, M., and Martin, R. V.: Sources of carbonaceous aerosols over the United States and implications for natural visibility, *J. Geophys. Res.*, 108 (D12), 4355, doi:10.1029/2002JD003190, 2003.
- Park, R. J., Jacob, D., Field, B. D., Yantosca, R., and Chin, M.: Natural and transboundary pollution influences on sulfate-nitrate-ammonium aerosols in the United States: Implications for policy, *J. Geophys. Res.*, 109, D15204, doi:10.1029/2003JD004473, 2004.
- Parrish, D. D., Holloway, J. S., Trainer, M., Murphy, P. C., Forbers, G. L., and Fehsenfeld, F. C.: Relationships between ozone and carbon monoxide at surface sites in the North Atlantic region, *J. Geophys. Res.*, 103, 13 357–13 376, doi: 10.1029/98JD00376, 1998.
- Parrish, D. D. and Fehsenfeld, F. C.: Methods for gas-phase measurements of ozone, ozone precursors and aerosol precursors, *Atmos. Environ.*, 34, 1921–1957, doi: 10.1016/S1352-2310(99)00454-9, 2000.
- Patoulias, D., Fountoukis, C., Riipinen, I., and Pandis, S. N.: The role of organic condensation on ultrafine particle growth during nucleation events, *Atmos. Chem. Phys.*, 15, 6337–

- 6350, doi:10.5194/acp-15-6337-2015, 2015.
- Penner, J. E., Andreae, M., Annegarn, H., Barrie, L., Feichter, J., Hegg, D., Jayaraman, A., Leaitch, R., Murphy, D., Nganga, J., Pitari, G., et al.: Aerosols, their Direct and Indirect Effects, in: *Climate Change 2001: The Scientific Basis, Contribution of Working Group I to the Third Assessment Report of the Intergovernmental Panel on Climate Change (IPCC)*, Chapter 5, edited by: Houghton, J. T., Ding, Y., Griggs, D. J., Noguer, M., Linden, P. J. v. d., and Xiaosu, D., Cambridge University Press, Cambridge, 289–348, 2001.
- Pérez, C., Nickovic, S., Pejanovic, G., Baldasano, J. M. Özsoy, E. Interactive dust-radiation modeling: A step to improve weather forecasts, *J. Geophys. Res.*, 111, D16206, doi:10.1029/2005JD006717, 2006.
- Pérez García-Pando, C., Miller, R. L., Perlwitz, J. P., Rodríguez, S. and Prospero, J. M.: Predicting the mineral composition of dust aerosols: Insights from chemical composition measurements at the Izaña Observatory, *Geophys. Res. Lett.*, 43, 19, 10520–10529, doi:10.1002/2016GL069873, 2016.
- Petäjä, T., Mauldin III, R. L., Kosciuch, E., McGrath, J., Nieminen, T., Boy, M., Adamov, A., Kotiaho, T., and Kulmala, M.: Sulfuric acid and OH concentrations in a boreal forest site, *Atmos. Chem. Phys.*, 9, 7435–7448, doi:10.5194/acp-9-7435-2009, 2009.
- Prospero, J. M. and Carlson, T. N.: Vertical and areal distribution of Saharan dust over the western Equatorial North Atlantic Ocean, *J. Geophys. Res.*, 77, 5255–5265, doi: 0.1029/JC077i027p05255, 1972.
- Prospero, J. M., Seba, D. B: Some additional measurements of pesticides in the lower atmosphere of the northern equatorial Atlantic Ocean, *Atmos Environ*, 6 (5), 363–4, doi: 10.1016/0004-6981(72)90202-8, 1972.
- Prospero, J. M., Schmitt, R., Cuevas, E., Savoie, D. L., Graustein, W. C., Turekian, K. K., Volz-Thomas, A., Díaz, A., Oltmans, S. J. and Levy, H.: Temporal variability of summertime ozone and aerosols in the free troposphere over the eastern North Atlantic, *Geophys. Res. Lett.*, 22 (21), 2925–2928, doi:10.1029/95GL02791, 1995.
- Prospero, J. M.: Long-term measurements of the transport of African mineral dust to the southeastern United States: Implications for regional air quality, *J. Geophys. Res. Atmos.*, 104 (D13), 15917–15927, doi:10.1029/1999JD900072, 1999.
- Prospero, J. M., Ginoux, P., Torres, O., Nicholson, S. E. and Gill, T. E.: Environmental characterization of global sources of atmospheric soil dust identified with the NIMBUS 7 Total Ozone Mapping Spectrometer (TOMS) absorbing aerosol product, *Rev. Geophys.*, 40 (1), 1–31, doi:10.1029/2000RG000095, 2002.
- Prospero, J. M., Landing, W. M. and Schulz, M.: African dust deposition to Florida: Temporal and spatial variability and comparisons to models, *J. Geophys. Res. Atmos.*, 115 (13), 46–63, doi:10.1029/2009JD012773, 2010.
- Prospero, J. M. and Mayol-Bracero, O. L.: Understanding the Transport and Impact of African Dust on the Caribbean Basin, *B. Am. Meteorol. Soc.*, 94, 1329–1337, doi:10.1175/BAMS-D-12-00142.1, 2013.
- Prospero, J. M., Collard, F. X., Molinié, J. and Jeannot, A.: Characterizing the annual cycle of African dust transport to the Caribbean Basin and South America and its impact on the environment and air quality, *Global Biogeochem. Cycles*, 28 (7), 757–773, doi:10.1002/2013GB004802, 2014.
- Prospero, J. M.: Characterizing the temporal and spatial variability of African dust over the Atlantic, *DUST*, 24, 68, 2014.

## REFERENCES

---

- Putaud, J. P., Van Dingenen, R., Mangoni, M., Virkkula, A., Raes, F., Maring, H., Prospero, J. M., Swietlicki, E., Berg, O. H., Hillamo, R. and Mäkelä, T.: Chemical mass closure and assessment of the origin of the submicron aerosol in the marine boundary layer and the free troposphere at Tenerife during ACE-2, *Tellus, Ser. B Chem. Phys. Meteorol.*, 52 (2), 141–168, doi:10.1034/j.1600-0889.2000.00056.x, 2000.
- Querol, X., Alastuey, A., Rodríguez, S., Plana, F., Mantilla, E. and Ruiz, C. R.: Monitoring of PM<sub>10</sub> and PM<sub>2.5</sub> around primary particulate anthropogenic emission sources, *Atmos. Environ.*, 35 (5), 845–858, doi:10.1016/S1352-2310(00)00387-3, 2001.
- Raes, F., Bates, T., McGovern, F. and Van Liedekerke, M.: The 2nd Aerosol Characterization Experiment (ACE-2): General overview and main results, *Tellus, Ser. B Chem. Phys. Meteorol.*, 52 (2), 111–125, doi:10.1034/j.1600-0889.2000.00124.x, 2000.
- Randerson, J. T., van der Werf, G. R., Giglio, L., Collatz, G. J., and Kasibhatla, P. S.: Global Fire Emissions Database, Version 4, (GFEDv4), ORNL DAAC, Oak Ridge, Tennessee, USA, doi: 10.3334/ORNLDAAC/1293, 2015.
- Ravelo-Pérez, L. M., Rodríguez, S., Galindo, L., García, M. I., Alastuey, A., and López-Solano, J.: Soluble iron dust export in the high altitude Saharan Air Layer. *Atmos. Env.*, 133:49–59, doi: 10.1016/j.atmosenv.2016.03.030, 2016.
- Ravishankara, A. R.: Heterogeneous and multiphase chemistry in the troposphere, *Science*, 276, 1058–1066, doi: 10.1126/science.276.5315.1058, 1997.
- Reid, J. S., Kinney, J. E., Westphal, D. L., Holben, B. N., Welton, E. J., Tsay, S. C., Eleuterio, D. P., Campbell, J. R., Christopher, S. A., Colarco, P. R., Jonsson, H. H., Livingston, J. M., Maring, H. B., Meier, M. L., Pilewskie, P., Prospero, J. M., Reid, E. A., Remer, L. A., Russell, P. B., Savoie, D. L., Smirnov, A. and Tanré, D.: Analysis of measurements of Saharan dust by airborne and ground-based remote sensing methods during the Puerto Rico Dust Experiment (PRIDE), *J. Geophys. Res.*, 108 (D19), 8586, doi: 10.1029/2002JD002493, 2003.
- Reid, J. S., Koppmann, R., Eck, T. F., and Eleuterio, D. P.: A review of biomass burning emissions part II: intensive physical properties of biomass burning particles, *Atmos. Chem. Phys.*, 5, 799–825, doi: 10.5194/acp-5-799-2005, 2005.
- Reischl, G. P., Mäkelä, J. M., Karch, R. and Ncid, J.: Bipolar charging of ultrafine particles in the size range below 10 nm, *J. Aer. Sci.*, 27, 931–949, doi: 10.1016/0021-8502(96)00026-2, 1996.
- Risebrough, R. W., Huggett, R. J., Griffin, J. J. and Goldberg, E. D.: Pesticides: Transatlantic movement in the Northeast Trades, *Science* (80), 159(3), 1233–1236, doi:10.1126/science.159.3820.1233, 1968.
- Rodríguez, S., Van Dingenen, R., Putaud, J. P., Martins-Dos Santos, S. and Roselli, D.: Nucleation and growth of new particles in the rural atmosphere of Northern Italy - Relationship to air quality monitoring, *Atmos. Environ.*, 39 (36), 6734–6746, doi:10.1016/j.atmosenv.2005.07.036, 2005.
- Rodríguez, S., González, Y., Cuevas, E., Ramos, R., Romero, P. M., Abreu-Afonso, J., and Redondas, A.: Atmospheric nanoparticle observations in the low free troposphere during upward orographic flows at Izaña Mountain Observatory, *Atmos. Chem. Phys.*, 9, 6319–6335, doi:10.5194/acp-9-6319-2009, 2009.
- Rodríguez, S., Alastuey, A., Alonso-Pérez, S., Querol, X., Cuevas, E., Abreu-Afonso, J., Viana, M., Pérez, N., Pandolfi, M., and de la Rosa, J.: Transport of desert dust mixed with North African industrial pollutants in the subtropical Saharan Air Layer, *Atmos. Chem. Phys.*, 11, 6663–6685, doi:10.5194/acp-11-6663-2011, 2011.

- Rodríguez, S., Alastuey, A. and Querol, X.: A review of methods for long term in situ characterization of aerosol dust, *Aeolian Res.*, 6 (1), 55–74, doi:10.1016/j.aeolia.2012.07.004, 2012.
- Rodríguez, S., Cuevas, E., Prospero, J. M., Alastuey, A., Querol, X., López-Solano, J., García, M. I. and Alonso-Pérez, S.: Modulation of Saharan dust export by the North African dipole, *Atmos. Chem. Phys.*, 15 (13), 7471–7486, doi:10.5194/acp-15-7471-2015, 2015.
- Rose, C., Sellegri, K., Freney, E., Dupuy, R., Colomb, A., Pichon, J. M., Ribeiro, M., Bourianne, T., Burnet, F., and Schwarzenboeck, A.: Airborne measurements of new particle formation in the free troposphere above the Mediterranean Sea during the HYMEX campaign, *Atmos. Chem. Phys.*, 15, 10203–10218, doi:10.5194/acp-15-10203-2015, 2015.
- Salisbury, G.; Williams, J.; Gros, V.; Bartenbach, S.; Xu, X.; Fischer, H.; Kormann, R.; de Reus, M.; Zoellner, M.: Assessing the effect of a Saharan dust storm on oxygenated organic compounds at Izana, Tenerife (July–August 2002), *J. Geophys. Res. Atmos.*, 111, D2230, doi:10.1029/2005JD006840, 2006.
- Salma, I., Borsós, T., Weidinger, T., Aalto, P., Hussein, T., Dal Maso, M., and Kulmala, M.: Production, growth and properties of ultrafine atmospheric aerosol particles in an urban environment, *Atmos. Chem. Phys.*, 11, 1339–1353, doi:10.5194/acp-11-1339-2011, 2011.
- Salvador, P., Almeida, S. M., Cardoso, J., Almeida-Silva, M., Nunes, T., Cerqueira, M., Alves, C., Reis, M. A., Chaves, P. C., Artúñano, B. and Pio, C.: Composition and origin of PM<sub>10</sub> in Cape Verde: Characterization of long-range transport episodes, *Atmos. Environ.*, 127, 326–339, doi:10.1016/j.atmosenv.2015.12.057, 2016.
- Savoie, D. L., Arimoto, R., Keene, W. C., Prospera, J. M., Duce, R. A. and Galloway, J. N.: Marine biogenic and anthropogenic contributions to non-sea-salt sulfate in the marine boundary layer over the North Atlantic Ocean, *J. Geophys. Res. Atmos.*, 107 (18), doi:10.1029/2001JD000970, 2002.
- Scanza, R. A., Mahowald, N., Ghan, S., Zender, C. S., Kok, J. F., Liu, X., Zhang, Y., and Albani, S.: Modeling dust as component minerals in the Community Atmosphere Model: development of framework and impact on radiative forcing, *Atmos. Chem. Phys.*, 15, 537–561, doi:10.5194/acp-15-537-2015, 2015.
- Schulz, M., Prospero, J. M., Baker, A. R., Dentener, F., Ickes, L., Liss, P. S., Mahowald, N. M., Nickovic, S., García-Pando, C. P., Rodríguez, S., Sarin, M., Tegen, I. and Duce, R. a: Atmospheric transport and deposition of mineral dust to the ocean: implications for research needs., *Environ. Sci. Technol.*, 46 (19), 10390–404, doi:10.1021/es300073u, 2012.
- Seinfeld, J. H. and Pandis, S. N., *Atmospheric Chemistry and Physics: From Air Pollution to Climate Change*, 2nd Edition, John Wiley and Sons, New York, ISBN: 978-0-471-72018-8, 2006.
- Shao, Y., Wyrwoll, K. H., Chappell, A., Huang, J., Lin, Z., McTainsh, G. H., Mikami, M., Tanaka, T. Y., Wang, X. and Yoon, S.: Dust cycle: An emerging core theme in Earth system science, *Aeolian Res.*, 2 (4), 181–204, doi:10.1016/j.aeolia.2011.02.001, 2011.
- Shi, Z., Krom, M. D., Jickells, T. D., Bonneville, S., Carslaw, K. S., Mihalopoulos, N., Baker, A. R. and Benning, L. G.: Impacts on iron solubility in the mineral dust by processes in the source region and the atmosphere: A review, *Aeolian Res.*, 5 (5959), 21–42, doi:10.1016/j.aeolia.2012.03.001, 2012.
- Simoneit, B. R. T.: Organic matter in eolian dusts over the Atlantic Ocean, *Mar. Chem.*, 5,

## REFERENCES

---

- 443–464, doi: 10.1016/0304-4203(77)90034-2, 1977.
- Sindelarova, K., Granier, C., Bouarar, I., Guenther, A., Tilmes, S., Stavrou, T., Müller, J. F., Kuhn, U., Stefani, P., and Knorr, W.: Global data set of biogenic VOC emissions calculated by the MEGAN model over the last 30 years, *Atmos. Chem. Phys.*, 14, 9317–9341, doi:10.5194/acp-14-9317-2014, 2014.
- Smith, S. J., van Aardenne, J., Klimont, Z., Andres, R. J., Volke, A., and Delgado Arias, S.: Anthropogenic sulfur dioxide emissions: 1850–2005, *Atmos. Chem. Phys.*, 11, 1101–1116, doi:10.5194/acp-11-1101-2011, 2011.
- Stein, A. F., Draxler, R. R., Rolph, G. D., Stunder, B. J. B., Cohen, M. D. and Ngan, F.: NOAA's HYSPLIT Atmospheric Transport and Dispersion Modeling System, *Bull. Am. Meteorol. Soc.*, 96 (12), 2059–2077, doi:10.1175/BAMS-D-14-00110.1, 2015.
- Steinbacher, M., Zellweger, C., Schwarzenbach, B., Bugmann, S., Buchmann, B., Ordóñez, C., Prevot, A. S. H., and Hueglin, C., Nitrogen oxide measurements at rural sites in Switzerland: Bias of conventional measurement techniques, *J. Geophys. Res.*, 112, D11307, doi:10.1029/2006JD007971, 2007.
- Stelson, A. W. and Seinfeld, J. H.: Relative humidity and temperature dependence of the ammonium nitrate dissociation constant, *Atmos. Environ.*, 16 (5), 983–992, doi: 10.1016/0004-6981(82)90184-6, 1982.
- Stohl, A., Wotawa, G., Seibert, P., and Kromp-Kolb, H.: Interpolation errors in wind fields as a function of spatial and temporal resolution and their impact on different types of kinematic trajectories, *J. Appl. Meteor.*, 34, 2149–2165, doi: 10.1175/1520-0450(1995)034<2149:IEIWFA>2.0.CO;2, 1995.
- Stohl, A. and Seibert, P.: Accuracy of trajectories as determined from the conservation of meteorological tracers, *Q. J. R. Meteorol. Soc.*, 125, 1465–1484, doi: 10.1002/qj.49712454907, 1998.
- Surratt, J. D., Murphy, S. M., Kroll, J. H., Ng, N. L., Hildebrandt, L., Sorooshian, A., Szmi-gielski, R., Vermeylen, R., Maenhaut, W., Claeys, M., Flagan, R. C., and Seinfeld, J. H.: Chemical Composition of Secondary Organic Aerosol Formed from the Photooxidation of Isoprene, *J. Phys. Chem. A*, 110, 9665–9690, doi:10.1021/jp061734m, 2006.
- Surratt, J. D., Lewandowski, M., Offenberg, J. H., Jaoui, M., Kleindienst, T. E., Edney, E. O. and Seinfeld, J. H.: Effect of acidity on secondary organic aerosol formation from isoprene, *Environ. Sci. Technol.*, 41 (15), 5363–5369, doi:10.1021/es0704176, 2007.
- Talbot, R. W., Dibb, J. E., and Loomis, M. B.: Influence of vertical transport on free tropospheric aerosols over the central USA in springtime, *Geophys. Res. Lett.*, 25, 1367–1370, doi: 10.1029/98GL00184, 1998.
- Tauler, R., Smilde, A., and Kowalski, B.: Selectivity, local rank, 3-way data-analysis and ambiguity in multivariate curve resolution, *J. Chemometr.*, 9, 31–58, doi: 10.1002/cem.1180090105, 1995b.
- Tauler, R.: Multivariate curve resolution applied to second order data, *Chemometr. Intell. Lab.*, 30, 133–146, doi: 10.1016/0169-7439(95)00047-X, 1995a.
- Tauler, R., Viana, M., Querol, X., Alastuey, A., Flight, R. M., Wentzell, P. D. and Hopke, P. K.: Comparison of the results obtained by four receptor modelling methods in aerosol source apportionment studies, *Atmos. Environ.*, 43 (26), 3989–3997, doi:10.1016/j.atmosenv.2009.05.018, 2009.
- Taylor, K. E., Stouffer, R. J., and Meehl, G. A.: An Overview of CMIP5 and the Experiment Design, *Bull. Am. Meteorol. Soc.*, 93, 485–498, doi:10.1175/BAMS-D-11-00094.1, 2012.

- ten Brink, H. M.: Reactive uptake of  $\text{HNO}_3$  and  $\text{H}_2\text{SO}_4$  in sea-salt (NaCl) particles, *J. Aerosol Sci.*, 29, 57–64, doi:10.1016/S0021-8502(97)00460-6, 1998.
- Textor, C., Schulz, M., Guibert, S., Kinne, S., Balkanski, Y., Bauer, S., Berntsen, T., Berglen, T., Boucher, O., Chin, M., Dentener, F., Diehl, T., Easter, R., Feichter, H., Fillmore, D., Ghan, S., Ginoux, P., Gong, S., Grini, a., Hendricks, J., Horowitz, L., Huang, P., Isaksen, I., Iversen, T., Kloster, S., Koch, D., Kirkevåg, a., Kristjansson, J. E., Krol, M., Lauer, a., Lamarque, J. F., Liu, X., Montanaro, V., Myhre, G., Penner, J., Pitari, G., Lamarque, J. F., Liu, X., Montanaro, V., Myhre, G., Penner, J., Pitari, G., Reddy, S., Seland, Ø., Stier, P., Takemura, T. and Tie, X.: Analysis and quantification of the diversities of aerosol life cycles within AeroCom, *Atmos. Chem. Phys.*, 6, 1777–1813, doi:10.5194/acpd-5-8331-2005, 2006.
- Tsamalis, C., Chédin, A., Pelon, J., and Capelle, V.: The seasonal vertical distribution of the Saharan Air Layer and its modulation by the wind, *Atmos. Chem. Phys.*, 13, 11235–11257, doi:10.5194/acp-13-11235-2013, 2013.
- TSI: Operation and service manual of aerodynamic particle sizer series 3321, P/N 1930064, Revision D, October 2005.
- TSI: Operation and service manual of electrostatic classifiers series 3080, P/N 1933792, Revision J, March 2009.
- Tsigaridis, K., Krol, M., Dentener, F. J., Balkanski, Y., Lathière, J., Metzger, S., Hauglustaine, D. A., and Kanakidou, M.: Change in global aerosol composition since preindustrial times, *Atmos. Chem. Phys.*, 6, 5143–5162, doi:10.5194/acp-6-5143-2006, 2006.
- Tsigaridis, K., Daskalakis, N., Kanakidou, M., Adams, P. J., Artaxo, P., Bahadur, R., Balkanski, Y., Bauer, S. E., Bellouin, N., Benedetti, A., Bergman, T., Berntsen, T. K., Beukes, J. P., Bian, H., Carslaw, K. S., Chin, M., Curci, G., Diehl, T., Easter, R. C., Ghan, S. J., Gong, S. L., Hodzic, A., Hoyle, C. R., Iversen, T., Jathar, S., Jimenez, J. L., Kaiser, J. W., Kirkevåg, A., Koch, D., Kokkola, H., Lee, Y. H., Lin, G., Liu, X., Luo, G., Ma, X., Mann, G. W., Mihalopoulos, N., Morcrette, J. J., Müller, J. F., Myhre, G., Myriokefalitakis, S., Ng, N. L., O'Donnell, D., Penner, J. E., Pozzoli, L., Pringle, K. J., Russell, L. M., Schulz, M., Sciare, J., Seland, Ø., Shindell, D. T., Sillman, S., Skeie, R. B., Spracklen, D., Stavrou, T., Steenrod, S. D., Takemura, T., Tiitta, P., Tilmes, S., Tost, H., van Noije, T., van Zyl, P. G., von Salzen, K., Yu, F., Wang, Z., Wang, Z., Zaveri, R. A., Zhang, H., Zhang, K., Zhang, Q., and Zhang, X.: The AeroCom evaluation and intercomparison of organic aerosol in global models, *Atmos. Chem. Phys.*, 14, 10845–10895, doi:10.5194/acp-14-10845-2014, 2014.
- U.S. Environmental Protection Agency: Technology Transfer Network Clearinghouse for Inventories and Emission Factors, National Emissions Inventory (NEI) air pollutant emissions trends data, <https://www.epa.gov/air-emissions-inventories/air-pollutant-emissions-trends-data> (last access: 12 April 2016), 2016.
- Usher, C. R., Michel, A. E., and Grassian, V. H.: Reactions on mineral dust, *Chem. Rev.*, 103 (12), 4883–4939, doi: 10.1021/cr020657y, 2003.
- Val Martín, M., Honrath, R. E., Owen, R. C., Pfister, G., Fialho, P., and Barata, F.: Significant enhancements of nitrogen oxides, black carbon, and ozone in the North Atlantic lower free troposphere resulting from North American boreal wildfires, *J. Geophys. Res.*, 111, D23S60, doi:10.1029/2006JD007530, 2006.
- Van Drooge, B. L., Grimalt, J. O., Torres-García, C. J. and Cuevas, E.: Deposition of semi-volatile organochlorine compounds in the free troposphere of the eastern North Atlantic Ocean, *Mar Pollut Bull*, 42 (8), 628–634, doi: 10.1016/S0025-326X(01)00064-9, 2001.

## REFERENCES

---

- Van Drooge, B. L., Fernández, P., Grimalt, J. O., Stuchlík, E., Torres García, C. J. and Cuevas, E.: Atmospheric polycyclic aromatic hydrocarbons in remote European and Atlantic sites located above the boundary mixing layer., *Environ. Sci. Pollut. Res. Int.*, 17 (6), 1207–16, doi:10.1007/s11356-010-0296-0, 2010.
- Van Drooge, B. L. and Grimalt, J. O.: Particle size-resolved source apportionment of primary and secondary organic tracer compounds at urban and rural locations in Spain, *Atmos. Chem. Phys.*, 15, 7735–7752, doi:10.5194/acp-15-7735-2015, 2015.
- Varotsos, C. A., Tzanis, C. G., and Sarlis, N. V.: On the progress of the 2015–2016 El Niño event, *Atmos. Chem. Phys.*, 16, 2007–2011, doi:10.5194/acp-16-2007-2016, 2016.
- Vehkamäki, H., Kulmala, M., Napari, I., Lehtinen, K. E. J., Timmreck, C., Noppel, M., and Laaksonen, A.: An improved parameterization for sulfuric acid-water nucleation rates for tropospheric and stratospheric conditions, *J. Geophys. Res.*, 107, 4622–4632, doi: 10.1029/2002JD002184, 2002.
- Venzac, H., Sellegri, K., Laj, P., Villani, P., Bonasoni, P., Marioni, A., Cristofanelli, P., Calzolari, F., Fuzzi, S., Decesari, S., Facchini, M. C., Vuillermoz, E., and Verza, G. P.: High frequency new particle formation in the Himalayas, *P. Natl. Acad. Sci. USA*, 105, 15666–15671, doi: 10.1073/pnas.0801355105, 2008.
- Wang, R., Tao, S., Balkanski, Y., Ciais, P., Boucher, O., Liu, J., Piao, S., Shen, H., Vuolo, M. R., Valari, M., Chen, H., Chen, Y., Cozic, A., Huang, Y., Li, B., Li, W., Shen, G., Wang, B. and Zhang, Y.: Exposure to ambient black carbon derived from a unique inventory and high-resolution model., *Proc. Natl. Acad. Sci. U. S. A.*, 111 (7), 2459–63, doi:10.1073/pnas.1318763111, 2014.
- Weber, J. R., McMurry, P. H., Eisele, F. L., and Tanner, D. J.: Measurements of expected nucleation precursors species and 3–500 nm diameter particles at Mauna Loa, Hawaii, *J. Atmos. Sci.*, 52, 2242–2257, doi: 10.1175/1520-0469(1995)052<2242:MOENPS>2.0.CO; 2, 1995.
- Weber, J. R., McMurry, P. H., Mauldin III, R. L., Tanner, D. J., Eisele, F. L., Clarke, A. D., and Kapustin, V. N.: New particle formation in the remote troposphere: a comparison of observations at various sites, *Geophys. Res. Lett.*, 26, doi: 307–310, 10.1029/1998GL900308, 1999.
- Whittaker, K. M., and Horn L. H.: Northern hemisphere extra-tropical cyclone activity for four mid-season months, *J. Climatol.*, 4, doi: 297–310, 10.1002/joc.3370040307, 1984.
- WHO, World Health Organization, 2014: Burden of disease from ambient and household air pollution, [http://www.who.int/phe/health\\_topics/outdoorair/databases/en/](http://www.who.int/phe/health_topics/outdoorair/databases/en/), last accessed: 23-feb-2016.
- Wiedensohler, A.: An approximation of the bipolar charge distribution for particles in the submicron size range, *J. Aerosol Sci.*, 19 (3), 387–389, doi:10.1016/0021-8502(88)90278-9, 1988.
- Winker, D. M., Tackett, J. L., Getzewich, B. J., Liu, Z., Vaughan, M. A., and Rogers, R. R.: The global 3-D distribution of tropospheric aerosols as characterized by CALIOP, *Atmos. Chem. Phys.*, 13, 3345–3361, doi:10.5194/acp-13-3345-2013, 2013.
- Wu, Z. J., Hu, M., Liu, S., Wehner, B., Bauer, S., Ssling, A. M., Wiedensohler, A., Petäjä, T., Dal Maso, M. and Kulmala, M.: New particle formation in Beijing, China: Statistical analysis of a 1-year data set, *J. Geophys. Res.*, 112 (D9), D09209, doi:10.1029/2006JD007406, 2007.
- Wu, S., Mickley, L. J., Kaplan, J. O., and Jacob, D. J.: Impacts of changes in land use and land cover on atmospheric chemistry and air quality over the 21st century, *Atmos. Chem.*

- Phys., 12, 1597–1609, doi:10.5194/acp-12-1597-2012, 2012.
- Xiao, S., Wang, Q. Y., Cao, J. J., Huang, R. J., Chen, W. D., Han, Y. M., Xu, H. M., Liu, S. X., Zhou, Y. Q., Wang, P., Zhang, J. Q. and Zhan, C. L.: Long-term trends in visibility and impacts of aerosol composition on visibility impairment in Baoji, China, *Atmos. Res.*, 149, 88–95, doi:10.1016/j.atmosres.2014.06.006, 2014.
- Xing, J., Mathur, R., Pleim, J., Hogrefe, C., Gan, C. M., Wong, D. C., Wei, C., Gilliam, R., and Pouliot, G.: Observations and modeling of air quality trends over 1990–2010 across the Northern Hemisphere: China, the United States and Europe, *Atmos. Chem. Phys.*, 15, 2723–2747, doi:10.5194/acp-15-2723-2015, 2015.
- Yli-Juuti, T., Riipinen, I., Aalto, P. P., Nieminen, T., Maenhaut, W., Janssens, I. A., Claeys, M., Salma, I., Ocskay, R., Hoffer, A., Imre, K., and Kulmala, M.: Characteristics of new particle formation events and cluster ions at K-pusztá, Hungary, *Boreal Environ. Res.*, 14, 683–698, 2009.
- Yli-Juuti, T., Nieminen, T., Hirsikko, A., Aalto, P. P., Asmi, E., Hörrak, U., Manninen, H. E., Patokoski, J., Dal Maso, M., Petäjä, T., Rinne, J., Kulmala, M., and Riipinen, I.: Growth rates of nucleation mode particles in Hyytiälä during 2003–2009: variation with particle size, season, data analysis method and ambient conditions, *Atmos. Chem. Phys.*, 11, 12865–12886, doi:10.5194/acp-11-12865-2011, 2011.
- Zanatta, M., Gysel, M., Bukowiecki, N., Müller, T., Weingartner, E., Areskoug, H., Fiebig, M., Yttri, K. E., Mihalopoulos, N., Kouvarakis, G., Beddows, D., Harrison, R. M., Cavalli, F., Putaud, J. P., Spindler, G., Wiedensohler, A., Alastuey, A., Pandolfi, M., Sellegri, K., Swietlicki, E., Jaffrezo, J. L., Baltensperger, U. and Laj, P.: A European aerosol phenomenology-5: Climatology of black carbon optical properties at 9 regional background sites across Europe, *Atmos. Environ.*, 145, 346–364, doi:10.1016/j.atmosenv.2016.09.035, 2016.
- Zhang, K. M. and Wexler, A. S.: A hypothesis for growth of fresh atmospheric nuclei, *J. Geophys. Res. Atmos.*, 107 (21), 44737, doi:10.1029/2002JD002180, 2002.
- Zhang, R., Suh, I., Zhao, J., Zhang, D., Fortner, E. C., Tie, X., Molina, L. T., and Molina, M. J.: Atmospheric new particle formation enhanced by organic acids, *Science*, 304, 1487–1490, doi: 10.1126/science.1095139, 2004.
- Zhang, Y., Mahowald, N., Scanza, R. A., Journet, E., Desboeufs, K., Albani, S., Kok, J. F., Zhuang, G., Chen, Y., Cohen, D. D., Paytan, A., Patey, M. D., Achterberg, E. P., Engelbrecht, J. P., and Fomba, K. W.: Modeling the global emission, transport and deposition of trace elements associated with mineral dust, *Biogeosciences*, 12, 5771–5792, doi:10.5194/bg-12-5771-2015, 2015.
- Zhuang, H., Chan, C. K., Fang, M., and Wexler, A. S.: Formation of nitrate and non-sea-salt sulfate on coarse particles, *Atmos. Environ.*, 33, 4223–4233, doi: 10.1016/S1352-2310(99)00186-7, 1999.
- Zishka, K. M., and Smith, P. J.: The climatology of cyclones and anticyclones over North America and surrounding ocean environs for January and July, 1950–1977, *Mon. Weather Rev.*, 108, 387–401, doi: 10.1175/1520-0493(1980)108<0387:TCOCOA>2.0.CO;2, 1980.

# List of Figures

Figure	Page
1 Aerosol size distribution in number (continuous line) and mass (dotted line). Major chemical species distribution, formation and removal processes are shown. Figure adapted from Seinfeld and Pandis (2006) and Gieré et al. (2010). . . . .	10
2 Annual mean aerosol loads of (A) sea salt, (B) mineral dust, (C) organic carbon, (D) black carbon, (E) sulphate and (F) nitrate. Simulations from Phase 5 of the Coupled Model Intercomparison Project (CMIP5) for 2000; source data: <a href="https://data.giss.nasa.gov/modelforce/trop.aer/">https://data.giss.nasa.gov/modelforce/trop.aer/</a> . . . . .	12
3 Expanse of the Saharan Air Layer (SAL) in winter (orange shade) and in summer (brown shade). Discontinuous lines mark the Intertropical Convergence Zone (ITCZ) band in January (Jan) and July (Jul). The location of Izaña-Tenerife is highlighted (red circle). Figure adapted from Garrison et al., 2014 and Rodríguez et al 2015. . . . .	17
4 Airstreams associated with the mid-latitude cyclones: (A) top view and (B) three-dimensional scheme. Figure adapted from Cooper et al., 2002 a. <b>WCB</b> : warm conveyor belt. <b>CCB</b> : cold conveyor belt. <b>DA</b> : dry airstream. <b>PCF</b> : post cold front. (C) Convection mechanism. . . . .	19
5 (A) New particle formation steps. Figure adapted from Kulmala et al. (2003). (B) New Particle Formation or ‘banana type’ event where the above named steps are pointed. Black dots indicate the growth of the particle geometric mean diameter. The gray line is the linear least-squares fit to these points. Figure adapted from Kulmala et al. (2012). . . . .	21
6 (A) Location of the Canary Islands. (B) Vertical cross-section of Tenerife, where the altitude of the Izaña Observatory and the Teide peak are indicated; the stratification of the troposphere at the Island and the wind regimen are also represented. Figure adapted from Rodríguez et al., 2009. (C) View of Izaña GAW Observatory; the main building of the aerosol program (J.M. Prospero Aerosol Research Laboratory) is highlighted. . . . .	26
7 Global Atmospheric Watch (GAW) stations ( <a href="http://www.wmo.int/pages/prog/arep/gaw/measurements.html">http://www.wmo.int/pages/prog/arep/gaw/measurements.html</a> ); Izaña GAW Station is highlighted in red. . . .	27
8 (A) Scanning Mobility Particle Sizer (SMPS, model 3996, TSI™). (B) Schematic diagram of the electrostatic classifier (TSI, 2009). . . . .	28
9 (A) Aerodynamic Particle Sizer (APS, model 3321, TSI™). (B) Schematic diagram of the APS (TSI, 2005). . . . .	29

---

10	(A) High volume air samplers (HVS; MCZ) and (B) the weighing room. . . .	30
11	Expanded uncertainty (U) of the gravimetric method for individual PM <sub>x</sub> samples as described in EN-14907. . . . .	30
12	Scheme of the inorganic and carbonaceous species analyzed and the amount of filter used. <b>TOT</b> : thermal-optical transmittance; <b>ICP-AES</b> : Inductively Coupled Plasma Atomic Emission Spectrometry; <b>ICP-MS</b> : Inductively Coupled Plasma Mass Spectrometry. . . . .	31
13	Scheme of the organic speciation analysis. . . . .	33
14	Examples of type of events and cases identified in the data analysis. . . . .	38
15	(A) Example of type Ia event. (B) Time evolution of the number of particles and of the geometric mean diameter (GMD) for the nucleation mode. Lines illustrate the fitting that are performed for determining the formation (blue) and growth (green) rates. . . . .	40
16	Summer mean dust at Izaña(August) vs. MEI·(-1) – Multivariate ENSO Index – averaged for Jul–Aug–Sep for Intense El Niño Events (1987, 1997, 2009 and 2015). . . . .	161
17	Summer 2015 (Jul–Aug) total dust concentrations at (A) Izaña, (B) Barbados and (C) Miami. ‘Dust impact’ days of the dust episode that started on 09 July at Izaña and finished on 18 July at Miami, are highlighted. . . . .	162
18	Tracking of the dust episode that started on 09 July at Izaña and finished on 18 July at Miami. Only days of ‘dust impact’ in each station are shown for the sake of brevity. <b>Sources</b> : <a href="https://worldview.earthdata.nasa.gov/">https://worldview.earthdata.nasa.gov/</a> (Modis), <a href="http://giovanni.gsfc.nasa.gov/giovanni/">http://giovanni.gsfc.nasa.gov/giovanni/</a> (Giovanni), <a href="http://forecast.uoa.gr/dust-indx.php">http://forecast.uoa.gr/dust-indx.php</a> (Skiron forecast) and <a href="http://www.cpc.ncep.noaa.gov/">http://www.cpc.ncep.noaa.gov/</a> (NCAR/NCEP). 163	163

# List of Tables

<b>Table</b>	<b>Page</b>
1 Type of events considered in this study. <b>FR</b> : formation rate. <b>GR</b> : growth rate.	39
2 Ratio soluble calcium to mineral calcium (Ratio-1) and soluble calcium to dust concentration (Ratio-2) at Izaña, Barbados and Miami for three identified dust pulses. . . . .	164



# Acronyms

a.s.l	Above sea level
ACE	Aerosol Characterization Experiment
AEROATLAN	Tendencia y variabilidad multi-década de las propiedades de los aerosoles en el Atlántico Norte
AEROCE	Atmosphere/Ocean Chemistry Experiment
AI	Aerosol Index
APS	Aerodynamic Particle Sizer
AVHRR	Advanced Very High Resolution Radiometer
BC	Black Carbon
BSRN	Baseline Surface Radiation Network
BVOC	Biogenic volatile organic carbon
CALIOP	Cloud-Aerosol Lidar with Orthogonal Polarization
Ca-sol	Soluble calcium
Ca-min	Mineral calcium
CCB	Cold conveyor belt
CMIP5	Coupled Model Intercomparison Project Phase 5
CoagS	Coagulation Sink
CPC	Condensation Particle Counter
CS	Condensation Sink
CSIC	National Research Council of Spain
CV	Cape Verde
Cv	Condensable Vapour
DA	Dry airstream
DAS	Data assimilation system
DMA	Differential Mobility Analyzer
dp	Particle diameter
EC	Elemental carbon
ECMWF	European Centre for Medium-Range Weather Forecasts
ENSO	El Niño/Southern Oscillation
EUSAAR2	European Supersites for Atmospheric Aerosol Research-2
FID	Flame ionization detector
FLEXTRA	Flexible Trajectories model

---

FR	Formation Rate
FT	Free troposphere
GAW	Global Atmosphere Watch
GC-MS	Gas-chromatography coupled to mass-spectrometry
GDAS	Global Data Assimilation System
GEOS-Chem	Goddard Earth Observing System
GFEDv4.1s	Global Fire Emissions Database Version 4 including small fires data
GMD	Geometric mean diameter
GOCART	Goddard Chemistry Aerosol Radiation and Transport
GR	Growth Rate
HPLC	High-performance liquid chromatography
HVS	High Volume Samplers
HYSPLIT	Hybrid Single-Particle Lagrangian Integrated Trajectory model
I2A2	Impact of African air mass intrusions on the air quality of the Canary Islands and the Iberian Peninsula: Conceptual model and monitoring
ICP-AES	Inductively Coupled Plasma Atomic Emission Spectrometry
ICP-MS	Inductively Coupled Plasma Mass Spectrometry
IDAEA	Institute of Environmental Assessment and Water Research
INFN	National Institute of Nuclear Physics
ITCZ	Intertropical Convergence Zone
LF	Lifetime
LIDAR	Laser Imaging Detection and Ranging
LSQ	Least squares quadratic
LVS	Low Volume Samplers
MBL	Marine Boundary Layer
MCAR	Median Concentrations At Receptor
MCR-ALS	Multivariate Curve Resolution Alternating Least Squares
MEI	Multivariate ENSO Index
MEGAN	Model of Emissions of Gases and Aerosols from Nature
MLRA	Multilinear Regression Analysis
MODIS	Moderate Resolution Imaging Spectroradiometer
NAFDI	North African Dipole Intensity
NAO	North Atlantic Oscillation
NCAR	National Centre for Atmospheric Research
NCEP	National Centre for Environmental Prediction
NIST	National Institute of Standards and Technology
NOAA	National Oceanic and Atmospheric Administration
NPF	New Particle Formation
nss	non-sea salt
OC	Organic carbon
OM	Organic matter
OMI	Ozone Monitoring Instrument
PAH	Polycyclic aromatic hydrocarbons
PCA	Principal components analysis

## ACRONYMS

---

PCF	Post cold front
PIXE	Proton-induced X-ray emission
PM	Particulate matter
POA	Primary organic aerosol
POLLINDUST	Composition, sources and multi-decadal evolution of the dust and particulate pollutants observed in the subtropical Saharan Air Layer
PRIDE	Puerto Rico Dust Experiment
Py	Pyrolytic carbon
Q	Source Rate
QA	Quality assurance
QC	Quality control
REDMAAS	Red Española de DMAs Ambientales
RG	Reactive gases
RH	Relative humidity
SAL	Saharan Air Layer
SDR	Short-wave downward radiation
SE	Selective electrode
SMPS	Scanning Mobility Particle Sizer
SN	Serial number
SOA	Secondary organic aerosol
ss	sea salt
SSS	Subtropical Saharan Stripe
TIL	Temperature inversion layer
TOMS	Total Ozone Mapping Spectrometer
TOT	Thermal-optical transmittance
TRF	Transport Route Frequency
U	Expanded uncertainty
uc	Combined standard uncertainty
UK	United Kingdom
U.S.	United States
U.S.A.	United States of America
VOC	Volatile organic carbon
WCB	Warm conveyor belt
WCCAP	World Calibration Centre for Aerosol Physics
WCRP	World Climate Research Programme
WES	Westerlies
WGCM	Working Group on Coupled Modelling



# Scientific Contribution

## Articles in peer-review journals

### Included in this thesis

**García, M. I.**, Rodríguez, S., González, Y., and García, R. D.: Climatology of new particle formation at Izaña mountain GAW observatory in the subtropical North Atlantic, *Atmos. Chem. Phys.*, 14, 3865–3881, doi:10.5194/acp-14-3865-2014, 2014.

**García, M. I.**, Rodríguez, S., and Alastuey, A.: Impact of North America on the aerosol composition in the North Atlantic free troposphere, *Atmos. Chem. Phys. Discuss.*, doi:10.5194/acp-2017-60, in review, 2017.

**García, M. I.**, Van Drooge, B. L., Rodríguez, S., and Alastuey, A.: Speciation of organic aerosols in the Saharan Air Layer and in the free troposphere westerlies, *Atmos. Chem. Phys. Discuss.*, doi:10.5194/acp-2017-108, in review, 2017.

### Other related publications

Boose, Y., Sierau, B., **García, M. I.**, Rodríguez, S., Alastuey, A., Linke, C., Schnaiter, M., Kupiszewski, P., Kanji, Z. A., and Lohmann, U.: Ice nucleating particles in the Saharan Air Layer, *Atmos. Chem. Phys.*, 16, 9067–9087, doi:10.5194/acp-16-9067-2016, 2016.

Ravelo-Pérez, L. M., Rodríguez, S., Galindo, L., **García, M. I.**, Alastuey, A. and López-Solano, J.: Soluble iron dust export in the high altitude Saharan Air Layer, *Atmos. Environ.*, 133, 49–59, doi:10.1016/j.atmosenv.2016.03.030, 2016.

Rodríguez, S., Cuevas, E., Prospero, J. M., Alastuey, A., Querol, X., López-Solano, J., **García, M. I.** and Alonso-Pérez, S.: Modulation of Saharan dust export by the North African dipole, *Atmos. Chem. Phys.*, 15(13), 7471–7486, doi:10.5194/acp-15-7471-2015, 2015.

Gómez-Moreno, F. J., Alonso, E., Artíñano, B., Juncal-Bello, V., Iglesias-Samitier, S., Piñeiro Iglesias, M., Mahía, P. L., Pérez, N., Pey, J., Ripoll, A., Alastuey, A., de la Morena, B. A., **García, M. I.**, Rodríguez, S., Sorribas, M., Titos, G., Lyamani, H., Alados-Arboledas, L., Latorre, E., Tritscher, T. and Bischof, O. F.: Intercomparisons of Mobility Size Spectrometers and Condensation Particle Counters in the Frame of the Spanish Atmospheric Observational Aerosol Network, *Aerosol Sci. Technol.*, 49 (9), 777–785, doi:10.1080/02786826.2015.1074656, 2015.

## Books and scientific reports

Gómez-Moreno, F. J., Sorribas, M., Alonso, E., Artíñano, B., Juncal, V., Piñeiro, M., López, P., Pérez, N., Pey, J., Alastuey, A., **García, M. I.**, Rodríguez, S., Titos, G., Lyamani, H., Alados-Arboledas, L., de la Morena, B. A. Intercomparaciones de la Red Española de DMAs Ambientales (REDMAAS) en la estación de sondeos atmosféricos del INTA en el Arenosillo, pp. 9–58, Instituto Nacional de Técnica Aeroespacial (INTA), 01/09/2013, ISBN 978-84-938932-1-7, 2013.

Cuevas, E., Milford, C., Bustos, J. J., del Campo-Hernández, R., García, O. E., García, R. D., Gómez-Peláez, A. J., Ramos, R., Redondas, A., Reyes, E., Rodríguez, S., Romero-Campos, P. M., Schneider, M., Belmonte, J., Gil-Ojeda, M., Almansa, F., Alonso-Pérez, S., Barreto, A., González-Morales, Y., Guirado-Fuentes, C., López-Solano, C., Afonso, S., Bayo, C., Berjón, A., Bethencourt, J., Camino, C., Carreño, V., Castro, N. J., Cruz, A. M., Damas, M., De Ory-Ajamil, F., **García, M. I.**, Fernández-de Mesa, C. M., González, Y., Hernández, C., Hernández, Y., Hernández, M. A., Hernández-Cruz, B., Jover, M., Kühl, S. O., López-Fernández, R., López-Solano, J., Peris, A., Rodríguez-Franco, J. J., Sálamo, C., Sepúlveda, E. and Sierra, M.: Izaña Atmospheric Research Center Activity Report 2012-2014, (Eds. Cuevas, E., Milford, C. and Tarasova, O.), State Meteorological Agency (AEMET), Madrid, Spain and World Meteorological Organization, Geneva, Switzerland, NIPO:281-15-004-2, WMO/GAW Report No. 219, 2015.

## Contributions to conferences and workshops

Trans-Atlantic African Dust Transport Under El Niño 2015 Scenario, 8th International Workshop on Sand/Dust storms and Associated Dust fall, 2016. **M. I. García**; J. M. Prospero; S. Rodríguez; P. Zuidema; E. Sosa; A. Alastuey; F. Lucarelli; G. Calzolari; J. Lopez-Solano.

Atmospheric aging of dust ice nucleating particles – a field approach, European Geosciences Union General Assembly 2016, 2016. Y. Boose; S. Rodríguez; **M. I. García**; C. Linke; M. Schnaiter; A. Zipori; I. Crawford; U. Lohmann; Z.A. Kanji; B. Sierau.

Ice nucleating particle properties in the Saharan air layer, Workshop – Microphysics of ice clouds, 2016. Y. Boose; F. Mahrt; **M. I. García**; S. Rodríguez; A. Alastuey; C. Linke; M. Schnaiter; U. Lohmann; Z. A. Kanji; B. Sierau.

Ice nucleating particle properties in the Saharan air layer close to the dust source, 2015 AGU Fall Meeting, 2015. Y. Boose; F. Mahrt; **M. I. García**; S. Rodríguez; C. Linke; S. Nickovic; U. Lohmann; Z. A. Kanji; B. Sierau.

Single particle chemical composition of natural dusts and its link to ice nucleation, European Aerosol Conference, 2015. B. Sierau; Y. Boose; F. Mahrt; **M. I. García**; A. Wélti; J. Atkinson; F. Ramelli; M. Abegglen; Z. A. Kanji; S. Rodríguez; U. Lohmann.

Temporal and Spatial Variation of the Atmospheric Particle Size Distribution at Seven Measurement Stations within Spain, European Aerosol Conference, 2015. E. Alonso-Blanco; F. J. Gómez-Moreno; B. Artíñano; S. Iglesias Samitier; V. Juncal; M. Piñeiro Iglesias;

P. López Mahía; N. Pérez; M. Brines; A. Alastuey; X. Querol; B. A. de la Morena; **M. I. García**; S. Rodríguez; M. Sorribas; G. Titos; H. Lyamani; L. Alados-Arboledas.

Chemical characterization of ambient atmospheric aerosol particles at high altitude in Tenerife, Spain, using an Aerosol Time-of-Flight Mass Spectrometer, Chemical Society, 250th National Meeting, 2015. F. Mahrt; B. Sierau; Y. Boose; **M. I. García**; S. Rodríguez; U. Lohmann.

Atmospheric Particle Size Distribution in the Spanish Network of Environmental DMAs (REDMAAS), 3rd Iberian Meeting on Aerosol Science and Technology – RICTA, 2015. E. Alonso-Blanco; F. J. Gómez-Moreno; B. Artíñano; S. Iglesias Samitier; V. Juncal; M. Piñeiro Iglesias; P. López Mahía; N. Pérez; M. Brines; A. Alastuey; X. Querol; B. A. de la Morena; **M. I. García**; S. Rodríguez; M. Sorribas; G. Titos; H. Lyamani; L. Alados-Arboledas

Single particle mass spectrometry of soil and dust particles – linking their chemical composition to ice-nucleation activity, Seventh Symposium on Aerosol-Cloud-Climate Interactions, 2015. B. Sierau; Y. Boose; F. Mahrt; J. D. Haskins; **M. I. García**; I. Steinke; C. Hoese; Z. A. Kanji; O. Möhler; S. Rodríguez; U. Lohmann.

Long term 1987–2012 trends of sulfate, nitrate and dust mixing in the Saharan Air Layer, Symposium on Atmospheric Chemistry and Physics at Mountain Sites, 2014. S. Rodríguez; J. M. Prospero; **M. I. García**; A. Alastuey; R. D. García; J. López-Solano; X. Querol.

Cloud nuclei properties in the Saharan Air Layer close to the source, American Meteorological Society 14th Conference on Cloud Physics, 2014. Y. Boose; L. Lachner; **M. I. García**; S. Nickovic; S. Rodríguez; U. Lohmann; Z. A. Kanji; B. Sierau.

The REDMAAS 2014 intercomparison campaign: CPC, SMPS, UPMF and Neutralizers, 2nd Iberian Meeting on Aerosol Science and Technology – RICTA, 2014. F. J. Gómez-Moreno; E. Alonso; B. Artíñano; S. Iglesias; M. Piñeiro; P. López; N. Pérez; A. Alastuey; B. A. De La Morena; **M. I. García**; S. Rodríguez; M. Sorribas; G. Titos; H. Lyamani; L. Alados-Arboledas; E. Filimundi; E. Latorre.

Ice nuclei properties in the Saharan Air Layer close to the source Results from the CALIMA 2013 field campaign, 94th AMS Annual Meeting, 2014. Y. Boose; **M. I. García**; S. Rodríguez; U. Lohmann; Z. A. Kanji; B. Sierau.

The Spanish network on environmental DMAs: the 2012 SMPS+UFP intercomparison campaign and study on particle losses in dryers, European Aerosol Conference, 2013. F. J. Gómez-Moreno; E. Alonso; B. Artíñano; V. Juncal; M. Piñeiro; P. López; N. Pérez; J. Pey; A. Alastuey; M. Sorribas; B. A. de la Morena; **M. I. García**; S. Rodríguez; G. Titos; H. Lyamani; L. Alados-Arboledas.

The REDMAAS 2012 SMPS+UFP intercomparison campaign, 1st Iberian Meeting on Aerosol Science and Technology – RICTA, 2013. F. J. Gómez-Moreno; E. Alonso; B. Artíñano; V. Juncal; M. Piñeiro; P. López; N. Pérez; J. Pey; A. Alastuey; B. A. de la Morena; **M. I. García**; S. Rodríguez; M. Sorribas; G. Titos; H. Lyamani; L. Alados-Arboledas.

Calibration and intercomparison results in the Spanish network on environmental DMAs, European Aerosol Conference, 2012. F. J. Gómez-Moreno; B. Artíñano; V. Juncal; M. Piñeiro; P. López; N. Pérez; J. Pey; A. Alastuey; M. Sorribas; B. A. de la Morena; **M. I. García**; S. Rodríguez; G. Titos; H. Lyamani; L. Alados-Arboledas.

Characterization of new particles formation events at Izaña Mountain Observatory (Tenerife, Canary Islands): formation, growth rates and influencing atmospheric parameters, European Aerosol Conference, 2012. **M. I. García**; S. Rodríguez; Y. González; R. D. García.



This thesis was performed with the financial support of the Canary Agency for Research, Innovation and Information Society (ACIISI) co-funded by the European Social Funds (Ref: TESIS20120054). The work was accomplished within the context of the projects POLLINDUST (CGL2011-26259), AEROATLAN (CGL2015-66299-P), TEAPARTICLE (CGL2011-29621), REDMAAS (CGL2011-15008-E) and GRACCIE (CSD2007-00067) supported by the Ministry of Economy and Competitiveness of Spain and the European Regional Development Fund, and FP7-ACTRIS (grant contract: 262254) supported by the European Union. Measurements at Izaña observatory were carried out within the context Global Atmospheric Watch networks with the financial support of the State Meteorological Agency of Spain (AEMET).



**Gobierno de Canarias**  
Agencia Canaria  
de Investigación, Innovación  
y Sociedad de la Información

canarias  
OBJETIVO de PROGRESO



**Unión Europea**  
Fondo Social Europeo



**GLOBAL  
ATMOSPHERE  
WATCH**

**AEMET**

Agencia Estatal de Meteorología

